University of Southampton

Faculty of Engineering and Physical Sciences

School of Electronics and Computer Science

E-Textile Sensor for Monitoring and Evaluation of Atopic Dermatitis in Skin

by

Alexandar Radoslavov Todorov

ORCID ID: 0000-0002-6126-753X

Thesis for the degree of PhD in Electronic and Electrical Engineering

February 2026

University of Southampton

Abstract

Faculty of Engineering and Physical Sciences

School of Electronics and Computer Science

Thesis for the degree of PhD in Electronic and Electrical Engineering

E-Textile Sensor for Monitoring and Evaluation of Atopic Dermatitis in Skin

by

Alexandar Radoslavov Todorov

Atopic dermatitis is one of the most common skin disorders, affecting nearly one fifth of the children and adolescents worldwide. It is characterised by relapsing skin lesions, which result in redness, itchiness, and dryness of the skin. Although research has discovered some of the reasons for the condition's emergence, a dysfunction of the epidermal barrier in the skin and its ability to retain water and repel outside influences, there has not been much progress in providing effective treatment and diagnosis. This is due mainly because such treatments are monitored qualitatively, by observation, rather than quantitatively, by empirical data.

This thesis presents the development of a novel e-textile interdigitated capacitor (IDC) system to quantitatively assess the severity and treatment of AD in vivo. The IDC is made bespoke to be highly sensitive towards detecting the dysfunction of the skin barrier by measuring the hydration in the superficial layers of the skin – the stratum corneum (SC) and epidermis (EP). This device provides an empirical and universal scale that can be used to tailor treatments based on the specific severity state of the patient's condition. It is housed in a compact, non-invasive and wearable package, to allow dermatologists to assess the patients' condition remotely and continuously, introducing a new dimension of data on AD. The thesis details the development of the sensor from concept to operating prototype, spanning simulation modelling and analytical solutions, fabrication of the device, tests on skin replicas, and trials on patients.

A novel multilayer skin model was created in COMSOL®, incorporating frequency-dependent dielectric spectra for skin with AD. The model was used to determine the best geometry of the IDC for the application by controlling the parameters of the design. This study revealed novel insights into the depth-resolution of IDC sensors when subjected to multilayer media, presenting evidence that shallower penetration of electric field lines results from smaller electrode gaps. Simulations demonstrated that optimised IDC geometries with 50 – 100 μm electrode gaps are most sensitive to hydration changes in the SC, with maximum sensitivity in the 10 kHz – 1 MHz frequency range.

Prototypes were fabricated using two methods: etched copper on copper-polyimide substrates and printing silver on textile. Products from both methods were assessed using a novel hydration-gradient skin replica (also known as skin phantom) which simulated skin with different severity levels of AD. The results validated the findings of the FEA study, and the IDC with an electrode separation gap of 100 μm was confirmed as the chosen design for the study, balancing sensitivity and fabrication complexity. The early prototypes were robust under temperature and mechanical deformation but were heavily affected by humidity and lacked repeatability in readings. An encapsulation layer of 50 μm was introduced to solve this, which decreased the sensitivity, but achieved stability and prevented artefacts attributed to poor contact or moisture build-up.

The finished printed silver sensor was integrated in a complete wearable system housed in an e-textile armband with a capacitance-to-digital converter, BLE-enabled transmitting microcontroller, and a custom graphical user interface. The system is designed to be portable and easy to operate, allowing for both clinicians and patients to use the device and collect readings both in clinic and at home.

Clinical trials on thirteen patients with the condition confirmed that the e-textile IDC sensor distinguished between different severity states of the skin (lesional and non-lesional) with 100% sensitivity and specificity for individual patients. It reaffirmed the findings of the simulation and empirical studies that the chosen design is the most sensitive towards biomarkers of AD, revealing the highest change in capacitance arising from changes in the severity state of the skin. Differences in measured capacitance between the skin states were in the order of 3 to 5 pF. The sensor correlated significantly with Corneometer® measurements, a gold-standard for skin hydration testing ($r = 0.595$, $p < 0.05$). Furthermore, the e-textile IDC sensor demonstrated tighter clustering of the readings compared to other methods of assessment, indicating better variability and repeatability.

These findings demonstrate, for the first time, that a textile-integrated IDC can provide stable, quantitative, and clinically relevant measurements of AD severity in vivo. The work establishes a foundation for objective, continuous, and remote monitoring of AD, paving the way towards digital dermatology tools that can transform both clinical practice and at-home patient management.

Table of Contents

Table of Tables

Table of Figures

Table of Figures

Table of Figures

Table of Figures

Table of Figures

Research Thesis: Declaration of Authorship

Print name: Alexandar Radoslavov Todorov

Title of thesis: E-Textile Sensor for Monitoring and Evaluation of Atopic Dermatitis in Skin

I declare that this thesis and the work presented in it are my own and has been generated by me as the result of my own original research.

I confirm that:

1. This work was done wholly or mainly while in candidature for a research degree at this University;
2. Where any part of this thesis has previously been submitted for a degree or any other qualification at this University or any other institution, this has been clearly stated;
3. Where I have consulted the published work of others, this is always clearly attributed;
4. Where I have quoted from the work of others, the source is always given. With the exception of such quotations, this thesis is entirely my own work;
5. I have acknowledged all main sources of help;
6. Where the thesis is based on work done by myself jointly with others, I have made clear exactly what was done by others and what I have contributed myself;
7. Parts of this work have been published as:

A. R. Todorov *et al.*, "Design of a Flexible, Wearable Interdigitated Capacitive Sensor for Monitoring Biomarkers of Atopic Dermatitis," *IEEE Sensors Journal,* pp. 1-1, 2023, doi: 10.1109/jsen.2023.3342992

A. R. Todorov, H. Dai, E. Y. H. Ko, L. S. Abdulkarim, N. Chupreecha, J. Fuller, E. Corden, Y. X. Teo, R. N. Torah, M. R. Ardern-Jones, and S. P. Beeby, “Wearable system using printed interdigitated capacitive sensor for monitoring atopic dermatitis in patients,” *IEEE Sensors Journal*, accepted for publication (in press), doi: 10.1109/JSEN.2025.3601742.

H. Dai, A. R. Todorov, S. Yong, R. Torah, M. Ardern-Jones, and S. Beeby, "High resolution reverse-offset printed wearable laminated textile capacitive sensor for continuous monitoring of atopic dermatitis," *npj Flexible Electronics,* vol. 9, no. 1, p. 78, 2025/08/02 2025, doi: 10.1038/s41528-025-00456-x.

A. R. Todorov, H. Dai, R. N. Torah, M. R. Ardern-Jones, and S. P. Beeby, "Wearable interdigitated capacitive sensor with flexible analog front end for superficial skin hydration measurements,"

presented at the *2025 IEEE International Conference on Flexible and Printable Sensors and Systems (FLEPS)* (22/06/25 - 25/06/25), 2025. [Online]. Available: https://eprints.soton.ac.uk/502032/.

A. R. Todorov, K. Goyal, R. N. Torah, T. Greig, M. R. Ardern-Jones, and S. P. Beeby, "Skin Model for Monitoring Atopic Dermatitis Using Interdigitated Capacitive Sensor," in *46th Annual International Conference of the IEEE Engineering in Medicine and Biology Society*, Orlando, FL, 2024 2024: IEEE, pp. 1-4, doi: 10.1109/embc53108.2024.10782789. [Online]. Available: https://dx.doi.org/10.1109/EMBC53108.2024.10782789.

A. R. Todorov, R. Torah, M. Ardern-Jones, and S. Beeby, "Fabrication of a Screen-Printed E-Textile Interdigitated Capacitive Sensor for Measuring Stratum Corneum Hydration," in *E-textiles 2023*, 2023: MDPI, doi: 10.3390/engproc2023052001. [Online]. Available: https://dx.doi.org/10.3390/engproc2023052001.

A. R. Todorov, R. Torah, M. R. Ardern-Jones, and S. P. Beeby, "Electromagnetic Sensing Techniques for Monitoring Atopic Dermatitis—Current Practices and Possible Advancements: A Review," *Sensors,* vol. 23, no. 8, p. 3935, 2023, doi: 10.3390/s23083935.

Y. Khan, A. R. Todorov, R. Torah, S. Beeby, and M. R. Ardern-Jones, "Skin Sensing and Wearable Technology as Tools to Measure Atopic Dermatitis Severity," *Skin Health and Disease,* vol. 4, no. 5, 2024, doi: 10.1002/ski2.449.

Signature: ..... Date:.....

Acknowledgements

A heartfelt thank you goes to my supervisors – Prof. Stephen Beeby, Prof. Michael Ardern-Jones and Dr. Russel Torah for their guidance and support throughout the progression of this project. Their dedication has been fundamental to the success of this project.

I would like to thank my incredible colleagues from SEMS research group: Mahmoud, Tom, Irfan, Abiodun, Mahdi and Sheng for their technical support in helping me shape the produced device. They have managed to help me solve a multitude of technical obstacles to achieve this. I would also express my gratitude towards Huanghao and Mengyang, who provided important support throughout the last stages of the project in fabricating the device and finding new applications for it. Finally, I would like to thank the team at the dermatology clinic in the University Hospital Southampton – Emily, Jai, James, April, and Chrissie, as they provided crucial support during patient trials.

Without this entire team, none of this would be possible – thank you!

Definitions and Abbreviations

AD ..... Atopic Dermatitis

AI ..... Artificial intelligence

AUC ..... Area under curve

CAD ..... Computer aided design

CCD ..... Charge-coupled device

CDC ..... Capacitance to digital converter

DFT ..... Discrete Fourier transform

DR ..... Dermis

DRI ..... Diffuse reflectance imaging

Epithelial barrier ..... Skin barrier, SC barrier, protects from external influences

EP ..... Epidermis

FEA ..... Finite element analysis

FLG ..... Filaggrin protein

IDC ..... Interdigitated capacitor

IDE ..... Interdigitated electrodes

ISF ..... Interstitial fluid

Lesion ..... Patch of abnormal skin

MCU ..... Microcontroller unit

MUT ..... Material under test

PDMS ..... Polydimethylsiloxane

Pruritus ..... Medical term for itchy skin

PVA ..... Polyvinyl acetate

RF ..... Radio frequency

ROC ..... Receiver operating characteristic

ROP ..... Reverse offset printing

SC ..... Stratum Corneum

SDS ..... Source-to-detector separation

SE ..... Sensing element

SNR ..... Signal to noise ratio

TARC ..... Serum thymus and activation-regulated chemokine

TDR..... Time-domain reflectometry

TEWL ..... Transepidermal water loss

TJ ..... Tight junction protein

TPU ..... Thermoplastic polyurethane

Chapter 1 Introduction

1.1 Motivation of Research

In the last decade, there has been an ever-increasing amount of innovation and interest in developing systems for personalized, at-home health care, assisted by advances in information and communication technologies also known as “e-health” [1]. The World Health Organization (WHO) calls the term a “worldwide phenomenon” and aims to provide suitable e-health solutions for everyone [2]. E-health encompasses a broad range of services such as providing remote specialist consultation and diagnosis, effective storage and management of patients’ clinical records and prescription of medicine via the Internet. Providing specialist medical care and advice through means of communication is highly sought from rural or remote areas, or when the patient is unable to leave their homes.

One area in medicine that has not seen much advancement since the introduction of e-health is dermatology and the study of lesions and skin inflammations. Diseases like melanoma (skin cancer), atopic dermatitis (AD), psoriasis have so far been diagnosed in person by a specialist dermatologist. In the case of AD, there is also no universally accepted treatment algorithm, thereby prescribed treatments of the same patient may vary depending on the dermatologist or the institution the patient attends [3, 4]. There have been attempts to introduce telemedical solutions such as machine learning and artificial intelligence (AI) to detect and diagnose melanoma [5] and psoriasis [6] by looking at pictures of patients with lesional (damaged) skin, which is a step in the right direction towards achieving a complete diagnosis through e-health systems, but these detection systems have limitations with accuracy [7]. This highlights the need not only for communication solutions for remote healthcare but for actual mobile medical devices that would assist in the diagnosis and treatments of patients in vivo. These devices have to be compact, cheap and non-invasive to the daily home routine of the patient.

Electronic textiles and wearable smart garments, cumulatively known as e-textiles attain all the aforementioned qualities in a comfortable platform that patients are already familiar with. E-textiles are wearable garments that include electronic components that are either placed in internal pockets or embedded (woven) inside the fabric [8]. These devices offer broad versatility, flexibility and allow for continuous monitoring, thus they have already been incorporated in the fields of worker safety and athletic performance tracking [9, 10]. E-textiles have also proven their usefulness in a variety of areas of medicine: breathing detection [11], ECG [12, 13], heart rate monitoring [14], temperature [15], movement disorders [16], neurological rehabilitation [17], and many others. Currently, there has been limited research into the usage of e-textile sensing

solutions in the monitoring and treatment of skin conditions, especially AD. Using the multifunctionality, breathability and conformability of e-textiles, a sensor for assessment of atopic dermatitis could be built, which will not only expand the field of e-health personalized solutions but will also provide insights for a universal criterion for evaluating this disease.

1.2 Objectives of the Research

The purpose of this study is to uncover what are the current means of monitoring AD in a clinical environment, and to explore ways of translating these methods into non-invasive and remote sensors. The goal of the research is to create a standalone device, with an application-specific sensing element, embedded into a garment or textile. This device would allow for quantifiable and empirical monitoring and evaluation of AD in both clinical environments and at the homes of patients. This sensor will detect for the change in a specific biomarker of AD – the stratum corneum barrier function, or the dehydration the outermost layers of the skin. The purpose of embedding it in textile is to expand the modality of operation, namely continuous assessment of the skin, rather than solely single-point-in-time measurements.

Different measurement principles will be considered throughout this study to construct a compact device that falls under the requirements of the research thesis for non-invasive and mobile monitoring. The performance and accuracy of the different types will be compared to highlight the best solution for AD monitoring.

The finalised prototype sensor will be tested in vivo onto the skin of humans with and without symptoms/lesions of AD. If the trials are successful, the device can compete for commercialization and adoption within the health industry.

1.3 Statement of Novelty

The author lists the following novelties of this project:

1. Application of targeted capacitive measurement of biomarkers of AD for the assessment of severity in patients. The literature presents various sensors for generic skin condition and hydration measurements, but none have been made bespoke for monitoring of AD and tested in vivo on patients.
2. Design of an interdigitated capacitor with a depth-selective sensitivity towards the outermost layers of the skin. This design was proven both through simulation and empirical studies on skin replicas and on patients. In the literature there are similar designs, but none of them are proven to be sensitive only to the outermost layers of the skin.

3. Determination of frequency window for high sensitivity towards hydration changes in the outermost layers of the skin, relevant to biomarkers of AD. Most publications in the literature use a fixed frequency for the excitation signal of capacitive sensors and this discovery fills an important gap in the literature.
4. Accurate layer-separated model of the skin for FEA studies, isolating the dielectric properties of individual skin layers. The model also reflects the frequency-dependence of the skin, allowing for frequency-resolved excitation signals to be investigated. To the knowledge of the author is the first such model presented in the literature.
5. Simulation model of skin with AD for FEA analysis. Following the layer-separated model of the skin, the dielectric properties of it were altered through empirical measurements to simulate patients' skin with the condition. A first in the literature.
6. Replica of the skin with a hydration-gradient profile, simulating various severity and hydration states of skin with AD. This is the first example in the literature of a skin phantom that can replicate multiple states of the skin at the same time.
7. First e-textile sensing system demonstrated on patients with AD. The novel sensor was integrated within a wearable and portable format and successfully tested in vivo on patients with the condition.

1.4 Publications Arising from This Thesis

The following publications have resulted from this thesis, each accompanied by a brief explanation linking it to one or more of the novelties described above:

1. A. R. Todorov *et al.*, "Design of a Flexible, Wearable Interdigitated Capacitive Sensor for Monitoring Biomarkers of Atopic Dermatitis," *IEEE Sensors Journal,* pp. 1-1, 2023, doi: 10.1109/jsen.2023.3342992.
    a. This publication introduces the bespoke design of the sensor, validated both through simulation studies and on the hydration-gradient skin replica, demonstrating novelties 2, 4, and 6.
2. A. R. Todorov, H. Dai, E. Y. H. Ko, L. S. Abdulkarim, N. Chupreecha, J. Fuller, E. Corden, Y. X. Teo, R. N. Torah, M. R. Ardern-Jones, and S. P. Beeby, "Wearable system using printed interdigitated capacitive sensor for monitoring atopic dermatitis in patients," *IEEE Sensors Journal*, accepted for publication (in press), doi: 10.1109/JSEN.2025.3601742.
    a. This publication introduces the complete e-textile system for monitoring and evaluating the severity of patients with AD, demonstrating novelties 1 and 7.
3. H. Dai, A. R. Todorov, S. Yong, R. Torah, M. Ardern-Jones, and S. Beeby, "High resolution reverse-offset printed wearable laminated textile capacitive sensor for continuous

monitoring of atopic dermatitis," *npj Flexible Electronics,* vol. 9, no. 1, p. 78, 2025/08/02 2025, doi: 10.1038/s41528-025-00456-x.

a. This publication details the novel fabrication method used to achieve the high resolution of the sensor for AD and includes testing which demonstrate novelty 2.

4. A. R. Todorov, H. Dai, R. N. Torah, M. R. Ardern-Jones, and S. P. Beeby, "Wearable interdigitated capacitive sensor with flexible analog front end for superficial skin hydration measurements," presented at the *2025 IEEE International Conference on Flexible and Printable Sensors and Systems (FLEPS)* (22/06/25 - 25/06/25), 2025. [Online]. Available: https://eprints.soton.ac.uk/502032/.

   a. This publication presents the development of the flexible e-textile system for targeted measurements of stratum corneum hydration, strengthening novelties 1 and 7.

5. A. R. Todorov, K. Goyal, R. N. Torah, T. Greig, M. R. Ardern-Jones, and S. P. Beeby, "Skin Model for Monitoring Atopic Dermatitis Using Interdigitated Capacitive Sensor," in *46th Annual International Conference of the IEEE Engineering in Medicine and Biology Society*, Orlando, FL, 2024 2024: IEEE, pp. 1-4, doi: 10.1109/embc53108.2024.10782789. [Online]. Available: https://dx.doi.org/10.1109/EMBC53108.2024.10782789.

   a. This publication presents the novel layer-separated simulation model of the skin and introduces the estimated dielectric properties of skin with AD to determine the high sensitivity range of the excitation signal used during capacitive measurements. This demonstrates novelties 3 and 5.

6. A. R. Todorov, R. Torah, M. Ardern-Jones, and S. Beeby, "Fabrication of a Screen-Printed E-Textile Interdigitated Capacitive Sensor for Measuring Stratum Corneum Hydration," in *E-textiles 2023*, 2023: MDPI, doi: 10.3390/engproc2023052001. [Online]. Available: https://dx.doi.org/10.3390/engproc2023052001.

   a. This publication introduced for the very first time an e-textile capable of high sensitivity measurements towards independent skin layers, in this case the hydration of the stratum corneum, demonstrating novelty 2.

7. A. R. Todorov, R. Torah, M. R. Ardern-Jones, and S. P. Beeby, "Electromagnetic Sensing Techniques for Monitoring Atopic Dermatitis—Current Practices and Possible Advancements: A Review," *Sensors,* vol. 23, no. 8, p. 3935, 2023, doi: 10.3390/s23083935.

   a. This publication is a review paper, summarising different methods that are used or can be used to assess AD empirically both in person and remote. This paper was created to fill a gap in the literature, bringing together isolated technical papers to elicit more focused interest into the field.

8. Y. Khan, A. R. Todorov, R. Torah, S. Beeby, and M. R. Ardern-Jones, "Skin Sensing and Wearable Technology as Tools to Measure Atopic Dermatitis Severity," *Skin Health and Disease,* vol. 4, no. 5, 2024, doi: 10.1002/ski2.449.
    a. This publication is a review paper, detailing the importance of wearable technology towards the monitoring AD.

1.5 Thesis Structure

This thesis is divided into 8 chapters.

Following the introduction, Chapter 2 presents the literature review of the project. First the structure of the skin is detailed, as it provides context for future references. Then the pathogenesis of AD is discussed, focusing on the skin barrier dysfunction and the symptoms that arise from it. It outlines measurable biomarkers relevant for disease monitoring. Then the focus of the review is of empirical monitoring of atopic dermatitis. A survey of invasive methods and non-invasive technologies are discussed. This section concludes with an in-depth review of a single monitoring technique – capacitive sensing. The literature review in this chapter was published in publication 7 and 8.

Chapter 3 contains the finite element analysis used to model the skin-sensor system and study the influence of geometric parameters, penetration depth, and frequency dependence. The chapter establishes the optimal IDC design tailored for the application. The work of this chapter was published in publications 1 and 5.

Chapter 4 details the fabrication of the first iteration of IDC sensors made of etched copper and their characterisation on replicas of the skin during varying environmental conditions. First in-vivo tests on volunteers are performed here, identifying challenges with the first iteration. The work of this chapter was published in publication 1.

Chapter 5 introduces the second iteration of IDC sensors made of printed silver and encapsulated with dielectric insulation. The second iteration are embedded into a wearable textile armband and evaluated for their repeatability and accuracy. Parts of this chapter were published in publications 3 and 6.

Chapter 6 expands the development of an e-textile system for monitoring AD by describing the custom hardware and software solution paired with the IDC textile sensor to create the system for monitoring on patients with AD. Patient trials demonstrate correlation with clinical standards. The work in this chapter is published in publications 2 and 5.

Chapter 7 summarises the research contributions and highlights the novelty of the approach and its potential impact in personalised dermatology care.

Chapter 8 includes a discussion on future work, indicating the future trials to be performed to bring the device closer to clinical adoption. The chapter also reveals designs for improving the resolution and utility of the device, by introducing the matrix IDC, capable of performing a spatial map of hydration.

1.6 Ethics Approval

The work in Chapters 4, 5 and 6 involved the participation of healthy volunteers and patients with AD. The testing procedure was risk assessed, and written consent was gathered. The data was processed in line with university and legal requirements. The study on healthy volunteers was approved by the University of Southampton's ethic process under study ID 70980 – the relevant consent form and participant information sheet are presented in Appendix E. The study on patients with AD was done in conjunction with the NOMAD study, ethics approval: NRES 330915.

Chapter 2 Literature Review

2.1 Biomarkers of Atopic Dermatitis

2.1.1 Skin Structure

The skin is the largest organ of the human body, acting as a layer of physical and chemical protection against external agents and influences [18]. The outermost layer of the skin, also known as the stratum corneum (SC) is the main barrier preventing against skin desiccation and challenges from the environment [19]. The stability of this barrier, also known as the epithelial barrier or epidermal barrier, preserves the integrity of the skin, making it durable and flexible, less susceptible to tissue damage or diseases. The thickness of this layer varies throughout the body, but it is on average around 20-40 μm, and it is composed of laterally stacked corneocyte cells, which are flat keratin filaments inside an envelope of cross-linked protein [18, 20]. These cells are dead and form a densely packed lipid matrix with very narrow transport channels, which is the reason for the naturally high impedance (around 1MΩ) of this layer. Its water concentration is around 20% and it is mostly hydrophobic [20].

Below the SC lies the viable epidermis (EP), the thickness of which is greatest on the palms of the hands and the soles of the feet, but it is on average around 100-150 μm. The keratinocyte is the predominant type of cell within this layer, and it creates different structural proteins and lipids to maintain the balance of the epithelial barrier (another name for the skin barrier) [21]. The epidermis is composed of four different layers, ordered from the deepest to the shallowest in the skin: the stratum basale, stratum spinosum, stratum granulosum and stratum lucidum. In the natural lifecycle of the keratinocytes, they traverse through these layers towards the SC, following a process called differentiation [20]. In the final phase of this process, the nucleus of these cells degrades, their bodies flatten out and they transform into corneocytes taking their place in the stack of lipids protecting from external stresses [22]. No blood vessels pass through the EP, and it is composed mostly of water and protein (40-50% each), which makes it a hydrophilic layer [20].

Underneath the EP is the dermis (DR), which is considerably thicker than the preceding layers, around 1 – 2 mm. It is home to blood vessels, hair follicles, sweat glands, sebaceous glands, and interstitial fluid (ISF), which is an information-rich fluid around cells, that is discussed further later in this chapter. The DR has similar water concentration to the EP (60%), has lower impedance than the stratum corneum and is hydrophilic [20]. Below the DR is the hypodermis, which is a layer of subcutaneous fat tissue, which spans several millimetres of depth. Figure 1 summarizes the structure of the skin, with all its important layers labelled.

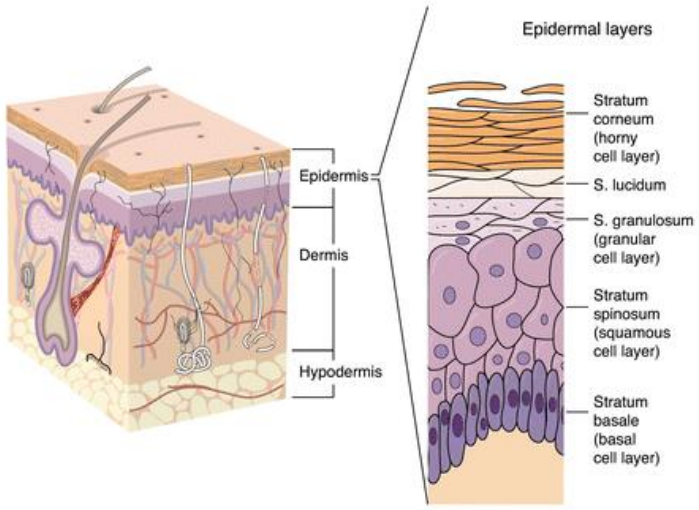

Figure 1 Structure of the skin with an expanded view on the narrowest layer - the epidermis, where the stratum corneum and the epithelial barrier reside. Image reproduced with permissions from [21].

Given the structure and composition of the different layers of the skin, it can be represented by a dielectric model with varying electrical properties. The stratum corneum, being the only hydrophobic layer within the model, has the highest impedance, in the range of 10^5 to 10^6 Ω [22]. Underlying layers have a higher concentration of water-soluble molecule, which act as charge transportation whenever an electric field is present, thus the impedance of the EP and DR is similar and is in the orders of 10^2 to 10^3 Ω [20]. These values and the physical properties of the skin layers (permittivity, resistivity, conductivity) vary depending on the location of the skin, the moisturisation (dryness) and the frequency of the excitation signal which is measuring these properties. Observation of these properties can provide insight into the hydration of the different skin layers.

2.1.2 Atopic Dermatitis

2.1.2.1 Definition

Atopic dermatitis, also known as eczema, is a chronic, relapsing skin disorder, which is characterised by recurring skin inflammation, pruritus (itchy skin), redness and dryness which results into visible cuts and lesions on the surface of the skin [23]. A lesion is a noticeable patch of abnormal skin on the human body and AD patients can experience the symptoms of the disorder (primarily itch) even if they do not have any apparent lesions – i.e. their skin is "non-lesional." In this report, when it is referred to the skin of AD patients or healthy subjects, it will be indicated whether the skin under study is lesional, non-lesional or from unaffected volunteers: non-AD (healthy skin), which is an important distinction, because even healthy-looking non-

lesional skin from an AD subject is different than normal skin [24]. It is one of the most common skin disorders worldwide, affecting nearly 20% of infants and children and around 3% of adults. It has been proven to negatively affect the quality of life on the patients, hindering their performance of daily activities [25]. Some of the negative side effects that children and adolescents suffering from this conditions experience are anxiety, lack of self-esteem, embarrassment, distress. It is not only detrimental to the children, but also impairs the lives of their parents, causing stress and financial burdens [25]. A study conducted in Scotland in 1995 estimated that annually £465 million pounds are spent in the United Kingdom to treat patients with AD, a staggering figure, more than half of which is being paid by the families of the patients [26].

Figure 2 presents two graphic photographs of the disorder and some of the common skin areas it usually outbreaks in. In children these areas are the face, mostly around the perioral (around the mouth) and periorbital (around the eyes) regions, the hands, wrists, ankles and popliteal (underside of the knee) and antecubital (underside of the elbow) areas [25]. Adolescents and adults tend to experience AD lesional involvement mostly on the dorsal side of the hand and in the periorbital regions, and rarely in other regions.

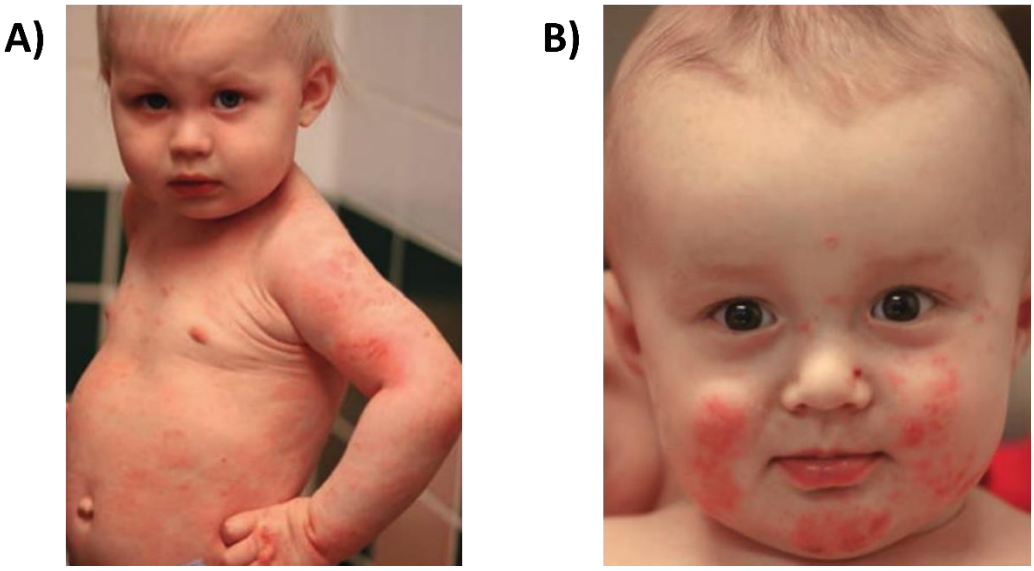

Figure 2 Photographs of babies with AD lesions on their A) body and B) face. Images reproduced with permissions from [27].

2.1.2.2 Pathogenesis and Biomarkers

The reasons behind the pathogenesis of the disease are still uncertain and there is not a singular hypothesis on the matter, but it is commonly believed that a dysfunction of the epithelial barrier plays an important role in the emergence of the disorder [23]. As discussed before, the barrier hinders the penetration of outside influences and allergens and keeps the hydration level of the

EP in normal state. One hypothesis suggests an “inside-out” approach that an immune-driven reaction triggers the dysfunction of the epithelial barrier, whereas another “barrier-driven” view believes an intrinsic epidermal abnormality causes the dysfunction of the barrier, thus preceding any immune activation and response [28]. Strong support for the epidermal barrier model comes from studies which have confirmed that the biggest genetic risk factor for AD occurs in the gene responsible for the filament aggregating protein Filaggrin (FLG) with an Odds ratio of 7-9 for development of AD in carriers. This protein has an important role in the formation of the rigid structure of the corneocytes in the SC [29]. Another research group found that AD patients often have polymorphic variants of the genes responsible for the tight junction (TJ) proteins, resulting in abnormalities in the protein production. The TJ proteins are fundamental for the effective function of the epithelial barrier as they solidify the matrix of corneocytes in the SC [30].

Thus, it can be inferred that AD can be detected by monitoring for abnormalities of the natural operation of the epidermal barrier and its ability to retain water and restrict outside influences (Figure 3 provides a graphical representation of this). The skin naturally loses water through the epithelial barrier, a process called transepidermal water loss (TEWL), but for healthy skin these water losses are minimal. Subjects with AD skin have been reported to have increased values of TEWL, which results in their visibly drier skin [31]. Therefore, a measurement of this property either through an external chamber or internal measurement of the moisture of the EP, would provide a sufficient basis for monitoring the severity and extent of this disease. This internal measurement of hydration will target the layers of the stratum corneum and the EP.

Other biomarkers that may provide insight into the severity of the condition are the sebum and the interstitial fluid (ISF). The sebum is an oily and waxy liquid secreted by the sebaceous glands of the DR and it is covering the outermost layer of the skin, thereby introducing the “oiliness” of the skin. According to some studies the chemical composition of the sebum may indicate the presence of a disease and in the case of AD, this results in a decrease of specific ceramide concentrations in the sebum [32]. The ISF on the other hand can also be investigated to profile the levels of chemokines proteins. A study in Japan concluded that the atopic skin has abnormally high levels of serum thymus and activation-regulated chemokine (TARC) [33]. These levels continue to remain high even when the disease is in remission, and there are no lesional outbreaks. Both fluids - sebum and ISF, require invasive methods for extraction and analysis, which defies the purpose of this report – to achieve non-invasive and continuous monitoring [34]. Thus, it is concluded that the measurement of the hydration levels in the outermost layers of the skin is the best approach in the pursuit of building a non-invasive skin sensor for AD. The next chapter will reveal the different methods and techniques used to assess AD currently. Established medical practises used for diagnosing AD will be presented and will be compared to

new non-invasive methods, which assess the skin barrier integrity by measuring the either TEWL or the water concentration within the SC and EP layers.

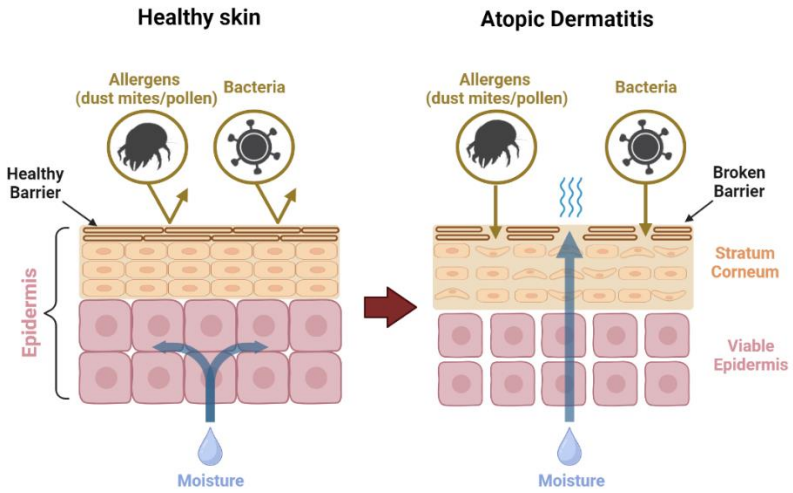

Figure 3 Comparison of cellular structure in healthy skin versus skin with AD. Breaches in the skin barrier result in excessive water evaporation and a decrease in cell size.

2.2 Monitoring Atopic Dermatitis Empirically

2.2.1 Introduction

The characteristics of the epidermal barrier and the skin hydration can be assayed using various methods such as external diffusion chambers, skin elasticity, electromagnetic and optical screening, all of which should provide a sufficient basis for monitoring the severity and extent of this disease [35]. Along with the measurement of water content, the vascular dilation associated with inflammation which can be seen as redness in white skin or darkening of darker skins, as well as surface scaling from keratinocyte disruption can be quantified. Machine learning through image recognition can be employed, like the systems applied for melanoma diagnosis [5, 36]. Alternatively, the impact of the condition on the lives of patients can also be measured. Since the lesions are often irritating and itchy, activity sensors can track how often patients scratch themselves providing an indication of how severe their condition is [37-39].

The purpose of this chapter is to identify the current methods of evaluation and monitoring of AD through the means of empirical data. First, standard medical practices that include invasive techniques are discussed, and then technology-enhanced approaches that allow for remote and non-invasive monitoring are presented. These methods have all been used in clinical trials on patients with AD to either diagnose, estimate severity or monitor the treatment. A summary on the methods of each branch is presented for easier comparison between them, outlining the most promising method for creating an e-textile sensor that can monitor and distinguish severity of AD in skin. In this case, this is capacitance measurements through the usage of arrays of electrode sensors in a specific alternating pattern. A section dedicated to this technique is presented separate from the other method, to provide more detail into the operation of the devices and what is currently done in the literature. This chapter also highlights alternative techniques that are applicable to the field of monitoring skin conditions and would advance the study of AD, but have not yet been tested on patients with AD. Finally, a discussion on each method's merits and demerits is presented, along with a critical conclusion on the most prominent technique for AD monitoring.

2.2.2 Medical Examinations and Tests

The National Institute for Health and Care Excellence (NICE) has laid out clinical guidance which recommends a holistic evaluation of AD during in-person consultations, considering the physical severity of skin and patient's quality of life. There are several diagnostic criteria for the assessment – mainly questionnaires like the Patient-Oriented Eczema Measure (POEM), the

Dermatology Life Quality Index (DLQI), the Hanifin and Rajka, the Millennium, the U.K. diagnostic criteria, and medical tests in addition [4, 25]. These are all based on a combination of visual inspections by a specialist with medical examinations such as blood serum, biopsy, and tape stripping. The lack of a unified empirical criteria means that diagnosis and distinction is sometimes subjective, based on the opinion of the acting dermatologist. Due to the complex nature of the condition and the lack of understanding on what the underlying cause is, the medical tests cannot fully empirically prove the condition and distinguish it from similar ones such as psoriasis or contact dermatitis [40]. Moreover, these tests are invasive and can induce anxiety and stress in the patients, which are predominantly children [26]. This section serves as an overview of what medical examinations are currently done in hospitals and clinics – biopsy, blood serum extraction and tape stripping. Figure 4 presents an infographic of the different chemical biomarkers that can be obtained through blood serum, biopsy or tape stripping. The methods presented do not fall in line with the e-health directive, and their drawbacks highlight the need for further research into the area of novel AD monitoring solutions.

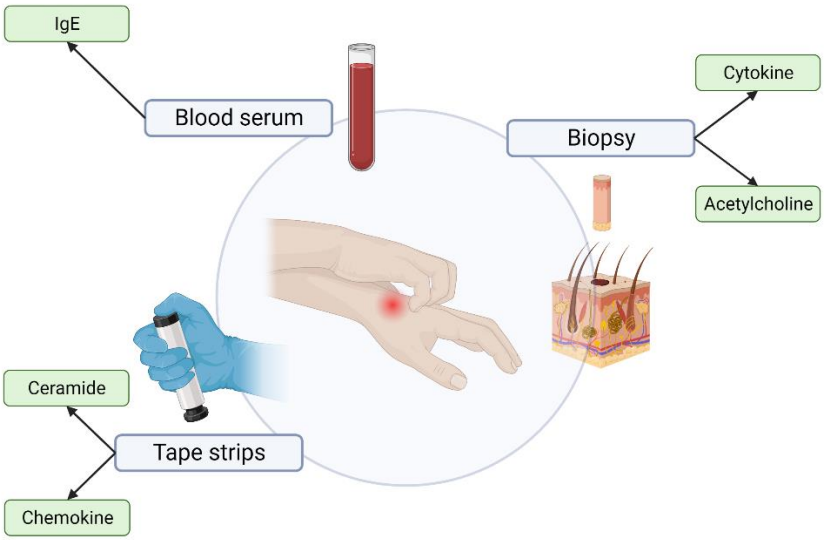

Figure 4 Methods of medical examination of AD and their corresponding potential biomarkers. The three main empirical methods are listed, all of which are performed under a controlled clinical environment. Figure created with BioRender.

2.2.2.1 Biopsy

Biopsy is a medical procedure in which a small sample of human tissue is sourced from a patient to be further examined to determine the presence of a specific disease. Obtaining a skin biopsy is a commonly used method in the diagnosis of skin cancer, as it provides the most insight into the extent of the condition [41]. Varying levels of specific molecules and compounds found within the biopsy may serve as evidence towards the presence of AD.

Wessler et al. present a study in which they linked increased levels of acetylcholine in 2 mm thick biopsies of AD patients [42]. Acetylcholine is a compound synthesized by epidermis cells that acts as signalling molecule that regulates cell adhesion and contact. The increase of acetylcholine in AD patients was found to be 14-fold, which makes is a solid biomarker of the condition [42]. The study also showed that injecting more acetylcholine in the skin, causes an itching sensation, similar to how AD pruritus feels. The researchers don't mention whether the increased levels apply only to lesional AD skin or to non-lesional as well.

Kägi et al. investigated the relationship between specific cytokine protein production and emergence of atopic dermatitis [43]. They sampled biopsies of lesional and non-lesional skin of AD patients and compared the presence of these proteins. The result was a completed protein profile of both types of skin in AD patients, so that the condition can be discovered even before skin inflammation and lesions have appeared [43]. While this might be beneficial for early discovery, due to its invasive nature it is a drastic solution to a "seemingly" healthy skin.

Salvador et al. states that biopsy is not a necessary method in diagnosing AD but can provide useful in distinguishing it among other conditions like psoriasis, dermatitis herpetiformis, and cutaneous lymphoma [44]. Overall biopsy is a stressful procedure that should resolve only to the most extreme conditions like melanoma, and in the case of diagnosing AD it is needless.

2.2.2.2 Blood Serum – "Liquid Biopsy"

An alternative to the biopsy procedure is to extract serum from the blood (also known as "liquid biopsy") and to measure the levels of Immunoglobulin E (IgE). IgE is an antibody that is produced by the immune system to combat allergens [45]. Thus, in the case of AD, a broken epidermal barrier would be penetrated more by outside influences and allergens, increasing the levels of IgE [24].

Kagi et al. and Liu et al. both researched this effect independently by extracting blood serum from the bodies of AD patients and concluded that high IgE levels are a biomarker for atopic dermatitis [43, 46]. This is a better assessment than single point biopsy but still involves the need for invasive extraction that must be performed by a specialist and then assessed in laboratory environment.

2.2.2.3 Tape Stripping

Tape stripping is a procedure where samples of clear tape with an adhesive on one side are gently pressed against the skin and then removed to be observed under a microscope. The collected tissue is mainly lipids from the SC, including corneocyte cells, linking proteins and fatty acids [47]. Since AD constitutes of a dysfunction in the barrier between the SC and the EP, information about the lipids in the SC is useful in determining the severity of the condition.

Yamamoto et al. obtained tape strips of patients with AD at varying skin locations and discovered that AD patients have a decrease in the proportion of the ceramide protein, responsible for cell linkage [47]. Røpke et al. sampled strips from both lesional and non-lesional skin areas of AD patients and concluded that levels of cytokine and chemokine proteins differentiate between the two, establishing another biomarker for AD [48]. The tape strip sampling process is visible in Figure 5. Koppes et al. employed the same tests as Røpke et al. but included tests on healthy subjects, to discover that chemokine protein is a better biomarker than cytokine [49]. Although tape stripping is proven to be an accurate and useful tool for non-invasive diagnosis of AD, it still needs to be performed in a laboratory environment, as sample contamination is a major risk. Moreover, there isn't a standardized procedure in performing the stripping – Yamamoto et al. and Koppes et al. repeatedly press and release the sample by hand, whereas Røpke et al. use a constant pressure instrument for a single press. Thus, tape stripping is not suitable for the purposes of e-health monitoring as it is not possible to effectively reproduce these tests at a remote location or at home.

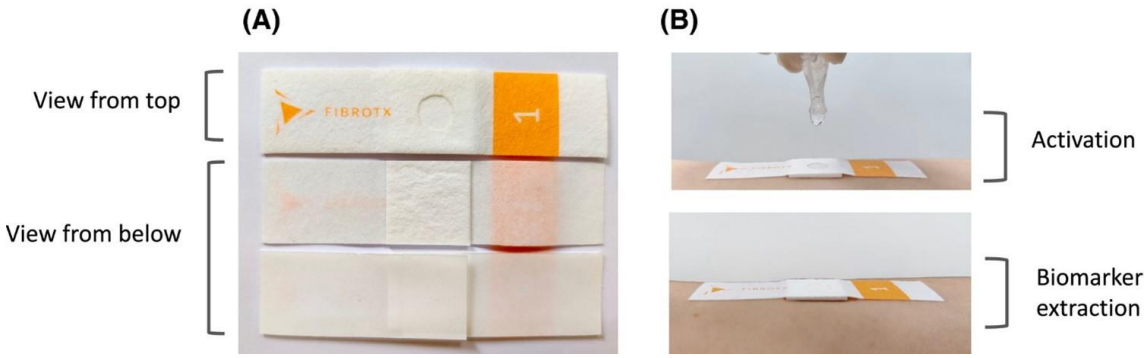

Figure 5 Tape stripping procedure illustrated with pictures. (A) presents the top and bottom view of the strip and (B) demonstrates the activation process used to extract the biomarkers. Image reproduced with permissions from [48].

2.2.2.4 Conclusion

Diagnosing and examining AD in medical practices is primarily done through visual assessment by looking at the skin lesions after the symptoms of the condition have emerged. New research has revealed that there are other biomarkers of AD in the skin of patients – such as IgE, chemokine, ceramide, and cytokine proteins, that can provide an empirical estimation of the severity of the disease and in the case of cytokine can even predict the emergence of the condition, without any apparent symptoms. These biomarkers can be obtained through the means of biopsy, blood serum extraction and skin tape stripping. These empirical examinations are much better than the conventional visual ones because they rely on measured data instead of subjective approach. Unfortunately, all these tests can only be performed in a controlled laboratory environment and require complex equipment and a qualified lab technician to

correctly assess the results. In the case of biopsy, the testing procedure can be very stressful for the patients. Thus, these methods cannot be used to provide a non-invasive and fully remote monitoring to patients around the world, and the need for a new generation of sensing technologies for skin condition diagnosis and monitoring becomes more apparent. Table 1 summarizes the current medical tests for AD diagnosis and highlights their drawbacks.

Table 1 Empirical medical tests for diagnosing and monitoring the severity of AD in vitro. None of the methods can be applied in a remote (non-laboratory) location and all require specialist operator.

Method	**Monitor and distinguish?**	**Estimate severity?**	**Can predict condition?**	**Biomarker**	**Requires clinic visit?**
Biopsy [41-44]	Yes	Yes	Yes	IgE	Yes
Blood serum [24, 43, 45, 46]	Yes	No	Yes	Cytokine Acetylcholine	Yes
Tape stripping [47-49]	Yes	Yes	No	Chemokine Ceramide	Yes

2.2.3 Technology-Enhanced Non-Invasive Measurements

New advances in medical technology have integrated non-invasive measurements as a highly sought-after alternative for monitoring patients. In some cases, like melanoma, they are gaining support to replace current medical examinations [36]. They are also widely used in monitoring other medical issues and vital signs including heart failure [50], respiratory [51], heart rate variability [52], fall detection [53], and anxiety [54]. These examples do not require complex laboratory equipment or a controlled environment and in most cases can be performed in the comfort of the patient's home [55]. Monitoring is performed typically using a standalone instrument or a wearable system, the latter of which can be used for continuous monitoring without obstructing the daily routine of the patient. The devices usually comprise a sensing/screening part, read by a controller unit that exports data to a computer or network, where the data can be easily accessed and interpreted by a doctor [55]. This section will highlight

technology-enhanced techniques reported in the literature for monitoring AD and comment on their accuracy in evaluating the severity and their reproducibility as a portable e-health device. The methods are grouped into subsection according to the specific biomarker that the device use to perform their measurements. Some of these devices have already seen commercialization as a full-scale product, although not yet accepted by any diagnostic criteria.

2.2.3.1 Transepidermal Water Loss (TEWL)

TEWL is the rate of water evaporation from the skin (in $g/m^2/h$), as water naturally permeates through the SC barrier. In healthy skin, this rate is minimal, and it varies based on the body site but an average value of TEWL in healthy skin is between 5 – 15 $g/m^2/h$ [56]. In damaged skin like the skin of an AD patient, the evaporation rate is higher, in the order of 15 – 25 $g/m^2/h$ since the barrier function is compromised [57]. Subjects with AD have been reported to have increased values of TEWL, which results in their visibly drier skin [31]. Therefore, a measurement of this property would provide a sufficient basis for monitoring the severity and extent of this disease. TEWL can be empirically measured by positioning an enclosed chamber probe onto the skin [58]. The probe has a hydration sensor built in to detect the increase in humidity in the chamber and the controller unit driving the sensor produces a value for TEWL [57].

Kim et al. used a commercial evaporimeter sensor (EP1, Servo Medical, Sweden) to evaluate severe lesions from five different skin sites of AD patients [59]. They discovered a significant correlation of severity with increased TEWL in all the five sites measured (postauricular (underside of ear), thigh, abdomen, forearm, popliteal fossa (underside of knee)). The results were compared to measurements of TEWL at the same sites in healthy subjects, confirming that a dysfunction in skin barrier's structure provokes higher TEWL values [59].

Werner et al used the same commercial evaporimeter as Kim but included TEWL measurements of clinically healthy sites of skin on AD patients and compared them to the skin of subjects without the condition [60]. They discovered that TEWL values in AD patients are increased even in the non-lesional areas, where there is no visual damage, inflammation, or redness present. This is an important distinction because it means that TEWL measurements can be used to predict the condition even before any symptoms have appeared. Given that current diagnostic procedures rely on observation of already visible lesions and symptoms, TEWL measurements are much faster in predicting the outcome and can be used to apply appropriate treatment the soonest. Xiao et al. compared two different commercial evaporimeters (the handheld battery powered VapoMeter®, Delfin, Finland and the wired pen-like AquaFlux® Biox Systems Ltd., UK, see Figure 6) to explore the effect of applying extra hydration to the skin [61-63]. They detected varying levels of hydration through the application of suntan lotions with TEWL values decreasing after the application of skin lotion. This needs to be investigated further but it affirms the claim

that hand creams and moisturisers assist the barrier function of the skin, thereby it is possible that constant application might decrease the severity of AD lesions.

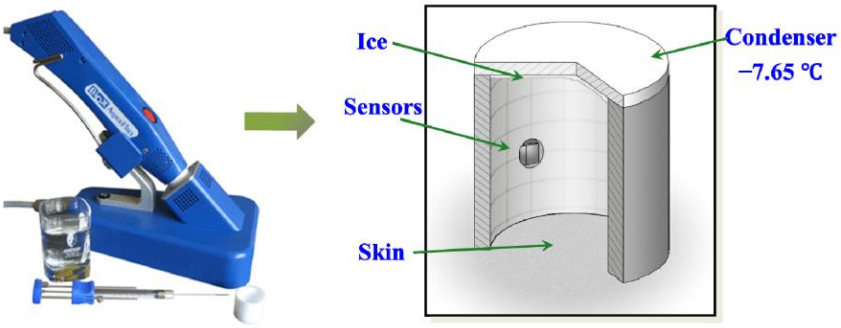

Figure 6 AquaFlux evaporimeter and its measurement principle. The chamber visible on the right is housed within the tip of the AquaFlux evaporimeter and contains the humidity sensors that detect the TEWL. Image reproduced with permissions from [61].

Sim et al. constructed their own TEWL measurement device following the same principle of operation used by the commercial devices, but they manage to house the sensor and the controller unit in a single pen-type package, as presented in Figure 7 [64]. The device was used to measure TEWL from a wetted artificially created skin and achieved a sensitivity of 0.0068 (%RH / ($g/m^2/h$)), meaning that for every gram of water molecules evaporated in time, the device detects tiny changes in the relative humidity of its internal chamber. The significance of Sim et al.'s device is that it also can measure other properties such as skin conductance and hardness, both of which are very relevant to the biomarkers of AD and will be introduced in the following subsections. This multimodality of measurement makes e-health devices more desirable, as they can use several measurands simultaneously to monitor patients more accurately. This idea will be expanded in the conclusion of this section.

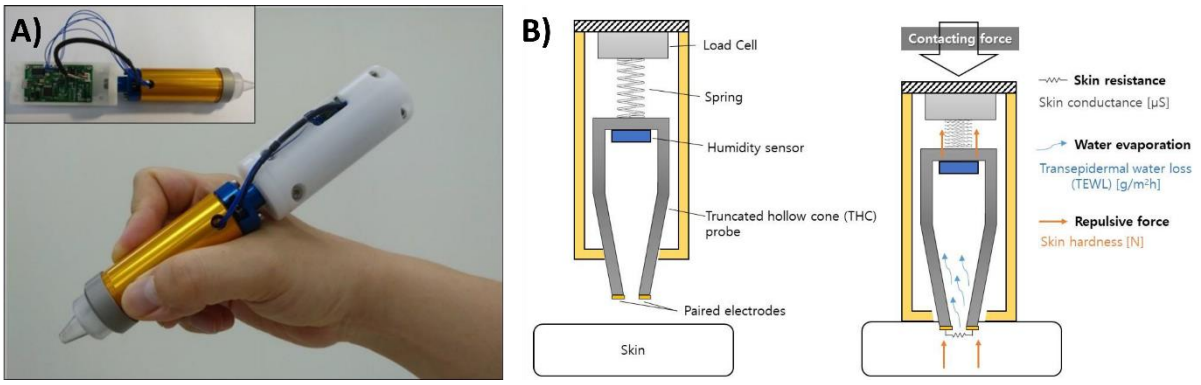

Figure 7 Images of multimodal device for measurement of TEWL, skin conductance and skin hardness constructed by Sim et al. A photograph is visible in A) (left) and in B) (right) its operating principle is presented. Images reproduced with permission from [64].

2.2.3.2 Skin Permittivity and Conductivity

As mentioned previously, the severity of AD can be linked with increased water evaporation rates and visible dryness of the skin. Martin et al. concluded that the TEWL and dryness biomarkers are correlated to a decrease in the size of corneocyte cells and a lower concentration of bulk (free) water molecules in the layers around the epithelial barrier [65]. Therefore, a measurement of water concentration within the SC and EP is also a valid biomarker for the condition. The presence of free water molecules in the skin is proven to affect composition and therefore change the skin's physical properties and parameters such as dielectric permittivity and conductivity.

The SC layer can be thought of as a dielectric material, and in the presence of an electromagnetic field, this dielectric is polarised to a certain degree, defined by the values of permittivity and conductivity [66]. In circuit theory, the polarisation of a dielectric media can be empirically measured by parameters such as impedance, capacitance, and conductance. Several studies have concluded that skin exposed to hydrating conditions is observed to have lower resistance values and higher capacitance values than normal and dry skin [67, 68]. Hydrating conditions, such as applying humectant or moisturising cream, assist the barrier properties of the skin, thereby increasing the ability to retain free water within the SC. The increased water concentration in the SC provides more conductive pathways for ionic charges, thereby increasing the conductivity and the dielectric constant, the latter of which is directly proportional to the value of capacitance and inversely proportional to the resistance [69]. Hence, by recording the values for impedance (capacitance and resistance) or conductance from the skin of AD patients, the severity of the condition can be empirically estimated.

The two predominant non-invasive and painless methods presented in the literature to determine the dielectric response of the skin are conduction measurements and capacitance/impedance measurements. Both require the placement of two or more electrodes on the skin, across which an excitation signal, usually AC voltage or current, is imposed. According to Yokus et. al. conduction measurements can be affected by factors on the skin surface such as oiliness, hairiness, environment temperature [68]. Conduction measurements usually require small electric current to be passed through the skin, and Abe et al. claims that since hair follicles and sweat glands have weaker permeability barriers than SC, they allow more movement of water molecules, thereby are likely to be a preferred path for current flow [22]. Capacitance measurements require the presence of an electric field, rather than electric current, and that is why they are less likely to be obstructed by hair follicles. Moreover, it has been discovered that conductivity measurements suffer from decreased sensitivity when distinguishing lower hydration states [70]. This makes capacitance measurements a better fit for the purpose of determining the severity of AD and distinguishing it from other skin conditions.

The dielectric properties of all materials vary with frequency of the applied excitation signal, and hence the measured impedance and capacitance vary too. This applies also to all human tissues, including skin, and in 1996 Gabriel et al. formulated a database consisting of the dielectric permittivity and conductivity of various human tissues in the frequency range of 10 Hz to 100 GHz [71]. The database visualised how different tissues have distinct dielectric responses across the frequency spectrum, thereby making it possible to distinguish materials solely on their response. Furthermore, the database included measurements from wet and dry skin, confirming that the properties change with the hydration state of the skin, as the dielectric permittivity of wet skin is close to ten times as large as the permittivity of dry skin in the lower frequency range between 100 Hz – 10kHz [72]. This property can be extrapolated to measure differences between severely dry skin like lesional AD skin and healthy or non-lesional skin.

This measurement technique is called electrical impedance spectroscopy (EIS) and involves sampling the impedance response across a spectrum of frequency bands, generating a unique impedance footprint based on the dielectric properties of the material under test (MUT). Rinaldi et al. used this technique to explore the integrity of the SC barrier of both lesional and non-lesional skin of AD patients over a long period of time [23]. They used a commercial spectrometer called Nevisence® (SciBase AB, Huddinge, Sweden) and were able to characterise both states of skin and revealed positive correlation between increase of EIS values and decreased pruritus and inflammation on the lesions, indicating that healing can be empirically measured [23, 73]. Nicander et al. used the same commercial equipment to detect lipid content within the SC and were successful in discriminating between healthy-looking skin from AD subjects and control skin [31]. The Nevisense® and similar spectrum impedance analysers constitute of a wired handheld probe connected to a bulky processing and visualisation unit and are advertised as melanoma detection instruments, but research has proven their applicability towards assaying AD.

Other commercial sensors include a limited or fixed scope of frequencies and thus are sometimes housed in more compact packages, allowing for easier operation and even home monitoring. There isn't a specified commercial sensor just for assessing AD, but skin hydration sensors have been widely utilised in determining the severity of AD in patients. The Corneometer® CM 825 (Courage + Khazaka, Cologne, Germany) is referred to as the "gold-standard" in capacitive skin measurements and is the most widely used equipment in monitoring AD in vivo [74]. The Corneometer® has an IDC structure on its sensing electrodes, as seen in Figure 8, which makes the capacitance readout more sensitive to changes in the dielectric permittivity of the MUT. Other notable commercial sensors that employ the same measurement technique are the MoistureMeterSC® by Delfin Technologies and the Novameter® DPM by Nova Technology Corp [75, 76].

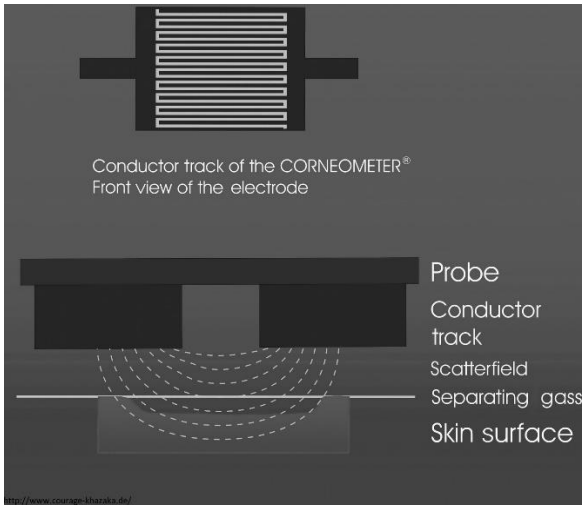

Figure 8 Measurement principle of the Corneometer® CM 825. On the top is the front view of the electrode, revealing its interdigitated shape and on the bottom is the side view, illustrating the scattered electric field. Image reproduced with permission from [77].

Grinich et al. compares three different commercial sensors – the Corneometer®, the GPSkin® (GPower Inc, Seoul, South Korea) and the TEWL Aquaflux® to monitor skin barrier function of AD patients. They indicated good correlation ($p > 0.80$) between decreased capacitance values and increased TEWL values from lesional skin, but none of the sensors were able to distinguish between different severity states of the condition [78, 79]. Matsumoto et al. employed the Scalar MY-707S Moisture Checker® (Scalar Corp., Tokyo, Japan) to measure the capacitance of the skin of infants, both healthy and with atopic dermatitis and they measured significantly lower capacitance readouts from atopic skin [80, 81]. Sator et al. used the Corneometer® on healthy and AD subjects to conclude that capacitance is not only decreased by the lower hydration values, but also because SC lipids have decreased in size. This strengthens the argument that SC hydration is a valid biomarker for AD, because a broken skin barrier results in smaller corneocyte cells (the building block of the SC) [82]. Chiang et al. explored the mean hydration improvement after different treatments applied to atopic skin such as bathing or applying emollient. They used a Novameter® DPM 9003 (Nova, Gloucester, MA) and Scalar Moisture Checker® and determined that emollient usage assists the skin barrier function, while bathing, although providing an immediate moisturisation, dehydrates the atopic skin in the long term [75, 83]. Table 2 summarises the various commercially available sensors used in the literature for assessing the skin hydration through measurement of the conductivity or permittivity of the outermost layers of the skin. Although these devices have been utilised in the literature, there is little information on the internal characteristics of the device, like the measurement frequency or the impedance analyzer circuit used to convert the capacitance values into units of hydration. Still, when designing new prototypes of skin hydration sensors, the existing commercial devices are used as an industry standard for calibration and accuracy.

Table 2 Summary of commercial devices for superficial skin hydration assessment used in the literature.

Name	Manufacturer	Probe Type	Electrode Shape and Area	Target Layer	Measuring Frequency	Measurement Time	Uncertainty
Corneometer® CM 825 [74]	Courage+Khazaka electronic GmbH	Wireless or wired	Interdigitated; 49 mm^2	SC	0.9-1.2 MHz	1 s	±3%
MoistureMeterSC [76]	Delfin Technologies	Wireless	Coaxial	SC	1 MHz	4 s	No information
Skin Moisture Sensor MY-808S [81]	Scalar Corporation	Wireless	Interdigitated	SC	No information	No information	No information
MoistSense [84]	Moritex	Wireless	Interdigitated	SC	No information	No information	No information
Novameter DPM 9003 [75]	Nova Technology Corp.	Wired	Coaxial (65mm^2)	EP	Sweeps to 1 MHz	No information	No information
Skicon-200EX [85]	Yayoi Co.	Wired	Coaxial (30mm^2)	EP	3.5 MHz	No information	±5%

While all the commercial sensors have proven to be useful in determining AD symptoms and severity and, due to their relatively small package, allow for mobile/remote monitoring, they still lack the ability to conduct continuous measurements to provide insight into how the condition progresses in time. To achieve a fully non-invasive telemedical device in constant contact with the skin, the sensor can be housed in a compact package, embedded in a wearable garment or patch. Jang et al. designed a textile-based wearable impedance sensor that was able to accurately distinguish different levels of skin hydration including severely dehydrated skin [86]. The sensor, as shown in Figure 6, comprises of two silver electrodes printed onto a flexible cotton substrate, allowing for conformal attachment to the skin. In the low frequency spectrum, the impedance varies by a factor of 100 between 10 kΩ to 1 MΩ for hydration measurements of moisturised and dry skin, respectively. The textile sensor's readings were calibrated against hydration readings measured using a commercial sensor [86]. Rie et al. utilised the same IDC design as the Corneometer® but housed the sensor in a device with total area of 2.3 x 4.6 mm^2 using CMOS technology. The device was tested for its suitability to measure the dehydration rate of the skin and exhibited higher sensitivity than commercial sensors and can be attached via

medical bandage onto the skin [87]. These advances prove that skin permittivity sensors can be embedded into a non-invasive wearable package for the purposes of continuously monitoring AD patients, but so far, no prototype has been presented.

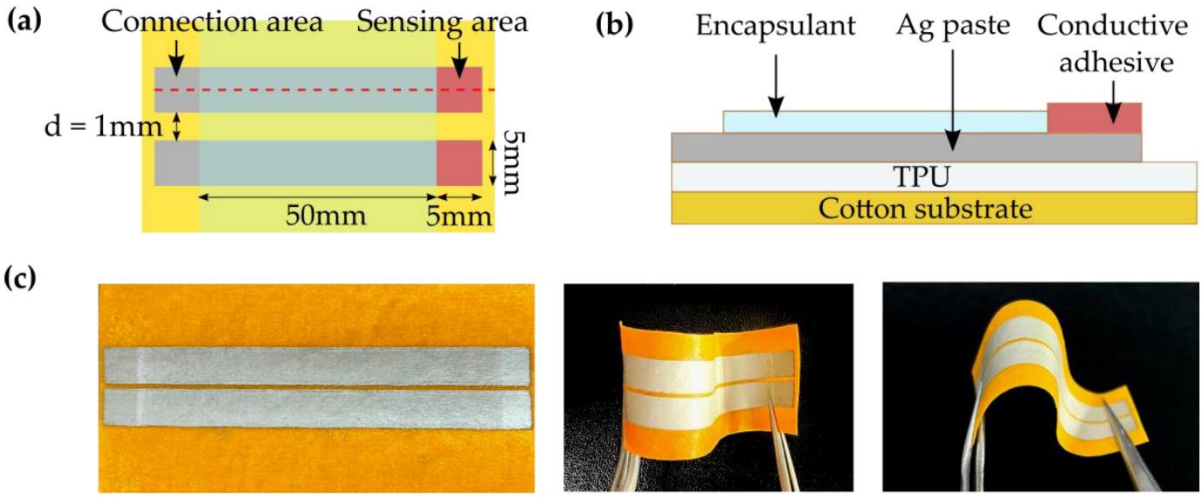

Figure 9 Images of the textile-based impedance sensor created by Jang et al. (a) and (b) present a schematic on the top (a) and side (b) view of the sensor, respectively, and (c) demonstrates its flexibility through photographs. Images reproduced with permission from [86].

2.2.3.3 Skin Elasticity

Skin elasticity is another biomarker of AD that can be empirically measured through telemedical techniques. The increased hydration loss caused by AD makes the skin more inelastic and susceptible to cracking [88]. A single commercial device, called the Cutometer® by Courage+Khazaka GmbH (Cologne, Germany) was used to quantify the elasticity of the skin of AD. The device has a rigid cylindrical hollow probe and a wired control unit and uses a suction method to mechanically deform the skin and a light source to determine how the skin resists to the negative applied pressure and its ability to return to the original position [89]. Montero-Vilchez et al. used the Cutometer® to demonstrate that skin elasticity values are lower on AD lesions of patients with the condition than on non-lesional areas or healthy subjects' skin (0.69 vs. 0.74, $p = 0.038$). They also highlighted that the negative correlation between age and skin elasticity was stronger in AD patients ($r = 0.494$), meaning that AD increases the inelasticity of skin as the patients age [90]. In another publication, Montero-Vilchez et al. compared the results from the Cutometer® with measurements from a Corneometer® and a TEWL Tewameter®, concluding that TEWL and SC hydration are better biomarkers for distinguishing between heathy and AD skin because of the bigger difference in the sensor output (TEWL ,9.98 vs. 25.51 g/m2/h, $p < 0.001$ and SC hydration 44.36 vs. 24.23 AU, $p < 0.001$, for healthy and AD skin respectively) [91]. Constantin et al. recorded the elasticity values of lesions on patients with dermatitis before and after

application of an emollient cream [92]. They reveal an increase in skin elasticity values after continuous application of the emollient, hence elasticity measurements can be used not only for distinction but for monitoring the progression of the treatment. Continuous measurements during treatment process are important because they provide insight into how the skin is responding to the treatment. The results may indicate whether the frequency or dosage of the treatment should be altered. Furthermore, there hasn't been any investigation whether skin elasticity can distinguish between different severity levels of AD or between different skin conditions such as psoriasis, urticaria, melanoma. The lack of a variety of measurement devices (currently only the Cutometer® is available) can also pose an obstruction to further investigation of the technique.

2.2.3.4 Scratch Activity and Frequency

A more abstract way of estimating the severity of AD and related conditions is to examine the effects on the daily lives of the patients. Dermatitis is characterised by pruritus and itchy lesions, causing sleep disturbance in the patients, which contributes to decreased performance, daytime fatigue, and irritability [39]. Thus, a record of how frequently the patient scratches their skin, would provide insight into the severity of the condition and subsequent treatment needed. Such measurement can be performed subjectively by the patient self-reporting or objectively with a wearable non-invasive sensor. Wrist actigraphy is an unobstructive technique that uses an accelerometer, mounted on a wristband to distinguish between scratching and other nocturnal movements of the hands [39]. Wrist activity measurements are much better option for monitoring nighttime AD scratches than polysomnography, which is the standard for identifying causes for sleep disturbances using heartrate and respiration, because it is less technically demanding as it tracks just the movements of the wrist [93].

Ebata et al. used a commercial wrist activity sensor called the ActiTrac® (IM Systems, Baltimore, MD, U.S.A.), alongside an infrared video camera to map data activity from scratching and noted significant correlation between the severity state of AD and the activity levels. Wrist activity due to scratching increased to 44 a.u. for AD patients, compared to 9 a.u. for controls [38]. Bender et al. used a different commercial device called the MicroMini Motionlogger® (Ambulatory Monitoring, Inc, Ardsley, NY, U.S.A.) to conclude that patients with AD have significantly more compromised sleep than controls, as high nocturnal activity measurements are linked with fatigue on the following day [39]. The device is shown in Figure 10 D) and the tested subjects have reported no complaints from its continuous usage. Noro et al. present an acoustic evaluation system for detecting scratches in patients with AD – illustrated in Figure 10 A), B) and C). The sensing element is a piezoelectric device which vibrates due to the sound caused by the scratching of the skin and the post processing system filters the signal to eliminate noise [94].

Kim et al. used a cloud-based mobile system to source data from textile wrist sensors and analyse it via web application, so that it can be easily accessible to health professionals worldwide [95]. Mahadevan et al. utilised machine learning techniques to sample data from a wristband sensor and to compare it to readings from polysomnography measurements to match sleep states. The wristband showed that scratching episodes match the wakefulness states, when the person is either woken up or sleeps very lightly, thus hindering the patient's ability to enter deep sleep [93].

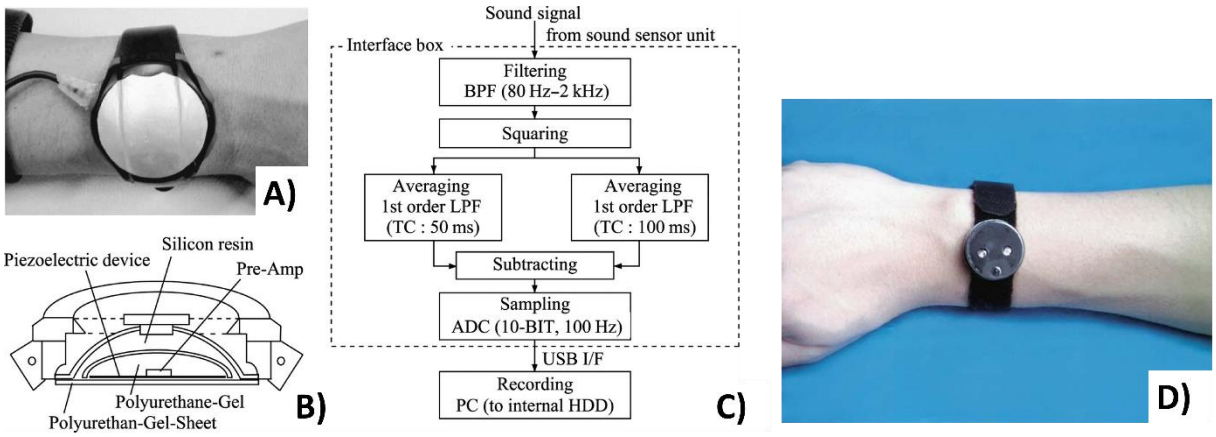

Figure 10 Examples of actigraphy sensors for scratch detection. A), B), and C) – Photograph, schematic and flow chart of the acoustic scratch detection sensor by Noro et al.; D) photograph of the MicroMini Motionlogger®, to showcase its compactness and non-invasiveness. Images reproduced with permissions from [39, 94].

Scratch activity sensors are a reliable way of estimating the severity of AD by measuring the disturbance on the sleep cycle of the patient. The device's low-profile footprint allows for continuous usage throughout the night without stressing the patient. Measurement throughout the day is possible, but currently a daytime scratch actigraphy sensor hasn't been demonstrated due to difficulties in distinguishing scratching from other typical daily activity [96]. Further research into these sensors must be provided to explore whether the sensor can also distinguish between other conditions that cause pruritus such as insect bites, infections, or allergic reactions.

2.2.3.5 Neural Network Imaging Systems

Another telemedical technique that has been used to identify and monitor the lesions of AD in human skin remotely is to employ an artificial intelligence (AI) algorithm, trained using datasets of images or a camera/imaging device, to detect the condition. Hsiao et al. compared the results from identifying mycosis fungoides, AD and psoriasis using a single shot multibox detector model but obtained low output sensitivity and precision when analysing AD images (80% and 86% respectively), concluding that this model has poor performance for AD distinction [97]. Padilla et

al. managed to differentiate between AD and Psoriasis using the MobileNet architecture based on a convolutional neural network (CNN). The network was trained using dermatology datasets online and when tested on 30 individuals using a Raspberry Pi camera it achieved a higher accuracy of 90% when classifying psoriasis and 88% in AD [98]. Pan et al. created an AD-focused computer vision model called the EczemaNet that can identify photographs of the condition and predict the severity and state of the disease [99]. The model achieved a 90% success rate in distinguishing the condition and a low root mean squared error of less than 2 for the severity prediction. An overview of the EczemaNet model is presented in Figure 11. Patella et al. explored the relationship between AD severity and exposure to air pollutants and environmental conditions using an artificial neural network (ANN) [100]. They found out that an increase in the diurnal temperature range (DTR), which is the variation between the highest and lowest temperature in a day, increased the severity of AD lesions by 200%. The ANN can be used to predict disease severity based on the environment and to alert the patients in advance to avoid possible irritants [100].

Neural network systems using cameras and imaging systems are a reliable and non-invasive way of classifying eczema and in some cases can effectively estimate the severity of the lesions. They allow for remote monitoring without the need of a clinician or specialist dermatologist, as patients can check their condition through their mobile phone camera. The only drawback is the inclusion of the camera to obtain the images, because the setup cannot be used to monitor the condition continuously for long periods of time, as that would require constant surveillance of the specific area of the skin. Current models also have a maximum reported accuracy of 90%. Further research into this field should seek to increase accuracy and to prototype a mobile device or app that would allow patients to use the power of the algorithm to assay their condition with confidence. Furthermore, experiments should be undertaken to explore the effect of emollient or moisturising cream on the sensitivity of the ANN, to see if treatment progression can be measured. Nevertheless, ANNs are a viable way of establishing remote assessment without the need of a clinician and can be used to classify other types of data, apart from visual and image based.

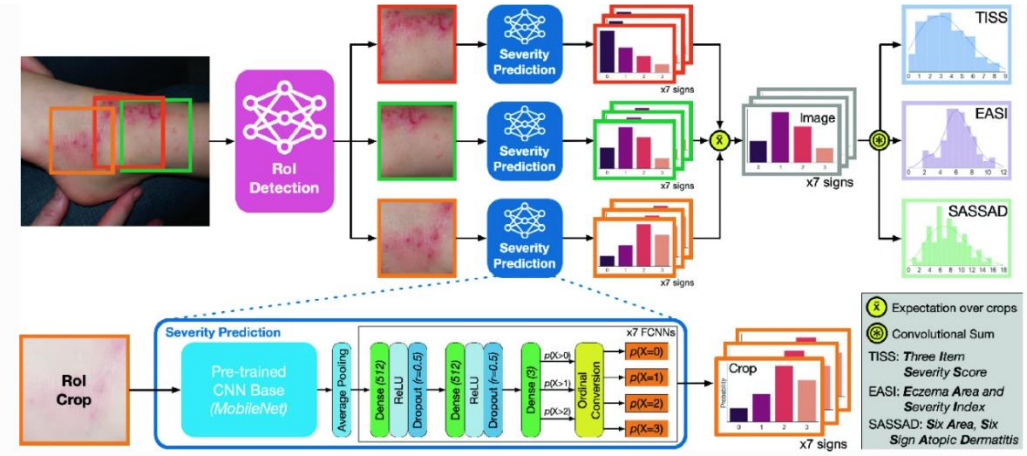

Figure 11 Schematic of the EczemaNet model created by Pan et al. The model can identify photographs of AD and predict the severity of the disease. Image reproduced with permissions from [99].

2.2.3.6 Conclusion

As presented in this section there are a variety of technology-enhanced methods already used to provide empirical measurements towards the monitoring of AD. These methods all fall in line with the e-health directive for achieving non-invasive and at-home monitoring, but not all of them can be used continuously as a portable device with little impact on the daily routine of patients. The individual advantages and drawbacks of each are summarized in Table 3. TEWL measurements are an accurate way of distinguishing atopic skin and predicting treatment using external relative humidity sensors, but they are occlusive and cannot be used for continuous measurements. Skin permittivity through capacitive and impedance measurements has problems with precision due to disturbances in the skin-sensor contact but can be housed in a non-invasive package for portable and continuous measurements. Furthermore, they have been shown to detect the condition, quantify the severity and monitor the response after treatment. Elasticity measurements have been tested against permittivity and TEWL measurements and demonstrate reduced accuracy in determining AD. The need to provide negative pressure eliminates the possibility of housing the method in a compact wearable package. Scratching actigraphy sensors are a proxy assessment by determining the severity of pruritus severity during nighttime, but these sensors have not been proven to discriminate between different conditions and have limited use during the daytime. Figure 12 illustrates the operation of all non-invasive techniques discussed in this section and reveals their respective measurand. Telemedical instrumentation does not induce any stress or harm onto the patient and thus it is the preferred method, when compared to invasive medical examinations. Research should be focused on establishing these methods of examination in a clinical setting rather than visual and blood test procedures as they provide an objective measure.

Table 3 Summary of technology-enhanced solutions used in the literature for monitoring and distinguishing AD in patients.

Method	**Monitor and distinguish?**	**Estimate severity?**	**Monitor treatment?**	**Allows continuous monitoring?**	**Suitable for e-textile?**	**Occlusive?**
TEWL [57-64]	Yes	Yes	Yes	No	Yes	Yes
Skin permittivity [23, 31, 74, 75, 77-83, 86]	Yes	Yes	Yes	Yes	Yes	Yes
Skin elasticity [88-92]	No	Yes	Yes	No	No	N/A
Scratching frequency [39, 93-96]	No	Yes	Yes	During nighttime	Yes	No
Neural network [97-100]	Yes	Yes	Yes	No	No	No

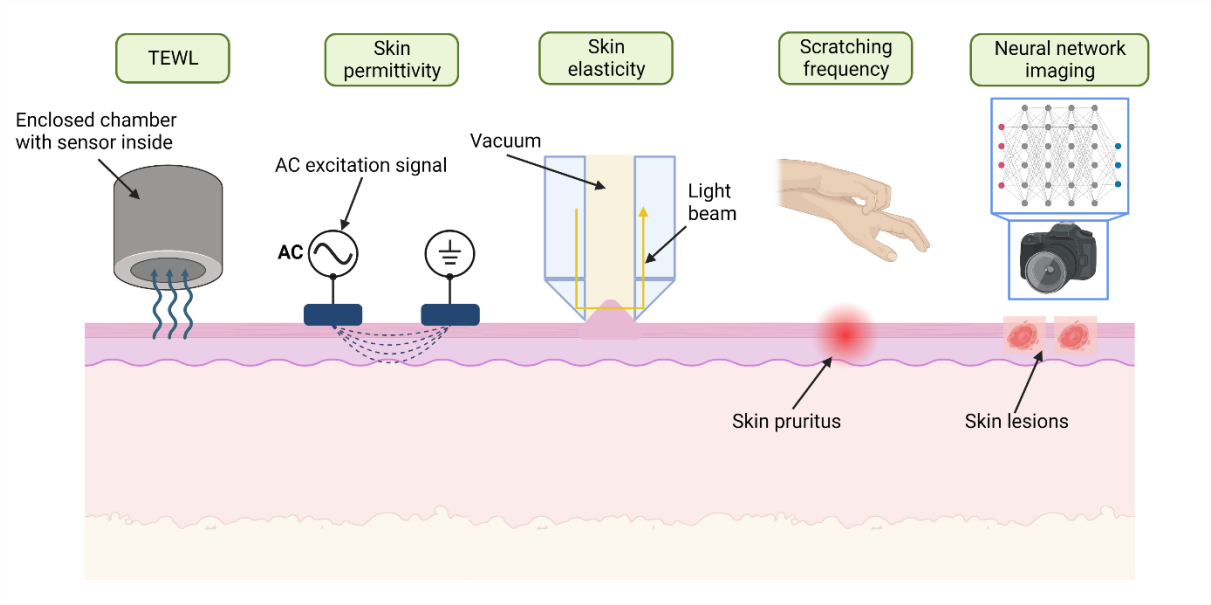

Figure 12 Illustration of different non-invasive telemedical methods for monitoring AD in vivo. The respective measurand parameters are presented on the top of each method illustration. The TEWL method features an enclosed chamber with a relative humidity sensor inside, so that water vapours from the skin affect its reading. The skin permittivity sensor consists of 2 or more electrodes in contact with the skin, of which one is a signal source and the other one a signal pathway (ground) to establish a scattered electric field through the skin. The skin elasticity sensor uses negative pressure to suction parts of the skin and emit light through it to test the skin's properties. The scratching frequency sensor detects when a person is scratching their AD lesions. The neural network imaging system uses a camera to distinguish lesions of AD from other similar conditions such as melanoma, skin burn, and psoriasis.

Following the classification laid out in Table 3, monitoring the skin permittivity via capacitive measurements appears as the most promising technique for the research focus of this thesis. This method has been proven to correctly assess the severity of skin conditions like AD and their flexible and scalable form-factor make them a perfect candidate for embedding into an e-textile sensor. Sensitivity towards biomarkers of AD can be achieved through the optimisation of the electrode pattern. Variations in the dimensions of these patterns would allow for measuring of the hydration of the SC and EP layers with the focus on the SC, which is characteristic for AD. The last section of this chapter will discuss in detail the operation and usage of the IDC sensor and will highlight resources from the literature that use IDC for skin hydration measurements.

2.2.4 Future Applicable Technologies

There are other applicable monitoring methods that have not yet been evaluated for use in AD applications but have shown been used to quantify similar conditions or to detect some of the biomarkers of eczema. Two methods highlighted here offer the potential for a non-invasive device for monitoring AD, but due to the complexity of the instrumentation used, at present their footprint is too large and expensive to be embedded into a wearable device and given to patients to use at home. Further research is needed in developing a more compact prototype sensor based on these methods and exploring that sensor's response from contact with atopic skin.

Since AD causes the skin barrier to permeate water molecules at an excessive rate and to dehydrate the EP and SC layers, a skin hydration sensor that targets those outermost layers can also estimate AD severity. This sensor would operate on a similar principle as the skin permittivity electrode sensors i.e., inducing an electromagnetic wave and measuring the reflected response. This electromagnetic wave can be a microwave in the radio frequency (RF) spectrum, or an optical light in the near infrared spectrum. Skin hydration sensors using radiation from these spectra have already been developed and this section will present the operation of these devices and discuss why they could be viable for distinguishing AD among other conditions.

2.2.4.1 Radio Frequency Reflectometry

It was previously established that free water molecules (not bound by lipids and proteins) inside the SC greatly affect the dielectric permittivity of the skin. Water has a significantly higher relative permittivity than dry skin, thus increased water content would translate into higher permittivity [101]. Using the Cole-Cole expression for complex dielectric permittivity, Arab et al. calculated that at 70 GHz the relative permittivity of wet skin is increased by 30% and conductivity increases by 10% when compared with dry skin [102]. At the millimetre and microwave frequency range, the effects of relaxation on water molecules dominate the dielectric spectrum of tissues [103, 104]. The emitted signals cause excitation of the water molecules, which absorb some of the energy carried by the wave. Thus, by monitoring the intensity of the reflected signal for a given frequency band, the water content can be estimated [105]. Therefore, this technique should be able to measure the dryness state of atopic skin and to distinguish it from similar conditions.

Time domain reflectometry (TDR) is a popular technique in the literature to quantify the variation in the reflected signal from a MUT. In TDR the input signal is usually a step-like voltage pulse, which is propagated along the sensing element (SE) or antenna in contact with the MUT with some relative permittivity εr. The TDR method calculates the reflection coefficient $\rho(t)$, which is the ratio between input and output voltage signals with respect to time, as given by Eq. 1 [101]:

$$\rho(t) = \frac{V_{refl}(t)}{V_{inc}(t)} \tag{1}$$

When analysing the reflectogram properties, the relative permittivity of the skin can be obtained from the reflection coefficient. Due to complications in analysing signals in the time domain, the TDR method can also be transformed to into the frequency domain, where the reflection is estimated using the reflection scattering parameter S_{11} [106]. The S_{11} parameter is calculated using a ratio of the discrete Fourier transform (DFT) of the reflection coefficient (Eq. 2):

$$S_{11}(f) = \frac{DFT[\rho(t)]}{DFT[\rho_i(t)]} \tag{2}$$

where $\rho_i(t)$ is the time-domain reflection coefficient when no material is measured by the SE. The parameter indicates the amount of energy that is lost or absorbed by the MUT. Scattering parameters (S-parameters) are easier to visualize against the measurement frequency and thus allow for better estimation of resonance frequencies of systems under test. The $S_{11}(f)$ can also be directly monitored using a vector network analyzer (VNA) to further simplify the technique [101]. VNAs are, however, typically bulky, and expensive benchtop devices for visualizing s-parameters, but there are compact models used in the literature that have been integrated into portable monitoring devices. Monti et al. used a nano VNA (HCXQS, Nanjing, China) operating in the frequency range of 0 to 3 GHz which is sufficient for RF reflectometry, but this is still quite bulky and has a high-power consumption [107]. The output of frequency coupled TDR, as visualized by a VNA, is a plot of the S_{11} parameter against the frequency. Schiavoni et al. used a parallel electrode SE in contact with three different states of skin based on their hydration. Setup and produced TDR readings are shown in Figure 13.

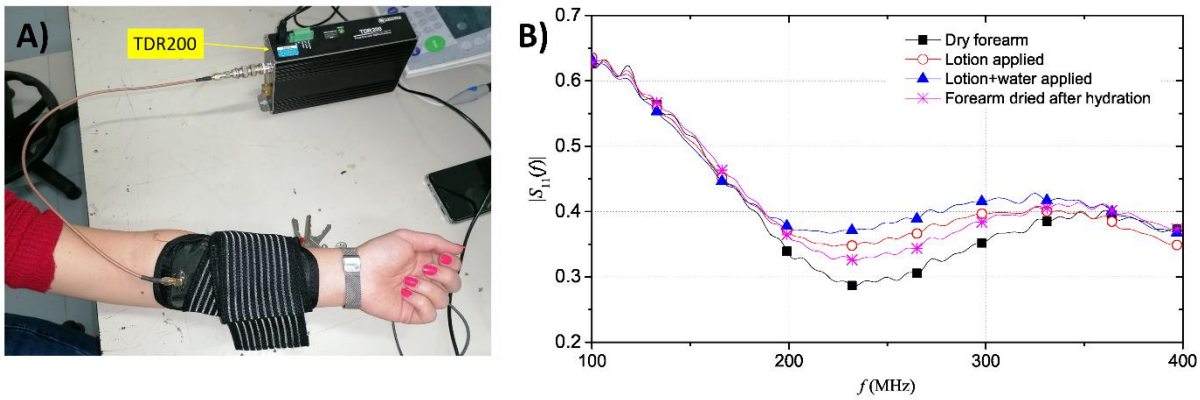

Figure 13 Experimental setup and results of RF reflectometry measurements performed by Schiavoni et al. A) Presents a photograph of the setup with the VNA used to perform the TDR calculations and B) measurement of s-parameters for four cases of forearm hydration. Images reproduced with permission from [106].

It can be seen from the plot that as the hydration levels increase, the magnitude of the reflection parameter around the resonance frequency of the skin-sensor system increases [106]. This is due to the increased permittivity and conductivity in hydrated skin, and this demonstrates the ability of TDR within the microwave frequency range to detect hydration change in the skin.

Table 4 presents a summary of the research papers that have investigated RF reflectometry for the purposes of measuring dry hydration state of the skin. Monti et al. present a tri-electrode sensor that can distinguish between three different states of hydration in the skin [107]. They discovered that around the resonance frequency of the system, the reflection parameters of dry skin are significantly lower, which means that dry skin lesions can be discriminated from healthy non-atopic skin. Schiavoni et al. utilized the tri-electrode sensor and integrated it in a wearable and flexible strap for mobile measurements and Cataldo et al. extrapolated its functionality to predict the hydration state of extra dehydrated skin [101, 106]. Eczema is characterized with severely dry skin and Cataldo et al.'s sensor should be able to distinguish this from normal skin and produce a reflection parameter value of around 0.165 based on the dry state prediction. Arab et al. fabricated a sensor with an open-ended coaxial probe that performed millimeter-wave reflectometry on skin cancer (melanoma) lesions [102]. Melanoma skin has distinct dielectric properties, much like atopic skin, and Arab et al.'s device demonstrated that the reflection parameters from melanoma skin are different to those of healthy dry or wet skin with an accuracy of tens of microns in lesion size [102]. While their design is not suitable for mobile measurements it proves the viability of RF reflectometry for detecting skin conditions. Mehta et al. employed a smaller coaxial probe to differentiate between normal skin, benign and malignant melanoma [108]. This is a very important distinction because it means that RF reflectometry might be utilised to discover skin conditions before the visual symptoms appear. Gao et al. use the reflectometry technique to classify burn degrees and can successfully distinguish 3 different degrees of burnt skin [104].

RF reflectometry has been demonstrated as an accurate tool to measure severely damaged skin and could be used to monitor the most severe cases in AD and psoriasis. Further research is required to explore the response of atopic and eczema skin under RF reflectometry and to see if it could be distinguished from other skin conditions such as melanoma and psoriasis. In addition, smaller, lower cost and low power alternatives to conventional VNAs are required for wearable, home based application of the approach.

Table 4 Summary of literature findings of RF reflectometry for the purposes of AD and skin condition monitoring.

Authors	**Probe type**	**Measurement frequency**	**Sensor placement**	**Range in S11 values between dry & wet skin states**	**Remarks**
Cataldo A et al., 2022 [101]	Tri-electrode array	0-600 MHz	Forearm and leg	0.165-0.268	Predicts values for extra-dehydrated skin.
Schiavoni R et al., 2021 [109]	Tri-electrode array	100-400 MHz	Forearm	0.185-0.290	Explores three skin hydration states. Housed in a wearable and flexible patch
Arab H et al., 2020 [102]	Open-ended coaxial	77 GHz	Hand	0.2-0.26	Tested on melanoma skin.
Brendtke R et al., 2016 [105]	Open-ended coaxial	7.35 GHz	Tested on phantom	-	Tested on various saline solutions in contact with skin phantom.
Monti G et al., 2021 [107]	Tri-electrode array	20-2000 MHz	Forearm, leg, arm, palm	0.224 – 0.282	Uses a compact VNA for mobile measurements.
Mehta P et al., 2006 [108]	Open-ended coaxial	300 MHz-3GHz	Forearm, cheek, palm, chest	0.08-0.14	Used for melanoma detection. Differentiates malignant and benign lesions.

Gao Y et al., 2017 [104]	Open-ended coaxial	26.5 - 75GHz	Tested on pig skin	-	Classifies burn degrees.

2.2.4.2 Optical Spectroscopy

When light from the optical spectrum (visible light and infrared with wavelengths from 400 nm to 1 mm and frequencies from 800 THz to 300 GHz) interacts with tissue or media, the phenomena of light scattering and light absorption occur [110]. During the process of scattering, the photons traverse in various directions among the cells or blood vessels until they are absorbed or remitted back outside of the tissue. The number of photons that get absorbed or get reflected is a probability function that depends on the inherent energy of each photon. This function can be quantified using the intrinsic optical properties of the tissue: the absorption coefficient (μ_a) and the scattering coefficient (μ_s) [110]. These properties depend on the chemical composition of the tissue and especially on the concentration of water molecules in the case of the human skin. Therefore, measurement of the optical absorption by analysing the input and output signals incident on the skin's surface can provide insight into the water composition within the skin.

To calculate the light absorption (A) through a specific media, the Beer-Lambert law is used, (Eq. 3):

$$A = log_{10}\frac{I_0}{I} = log\frac{1}{R} \quad (3)$$

Here I_0 is the intensity of the input light, I is the intensity of the output, and R is the reflectance [111]. The output intensity depends on the absorption and scattering parameters, μ_a and μ_s, and on the distance ρ_0 between where the incident light enters the tissue and where the reflected light exits. The ratio between the input and output is the reflectance and from it the absorbance can be calculated using Beer's law. Modern spectrometers do this calculation automatically and provide absorption measurements directly in units of log (1/R). Since the μ_a and μ_s coefficients depend on the frequency/wavelength of the incident light, the absorption values are commonly graphed on a wavelength spectrum. Absorbance peaks at specific wavelengths because some combinations of molecules begin vibrating and absorbing photons at an accelerated pace [112]. The same is valid for other measurands arising from Beer-Lambert's law such as the reflectance or intensity of scattered signal, which can be obtained through various measurement techniques and plotted against the frequency. This frequency-dependent behaviour provides insight into the chemical composition of the MUT, by highlighting distinguishable segments of absorption/reflectance increase, which indicates the presence of specific compounds [111].

There are various methods of performing these measurements based on the frequency range, equipment setup, light source and the targeted measurand. This review covers methods demonstrated in the literature as viable skin hydration sensors and in some cases that have been used on skins with eczema. Raman spectroscopy focuses on the scattering of light, and it measures the intensity of scattering events occurring at specific wavelengths thereby estimating the concentration of molecules with known scattering effects at these frequencies [113]. Near Infrared Spectroscopy (NIRS) monitors the absorption intensity from the reflectance spectrum of an exposed tissue or material within the near infrared band (wavelengths of 0.8 to 2.5 mm). The absorption is linearly correlated with the concentration of specific molecules at unique band levels and by selecting the specific NIR waveband, insight into the presence of individual molecules can be determined [114]. Diffuse reflectance spectroscopy (DRS) is another widely used technique to determine chemical composition by measuring the remitted light after interaction with the MUT. It considers the lateral distance travelled by the light within the MUT, affected by scattering and absorption events, allowing for a spatially resolved measurement [115]. The methods described here are all accurate enough to be used as AD monitoring devices, but yet a fully portable and mobile version of these devices has not been developed.

2.2.4.2.1 Raman Spectroscopy Measurements on Skin

Confocal Raman Micro-Spectroscopy (CRM) is a type of Raman spectroscopy that can be used to perform non-invasive in vivo measurements on independent layers of the skin, as it can determine the biomolecular composition at depths up to several hundred micrometres [113]. The method uses the variance in scattered protons depending on the chemical content to provide a unique signature Raman spectrum for each material measured. AD affects the chemical composition of the skin, not only by reducing the free water molecules inside but also eliciting other molecular biomarkers. Dev et al. explored the Raman intensity at different wavebands from 400 to 1800 cm^{-1} to classify the differences between atopic and healthy skin [113]. The probe used was handheld and portable, but the light source and the spectrograph required for the measurements are bench top equipment and therefore this approach is not portable, as visualized in Figure 14. They record differences in the Raman spectra at the wavebands corresponding to water, ceramide and urocanic acid, the latter of which features the highest separation at the wavelength of 6098 nm [113]. This is an important metric for the discovery of other biomarkers of AD. Ho et al. used the same method to discover that AD skin had 51% and 52% lower concentration of water and urocanic acid, respectively, compared to healthy control skin [116]. Their device was also tested against different severity levels and was able to distinguish between mild and moderate, but not between moderate and severe states of eczema. Results were also compared with TEWL measurements and the TEWL exhibited a 32% increase in sensitivity compared with CRM in distinguishing between the mild and moderate severity states

[116]. Gonzalez et al. used a commercial benchtop Raman spectrometer to detect AD early in infants based on the presence of a key skin barrier maintenance protein called filaggrin (FLG) [117]. It was discovered that the infants with lower FLG concentration were the ones that developed AD, identifying it as a valid biomarker for the condition.

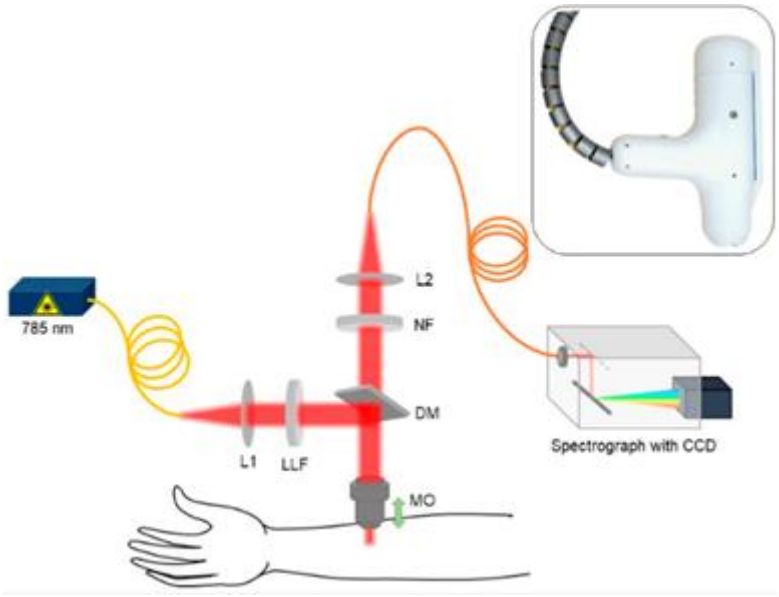

Figure 14 Schematic of handheld in vivo CRM system utilized by Dev et al. The system is housed within the handheld probe visible in the top right corner – the cable on the left is connected to the laser source and the cable connecting to the spectrograph is not illustrated. Image reproduced with permissions from [113].

CRM is a highly accurate tool for discriminating the biomarkers of AD, but its requirement of a multi-lens arrangement, along with a halogen light source and CCD spectrograph make it unsuitable for portable, home-based application at present.

2.2.4.2.2 Near Infrared Spectroscopy Measurements on Skin

The absorbance spectrum of water and porcine skin in the near infrared range (NIR) is compared in Figure 15. It is evident that the skin spectrum follows the spectrum of the water and peaks at the same wavelengths of around 1450 and 1900 nm. This is because at these bands the combinations of OH and HOH molecule groups of water begin vibrating [112]. These groups are attributed to the bulk water content within the SC which is one of the biomarkers of AD. Therefore, skin with lower free water content, such as atopic skin, will have lower absorbance values at these specific wavelengths than normal, healthy skin and a device that can estimate the scattering, absorbance, or reflectance of light through the skin would be useful in monitoring skin conditions such as AD.

NIR Spectroscopy (NIRS) devices perform absorbance measurements across the frequency range to detect deviations between the measurand and a control unit, indicating the differences in the chemical composition between the two. NIRS has already been employed and widely used in determining melanoma spots, as Fioravanti et al. have presented a portable, but not yet wearable, device that complements histopathological measurements to prevent misdiagnosis [118]. The wavelength used is tailored to detect discrepancies in the methylene absorption, as it is an indicator for melanoma. By changing the frequency, it should be possible to detect the biomarkers of AD such as water molecules, FLG, ceramide and chemokine [27, 33, 65, 117]. Shin et al. have used NIR to monitor molecule changes during acute barrier disruption in the SC, which was artificially induced via tape stripping. They have discovered the same peaks of methylene absorption as with melanoma, and additional insight into the protein and lipid composition of the SC [119]. This confirms that NIRS can analyse the lamellar structure of SC and monitor the ceramide protein levels, rendering it another possible approach for monitoring AD. Zhang and Meyers et al. have created a NIR imaging system using an InGaAs array detector and two tungsten halogen lamps to detect hydration changes of the skin in the range 800 - 1800 nm [114]. The skin was treated with different products such as humectant cream and moisturizing body wash, which are both remedies for the symptoms of AD. The results were compared to visual and electrical methods of hydration assessment, and it was shown that the NIR method related more closely to the visual assessment performed by a clinician, than to the electrical ones, even though the latter showed higher sensitivity to the humectant cream [114].

NIRS has the potential to be an accurate tool of identifying the biomarkers of AD but has not yet been tested to assay the condition, but Zhang and Meyers et al. stated the method cannot target the outermost layers for hydration detection, and that it measures the overall hydration in the skin [114]. Further research is required to determine if NIRS can distinguish AD from other skin conditions like skin burns.

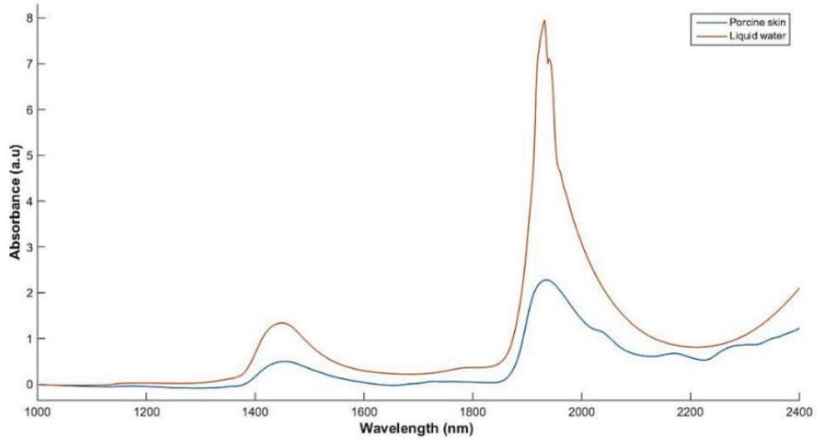

Figure 15 Absorbance spectrum of water and porcine skin in the NIR range. The absorbance peaks around 1400 nm and 1900 nm match almost perfectly, indicating that the

absorbance response in the skin is due to the water concentration. Image reproduced with permissions from [112].

2.2.4.2.3 Diffuse Reflectance Spectroscopy Measurements on Skin

Diffuse reflectance spectroscopy (DRS) is commonly performed in the IR range, and it utilizes a two-probe arrangement, connected with a spectrometer, to establish the optical parameters of a MUT. The optical probes are employed as an emitter and collector and are positioned on the surface of the MUT with a defined separation between each probe [110]. When an emitted photon package passes through the MUT, part of it is absorbed and the rest undergoes scattering and emerges at some distance from the input. The levels of absorption and scattering will vary depending upon the inherent optical properties and coefficients of the MUT [111]. From the intensity of the reflected signal and the distance it has diffused from the input, a depth-resolved image of the MUT can be estimated, thus providing insight into the chemical composition of tissues at different layers. The separation distance between the source and detector is determined by the probe placement and by varying this distance measurement at specific depths can be achieved [111]. Therefore, the DRS sensor can be set to detect the concentration of AD biomarkers in the outermost layers of the skin at a specific point on the skin using the two probes and electronics for analysing the reflected light.

Since DRS is operating in the IR range, and the absorbance peak bands of specific molecules in the IR range are already known, the total footprint of a DRS measurement device can be reduced to a simple light emitting diode (LED) with fixed wavelength and a photodiode (PD) or camera to capture the reflected signal. The wavelength of the LED will be matched to the absorbance peaks of the relevant AD biomarker molecules such as water, methylene, FLG, ceramide. Anker et al. have used a multi-LED arrangement around a camera setup to visualize epidermal keratin and dermal collagen structure for the purposes of understanding abnormal keratin formation in ichthyosis, a condition similar in severity to AD and commonly in infants [120]. They were able to link the abnormal keratin structure to gene mutations, like the mutations in AD patients that cause the breakdown in the linkage proteins within the SC barrier. To optimize the DRS sensor arrangement, multi-wavelength LED setups can be employed to detect other absorption peaks. Yan et al. have presented an opto-electronic patch sensor that features four channels of different wavelengths ranging from 525 nm to 870 nm around a single PD cell [121]. The sensor (visible in Figure 16) is housed in a compact and wearable packaging and was used to detect the heartrate of the subject while per-forming daily activities.

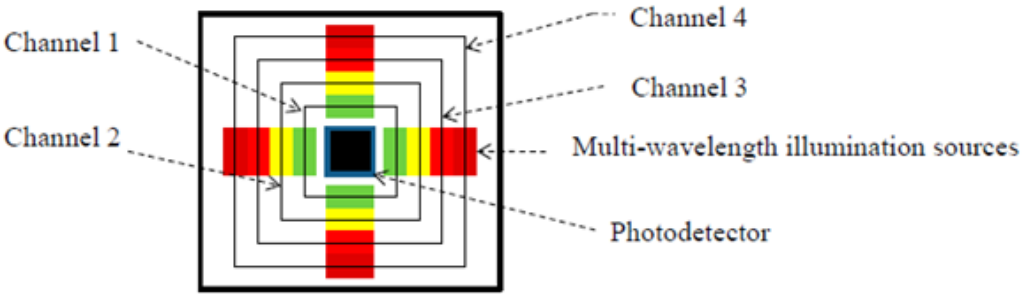

Figure 16 Schematic of opto-electronic patch sensor created by Yan et al. Four channels of NIR LEDs are positioned around a single PD cell. The channel can emit light with varying wavelengths to achieve a higher sensitivity. Image reproduced with permissions from [121].

Mamouei et al. employed the same multi-LED sensor arrangement but used three LEDs with wavelengths of 970, 1200 and 1450 nm to determine dermal skin hydration. These wavelengths correspond to the absorbance peaks in Figure 15 [112]. The sensor has been simulated to target the EP and DR layers, but by tweaking the SDS distance, the penetration depth can be altered, to target the AD-relevant SC layer. The device, visible in Figure 17, is incorporated into a coin-sized non-invasive package and has been tested on skin phantoms using gravimetric testing, which involves wetting the skin phantom and positioning it onto a fine scale and record the weight of the evaporated water from the surface of the phantom [112]. The authors claim that the sensor has noise immunity from other physiological influences on the skin, but has not been tested in vivo, so further testing is required.

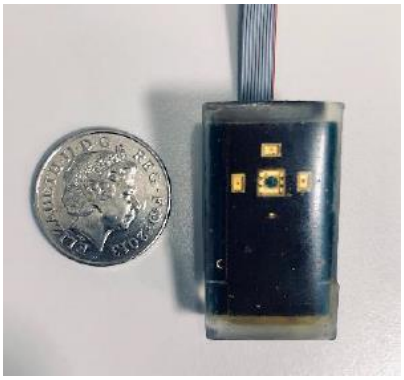

Figure 17 Photograph of the LED/PD sensor. Image reproduced from [112].

The standard two-probe DRS method is limited to monitoring a single point, but with an image filter or optic plate, the measurement can be extended over a two-dimensional area. This type of DRS is called diffuse reflectance imaging (DRI) [110]. DRI can be performed over an area of pixelated sensor probes to gather spatially resolved information about the MUT [115]. The source of light within DRI would be a single LED pixel, usually placed in the middle of a matrix of PD pixels to pick-up the reflected signal. Such an arrangement would not only allow water content estimation across an area but would be able to pinpoint how the water content varies with depth.

If the water molecule absorption at the shallower layers is low, then photons will traverse deeper into the tissue and would remit further from the source [110]. Thereby, since AD skin is dryer, the intensity measurement of the outer pixels should be higher than that of the inner ones. Petitdidier et al. proposed such spatially resolved DRI sensor using CMOS technology to fabricate a pixelated sensor with a single light emitter and a matrix array of PDs to determine the absorption and scattering coefficients of the skin [115]. A fiber optic plate (FOP), which is a grid of parallel vertically oriented fibers, guides the reflected light from the surface of the MUT to the pixels of the sensor. The sensor was able to accurately calculate the optical properties of the skin but has not been tested in vivo on skin conditions to determine its efficacy.

2.2.4.2.4 Conclusion

Optical spectroscopy is a valid future method for determining the physiological characteristics of damaged skin and has already proved its usability in monitoring conditions similar to AD. Optical based approaches are immune to electrical noise arising from hair follicles and skin pores and their response is not affected by the skin-sensor contact pressure, unlike methods such as RF reflectometry and electrical impedance. Table 5 summarises the most prominent spectroscopic devices. The methods require further work to evidence their usability for examining AD specifically. Raman Spectroscopy is the only optical method that has been tested on AD patients, but due to the complexity of the equipment, it cannot be classified as a portable e-health device that does not require the input of an expert operator. Further research to reduce the size of spectroscopic devices and simplify their implementation is required to enable them to be used by the patient in a home monitoring scenario.

Table 5 Summary of literature findings of optical spectroscopy for the purposes of AD and skin condition monitoring.

Authors	Technique	Sensor placement	Sensor footprint	Skin Condition	Wavelength (nm)	Remarks
Dev et al. 2022 [113]	Confocal Raman Micro-Spectroscopy	Volar forearm	Handheld probe, connected to bench spectrometer	AD	5550-25000	Highest sensitivity to urocanic acid.
Ho et al. 2020 [116]	Confocal Raman Micro-Spectroscopy	Volar forearm	Handheld probe with built in spectrometer and light source; bulky package	AD	5000-16000	Compares device to TEWL and conventional AD scoring system.
Gonzalez et al. 2011 [117]	Raman Spectroscopy	Right thigh	Commercial benchtop Raman spectrometer	AD	5550-50000	Tested on infants.
Fioravanti et al. 2016 [118]	Near Infrared Spectroscopy	Biopsy	Multi-lens benchtop setup, connected to a computer and IR emitter	Melanoma	3350-3550	Detects abnormalities of methylene absorption in melanoma patients.
Shin et al. 2018 [119]	Near Infrared Spectroscopy	Facial cheek	Commercial benchtop spectrometer	Barrier disruption	1450-2500	Performs skin stripping to induce barrier disruption. Can

Authors	Technique	Sensor placement	Sensor footprint	Skin Condition	Wavelength (nm)	Remarks
						monitor protein and lipid alterations.
Zhang et al. 2005 [114]	Near Infrared Spectroscopy	Outer lower leg	Benchtop detector and camera setup with two separate light sources	Skin hydration	1100-1630	Claims NIR cannot be used to target individual layers. Compares against electrical methods.
Anker et al. 2021 [120]	Diffuse Reflectance Spectroscopy	Various locations on infants' skin	LEDs around a camera.	Ichthyosis	405	Monitors mutations of keratin-forming genes.
Yan et al. 2017 [121]	Diffuse Reflectance Spectroscopy	Palm	Multi-LED and PD patch of size 324mm^2	Physiological skin changes	525-870	Compact and wearable package.
Mamouei et al. 2021 [112]	Diffuse Reflectance Spectroscopy	Skin phantom	Coin-sized Multi-LED and PD probe	Skin hydration	970-1450	Has not been used on skin, only on fake tissue to predict water evaporation.
Petitdidier et al. 2021 [115]	Diffuse Reflectance Spectroscopy	Skin phantom	Coin-sized pixelated sensor with holder.	Physiological skin changes	645	Uses CMOS technology for very small separation distances.

2.2.5 Capacitive Measurements of Skin Hydration

2.2.5.1 Introduction

Out of all highlighted methods for measuring the hydration of the outermost layers of the skin, the capacitance measurement seems to be the most suitable approach for determining biomarkers of AD. The technique has also been adopted in commercial devices like the Corneometer® and MoistureMeterSC® [74, 76]. The sensing element also be easily embedded into e-textile format, as evident by Jang et al.'s flexible skin dehydration sensor presented in Figure 9 [86]. The sensing element consists of pairs of electrodes from opposing polarity, onto which an alternating voltage source is imposed, creating a varying electric field between them [122]. As established in section 2.2.3.2, the strength of this electric field depends on the dielectric properties of the material between the electrodes, which in this case is the AD skin. By employing a specific pattern of electrodes, the properties of specific skin layers can be assessed to determine the hydration of these layers. Two arrangements of the sensing electrodes are predominant in the literature – the coaxial and the interdigitated electrodes. This section will expand on the information provided in section 2.2.3.2 by investigating how both capacitive sensors operate: the underlying physical properties measured and how the parameters of the sensors affect the measurement. Then more examples from the literature will be presented, in which the capacitive sensors were used for general skin hydration measurements, not only for AD dehydrated skin.

2.2.5.2 Modelling the Dielectric Properties of the Skin

Before discussing how the capacitive sensors work, it is important to understand how the skin behaves when subjected to the electric field arising from the sensor. The skin is a dielectric material, and as such it is capable of storing electrical energy based on its properties [123]. That ability is defined as capacitance, and its value is directly proportional the dielectric properties of the material – namely the permittivity. Eq. 4 presents the basic formula for capacitance, independent of frequency, where *A* is the cross-sectional area of the medium, *d* is the length, ε_r is the relative permittivity of the material, and ε_0 is the absolute permittivity of vacuum.

$$C = \frac{\varepsilon_r \varepsilon_0 A}{d} \tag{4}$$

The skin is not an ideal dielectric, but a complex material with a heterogeneous structure with ionic and molecular components that contribute to a complex impedance behaviour, consisting of both capacitive and resistive effects [122]. Thus, the skin can be modelled as a series and parallel combination of resistors and capacitors, whose effect varies with the frequency of the

imposed electric field. At low frequencies, resistive components dominate due to ionic conduction, whereas at higher frequencies dipole polarisation occurs, leading to high capacitive contribution. This is also known as the RC equivalent circuit of the skin, and it represents each layer as an effective filter, which obstructs different bandwidth of frequencies. That is also why high frequencies can penetrate deeper into the skin [20]. Therefore, to accurately reflect the complex behaviour of the skin, Eq. 5 should be updated to include the frequency-dependent complex permittivity ($\hat{\varepsilon}(\omega)$):

$$C(\omega) = \frac{\hat{\varepsilon}(\omega)\varepsilon_0 A}{d} \tag{5}$$

The complex permittivity has two terms – a real part, the ability to store charge attributed relative permittivity, and an imaginary part, the ability to dissipate energy due to conductivity (σ). Eq. 6 shows the relationship between conductivity and permittivity, where *j* is the imaginary unit and ω is the angular frequency:

$$\hat{\varepsilon}(\omega) = \varepsilon_r - \frac{j\sigma}{\omega\varepsilon_0} \tag{6}$$

The dielectric spectrum of all biological tissues follows this complex behaviour. A more detailed characterisation of this spectrum can be achieved by considering the RC equivalent model. This approach allows us to identify multiple relaxation regions, where distinct dipole polarization mechanisms dominate at different frequency ranges. These relaxation processes, known as dispersions, each describe a particular response of the tissue to an applied electric field [124]. A mathematical framework that effectively models this dielectric response is given by the Cole-Cole equation:

$$\hat{\varepsilon}(\omega) = \varepsilon_\infty + \sum_{i=0}^{n} \frac{\Delta\epsilon_n}{1 + (j\omega\tau_n)^{(1-\alpha_n)}} + \frac{\sigma_i}{j\omega\varepsilon_0} \tag{7}$$

The Cole-Cole equation expands the existing single relaxation models, as it accounts for non-ideal behaviour with distributed dispersions. The different terms of Eq. 7, that have not been introduced so far, are as follows: ε_∞ is the permittivity of frequencies where $\omega\tau_n \gg 1$; $\Delta\epsilon_n$ is the magnitude of dispersion; α_n is the distribution parameter, a measure of the broadening of the dispersion; σ_i is the static ionic conductivity [71]. The parameters of Eq. 7 dictate the permittivity and capacitance response and are also dependent on the individual layers of the skin and their composition. Therefore, with this equation different hydration states of the SC, EP and DR layers can be modelled, to investigate the capacitive behaviour under varying frequency spectrum.

In the introduction of this chapter, it was established that hydrated skin exhibits higher values of dielectric permittivity and conductivity than dry skin. High water content in the SC increases the number of ionic pathways for electrons, by introducing more dipoles, and makes the SC keratin layer more flexible, thus enhancing the skin's response to applied electrical fields and increasing the amount of electrical energy that can be stored [103]. Gabriel et al. compiled the measured dielectric properties of different tissues in the literature across a spectrum between 10 Hz and 100 GHz and found out that the response aligns with the Cole-Cole equation for the complex relative permittivity with 4 dispersion regions [71]. The authors then fitted the measurements to the Cole-Cole model and found the parametric solution to satisfy the complex behaviour of both wet and dry skin. This has formulated a database that has been the cornerstone of nearly all skin modelling within the literature and the basis for impedance sensing on the skin.

Figure 18 depicts the dielectric spectrum of dry skin, as measured by Gabriel et al. and Raicu et al. [72]. It is seen that at lower frequencies (less than 10 kHz) the permittivity plateaus between 1100 – 10000 and as the frequency increases, the permittivity drops to 10. Conductivity runs the opposite: at lower frequencies it is around 0.0001 S/m and climbs up to 1-10 S/m with frequency increase. Gabriel et al. also discovered that these values change based on the hydration of the skin – wet skin has a higher relative permittivity and conductivity at the lower frequency spectrum, which agrees with the theory laid out in the introduction [71].

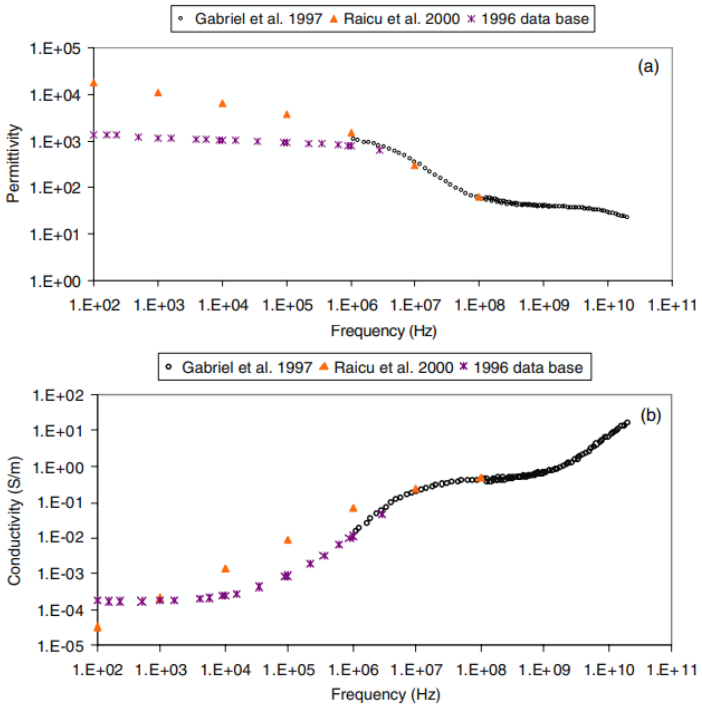

Figure 18 Permittivity and conductivity spectrum of dry skin. Reproduced from [72].

Furthermore, Gabriel et al.'s permittivity measurements show that the highest difference in the permittivity values between dry and hydrated skin occurs at the low to mid frequency range (kHz

to MHz). At this frequency range, β-dispersion occurs according to the Cole-Cole model, and the capacitance is strongly influenced by polarisation of bound charges (water molecules) in the SC and EP tissues [125]. At lower frequencies the SC behaves more resistively and acts as a high impedance barrier. At higher frequencies the electric field penetrates deeper, therefore capacitance is influenced more by the deeper layers such as the dermis. Therefore, a sensor that utilises the mid frequency range (10 kHz to 10 MHz) should be an effective tool in determining the hydration factor in the SC. Further modelling will be conducted to validate that hypothesis.

2.2.5.3 IDC and Concentric Scatter-field Capacitors – Operation and Application for Skin Hydration Measurements

Capacitive sensors utilise complimentary pairs of coplanar electrodes in contact with the skin with different arrangements to achieve different sensitivity. One of the electrodes carries the signal – periodic AC voltage wave and the other provides a ground reference. Hence, a scattered electric field, penetrating the skin, is established between the plates. The system can be approximated as a spread-out capacitor, as seen in Figure 19. The figure presents an illustrative version of the electric field lines, as in reality the emitted field is present on the other side of the electrodes too. In the case where the dielectric permittivity of the MUT is much greater than the permittivity of the substrate onto which the electrodes are placed (like Kapton, or for simplicity, air), the measured capacitance depends primarily on the dielectric properties of the MUT, mainly the relative permittivity as it is shown in Eq. 5.

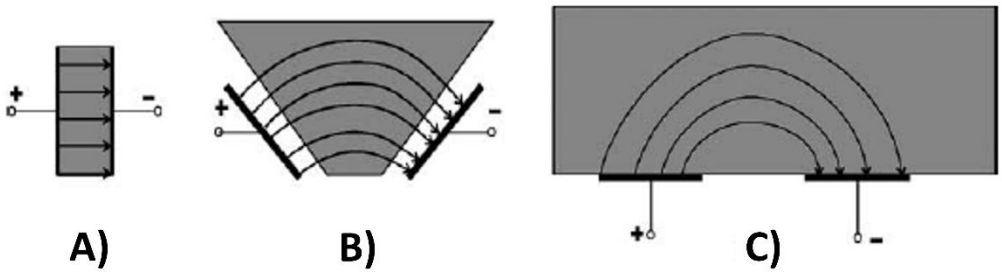

Figure 19 Illustrative example of a scatter-field capacitor and the electric field lines penetrating just the MUT. Reproduced from [126].

By measuring the capacitance, the change in relative permittivity can be detected, which has been proven to reflect a change in hydration status. The penetration depth of the field can be controlled by varying the gap between the electrodes and the frequency of the excitation signal [126]. The bigger the gap, the deeper will the electric field penetrate, thus, to measure the hydration around the SC barrier, a narrower gap will be utilised [127]. The penetration depth is not a fixed point but a range in which the strength of the electric field is the strongest. To monitor biomarkers of AD, this range should be within the SC and EP layers.

Two prominent designs for the shape of the coplanar electrode plates are found in the literature – coaxial and interdigitated. Coaxial electrodes consist of a circular electrode and a separated coaxial ring placed around it, presented in Figure 20 A). Usually, the inner electrode is the signal carrying one and the outer ring is the ground reference. The interdigitated shape consists of two electrically insulated comb-like electrodes that are positioned facing each other, like in Figure 20 B). The interdigitated electrodes (IDE), also known as interdigital capacitor (IDC), is the most common type of electrode transducer used in the literature and in commercial sensors, especially for the purpose of assessing skin hydration [128]. The purpose of the IDC is to maximise the output capacitance, while minimising the sensing area. Due to its layout, the IDC can be thought of as *N-1* capacitors connected in parallel, where *N* is the number of fingers (digits). This effectively amplifies the output capacitance, making it easier to measure, because the output of an IDC is usually in pF or nF. The geometry of the IDC affects the penetration depth and the total capacitance read-out. To achieve a desirable penetration depth the gap between fingers is varied – smaller gaps achieve shallower measurement depths. The finger length, width and number determine the overall area of the electrodes. The IDC also measures a bigger area than the coaxial sensor, eliminating potential outliers and sources of error.

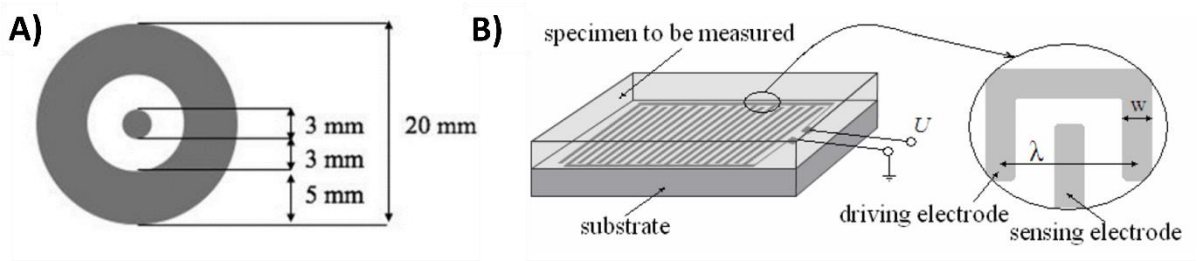

Figure 20 Examples of A) coaxial electrode and B) interdigitated electrode. Images reproduced from [129] and [127].

The sensing part is usually made of copper (Cu), silver (Ag), gold (Au) or platinum and it is etched through photolithography or deposited by a screen-printing method onto a substrate [130]. Silver and copper are the least expensive and provide adequate measurements but have problems with long term stability [131]. Gold and platinum are more expensive and highly reliable options, but studies indicate that platinum does not adhere well with the substrate and can be peeled off [131]. The substrates are usually made of different types of polymers because of their non-toxicity and resistance to heat and abrasion – PDMS, polyimide, PVA [126, 132]. The substrate can be a solid piece or conformal thin sheet, that adheres to the skin. The latter one provides better contact with the skin, but the former is more rigid with a defined geometry for better accuracy and repeatability. The IDC can also be placed in a closed chamber, not in direct contact with the skin to measure TEWL values. Mundlein et a. tested an IDC gas and humidity sensor placed inside a closed chamber on top of the skin and managed to measure accurate TEWL values and relate

them to severity of skin dryness [57]. The purpose of this study is to house the sensing component into a non-invasive patch, thus the solutions that utilise thin films or flexible substrates are more attractive. The areas of the sensors in the literature range between 5 mm^2 to 300 mm^2. Utilising a bigger area may be more effective for getting a broader picture of the disease severity, but that often comes at the expense of sensitivity. Huang et al. and Rie et al. solved this issue by introducing a matrix of individual coaxial and IDC sensors that cover a bigger area and achieve fine scale sensitivity [87, 133]. Measurements are usually performed on the volar forearm because it is easily accessible, but if the sensor is mobile enough, measurements can be taken from anywhere where AD lesions occur. The output measured by a coaxial or IDC sensor is the internal impedance in the form of capacitance or resistance. Works from the literature use commercial LCR meters or various impedance analyser circuits to calculate the impedance at different frequencies or different hydration levels. Varying hydration levels are usually achieved by introducing moisturizer agents and lotions onto the skin. The impedance range is usually in tens to thousands of kΩ for resistance values and in tens of nF or pF for capacitance, depending on the sensing area. The values for impedance or capacitance are mostly related to arbitrary units of hydration (in a.u. or %) taken from a commercial sensor placed on the same spot on the skin. As discussed in the introduction high hydration levels would translate into high capacitance values and low resistance values, and low hydration levels would be the opposite. In Ivanic et al.'s paper the impedance values are compared against the relative permittivity of the skin, and they exhibit the same relationship as with arbitrary hydration levels – impedance decreases, whereas capacitance increases with increasing permittivity [134]. Yang et al. determines the range for permittivity and conductivity values of the skin within the low frequency range: relative permittivity varies between 4500 and 13000, and conductivity varies between $1.25x10^{-4}$ and $2.3x10^{-4}$ S/m [66]. Table 6 summarises the most notable publications from the literature that utilise IDC or coaxial electrodes to perform electric field screening onto the SC or the EP. For each reference the geometric features and compositions are highlighted, along with signal voltage (peak to peak values) and frequency, sensor placement and sensitivity, which is the change in impedance per 1 unit of change in hydration levels taken from commercial sensors either in arbitrary units (a.u.) or in percentage (%).

2.2.5.4 Conclusion

The best method for monitoring AD through capacitance measurements would be to use an IDC sensor due to its ability to be tailored for precise measurements. By varying the geometric parameters of the IDC, the sensing can be optimised for detecting only the outermost layers of the skin, the SC, where the AD biomarkers are present. The IDC electrodes can easily be integrated into a wearable garment, allowing for the continuous severity monitoring. This can be done with common fabrication processes like screen printing or etching. Although a cost-

effective and easy to implement solution, this measurement technique comes with several drawbacks. One of those issues is the contact between the electrodes and the skin, as poor contact can introduce too much electrical noise in the output. Many of the designs considered within this literature review utilize pressure system like a sensor or a spring to control the amount of pressure applied between sensor and skin [87, 135]. Others use a completely conformal sensor that adheres to the skin fully, but that introduces another issue – the patch prevents the humidity from the skin to evaporate normally, thereby hindering the accuracy. Matsukawa et al. suggests making the substrate and sensor water permeable to avoid occlusion. Since textiles are naturally breathable, an electrode sensor housed within a textile should provide a promising prototype for constructing a standalone devise for monitoring AD.

Table 6 Summary of relevant literature on electric field hydration sensing.

Authors	Electrode shape and area	Electrode material	Substrate	Signal voltage	Measurement frequency	Sensor placement	Sensitivity	Remarks
Huang X et al., 2012 [133]	Coaxial, IDC, Meander; 25mm^2	Chromium / Gold	5µm silicone film	2 Vpp	1-100 kHz	volar forearm	20 kΩ/a.u.	Uses two probes and measures the difference between them to eliminate noise. Highest sensitivity is at low frequency (15 kHz).
Huang X et al., 2013 [135]	Coaxial; 0.8mm^2	Chromium / Gold	5µm silicone film	2 Vpp	20 Hz-20MHz (best 15 kHz)	volar forearm	9 kΩ/a.u.	Utilizes a matrix arrangement of individual sensors. Made onto a thin film that conforms to the skin.
Benjamin H et al., 2005 [136]	Circular array of electrodes; -	Chromium / Gold	Glass	250 mVpp	10 kHz-1MHz	-	-	Electrodes are placed in a circular array. Claims SC dielectric spectrum does not fit Cole-Cole curve fully.
Huang T et al., 2008 [128]	IDC; -	Copper	FR4	300 mVpp	100 kHz	-	0.035 pF/%	Sensitivity is calibrated against a commercial sensor.
Yao S et al., 2017 [69]	IDC; 480mm^2	Silver NanoWires	PDMS thin film	2 Vpp	100 kHz	volar forearm	0.9 nF/a.u.	Sensor is made of breathable nanowires and PDMS substrate and is tattooed on the skin.

Authors	Electrode shape and area	Electrode material	Substrate	Signal voltage	Measurement frequency	Sensor placement	Sensitivity	Remarks
Rie H et al., 2020 [87]	IDC; 0.185mm^2	-	CMOS chip	1.5 Vpp	600 kHz	-	0.25 %/min	Houses an array of IDC sensors in a single CMOS chip. Can select individual pixels of this array.
Yokus M et al., 2016 [68]	IDC; 144mm^2	Gold	Polyimide	1Vpp	10 Hz - 0.1 MHz	simulation	-	Uses meandering electrodes for the IDC fingers.
Ivanic R et al., 2003 [134]	IDC with non-symmetric fingers; -	Platinum	Alumina	100 mVpp	1 kHz	hand	0.65 µA/ 1 unit of relative permittivity	Tests non-symmetric arrangement of fingers. Measures the output current and relates it to dielectric permittivity.
Matsukawa R et al., 2020 [137]	IDC; 120mm^2	Gold nanomesh	PVA nanofibres	-	100 Hz	volar forearm	4 kΩ/a.u.	Sensor is breathable to avoid noise from occlusive properties.
Mundlein M et al., 2003 [57]	IDC; 5.5mm^2	Molybdenum	Ceramic	100 mVpp	500 kHz	arm	-	Sensor is housed in an enclosed chamber. Tested on skin with AD.
Ramanathan S et al., 2020 [138]	IDC; -	Aluminium	PDMS	2 Vpp	-	tested on samples	-	Sensors is used to analyse sweat samples.

Authors	Electrode shape and area	Electrode material	Substrate	Signal voltage	Measurement frequency	Sensor placement	Sensitivity	Remarks
Sekiguchi N et al., 2001 [139]	IDC; 5.5mm^2	Molybdenum	Ceramic	100 mVpp	100 kHz - 2MHz	-	0.05 pF/a.u.	Concludes that normal skin has higher capacitance than atopic skin for given frequency measurement.
Yang B et al., 2016 [66]	IDC, 46.5mm^2	Gold	FR4	800 mV	600 Hz – 10kHz	volar and dorsal hand	-	Uses a square wave signal, not a sine wave.
Guzman et al., 2017 [129]	Coaxial; 314mm^2	Silver	Ethyl celulose thin film	30 mVpp	0.1 Hz - 1MHz	volar forearm	-	Sensor is tattooed on body. Used for whole body analysis but design suggests that it penetrates only the SC.

2.2.6 Conclusion

There is not a single best method for assessing AD severity empirically. As outlined above, each have their own merits and demerits. Medical tests are the current diagnostic standard supplementing the visual observation carried out by the dermatologists but require painful and invasive techniques in a clinical environment. New innovative technologies have been applied in the field to test replacement of medical and visual examinations, but none of them have achieved full clinical adoption. These techniques feature measuring TEWL, skin permittivity, skin elasticity, scratch frequency or automate distinguishing lesions in skin through CNN on photographs. There are also other methods that are gaining traction, due to their application in skin hydration tests, but have not been employed in the field of AD monitoring – RF reflectometry and optical spectroscopy. The new methods, although promising, require high complexity of sensor design and equipment, rendering them difficult to integrate in a wearable format. Of the possible mentioned techniques, the skin permittivity measurement through IDC is the most prominent because it is non-invasive, cheap to produce, and easily accessible to patients worldwide, and has shown sufficient capability in predicting the symptoms, evaluating the severity, and monitoring the treatment of AD. That is why the IDC sensor is chosen as the focus of this thesis to produce a wearable sensor capable of monitoring AD in skin.

Chapter 3 Design, Analysis and Optimisation of an IDC Sensor for Monitoring AD

3.1 Introduction

Based on the findings from the literature review, the best sensor for empirically measuring the severity state of skin with AD in a wearable format is the capacitance sensor utilising the IDC design. This is because it can detect biomarkers of AD, has a low cost of production and simple method of operation. It features a thin electrode pattern which can be etched from a thin flexible film or printed onto a textile substrate. That is why this chapter will focus on understanding its operation, testing how its parameters affect the measurement sensitivity and conduct analytical studies to determine the most optimised parameter setup for the application. The literature revealed limited work on IDCs being tested on skin with AD, so this study is novel and necessary to produce an accurate sensor.

As introduced in the previous chapter, the IDC is a specific arrangement of intertwined electrodes, placed in an alternating pattern with uniform gaps of air or other insulation. A schematic of this arrangement is presented in Figure 21 A). The electrodes are usually made of metal but can also be conductive polymers like carbon. To limit the scope of this study and to focus only on the properties of the skin permittivity, only metal electrodes will be investigated, as the conductivity is the highest.

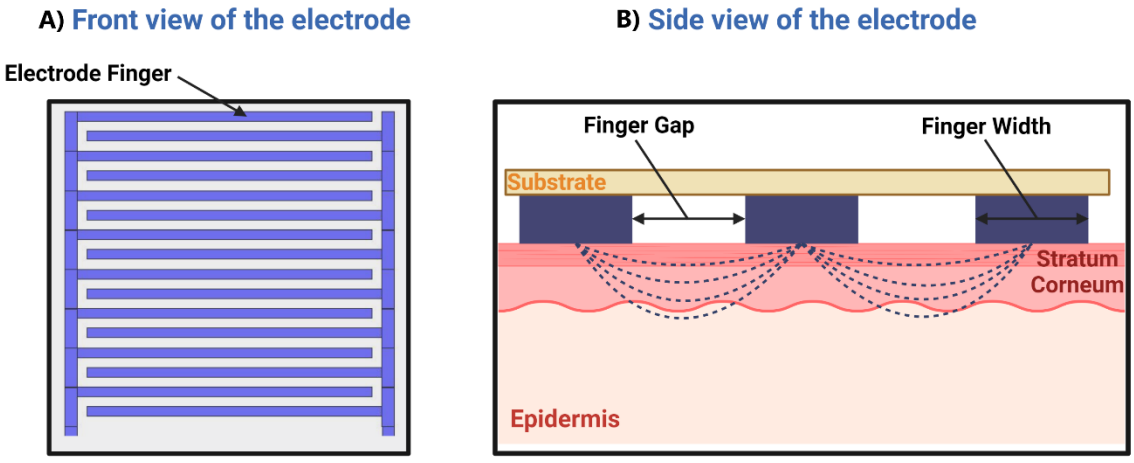

Figure 21 Generic layout of the IDC sensor used. A) Plan view of a standard IDC sensor arrangement - two vertical electrodes, called arms, with protruding fingers insulated from each other; B) Side view of the IDC electrode in contact with the skin and the produced electric field.

When a power supply is connected across the arms, charges build up on the edge of the fingers and an electric field is established across the gaps. Because the electrodes are thin, most of the electric field lines radiate in the Z-direction, out of the plane of the IDC. When the sensor is placed flat on a material with a higher dielectric permittivity than air, the electric field lines focus within the material, because of the higher number of ionising particles. That is why on the opposite side of the electrode, there is almost no imposed electric field. The greater number of electric dipoles result in a larger ability to store electric charge, which is physically represented as higher dielectric permittivity and higher capacitance. Thus, the IDC's capacitance is sensitive only to changes in the dielectric properties of the MUT in contact with, and from measuring the capacitance the latter can be calculated. The geometry of the IDC affects the strength of the emitted electric field and hence the measured capacitance. That is because the penetration depth of the electric field is dependent on the geometry. Since the skin is a heterogeneous material with distinct layers the geometry of the IDC plays a pivotal role to focus the electric field at a specific depth. As it was presented in Eq. 4, capacitance is also influenced by the area and distance separation between the electrodes. Therefore, the dimensions of the IDC all play a role in the capacitance measurements – gap width, finger width, finger length, number of fingers, electrode thickness. There are limited resources in the literature investigating IDC sensors on a multi-layered MUT like the skin. Furthermore, there is no accurate multi-layered model of the skin for simulating the response of various electrical sensors, as most models represent the skin as a single unified block of constant dielectric permittivity. That is why this chapter will introduce a new medically accurate skin model and will study the effects of varying different IDC parameters on the measured capacitance with the goal of finding the best geometry with the highest sensitivity towards changes of the dielectric properties of the outermost layer of the skin – the SC, indicator of AD severity. To achieve this, finite element analysis will be conducted.

3.2 Finite Element Modelling of IDC Sensor

Finite element analysis (FEA) is a valuable tool in approximating the behaviour of complex shapes and devices, without the need of producing them in real life. The method segregates the simulated design into thousands of elements of the similar area and volume and solves fundamental mathematical and physical equations for each element individually. The process is performed iteratively, until all elements are accounted for and then the individual solutions are combined to achieve a final answer. The number of individual elements can be controlled to arrive at a finer or broader solution, depending on computational power and time limits. The drawback to FEA is that it cannot fully simulate the nature and interactions of the skin-sensor system and can be less accurate. Nevertheless, it is a necessary tool for optimizing the IDC design and tailoring its parameters to the specific problem.

COMSOL Multiphysics ® was chosen as the preferred FEA software of this project because of its versatility, intuitive user interface, and large computational power. COMSOL houses an advanced computer aided design (CAD) interface for model building and can perform both stationary and transient studies in the frequency and time domains. It also includes a large catalogue of physics modules, which has built-in partial differential equations for computation, so the user does not have to manually input his own. These modules can solve problems from the fields of electromagnetism, acoustics, fluid flow, heat transfer, semiconductor, electrochemistry, mechanics, etc. Moreover, modules can be combined to analyse complex devices that undergo various physical phenomena. The software can also perform stationary and transient analysis both in the frequency and time domain, thus the IDC response can be evaluated at a spectrum of signals. COMSOL was also the preferred choice of analysis for IDCs within the literature, thus it was selected for consistency and comparable results.

3.2.1 Physics Study and Governing Equations

The goal of the simulation study is to determine the electrical behaviour of the device given geometrical parameters and material properties. The output of the simulation should be values for capacitance/impedance. Hence, the AC/DC module with its physics interface for electric currents (EC) and/or electrostatics (ES) were used for the computation. Both interfaces can be used to calculate the electric field and potential distributions of dielectrics and conductors, with the ES focusing on charge distribution following Gauss' Law and EC computing current density using Ohm's Law. The governing equations of both are listed below (Eq. 8 – 11).

$$\nabla . D = \rho \tag{8}$$

$$D = \varepsilon_0 \varepsilon_r E \tag{9}$$

$$\nabla . J = j\omega\rho \tag{10}$$

$$J = \sigma E + j\omega D + J_e \tag{11}$$

Here D is the electric displacement, ρ is the electric charge density, E is the electric field intensity, ε_0 is the permittivity of vacuum, ε_r is the relative permittivity, J is the current density, $\omega = 2\pi f$ is the angular frequency, σ is the electrical conductivity and J_e is the externally created current density.

Because the dimensions of the system are negligibly smaller compared than the wavelength of the applied signal, a quasi-static approximation of Maxwell's equation can be used with a curl-free state of the electric field and is therefore applied with a gradient of the voltage, described respectfully by Eq. 12 and 13 [140]:

$$\nabla \times E = 0 \tag{12}$$

$$E = -\nabla V \tag{13}$$

This approximation is common for both modules and by combining Eq.13 with Eq. 11 and Eq.9, the continuity equation for electric potential is established:

$$-\nabla.(j\omega\varepsilon\nabla V + \sigma V - j\omega D) = 0 \tag{14}$$

The continuity equation is solved iteratively for each element in the analysis and values for the electric field and electric potential distribution can be obtained from it. Thus, values for the impedance and capacitance can be evaluated.

3.2.2 Skin-Sensor System Model

The skin model used in the simulation studies in this chapter is the multi-layered skin. The different layers have different dimensions and dielectric properties. The bottommost layer is the DR, followed by the EP and the SC on the top, the latter of which comes in contact with a metal electrode. Copper was chosen as the material of the electrodes for the simulation because it is commonly used in the literature and all its dielectric properties were already available in the COMSOL materials' library. Silver was also selected during one test, but no measurable difference was found in the capacitance, so copper was used throughout all the simulations. The reason behind this is because in COMSOL's built-in library for the ES and EC studies, all conductor materials have the same dielectric properties. Figure 22 presents a drawing of the entire model, not to scale, and the dimensions are laid out in Table 7.

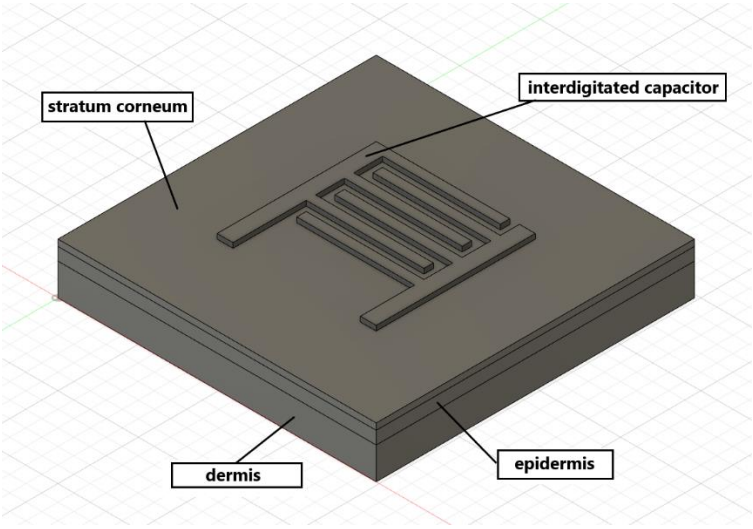

Figure 22 Skin and sensor model for FEA analysis with labels of the different layers. Graphical representation of dimensions is not to scale.

Table 7 Dimensions of the different components of the model presented in Figure 22.

Geometry	Value (mm)
Skin block width	20
Skin block length	20
Dermis thickness	1
Epidermis thickness	0.15
Stratum corneum thickness	0.025
Electrode thickness	0.02

To fully simulate the real environment, a thin layer of Kapton with the same size of the IDC was simulated to see if there would be any changes to the output and the entire assembly was covered by a block with the dielectric properties of air. It was observed that these surrounding media induce no alteration of the capacitance output, because their relative permittivity is negligible compared to that of the skin-sensor interface. The variation of the size of the skin block was also examined, as it was reasoned that since it is the main factor driving the capacitance calculation a bigger skin block with big permittivity values should have effect. It was discovered that if the block's top area is at least four times as big as the IDC sensor's area, the capacitance read-out does not depend on the sizing. Finally, the thickness of the electrodes was varied but it was discovered that the capacitance changed with less than 2% after increasing the thickness from 20 μm to 500 μm. These values were selected from standard etched copper electrode values to exaggerated numbers in order to determine the impact of electrode thickness. Therefore, the geometry of the surrounding media does not interfere with the capacitance measurement, and the variables that directly affect it are the internal dimensions of the IDC such as the gap between fingers (G), number of fingers (N), finger width (FW) and length (FL), because these affect the produced electrical field that passes through the skin and the area of the electrode.

3.2.3 Dielectric Properties of Multi-Layered Skin Model

As discussed in the literature review, skin with AD symptoms features a dysfunction in the barrier integrity of the outermost skin layers, resulting in a specific dehydration of the SC layer and upper parts of the EP. Since the presence of free water molecules affects the dielectric properties of these layers, by changing the relative permittivity of the SC and EP layers, different severity states of the condition can be simulated. In COMSOL the variation of the relative permittivity of any

material can be easily achieved when selecting the material properties for each component of the model. As the model is a multi-layered skin block, this permittivity control will only be applied to the SC and EP layers, and the DR layer will be kept constant, because in AD the DR layer is not severely dehydrated. COMSOL does not have a bult-in material for human skin, so a new material will be created, and the relative permittivity and electric conductivity will be input manually. The prevalent source from literature regarding these values is Gabriel et al.'s database, which was discussed in section 2.2.5.2. It features permittivity and conductivity values for wet and dry skin (in this case clinically normal skin) in the range 10 Hz – 10 GHz [71]. As discovered in the literature review, the frequency range for the excitation signal of the IDC to be sensitive to changes in the outermost layers of the skin is between 10 kHz and 10 MHz, and most commercial skin hydration sensors utilize 1 MHz. The corresponding value of relative permittivity at 1 MHz from Gabriel et al.'s database is around 1100 for dry skin and around 30000 for wet skin. No empirical measurements were ever performed to measure the permittivity of severely dehydrated skin or skin with AD. Yao et al. used an extrapolation method to simulate dryer and wetter skin, based on Gabriel's database [69]. The same extrapolation method was applied in the studies performed here, to simulate permittivity values of skin with AD.

3.2.4 Overview of COMSOL Studies Performed

Three independent studies were conducted to simulate the behaviour of the IDC based on controlled conditions. The goal with each study is to discover the variables that increase the sensitivity of the IDC – greatest change in capacitance per change in permittivity of skin with AD. The first test varied the geometric dimensions of the IDC to determine how they affect the sensitivity. The second test investigated the strength of electric fields penetrating the skin, based on the different gaps discovered in the first test. The final test introduced the frequency dependence on the skin-sensor system to explore how the frequency of the excitation signal affects the measurement depth and sensitivity.

3.3 Study on the Geometric Parameters of an IDC

3.3.1 Study Setup

The goal of this study is to determine how the geometric dimensions of the IDC affect the capacitance when in contact with a multi-layered MUT. Resources in the literature were limited for this application, that is why this test was undertaken. The hypothesis from the literature is that smaller gaps between fingers result in shallower penetration of electric field lines and therefore increased sensitivity towards superficial skin layers. Other variables such as FW, FL and N should

act as scaling parameters for the capacitance, but it is important to investigate their behaviour as well.

The stationary analysis study with a parametric sweep and the EC physics interface was the chosen method of computation. This setup allows for easy evaluation of capacitance, as COMSOL has a built-in solver for global evaluation. The method of evaluation was also checked against a fabricated IDC sensor in the literature made by Yao et al, and it produced similar capacitance read-outs [69]. Terminal voltage conditions with values of 1 V and 0 V were set on the two electrode arms. The physics-controlled mesh with a fine element size was selected. New material was created for the study and applied to the skin layers with its relative permittivity set as a parameter. The parametric sweep allows to simulate varying hydration conditions of the skin with AD by sweeping across a range of values of the relative permittivity of the SC and the EP. For severely dry skin the permittivity will be really low, whereas for hydrated – very high. There is no empirical data on the permittivity of skin with AD from the literature, that is why the range of values were extrapolated from Gabriel et al.'s database following a technique used by Yao to simulate really dry skin [69, 71]. The range of values used in the parametric sweep was: 50, 100, 200, 500, 700, 900, 1000, 1100, 1200, 1500, 2000, 3000, 5000, 7000, 10000, 12000, 15000, 20000, 25000, 30000. This range was applied to the permittivities of the SC and the EP only, because that is where the AD barrier dysfunction is most prominent, and the permittivity of the DR was kept constant at 1100. The output of the entire system is the values of capacitance of the sensor at each permittivity step.

3.3.2 Gap Between Fingers

The gap between the IDC fingers is an important metric in determining the capacitance because it determines the depth of the penetrating field [126]. According to the literature, smaller gaps result in finer measurements and higher sensitivity. The lower limit for element size within standard fabrication equipment available is 50 μm. Anything below that incurs too high cost of production. The range of gap sizes explored within this analysis will be 50, 100, 200, 300, 400, 500 μm, as the trend becomes apparent. Larger gaps are investigated later, when the scaling up of the IDC is investigated. All other IDC dimensions were kept constant: finger width (FW) was 200 μm, finger length (FL) was 3mm, number of fingers (N) was 8. The results are presented Figure 23.

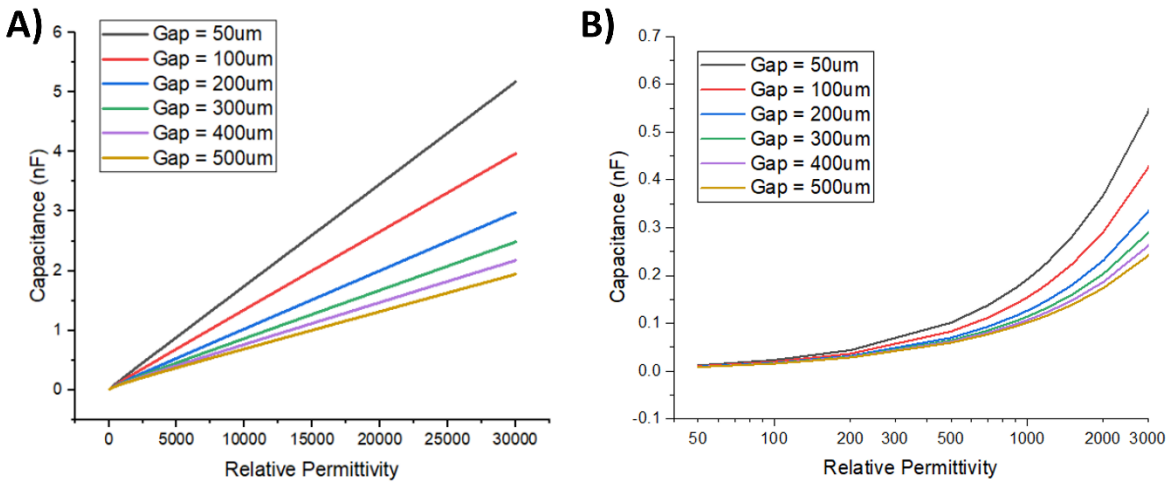

Figure 23 Capacitance vs. relative permittivity of SC with variation of gap between electrodes. Full permittivity range in A) and a magnified view of lower permittivity end in B).

The results confirm the hypothesis laid out by the literature – finer gap sizes result in a greater capacitance change per change of relative permittivity. The effect takes on an exponential behaviour, as seen in Figure 23, where 50 µm gap size is presenting the best performance, but it is the most difficult to fabricate. Due to these limits, IDCs with gaps of 100 and 200 µm will be the focus of this research, as they offer the second-best sensitivity. To confirm the validity of the results, a contour of the electric field passing through the skin was plotted, presented in Figure 24. Most of the electric field lines pass through the SC and the EP, and the field is considerably stronger in the SC, thus electric screening for hydration is performed in the right place.

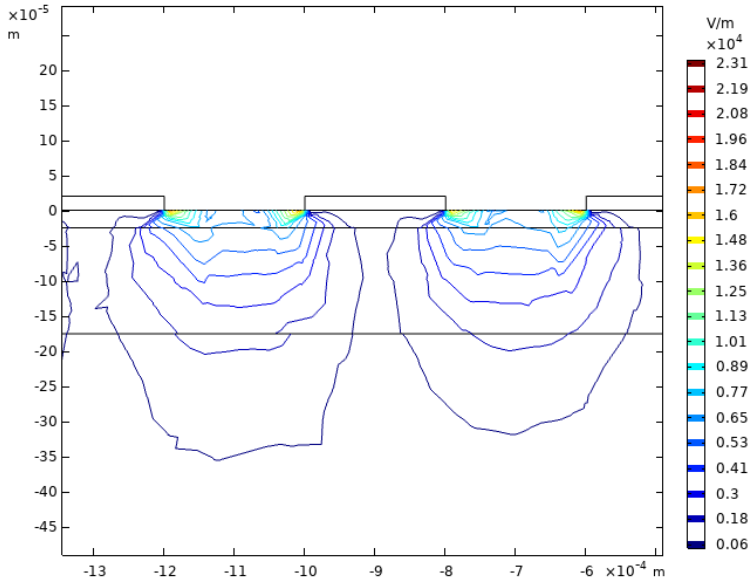

Figure 24 Contour plot of the electric field lines penetrating the SC and the EP layers of the skin. The gap between the electrodes and their FW are both 200 µm. Contour tool was used to only present the electric field within the skin layers.

3.3.3 Number of Fingers

An IDC can be approximated as consecutive capacitors all connected in parallel. The number of fingers dictates the number of capacitors connected. Thus, by having more fingers the capacitance output should increase, because capacitors connected in parallel sum up their capacitance. Zoric et al. states a formula for the capacitance of an IDC, where C_{uc} is the capacitance between any two pairs of fingers and L is the length of the fingers, and N-1 is effectively the number of gaps [141]:

$$C_{TOTAL} = C_{uc}(N-1)L \tag{15}$$

During this simulation the gap size was kept at 200 µm, the FW was at 200 µm, and the FL was at 3 mm. The number of fingers was increased by 2 (to keep the symmetry) from N=6 to N=14. Figure 25 illustrates the results.

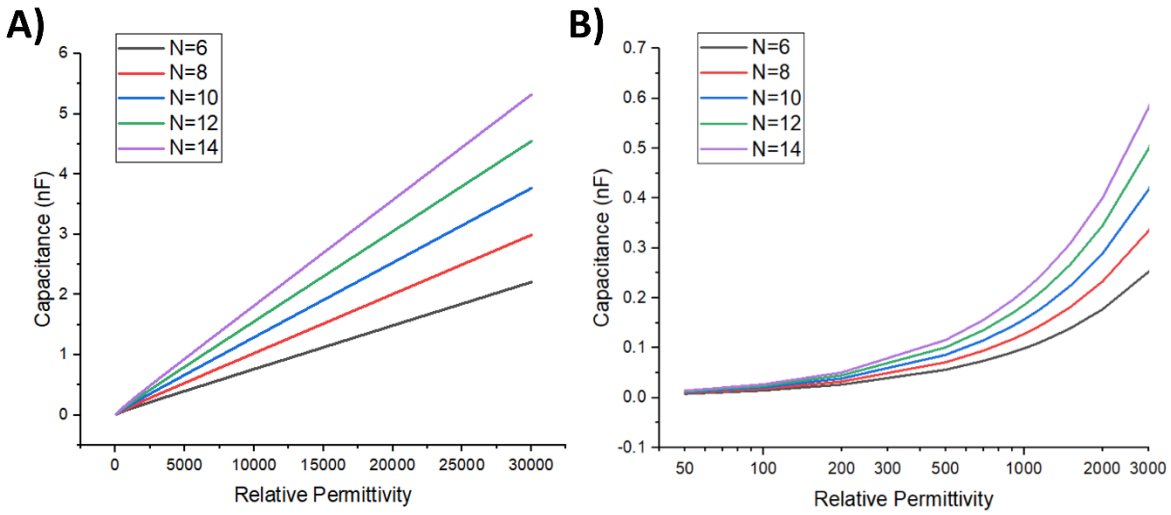

Figure 25 Capacitance vs. relative permittivity of SC with variation of number of electrode fingers. Full permittivity range in A) and a magnified view of the lower permittivity end in B).

It is observed from the graphs that each pair of electrode fingers added to the IDC increases not only the total capacitance but also the sensitivity as the slope of the lines becomes steeper. Hence, a build with as much fingers as permitted by the sensing area will be incorporated in the final design of the IDC sensor.

3.3.4 Width of Fingers

The fingers are the capacitance plates onto which charges build up and establish the electric field. Bigger plate area would suggest more space for charges to accumulate and thus higher capacitance values. The FW was tested with the same range of values as the gap, because in the

literature usually these two parameters have the same dimension: 50, 100, 200, 300, 400, 500 µm. The gap was kept at 200µm, FL at 3mm and N at 8.

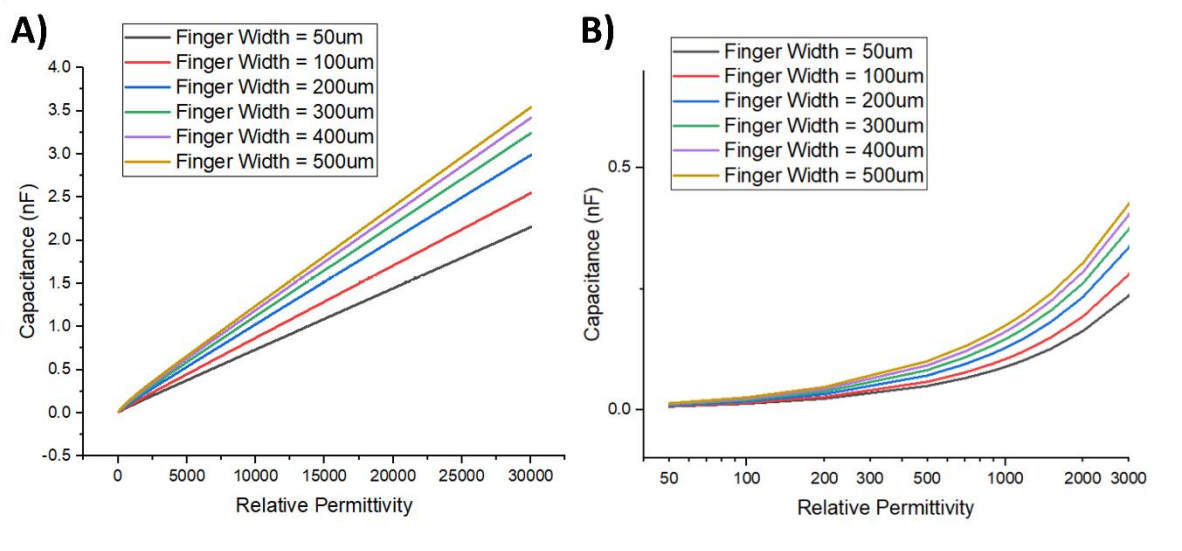

Figure 26 Capacitance vs. relative permittivity of SC with variation of width of electrode fingers. Full permittivity range in A) and a magnified view of the lower permittivity end in B).

The variation of the FW has limited effect on the sensitivity of the sensor, especially in the lower end of the permittivity range. Because the gap was kept constant, the increased sensitivity and capacitance values at the higher FWs could be since the fingers appear closer to each other in comparison to their width. During this project, the fingers will be kept the same width as the gap, for consistency with the results from the literature.

3.3.5 Length of Fingers

The FL affects the area of the fingers, thus introduces more area for charge storage. Zoric et al. discovered that the total capacitance of an IDC sensor increases linearly with the increase of the finger length [141]. To test this claim, the length of the fingers was increased in the following manner: 2, 3, 4, 6, 8, 12 mm. The gap and the FW were set at 200 µm, and N was 8. The results presented in Figure 27 agree with the literature. The capacitance read-out at any permittivity value effectively doubles as the FL is doubled. Thus, a longer IDC sensor would be easier to measure and less susceptible to noise. Since the same conclusion was discovered for the increase of N, a comparative test of the sensitivity of each is done. Sensitivity, or the change of capacitance per change in optimized parameter, is better than measuring total capacitance, because it is more challenging to keep the sensor area the same when varying the different parameters. Thus, for a value of permittivity of 1000, which is the average for healthy skin, the change in capacitance was measured after doubling FL in one test and doubling N in another (all other parameters were kept constant G=200, FW=200). In both cases, the total capacitance approximately doubled, with a

difference between the sensitivity of less than 1%. So, both FL and N act as scaling parameters that can be used to increase the capacitance range to higher values, which are easier for measurement.

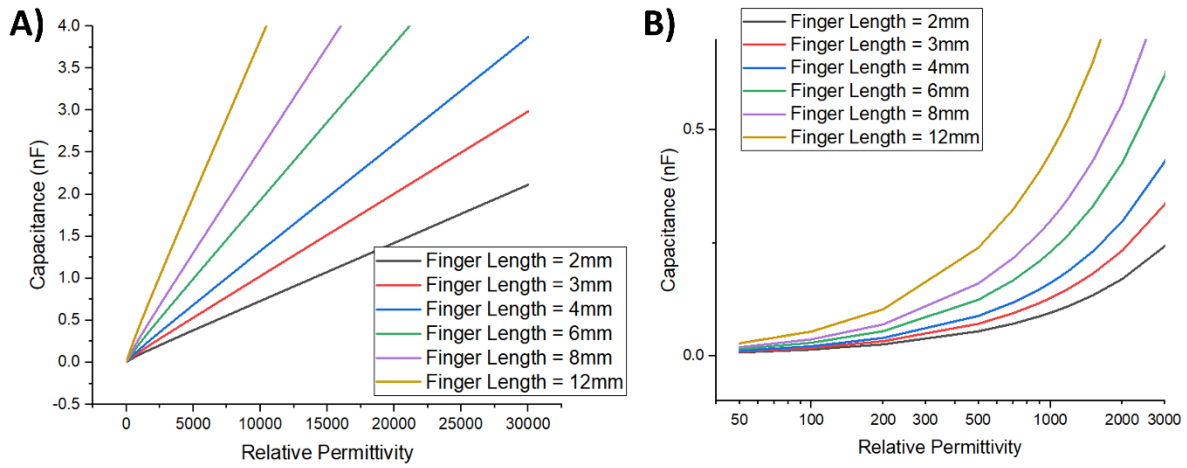

Figure 27 Capacitance vs. relative permittivity of SC with variation of length of electrode fingers. Full permittivity range in A) and a magnified view of the lower permittivity end in B).

3.3.6 Scaled-up IDC

So far it was established that the area of the finger electrodes influences the capacitance, as a sensor of larger area (longer fingers) has a bigger capacitance output. It is worth exploring the behaviour of a scaled-up version of an IDC, where all dimensions are increased by the same order of magnitude. The ratio between the area of the IDC and the area of the skin block were kept the same, to make sure that the changes in sensitivity do not arise from a mismatch between the size of the IDC and the skin block. The FW was increased to 1mm, N was kept at 8, the electrode arms width and length were 1mm and 20 mm, respectfully and the skin block's width and length were both 40 mm. The same parametric sweep was simulated on this setup, and the gap was varied in size – from 0.5 mm to 2 mm. It was hypothesised that due to the increase in overall area, the capacitance should also increase accordingly. The response is illustrated by Figure 28.

The scaled-up version of the IDC does not achieve a higher capacitance as evident from the graph. The G=1 mm, FW=1 mm model produces the same capacitance/permittivity plot as the G=0.1 mm, FW=0.1 mm model. Bigger gap sizes than 1 mm degrade the sensitivity of the IDC, which can be explained by the deeper penetration of the electric field. If the electric sensing is performed deeper than the SC and the EP, the influence of the latter two's high permittivity decreases and thus the capacitance depends on the permittivity of the DR, which stays constant. Thus, big IDC models with large gaps are rendered useless for sensing the hydration within the

SC and EP. Another problem arising from modelling the big IDC is that the mesh has to be refined to accommodate all elements of the study, as the SC thickness and copper thickness are too small compared to the other dimensions in the model. This requires more computational power and time, so the performance will also be assessed in practice, alongside the testing of the other IDCs after their fabrication.

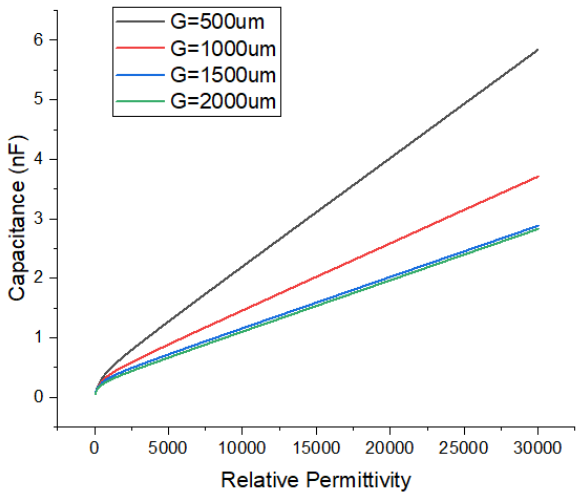

Figure 28 Capacitance vs. relative permittivity of SC with variation of gap sizes in scaled-up IDC model.

3.3.7 Summary of Results

In this study the geometric parameters of the IDC were investigated for the purpose of increasing sensitivity towards distinguishing varying severity of skin with AD. It was discovered that the G distance between neighbouring fingers plays major role in determining the measurement depth of the electric field lines and thereby the sensitivity towards dielectric changes in that layer. Gaps of 200 μm or less are suitable for screening in the SC and EP layers. The G of 50 μm is the best, but it will impose challenges in fabrication, that is why G of 100 and 200 μm will be the focus of this research paper. Oher geometric parameters such as N, FW, and FL affect the capacitance as a scaling factor, but do not change the sensitivity. It was also discovered when scaling all parameters together (with a G of 500 μm and N = 10), the capacitance does increase slightly in value, but sensitivity actually decreases, as the larger gap means deeper penetration in the skin. This will be tested in vivo as well, but it introduces the importance of constant area when comparing between IDCs designs to focus only on capacitance changes due to increased sensitivity.

To ensure comparability between different G sizes of IDCs when testing sensitivity further, the sensing area will be kept constant. Larger numbers increase the measured capacitance range, making it easier for electrical equipment to read it. But the total area of the IDC should not be too

big, because it then loses resolution when testing in vivo on lesions of AD, because it will encompass neighbouring skin in addition to the lesion. Therefore, it is decided that the FL will be kept constant across all IDCs at 6 mm and FW will be the same as G. N will then be varied, according to the value of G, in order to keep the sensing area of each IDC constant at 0.384 cm^2. Starting at a G = 50 µm, and N = 64, other IDC solutions can be built by doubling the G by 2 and dividing the N by 2. Table 8 introduces all possible configurations of the IDC. Not all of them will be empirically tested as the focus is on the smaller G size IDCs, and the larger ones will be used to prove insensitivity towards skin with AD. The naming convention is also outlined.

Table 8 IDC sensor configurations designed within the scope of this project to determine the most optimal one for the application of AD severity measurement.

IDC Name	Gap (µm)	Number of Fingers
G50 N64	50	64
G100 N32	100	32
G200 N16	200	16
G400 N8	400	8
G800 N4	800	4
G1600 N2	1600	2

3.4 Study on the Penetration Depth of IDC Electric Field

3.4.1 Study Setup

To further solidify the findings that a narrow gap IDC would be most suitable for screening the SC and the EP and not the DR a different study in COMSOL was performed. AD affects only the hydration state of the SC and the EP so the sensor must be most sensitive to permittivity changes in those two layers. There is no fixed penetration depth for electric field lines emerging from IDC, as theoretically the electric field lines spread into infinity, but their intensity decreases exponentially the further they are from the source [131]. For an IDC, the penetration depth would be the region where the strength of the electric field is higher and where a change in the dielectric properties of the medium would result in the greatest variation of the electric field intensity and

in return, a change in measurable impedance or capacitance. That is why a new set of experiments was performed in which the electric field intensity was measured along the negative z-axis (penetrating into the skin) as the permittivity's of the different layers were individually variated to simulate different states of hydration. This study was done for several types of IDC from Table 8 – from G100 N32 to G1600 N2, where total sensing area was kept constant and just the G and N were varied.

A parametric sweep study was setup in COMSOL, in which the permittivites of SC, EP and DR were individually parametrized to be from a set of predefined values. The range of values was limited in comparison to the previous studies, to significantly reduce the total computational time, as in a parametric sweep study, COMSOL solves the system for each possible combination of the three parameters. The set of permittivity values chosen here was [100, 500, 1000, 2000 and 5000] – where 1000 is considered again to be the permittivity of normal healthy skin layer, 100 would be severely dehydrated skin layer and 5000 would be artificially wetted skin layer. Each of the layers could be assigned a permittivity value from the set, independent of the other layers, resulting in a total of 5x5x5 = 125 total cases solved. For AD, it is known that the SC and the EP are severely dehydrated, whereas the DR is normal – so the combination of layer's relative permittivites that would apply to this case would be: (100, 100, 1000) for the SC, EP and DR, respectfully. Therefore, by looking at other combinations of layer's dielectric constants (simulating varying skin conditions), this study can confirm the correct design for an IDC to be used in AD monitoring and is possible to uncover a different application for IDCs. All other study and physics settings were kept the same as in the previous study.

For each of these individual combinations of layer's dielectric permittivity, the normal electric field along the negative z-axis was calculated. This is the electric field inside the skin, and its values change with depth and with the dielectric constants of the medium it passes – in this case the SC, the EP, and the DR. The axis used to calculate the field was positioned in the centre of the IDC, for symmetry, and in the middle between two adjacent fingers, because that is where individual electric field lines emerging from the signal electrode finger should reach their maximum depth before converging into the adjacent ground finger.

3.4.2 Electric Field Strength against Depth

In Figure 29 the electric field graphs for G100 N32 are presented, where both the SC relative permittivity and the DR relative permittivity are independently varied. They are most indicative of the thesis that smaller IDC gaps are more sensitive to shallower layers of the skin. The full depth of the model is not shown, as the lines converge around the point 300 μm.

In Figure 30, the electric field graphs of the G1600 N2 IDC are presented, where the increase in sensitivity in the deeper layers like the DR is observed. Here, the full depth of measurement is shown, as the change in electric field at deeper levels is significant.

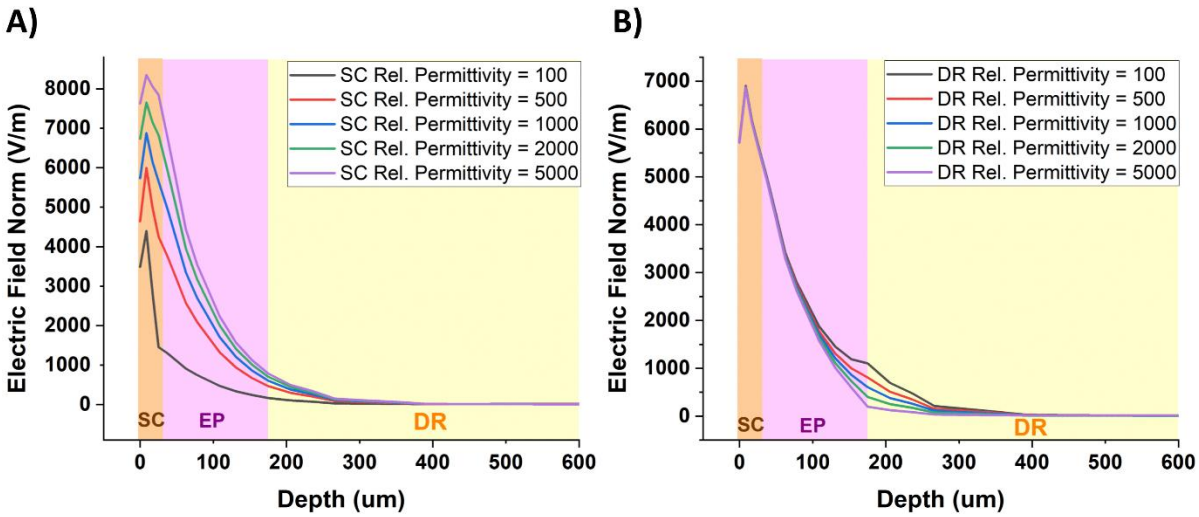

Figure 29 Electric field against depth of a G100 N32 IDC with a varied relative permittivity of: A) the SC; B) the DR. The layers of the skin are colour coded according to their depth.

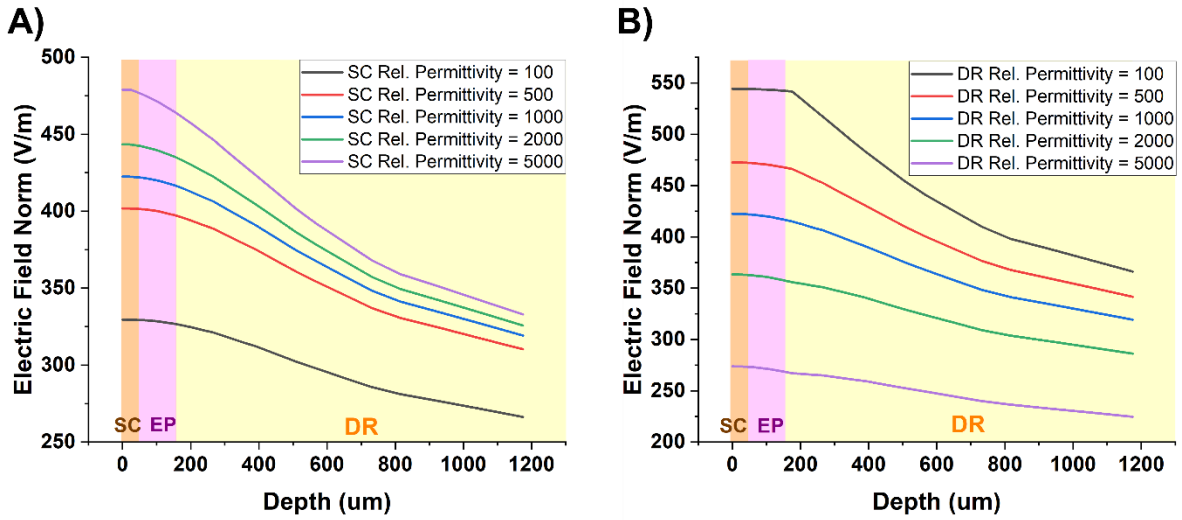

Figure 30 Electric field against depth of a G1600 N2 IDC with a varied relative permittivity of: A) the SC; B) the DR. The layers of the skin are colour coded according to their depth.

It is evident from Figure 29 B) that for the G100 IDC, the change in the dielectric properties of the DR elicits almost no change in the electric field at the depths of interest – below 150 µm, where the EP layer ends. At the same time in Figure 29 A) the SC permittivity does have a significant effect on the spread of the electric field lines. This confirms that smaller gaps such as the G100 are the most optimised for measuring in the shallow layers of the skin. In Figure 30 the opposite is observed - the electric field intensity along the negative z-axis arising from larger IDC electrode

gaps is influenced more by the deeper layers of the skin. The change in permittivity in the DR affects the electric field intensity more than the change in the permittivity of the SC. This means that the change in the dielectric properties of the DR would result in a larger change in overall capacitance than the change in the dielectric properties of the SC. Thus, wider gap IDCs are less sensitive to changes in the shallow SC and EP layers than the narrow gap IDCs and are instead sensitive to changes in the deeper DR layer.

3.4.3 Capacitance vs. Variation of Permittivity

To further test the insensitivity to smaller gap IDCs towards permittivity changes below the EP, a new computation is performed, where instead of electric field, the total capacitance is calculated as the permittivity of individual layers is varied.

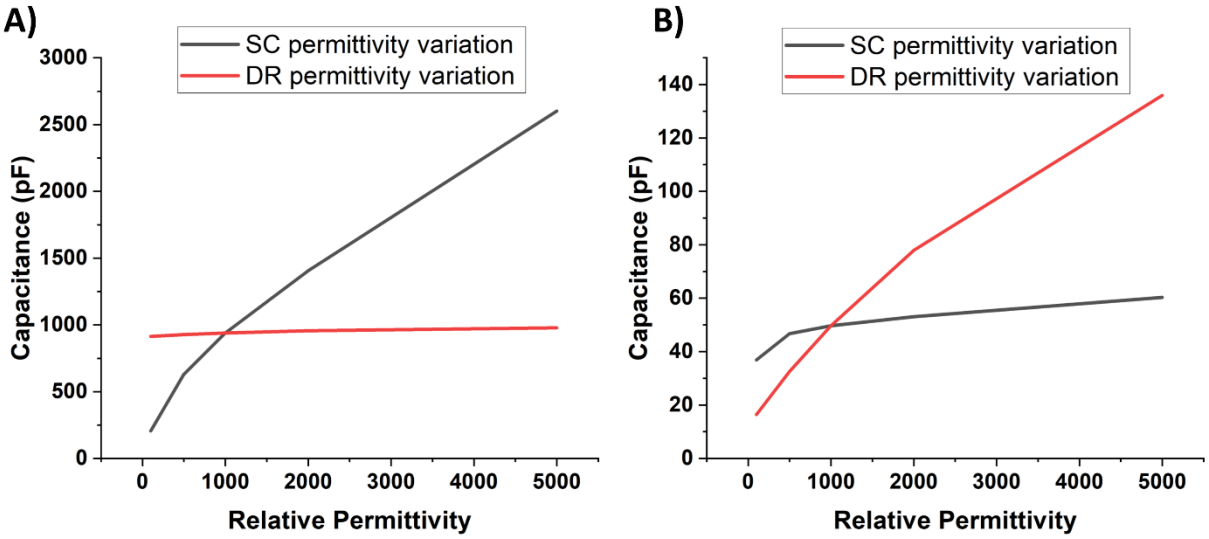

Figure 31 Capacitance vs. relative permittivity, where the permittivities of SC and DR layers of the skin are independently varied. A) is the capacitance plot of a G100 N32 IDC and B) is the capacitance plot of a G1600 N2 IDC.

It can be seen from Figure 31 A) that in the G100 case a change of dielectric properties in the DR layer would amount to no change in overall measured capacitance. On the other hand, the G100 is very sensitive to changes in the SC, as the capacitance varies by orders of magnitude. In Figure 31 B) the opposite is observed for the G1600 case – a greater variation of impedance is caused by the change in the DR, making it more sensitive to that layer than to the SC layer.

This results in an overall deeper penetration depth for larger IDC gap sizes, and shallower penetration depth for lower IDC gap sizes. Considering AD is most prominent in the SC and EP regions, a smaller gap IDC would be most suitable for this application.

3.4.4 Analytical Solution

An analytical solution was also used to calculate the capacitance of the IDC using the relative permittivity values obtained from Gabriel's database [71]. This was done to confirm the validity of the simulation results. The theoretical capacitance calculations also serve as closed-form validation for the COMSOL simulated capacitances. To perform the analysis, Eq. 15 from Zoric et al. and Angkawisittpan et al.'s formulae for the capacitance of an IDC were used and fitted following the notation of parameters so far [141, 142]:

$$C_{UC} = \varepsilon_0 (\frac{\varepsilon_1 + \varepsilon_2}{2}) \frac{K(\sqrt{1-k^2})}{K(k)} \tag{16}$$

$$k = \frac{G}{G + FW} \tag{17}$$

Here C_{UC} denotates the unit cell capacitance, or the capacitance between two neighboring electrode fingers; N is the number of fingers; L the length of single electrode finger; ε_0 - the free space permittivity (8.854 x 10^{-12} F/m); ε_1- the relative permittivity of the substrate (polyimide); ε_2- the relative permittivity of the skin; and *K*[x] is a complete elliptic integral of the first kind. An approximation can be made to shorten Eq. 16: since the permittivity of the skin is much larger than the permittivity of the substrate (around 3.5), the latter's component can be disregarded and thus Eq. 16 reduces to:

$$C_{UC} = \varepsilon_0 \frac{\varepsilon_{skin}}{2} \frac{K(\sqrt{1-k^2})}{K(k)} \tag{18}$$

Using Eq. 15, 17 and 18, and the parameters in Table 7, the forward solution is calculated using MATLAB® software – obtaining capacitance values from relative permittivity/hydration variation. The value of 1000 was selected for the relative permittivity of the skin, as in Gabriel et al.'s database it is the value of normal (non-moisturized) skin [71]. The computed capacitance was 1083 pF for the G100 N32 IDC, 524 pF for G200 N16 IDC, and 58 pF for the G1600 N2 IDC. The corresponding values obtained by the FEA simulation performed in section 3.4.3 were 940 pF for the G100, 460.4 pF for the G200 and 49.7 pF for the G1600. The small difference between the values confirms the validity of the FEA study.

3.4.5 Summary of Results

In this study it was proven that smaller IDC gaps – such as G100 or G200 are most suitable for the application of monitoring in the SC and the EP, because the capacitance measured these IDCs is the most sensitive to changes in the properties of the SC and EP. Bigger IDCs such as G800 and G1600 measure deeper into the skin and are suitable for detecting changes in the DR and deeper

skin layers – such as hypodermis or even muscle tissue. The method used to perform these simulation studies was also validated by solving an analytical solution using conventional equations of an IDC's capacitance and arriving at the same calculated capacitance value.

3.5 Study on Frequency-Dependence of Skin Dielectric Properties

3.5.1 Study Setup

The final study performed in this chapter builds upon the discoveries by previous simulations by employing the most optimised solution so far (when considering fabrication limitations) – the G100 N32 and testing it against a skin model with complex dielectric properties. This method was published and is novel to the literature, as it simulates the frequency-dependent relative permittivity and electrical conductivity of independent skin layers, making it possible to isolate the capacitive response of a sensor from a specific measurement depth [124]. Thus, with this layer-separated model skin an accurate representation of skin with AD can be simulated, by ensuring that the SC layer is severely dehydrated, whereas the DR layer is not. Frequency is an important parameter to account for, because the IDC uses an excitation alternating voltage signal to impose a variable electric field on the skin and measure the capacitance. If the skin layers have different permittivity based on the excitation frequency, then the capacitance read-out will be different. Thus, the goal of this study is to determine a frequency range which increases the IDC's sensitivity towards changes in the complex dielectric properties of the SC.

In this case the EC interface was used, instead of the ES physics. The interface solves a current conservation equation based on the current density form of Ohm's law using scalar electric potential as the dependent. A terminal boundary condition with a voltage of 1 V was applied to one of the IDC's electrodes and the other one was grounded. A frequency-domain study is conducted which sweeps through a range of frequency values, solving the continuity equation for every node in the model. The range of frequencies is from 10 Hz to 10 GHz with 5 frequency values per decade. Each frequency would result in a different complex permittivity value for the SC. The same model geometry was used as in the previous studies, but this time only one IDC was simulated – the G100 N32. The full model details along with graphical illustrations are available in Todorov et al.'s publication [124].

3.5.2 Prediction of the Complex Permittivity of Skin with AD

There are no resources available in the literature concerning the complex dielectric properties of independent skin layers or specific skin types. Thus, it was decided to come up with a model that can accurately predict these properties. Gabriel's database was used again as a starting point,

as it parametrizes the complex permittivity and conductivity of dry and wet skin using a dispersion equation. This was explained in more detail in section 2.2.5.2, and so a brief overview will be presented here.

Body tissues, such as the skin, have a dielectric spectrum characterised by 3 to 4 relaxation regions at different frequency ranges and other minor dispersions [71]. These dispersions cause their dielectric properties to be complex, changing with frequency. Gabriel et al. have produced a dataset, in which they've experimentally calculated the complex permittivity of various skin tissues in the range 10 Hz – 100 GHz and have fitted a parametric equation to the dielectric behaviour. This equation is known as the Cole-Cole dispersion equation and in Gabriel et al.'s work it features 4 dispersion terms with 17 parameters in total to characterize the dielectric response of any biological tissue against frequency, presented in Eq. 19:

$$\hat{\varepsilon}(\omega) = \varepsilon_\infty + \sum_{n=1}^{4} \frac{\Delta\epsilon_n}{1 + (j\omega\tau_n)^{(1-\alpha_n)}} + \frac{\sigma_i}{j\omega\varepsilon_0} \tag{19}$$

where $\hat{\varepsilon}(\omega)$ is the complex permittivity of the material, ε_∞ is the permittivity at frequencies where ωτ >> 1, $\Delta\epsilon_n$ is the magnitude of dispersion, ω is the angular frequency, τ_n is the time constant for each dispersion, α_n is the distribution parameter, a measure of the broadening of the dispersion, σ_i is the static ionic conductivity, and ε_0 is the permittivity of free space [71]. This equation can be split into a real and imaginary term, thereby obtaining relative permittivity and conductivity of the selected tissue, as described in Eq. 6 from Section 2.2.5.2 [124]. Gabriel et al. used this equation and found the parameters that satisfy it to approximate the relative permittivity and electrical conductivity of clinically healthy skin.

In this study, data from Gabriel et al.'s work is extrapolated to cover the dehydrated spectrum of the skin, and this data is applied to each skin layer individually, to enable the separation of the dielectric properties of the skin layers. Values for relative permittivity and conductivity were extrapolated from Gabriel et al.'s clinically normal skin using a method by Yao et al. to create two different dielectric spectra - one of skin with AD and one of severely dehydrated skin [69]. Eq. 19 was then fitted to the curve using MATLAB® R2021a to find the unknown parameters of the new dielectric spectra.

The parameters for Gabriel et al.'s clinically healthy skin and this study's skin with AD and severely dehydrated skin are presented in Table 9 and the resulting plots are shown in Figure 32. The parameters for the third and fourth dispersion are omitted, since in Gabriel et al.'s database they are all equal to 0. The parametric solution was then used in COMSOL® to create three new materials: SkinNormal, SkinAD, and SkinSevereDry - each of them had a local function with the

corresponding parameters that uses the frequency as an input and returns the relative permittivity and conductivity. Initially, SkinNormal was applied to all skin layers, then only the material for the SC layer was changed to SkinAD and SkinSevereDry and the model was solved again for each case. As discovered in the previous studies the IDC for AD monitoring should be as sensitive as possible for the outermost layer of the skin, and to ensure that only the SC layer will be simulated here.

Table 9 Parameters of the Cole-Cole equation used to predict the dielectric spectrum of different states of hydrated skin.

Skin Hydration State	ε_∞	$\Delta\epsilon_1$	τ_1 **(ps)**	α_1	$\Delta\epsilon_2$	τ_1 **(ns)**	α_2	σ_i
Clinically Normal Skin	4.0	32.0	7.23	0	1100	32.48	0.2	0.0002
Skin with AD	4.0	34.0	7.23	0	600	8.42	0.2	0.00015
Severely Dehydrated Skin	4.0	34.0	7.23	0	300	3.37	0.2	0.0001

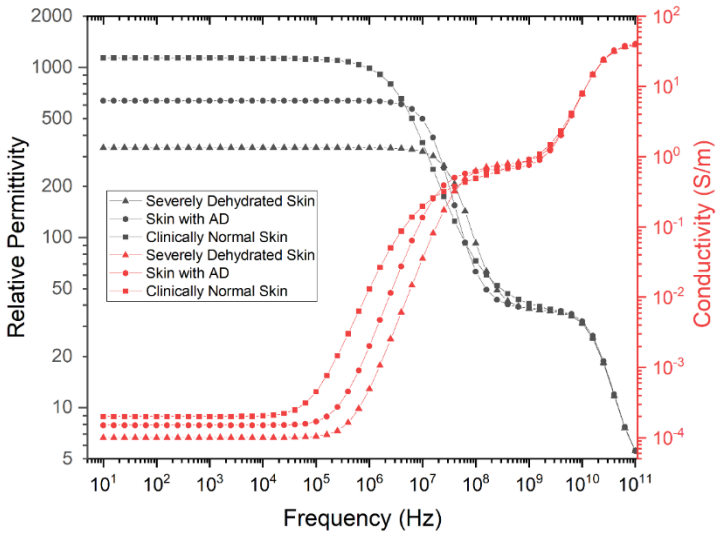

Figure 32 Predicted permittivity and conductivity of three states of skin – clinically healthy skin, skin with AD, and severely dehydrated skin.

3.5.3 Study Results

Global evaluation tool was used to calculate the total capacitance between the terminals of the IDC. To calculate the capacitance in COMSOL®, the imaginary value of the complex impedance Z between the terminals was obtained and then multiplied by the angular frequency and plugged in

as a divisor of 1. The phase was calculated similarly, taking the inverse tangent of the ratio between the imaginary and real components of Z.

Figure 33 presents the resulting plots across the frequency range. It is evident from Figure 33 A) that the plots start aligned, then diverge around 10^4 Hz, and converge back around the 10^8 Hz. Figure 33 B) focuses within this frequency range to highlight capacitance spread. There is about a 200 pF difference between the different hydration states in this region, which is more than enough to be detected by capacitive read-out circuits, thereby allowing a distinction between the severity levels of skin with AD and clinically healthy skin. In Figure 33 C) the phase against frequency is plotted, which reveals an initial RC circuit shape up to 10^4 Hz. In the same frequency range as the one with the highest capacitance spread, the behaviour of the circuit is purely capacitive, resulting in a -90° phase. After that, the phase begins increasing again, indicating some resistive properties, arising from deeper layers of the skin.

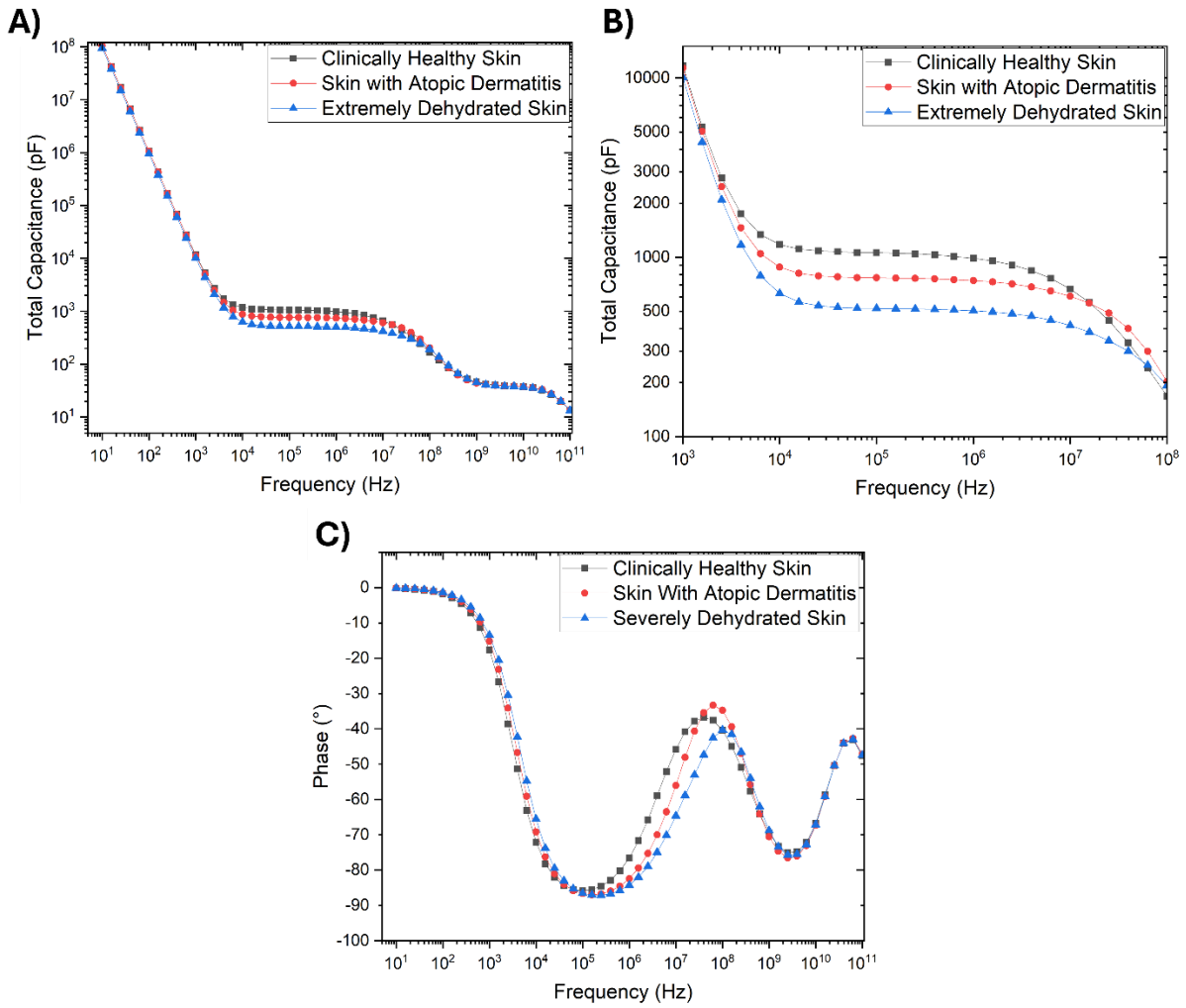

Figure 33 Measurement of IDC sensors' output against frequency for 3 states of skin – clinically healthy skin, skin with AD, and severely dehydrated skin: (a) Capacitance; (b) Inset of Capacitance plot for frequency range of 10^3 to 10^8 Hz, (c) Phase.

To further confirm that the IDC sensor is sensitive only to dielectric changes in the SC, another computation was performed in which the severely dehydrated skin dielectric spectrum was applied to the DR layer of the skin, and the SC and EP layers were kept as SkinNormal or clinically healthy skin. Figure 34 reveals the comparison of the capacitance sweep for clinically healthy skin, skin with AD, and skin with a dehydrated DR layer and there is no measurable difference between the healthy skin and the skin with a dehydrated DR layer.

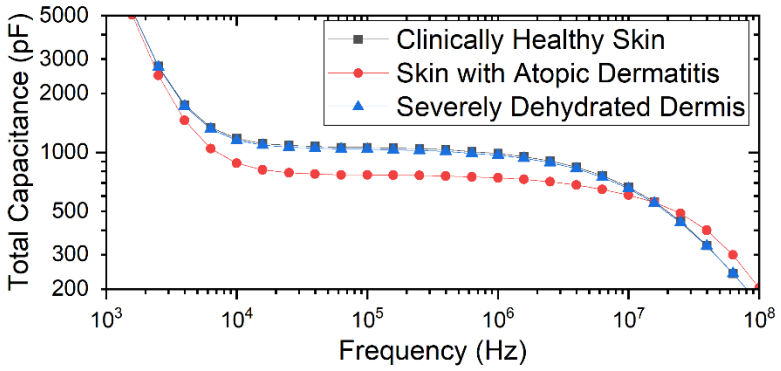

Figure 34 Comparison of capacitance versus frequency sweep for three hydration states of the skin: clinically healthy skin, skin with AD, and skin with severely dehydrated DR layer.

3.5.4 Summary of Results

The simulation shows that an IDC sensor with the geometry of 100 µm gap and finger width is most sensitive towards changes in the dielectric properties of the SC when using an excitation signal frequency between 10 kHz and 10 MHz. This frequency range produces a 200 pF spread between the capacitance spectra of the IDC, which is easily measurable by commercial benchtop impedance analysers like the Wayne-Kerr 6500b, or even small integrated circuit impedance converters such as the AD5933. The phase plots also reveal that at frequencies above 10^6 Hz, the RC behaviour of the SC can be bypassed, introducing impedance terms dominated by the resistive properties of the lower tissue layers. When the SC layer is less hydrated, this transition occurs at a higher frequency value because the capacitance of the SC is lower with low water content. Thus, the optimal excitation signal frequency remains between 10 kHz to 1 MHz.

3.6 Conclusion

The COMSOL simulations of the IDC sensor and its interaction with skin with AD revealed that the total capacitance of the IDC is dependent on the area, whereas the sensitivity towards dielectric changes of specific skin layers is attributed to the gap separation between electrodes.

To achieve a comfortable and easily measurable total capacitance range, a large number of electrodes was chosen over a specific area. It was discovered that scaling the area does not

affect the sensitivity of the measurements, thus the area has been kept constant at 0.384 cm^2 to ensure that it remains smaller when compared to the size of a standard AD lesion – this was done to achieve high resolution in screening. Gaps such as 50, 100 and 200 µm were discovered to be the most sensitive towards changes in the SC and EP layers, whereas IDCs with gaps of 800 and 1600 µm were sensitive towards dielectric changes in the DR layer. Thus, it was proven that smaller gap IDCs are better for the application of distinguishing severity states of AD. A series of standardised IDCs with constant area and variable gap is proposed to be tested empirically to confirm the simulation proof. The G100 N32 IDC emerged out of the study as the best solution, due to the balance between maximum sensitivity and fabrication feasibility.

A novel multi-layered frequency-dependent skin model is presented, which can be used to predict the complex dielectric properties of skin with AD. The model features a parametric solution for the Cole-Cole dispersion and has been published in the literature for other researchers to build upon [124]. With this model a specific measurement range for the excitation signal of an IDC is discovered, to yield maximum sensitivity towards changes in SC layer, and minimum disturbance from changes in the DR layer. The G100 N32 IDC was tested against it, and it was proven to be only sensitive towards SC changes in the range of 10 kHz to 10 MHz.

The proposed sensors in the next chapter will be fabricated to test their performance in a real environment. Simulation software is good for initial analysis but cannot fully simulate all the processes and phenomena that such a system would exhibit. The software relies on assumptions and approximations to reduce computational power, such as isotropic behaviour of the materials and homogeneous density. The skin layers are not homogeneous blocks of uniform density and fixed boundaries; thus, FEA software cannot ensure perfect accuracy.

Chapter 4 Flexible Etched Copper IDC Sensor

4.1 Introduction

The results in the previous section revealed several IDC designs suitable for the application of monitoring skin barrier function in vivo. In this chapter some of these patterns will be fabricated to test the simulation results. The goal of this chapter is to validate the results from the COMSOL® simulation on the sensitivity of the IDC designs. Only specific designs will be manufactured to empirically test whether capacitance sensitivity towards changes in the SC is increased with the decrease of the G distance and if the sensor area affects the sensitivity.

The chapter presents a description of the fabrication method, and the designs used. Following that a characterisation study is performed using a novel multi-layered skin replica that variates different severity levels of skin with AD. The study is repeated under different environmental conditions to determine the range and stability of the flexible IDC sensor's readings. The IDC sensors are also tested on healthy volunteers – measuring the capacitance of the skin after the application of a humectant cream that strengthens the SC barrier properties. Finally, a discussion on the IDC sensor response is presented with conclusions identifying the IDC sensors to be used for further testing on patients.

4.2 Design and Fabrication

An EDA software will be used to design layouts of the sensors. The software of choice is L-edit IC by Tanner Tools, because of its efficiency in design of recurring elements. L-edit uses a hierarchical physical layout procedure, where changes in the design of individual components are automatically updated across any instances of those components in the project. The final drawing will be exported into gerber format, which will be fabricated onto a printing mask. This mask can be used to fabricate metal sensors using screen printing or etching methods.

4.2.1 Copper Etching

Crystal etching refers to a process in which copper traces are etched out of a copper-polyimide laminate sheet following UV exposure through an acetate mask and development. The method of fabrication is taken from Komolafe et al.'s paper [143]. The sheet is cut into the shape of a silicon wafer. To provide a rigid base, the sheet is bonded to a silicon wafer using a photoresist S1813 (Shipley®, Marlborough, USA). Once bonded, the photoresist is dispensed on the copper sheet and spin coated at a 1500 rpm. The resist-coated copper sheet is baked in a carbolite oven at

110 °C for 3 mins. The circuit patterns are transferred onto the resist-coated copper sheet by UV exposure. The acetate mask designed in the previous section was attached to a glass to ensure the patterns are flat and the UV light can pass through. The UV exposure is for 30 seconds. After this, the sheet is developed in a solution of AZ400K developer and water (in a 1:4 ratio) for 10 seconds. The sheet is rinsed in water afterwards. The regions of photoresist that were exposed to the UV light dissolve in the developer, thereby creating regions of exposed copper. Finally, the substrate is ready to be etched in an etch tank containing a solution of fine etch crystals (sodium peroxidsulfate) for 8 mins to remove the exposed copper. The sheet is rinsed in water after etching and the undeveloped resist on the remaining copper is wiped off with acetone.

This method allows for fast and relatively clean fabrication of IDC electrodes on polyimide film substrate. The only drawback is the lack of material variety – the electrodes can only be made of copper. While copper is a good conductor, it reacts with the surrounding oxygen and with the salinity of the skin, causing a redox reaction, which degrades its performance [131]. Polyimide (Kapton) is a stable and biocompatible substrate that has been extensively used to embed circuitry in textiles [143].

4.2.2 Range of IDC Designs

FEA simulations in the previous chapter concluded that the IDCs of gap (G) / finger width (FW) size 50, 100 and 200 µm and subsequent finger numbers (N) of 64, 32, and 16 are best for isolating measurement of the SC hydration. Out of the 3 the G100 N32 IDC is the best balance between sensitivity and fabrication feasibility, as the 50 µm resolution of the G50 N64 is difficult to achieve with the crystal etching method. All the previously mentioned IDC patterns, listed in Table 8, were designed in L-Edit software, as to be ready for fabrication. To confirm the validity of the simulation results 3 different IDCs were fabricated initially for testing the effect of gap and area variation on the sensitivity to SC measurements. These were the G100 FW100 N32 IDC, the G200 FW200 N16 IDC and the G500 FW500 N10 IDC. They were chosen following the results of the COMSOL simulation study – the G100 and G200 were the most sensitive to changes in the SC layer, and the G500 was selected to feature a variation in the sensing area to confirm that boosting the capacitance output by increasing the area will not affect the sensitivity and the wider gap size of 500 µm would be more sensitive to the deeper layers. The first two sensors have an overall sensing area of 38.4 mm^2, whereas the last one has an area of 100 mm^2. Figure 35 A) – C) present the detailed dimensions of the G100, G200 and G500 IDCs respectively. Figure 36 shows a photograph and an optical micrograph of one of the IDC created – the G200 N16.

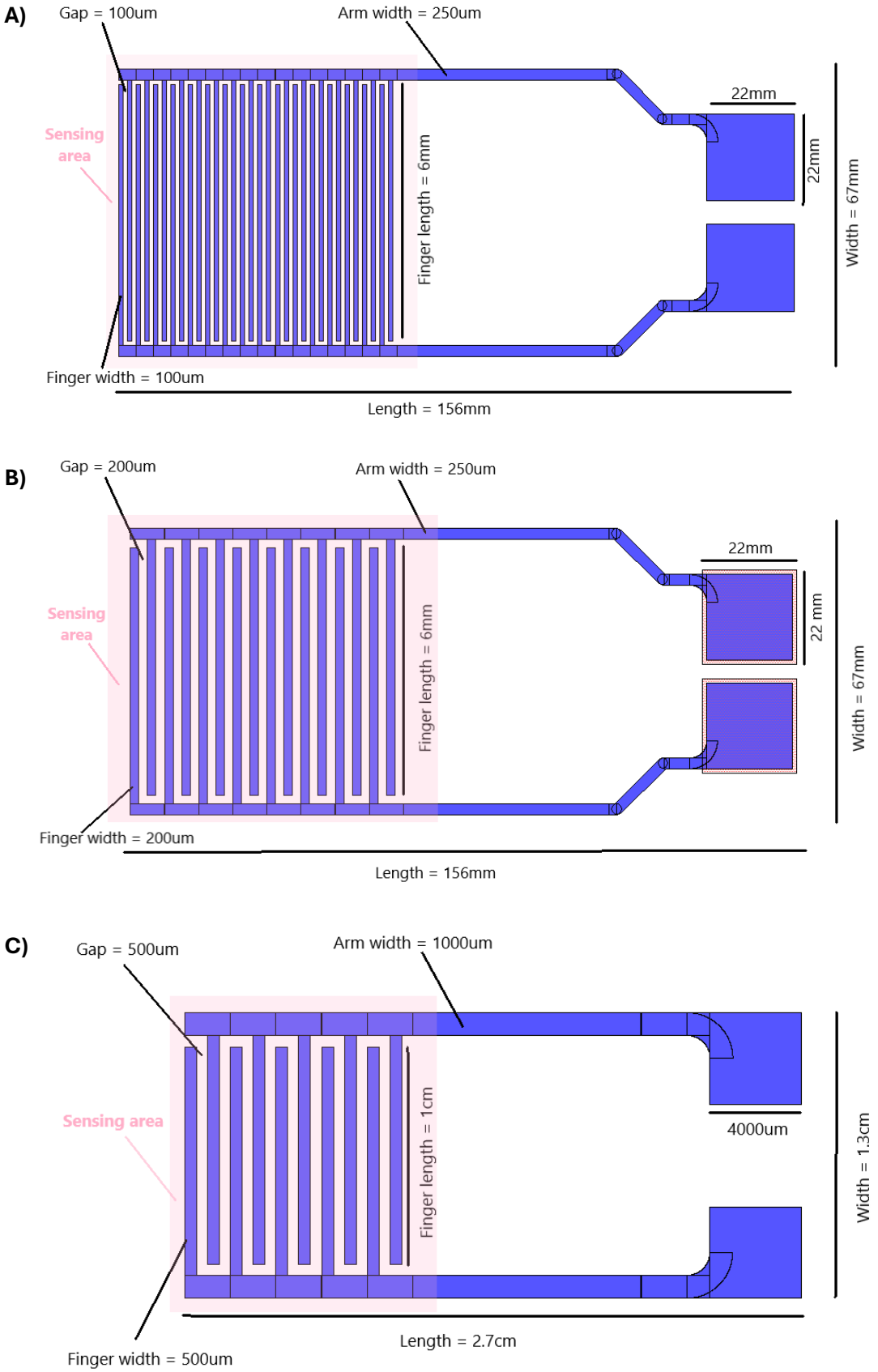

Figure 35 Dimensions of the fabricated IDC designs used in the characterisation study. A) and B) present the G100 N32 and the G200 N16 with the same sensing area of 38.4 mm^2 and C) presents the G500 N10, with its scaled sensing area of 100mm^2.

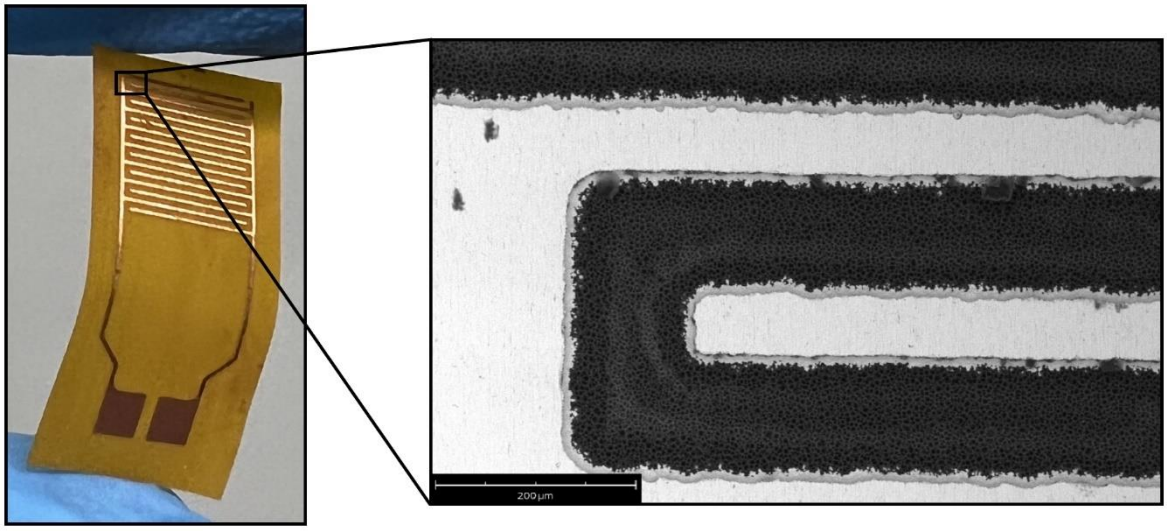

Figure 36 Photograph and a micrograph taken using a scanning electron microscope. The flexibility of the fabricated IDC is presented in the photograph.

4.3 Sensor Characterisation

A thorough characterisation study was conducted using the fabricated IDCs to verify the results of the FEA analysis and to discover the limitations of the sensors. This is a necessary step before continuing tests on volunteers and eventually patients. A novel skin replica with a controllable gradient depth-resolved hydration is produced specifically for this purpose. Also known as a skin phantom, this testing media allows to simulate in vivo various hydration states of the skin, including skin with AD, while controlling the relative permittivity of the phantom. Impedance and capacitance against frequency measurements were performed on the skin phantom using the three IDC sensors. Finally, the effect of environmental conditions is investigated.

4.3.1 Skin Phantom Fabrication

A novel replica of the skin, known as a skin phantom, is used to mimic the effects of severely dry skin. Skin phantoms have been widely used in the literature to test electrode hydration sensors, but none of them replicate the drier spectrum of the skin, which is the focus of the phantom presented here. The phantom features two dielectric layers – the top one, named the SC layer, mimics the properties of a combined SC and EP and the bottom one replicates the DR layer. To control the level of dehydration within the SC layer, the porosity of this layer is varied by cutting a defined number of holes in it. The hydration control via porosity and the fabrication method are explained in detail and adapted from work by Goyal et al [123]. The top SC layer has a thickness of 100 µm and it consists of a mixture of PDMS with 2.5% W/W carbon black powder to increase the conductivity, and 40% W/W Barium Titanate to increase the permittivity. The bottom DR layer has a thickness of 5 mm, and it is a PVA cryogel solution developed using 8.8g of PVA powder

mixed in 50 ml of 0.9% W/W saline solution (0.9 g of NaCl in 99.1 g of DI water). These specific mixtures create a soft and flexible phantom that closely resembles the structure of the skin. In the previous publication by Goyal, this phantom was measured to have an average impedance of 1MΩ and capacitance of10 nF [123].

In this work, the author implements a hydration gradient across a single skin phantom by fabricating regions with different porosities but with the same underlying hydrated DR layer, so that the base is consistent among the tests and the variation relies solely on the SC layer. The different porosities each correspond to a state of dehydration. A 0% porosity SC layer means that there are no pores, the phantom is effectively a pure dielectric, and its behaviour is only capacitive. In reality, skin can never be this dry and will always have some resistive properties, so this region on the phantom was produced to set the baseline. A 0.16% porosity SC layer represented very dry skin, and a 0.28% porosity phantom resembled normal dry skin. The 0.16% porosity layer should approximate the dielectric behaviour of skin with AD. Figure 37 presents an illustration of the skin phantom.

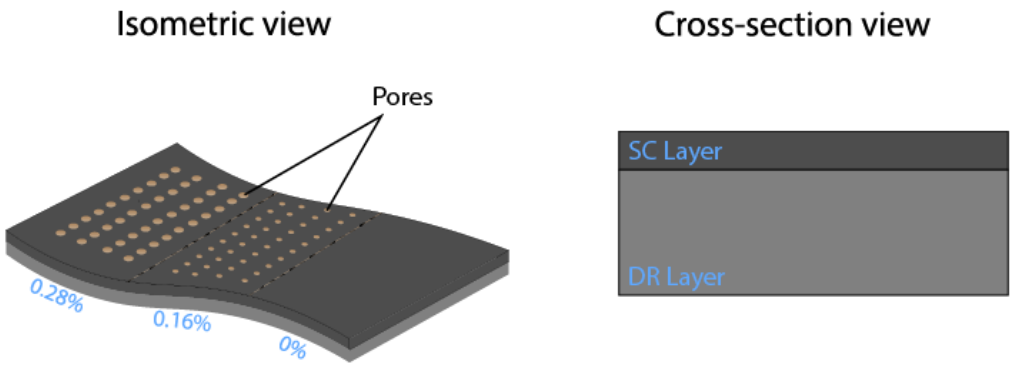

Figure 37 Isometric and cross-sectional view of the novel fabricated hydration gradient skin phantom. The different hydration regions are labelled with their corresponding porosity. The layers of the phantom are labelled in the cross-sectional view with the SC layer replicating a combined SC and EP, and the DR layer replicating DR and deeper tissues. The image and number of holes are not to scale.

4.3.2 Measurement Setup

To obtain impedance measurements from the IDCs, a Wayne-Kerr 6500B Impedance Analyzer was used across the two terminals of the IDC (Wayne Kerr Electronics, Bognor Regis, England). The IDCs were individually tested by being placed directly on top of the SC layer of the skin phantom, and a 5N weight was placed on top to ensure constant pressure. 5N is selected as similar to the force which the final armband holding the sensor would exert on the skin. The weight is made of PLA, an insulator, to ensure that it does not affect the readings. Figure 38 depicts the experimental procedure – during testing the IDC was positioned with the electrodes in contact

with the skin phantom and the weight was placed on top of the IDC. Five measurements on different sites on the phantom's surface were taken, and an average value was calculated. Studies were conducted to source readings for impedance, phase, and capacitance for the frequency band of 100 Hz – 15 MHz.

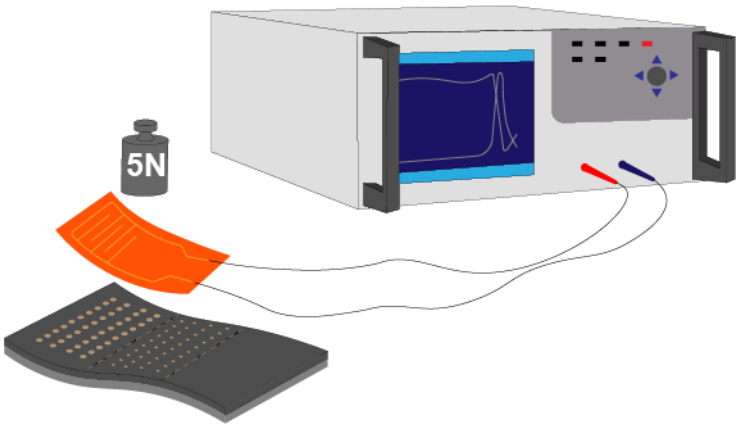

Figure 38 Graphical illustration of the experimental setup consisting of an Impedance Analyzer, constant weight, IDC sensor and hydration gradient skin phantom. The image is not to scale.

To verify the measurements, results were compared to a commercial skin hydration measurement device, a Corneometer® (Courage + Khazaka, Cologne, Germany). The Corneometer® is widely used as a validation for new hydration sensors, and it is considered the gold standard for the field [74].

4.3.3 Characterisation Measurements

The absolute value of complex impedance (|Z|) and phase (θ) of the IDCs were plotted against frequency for the different hydration states, expressed in porosity percentages. Figure 39, 40 and 41 depict the plots of the G100 N32 IDC, the G200 N16 IDC, and the G500 N10 IDC, respectively. The impedance values were normalised with respect to area, to account for the dimension differences between the three IDCs. The phase plots of the 0% porosity for all the IDCs reveal a near positive 90 degrees, which means that the behaviour is purely capacitive, and this is also confirmed by the linearity of the impedance. Therefore, the capacitive elements are prevalent in the complex response, thus measuring capacitance is a valid indicator for the performance of the IDC.

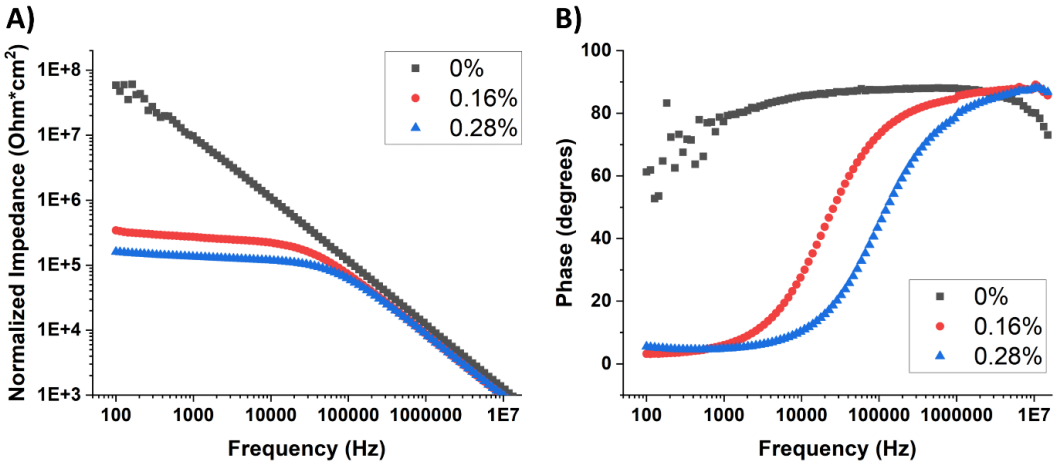

Figure 39 Measurements for G100 FW100 N32 IDC at different porosity regions against frequency: A) Absolute value of complex impedance normalised and B) Phase in degrees. Porosity values are expressed in percentages and correspond to extremely dehydrated (0%), dehydrated (0.16%), and normal (0.28%) SC layer.

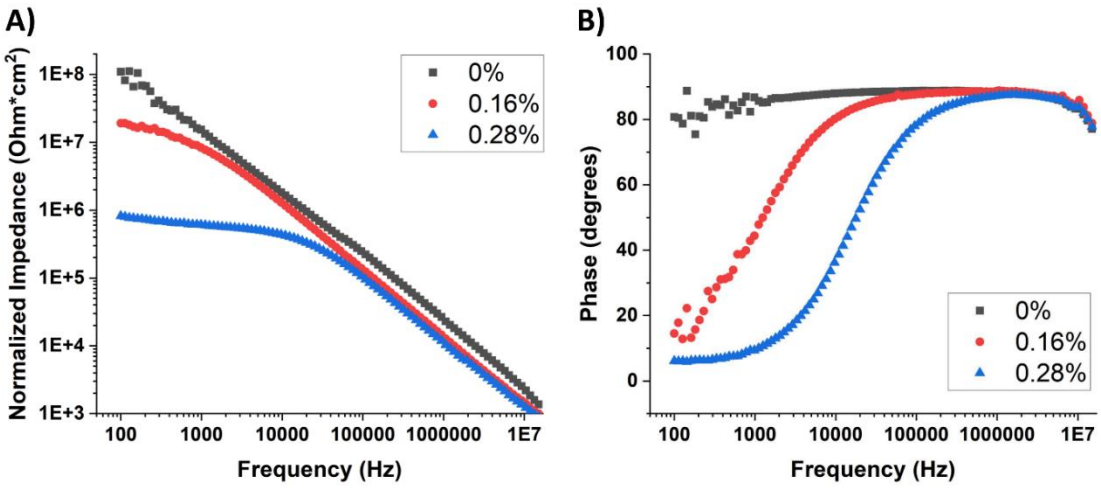

Figure 40 Measurements for G200 FW200 N16 IDC at different porosity regions against frequency: A) Absolute value of complex impedance normalised and B) Phase in degrees. Porosity values are expressed in percentages and correspond to extremely dehydrated (0%), dehydrated (0.16%) and normal (0.28%) SC layer.

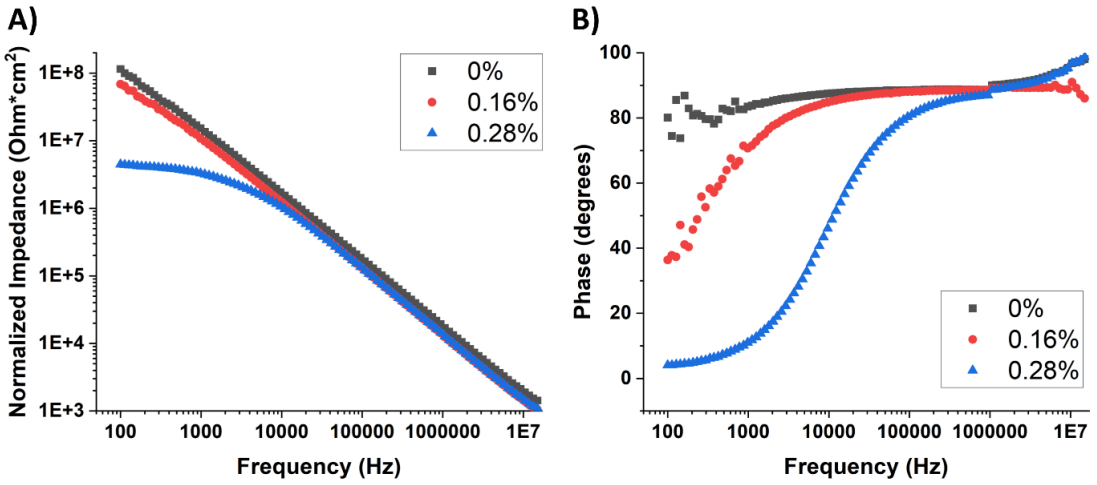

Figure 41 Measurements for G500 FW500 N10 IDC at different porosity regions against frequency: A) Absolute value of complex impedance normalised and B) Phase in degrees. Porosity values are expressed in percentages and correspond to extremely dehydrated (0%), dehydrated (0.16%) and normal (0.28%) SC layer.

Across all devices a specific frequency is observed at which the different porosity plots converge. This frequency is around 100 kHz for the G100 IDC, close to 40 kHz for the G200 IDC, and 8 kHz for the G500 IDC. In the phase graphs, as the G size is increased, the phase plots shift towards the 0% porosity plot at 90°, and the frequency band, at which capacitive properties dominate, is increased. The skin-sensor system can be fundamentally simplified to a resistor and capacitor in parallel. At lower frequencies there is resistive behaviour arising from the ionic pathways of the water molecules, which allow for current to pass through easily, thereby decreasing the total impedance. This is visible in the impedance graphs, in the plots for 0.16% and 0.28% porosity on all IDCs. In the 0.28% porosity phantom, this effect is the strongest, because it is the most hydrated of all other phantoms. As the frequency is increased, this resistive effect disappears, and the skin becomes a pure capacitor. Therefore, to quantify the hydration of the outermost layers of the skin, an excitation signal with a frequency below this limit should be used.

As it was discovered in the COMSOL simulation, the gap size of the IDCs affects the penetration depth the most, and that is also visible in the impedance plots here. The G500 IDC is more influenced by the deeper PVA layer of the phantom, that is why changes in the SC layer introduce little resistive effect on the total impedance (Figure 41 A). In contrast, for the G100 IDC, there is a considerable spread between the impedance values of the different porosity states, because it is most sensitive to changes in the SC layer.

The capacitance versus frequency for the different porosity states is plotted for all IDCs in Figure 42. The same area normalisation was applied as with the complex impedance, and the graphs are plotted in separate windows because of the exponential difference in the measurements for the

G100 N32 IDC and the other two IDCs. The capacitance plots agree with the conclusion that the G100 IDC is the best design as it provides the highest sensitivity and achieves a measurement depth to distinguish dehydration levels of the SC. The G200 and the G500 IDC do show increasing capacitance values for the 0.28% porosity region versus frequency, but they cannot distinguish between the other two porosity levels. Given the plots, the frequency band between 1 kHz – 1 MHz is a reasonable value for the excitation signal, as the capacitance exhibits the highest sensitivity to different hydration states.

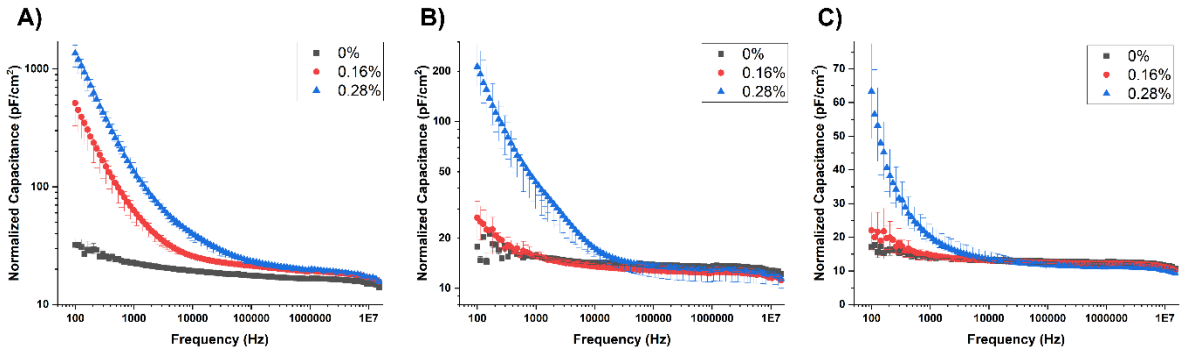

Figure 42 Measurements for the normalized capacitance against frequency at the different porosity phantoms of a: A) G100 FW100 N32 IDC; B) G200 FW200 N16 IDC; C) G500 FW500 N10 IDC. Porosity values are expressed in percentages and correspond to extremely dehydrated (0%), dehydrated (0.16%) and normal (0.28%) SC layer.

To validate the sensor's capacitance readings, the measured capacitance of the different IDC sizes at 1 kHz were compared to the hydration readings of the Corneometer®, which is a commercial skin hydration device. It yields hydration readings in arbitrary units (A.U.) and was used to measure the skin phantom's hydration - the comparison is presented in Figure 43.

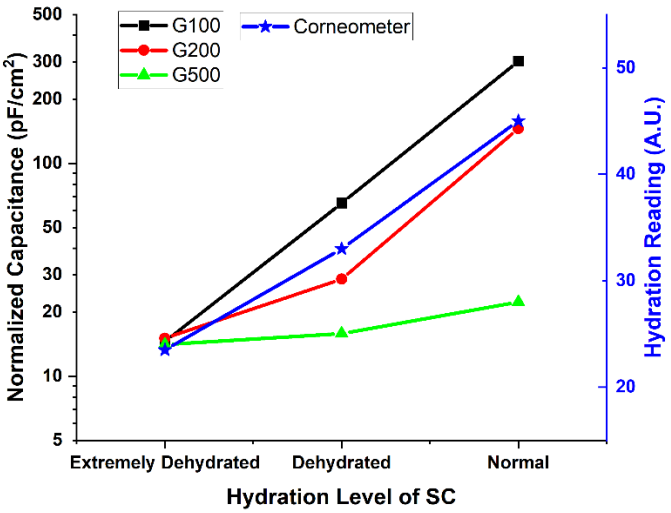

Figure 43 Capacitance readings from different IDCs explored in this paper and hydration readings from Corneometer® against the three different hydration levels of the SC, achieved by the hydration gradient skin phantom.

From the graph, all IDCs follow the trend of increasing capacitance with hydration level. The sensitivity of the individual IDCs can be mapped against that of the Corneometer®, by dividing the change in capacitance of the IDCs between hydration levels by the change in A.U. of the Corneometer® between the same levels. The formula used is presented in Eq. 20:

$$S = \frac{\Delta C}{\Delta H} \tag{20}$$

where ΔH is difference in the commercial sensor's responses for different hydration levels. This results in a sensitivity of 13.1 pF/cm^2 per 1 A.U. for the G100 IDC, 6.08 pF/cm^2 per 1 A.U. for the G200 IDC, and 0.38 pF/cm^2 per 1 A.U. for the G500 IDC. The G100 IDC demonstrates a higher sensitivity towards changes in the SC hydration than the other IDCs, and therefore it is the most optimal for the purposes of AD monitoring.

To equate the impedance and capacitance readings to relative permittivity values, the analytical approach was again used. Following Eq. 15, 17, and 18, the inverse solution was input in MATLAB to calculate relative permittivity values or hydration states from capacitance readings from the experiments. The readings from the 0.28% porosity region were taken, which would equate to normal SC hydration. The capacitance of both the G100 and the G200 IDC at 1 kHz were much lower than the simulations – around 126 pF and 59 pF, respectively, so the computed relative permittivity's were also lower – 116 and 110, which is very different from Gabriel et al.'s values. In the initial conditions of the analysis, it was stated that those values were not for the SC layer specifically, but rather for the skin as a single block. There are other sources in the literature claiming that the relative permittivity of individual SC cells is around 86 – 90 but have not proven it empirically [144]. Moreover, using Gabriel's database for determining the optimal frequency for sensing the capacitance yielded a great sensitivity around 1 MHz, whereas in phantom testing, that is lower, closer to 1 kHz. Thus, Gabriel et al.'s database might not be applicable or appropriate for the purposes of this study. Empirical testing on in-vivo skin will be the determinant for the most appropriate frequency, but skin phantom and FEA analysis uncovered the approximate range for the measurement frequency to be 1 kHz – 1 MHz.

Finally, a stepwise response investigation was undertaken to determine the behaviour of the sensor when placed on and off the phantom. Parameters such as the response and recovery times provide more insight into the operation of the sensor. For this test only the G100 IDC was used, since it was discovered to be optimal for the purposes of SC hydration sensing. The test conducted was to repeatedly press and release a single G100 IDCs onto the different porosity areas of the hydration gradient phantom whilst continuously sampling capacitance data from the impedance analyser every 0.2 seconds. The testing procedure was distributed as follows: 5 seconds off-time (no contact to skin phantom, sensor is in air), followed by 5 seconds on-time

(pressed to the skin phantom with the same 5N weight as used before), 5 seconds off. This was repeated with each of the 3 different porosity sections tested 2 times during the 75-second test. The results are shown in Figure 44.

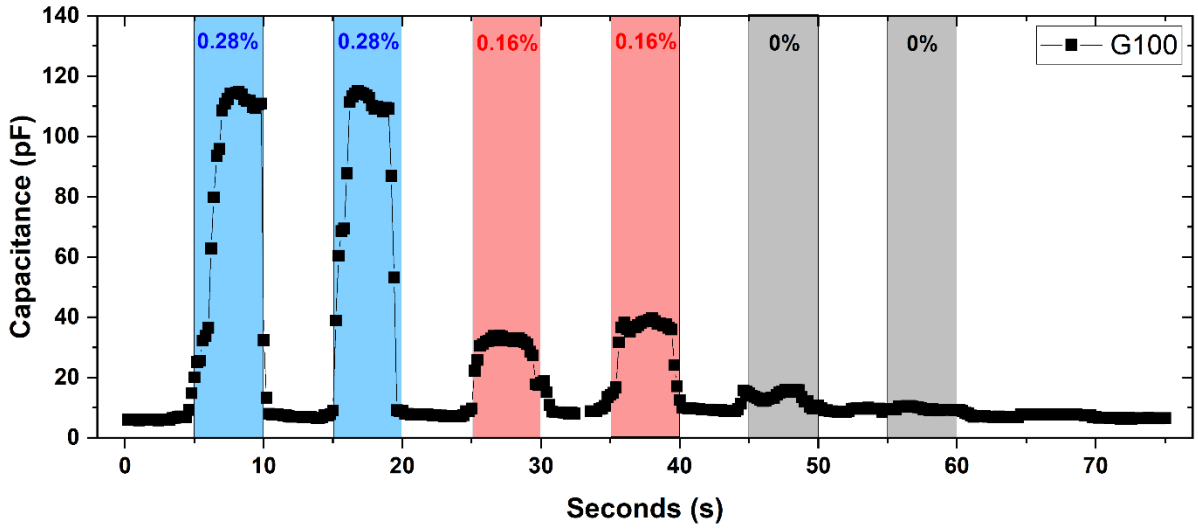

Figure 44 Step-response of a G100 N32 IDC sensor on a hydration-gradient skin phantom with 3 porosity levels. Excitation signal of the impedance analyser was 1 V at 1 kHz.

As expected, the readings of the G100 IDC match the frequency sweep measurements at the given frequency band (1 kHz) before normalisation and the distinction between the different porosity levels is evident.

Using the stepwise response graph, the parameters of response and recovery times can be calculated. For the first period in contact with the 0.28% porosity phantom, the capacitance begins increasing first slowly, then more rapidly and it raises from around 9.3 pF to 108.6 pF in 2.4 seconds. This is a response of about 41.4 pF/s when in transition between air and normally hydrated skin. The following recovery time is much faster – it goes from 110.9 pF to 8 pF in 0.6 s, which is a recovery time of 171.5 pF/s. During the second period in contact with the 0.28% porosity phantom, the response time is much faster, 85.4 pF/s, whereas the recovery time is approximately the same. For the two contact periods with the 0.16% porosity the response and recovery times are close to each other at around 26 pF/s, but that is expected since this is replicating the drier spectrum of skin hydration. Response and recovery times could not be calculated for the 0% porosity phantom, due to the marginal change in the capacitance measurements. The stepwise response shows stable and repeatable operation when performing quick sampling measurements using the IDC sensor on the skin phantom.

4.3.4 Environmental Stability Test

4.3.4.1 Effect of Environmental Humidity

To fully understand the measurements of the IDC sensor, the possible effect of environmental humidity must be investigated. Since the IDC is sensitive to the presence of water molecules in the media it is measuring, environments with high humidity should have an effect on the IDC, thus increasing the capacitance readings.

All the produced IDCs in this work were patted down with a cloth to dry them and then were individually tested inside a climate chamber (WKL 100, Weiss Technik) and their capacitance was continuously sampled every 30 seconds using the Wayne Kerr 6500b Impedance Analyzer and a LabView® script for 20 minutes while the chamber's humidity was raised linearly from 50% (relative humidity of room) to 95%. The excitation signal from the impedance analyser was the same as used in the initial capacitance testing – 1 V at 1 kHz. Temperature was kept the same throughout the measurements at 25ºC. Results are portrayed in Figure 45, 46, and 47.

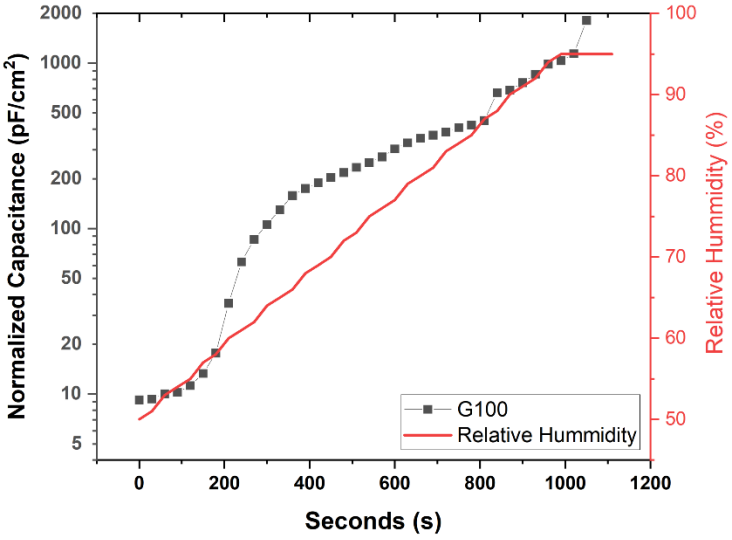

Figure 45 Capacitance versus time for a G100 N32 IDC sensor placed inside an environmental chamber with varying relative humidity between 50% and 95%.

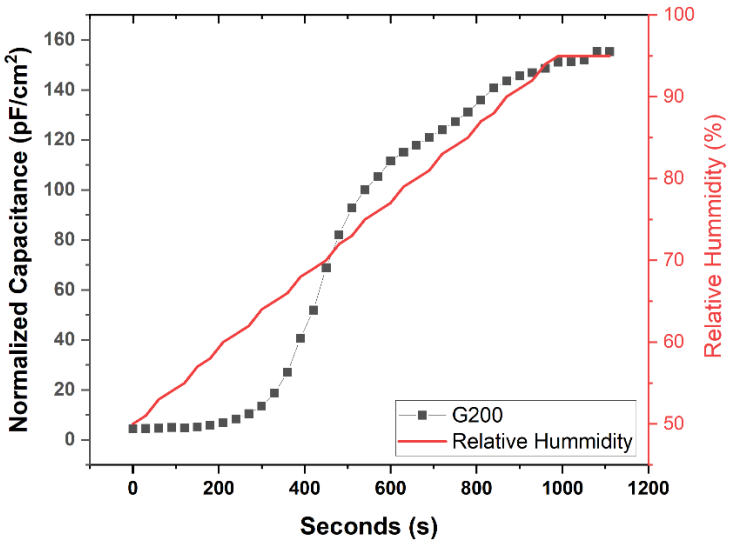

Figure 46 Capacitance versus time for a G200 N16 IDC sensor placed inside an environmental chamber with varying relative humidity between 50% and 95%.

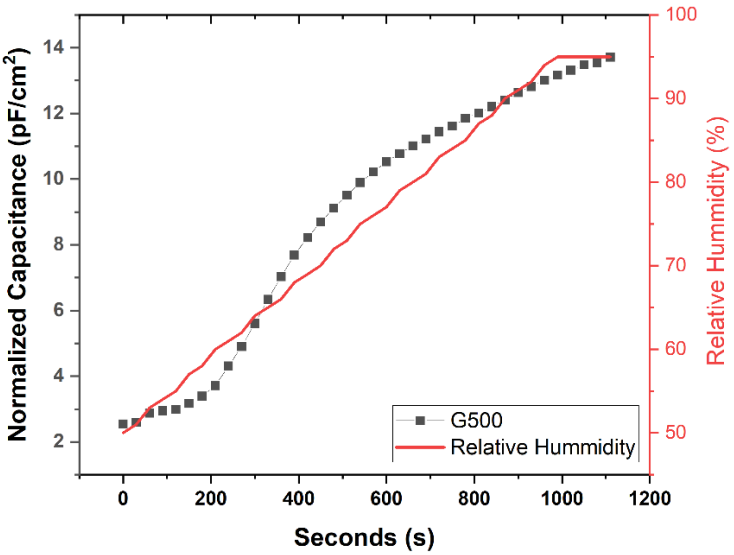

Figure 47 Capacitance versus time for a G500 N10 IDC sensor placed inside an environmental chamber with varying relative humidity between 50% and 95%.

In all graphs it is evident how the capacitance increases with several orders of magnitude due to the increase of relative humidity above a certain threshold. For the G100 and the G500 that threshold is about 60%, and for the G200 it is about 70%. This shows the sensors have a working range of 40-60% relative humidity, which is consistent with typical room conditions. After this threshold is passed, there is an initial sharp increase in capacitance, visible in the G200 and G100 plots, after which the gradient changes. In the later stages of the humidity test on the G100 IDC, around the 800th and 1100th seconds, there is a sharp increase that almost doubles the capacitance. Since these all occur at high humidity, it is believed that this is caused by condensation of water molecules onto the surface of the IDC. The G100 IDC has the smallest separation distance between the electrodes and is most sensitive to changes in the dielectric

medium arising from water molecules forming on the sensor. After the testing was finished, and the sensors were brought back to normal room humidity all of them returned to their original capacitance values. Unlike the G200 and the G500, the G100 IDC's capacitance values remained high for a long period of time after testing ended – this is attributed to the smaller gap between electrodes, allowing for higher formation of water droplets due to condensation that bridge the gap.

To increase the range of humidities the sensor can function over and mitigate condensation effects a possible solution would be to implement an encapsulation layer, but that would decrease the sensitivity and offset the measurement depth.

4.3.4.2 Effect of Environmental Temperature

Similarly to humidity, the effect of temperature on the capacitance readings of the sensor is also investigated. The IDCs sensors were again placed individually inside an oven and the temperature was gradually increased from 25ºC to 100ºC, while keeping average room relative humidity at 50 %. Testing took 20 minutes, and data was sampled every 1 minute using a Wayne Kerr 6500b Impedance Analyzer with an excitation signal of 1 V at 1 kHz and a LabView® script. Results are on Figure 48.

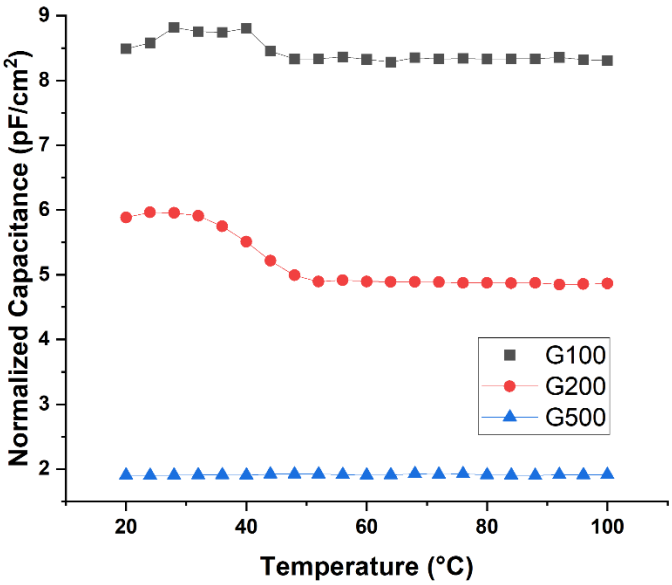

Figure 48 Normalized capacitance versus temperature for 3 types of IDCs: G100 N32, G200 N16 and G500 N10. The capacitance values were normalized to account for the area differences between the IDC sensors.

As it is seen on the graph, the effect of temperature on the IDCs readings is negligible compared to the range of readings when comparing different hydration levels. In the G100 and G200 IDCs there is a slight decrease in readings before stabilising, which is attributed to evaporation of any

residual water molecules that might be present on the surface of the sensor from the ambient air humidity.

4.3.4.3 Effect of Bending

The effect of bending radius is also investigated as an external variable since the IDCs are printed on a flexible substrate. The same impedance analyser setting was used as with the previous external variables testing. Three different cylinders with varying radii of 15 mm, 10 mm and 5 mm were 3D printed from PLA and the IDC sensor was bent around the cylinders with the electrodes facing inwards. Given that the length of the G100/G200 IDCs is around 6.4 mm and that of the G500 is 10 mm, the smallest radius would cause a total bend of approximately 90°. As PLA and Kapton are both polymers with comparable dielectric permittivity, this would introduce no capacitance changes, so any variations in capacitance should arise from the effect of the sensor being bent. The results in Figure 49 reveal that there is no significant effect of bending radii on the capacitance of the IDC in air and hence the IDCs can effectively be used in wearable applications where bending may occur in use.

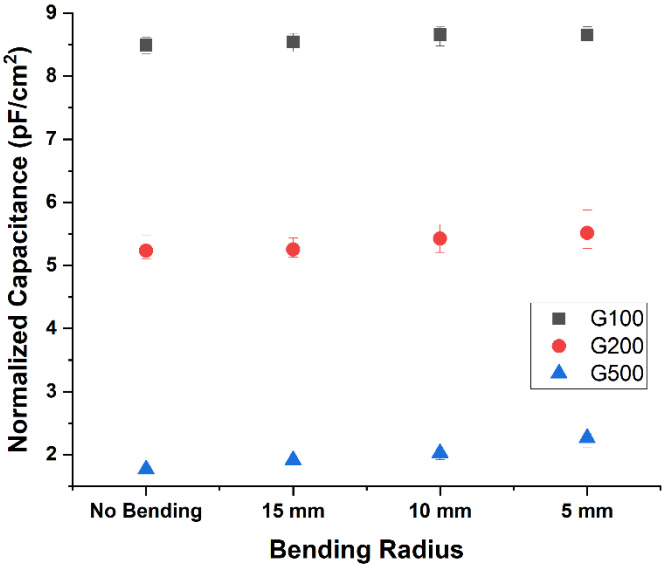

Figure 49 Normalized capacitance versus bending radii for 3 different IDC sensors (G100 N32, G200 N16 and G500 N10). Several tests were conducted, and the average value was taken; error bars indicate the range of values obtained.

4.3.5 Conclusion

The characterisation study revealed that the optimised IDC sensor can accurately distinguish between levels of hydration of the SC layer and therefore can help in estimating the severity of the AD or monitoring its treatment. The G100 N32 IDC emerged out of both the FEA simulation and the skin phantom study as the most optimal solution for the application, given the fabrication

limitations. The frequency scope of 1 kHz – 1 MHz proposed by the simulation study was affirmed by the empirical tests and will therefore be used going forward. Environmental conditions have no significant effect on the performance of the IDC, apart from humidity, which only has an effect at above-average room humidity levels of more than 60%. Bending the materials does not inhibit a major deviation on the capacitance measurements, meaning that the flexible IDC can comfortably be used in wearable garments for portable and longitudinal monitoring of AD severity.

4.4 In Vivo Healthy Volunteer Tests

In vivo testing refers to testing that is conducted on the skin of living human subjects. Testing on healthy human subjects is a necessary step towards conducting clinical trials on patients with AD. Unlike controlled skin phantom testing, in vivo skin testing brings extra factors that could affect readings such as a non-homogeneous material composition, curvature of the surface of the skin, pressure implications, motion artifacts, and longitudinal wear. This section will explore some of those effects in the pursuit of eliminating them and creating a stable device that can yield repeatable and controlled results.

4.4.1 Study Setup

Volunteer testing was performed under the study "Non-invasive textile sensor for skin hydration monitoring", following ethics approval (ERGO: 70980). Only 1 healthy volunteer was tested at this part of the study, as wider testing would be conducted once the sensor is fully developed and characterised. The participant was allowed to rest for 30 mins in a room with a temperature of 22ºC and 40% relative humidity. Although in Section 4.3.4 it was discovered that standard room environment conditions do not have an effect on the performance of the sensors, these values were monitored throughout the study, to eliminate potential environmental noise on the readings. IDCs sensors fabricated out of copper will be used, following the procedure laid out in Section 4.2.1, and will be the G100 N32, G200 N16 and G500 N10. The copper IDC's readings will be compared to Corneometer® measurements, performed alongside the different tests.

The goal of the thesis is to produce a wearable sensor, so a suitable substrate for housing the IDC, while being worn on the skin, was researched. Several options were considered, including sleeves, gloves, and wrist bands but finally a forearm band was selected, because it had an adjustable strap. The strap allowed for the tightness of the armband to be controlled, therefore controlling the pressure which the IDC sensor exerts on the skin – an important variable for investigation. Furthermore, the armband had a cushion which ensured that the IDC sensor conforms nicely to the curved surface of the forearm. The forearm was chosen as the skin area

for measurements, due to its easy accessibility and general flatness. Comparative studies in the literature also choose the forearm for the characterisation of skin sensors and interfaces.

The copper IDCs were taped to the volar forearm using breathable medical tape and the armband was positioned on top of it. The tape exerted negligible pressure onto the sensor; thus, the strap was necessary to establish proper sensor conformity. The strap's length was marked at equal distances in order to indicate the level of tightness and thus to achieve the same level of compression during each testing. Figure 50 A) reveals a photograph of the armband used in this study and B) shows the armband positioned on a forearm.

Figure 50 Photograph of A) the armband used as a substrate to the IDC sensor; B) its position on the volar forearm of a volunteer.

Capacitance measurements were taken using a Wayne-Kerr 6500b Impedance Analyser (Wayne Kerr Electronics, Bognor Regis, England). The same voltage excitation and frequency sweep range was used as in the sensor characterisation from section 4.3.3: 1V at frequency range 100 Hz – 15 MHz. Whenever frequency isolation was required (for time-based tests), excitation frequency was kept at 10 kHz, because it is in the high sensitivity range of 1 kHz – 1 MHz as discovered by previous chapters. Three levels of tightness were marked on the strap (subsequently named Tightness Level (TL) 1, 2 and 3), which were measured using a thin film pressure sensor (FSR06, Ohmite, Warrenville, USA) to be approximately equal to applying a force of 1 N, 2.5 N and 5 N. Table 10 summarises the pressure standardisation procedure, where the pressure in kPa was calculated by dividing the measured force by the area of the sensor (in this case 0.384 cm^2 for the G100 N32 and G200 N16 and 1cm^2 for the G500 N10). Section 4.4.3 will investigate the pressure relationship in more detail, but for initial testing the tightness at TL 2 was selected, as it ensured proper skin-sensor contact.

Table 10 Tightness/Pressure standardisation levels used with the arm band, pictured in Figure 50. The strap was marked at equal intervals of 2 cm, and the different levels were

achieved by tightening the strap to the next marker. This resulted in controllable and repeatable pressure application for the flexible sensor.

Tightness Level (TL)	FSR06 resistance (kΩ)	Approx. force (N)	Approx. pressure (kPa)
1	27.5	1	26.04
2	9.53	2.5	65.1
3	2.41	5	130.21

4.4.2 SC Hydration Capacitance Measurement

To simulate varying levels of SC hydration, measurements were performed before and after the application of a standard humectant cream that improves the SC barrier properties by providing necessary ceramide molecules that strengthen the integrity of the barrier (Eucerin®, Birmingham, UK). This is a valid test to approximate the skin of patients with AD, a similar procedure will be undertaken when testing the effectiveness of treatments in patients. The test subject was allowed to rest for 30 minutes prior to testing to allow any sweat to evaporate. First the Corneometer® was used to take hydration reading of a specific area on the volar forearm. Afterwards the armband with sensor was positioned on exactly the same area and tightened to TL 2. Frequency sweep measurement was recorded, after which the sensor and strap were removed to apply the humectant cream. Testing was repeated 15 minutes after application of cream, to ensure proper absorption of the ceramide molecules into the SC.

The capacitance results are presented in Figure 51. All 3 IDC which were tested on the skin phantom were tested here – the G100, G200 and G500, in order to compare between the phantom and the in vivo tests. In all three cases, the copper IDCs successfully distinguished between different hydration states of the skin, as verified by the Corneometer®. It is observed that the G100 N32 IDC again showcases the highest sensitivity towards hydration changes in the SC, as the difference between the dry and the treated skin in terms of capacitance is the greatest across the broader frequency range. This is in-line with simulation analysis and with skin phantom tests – concluding that finer IDC sizes such as the G100 are best suited for the application. The range of capacitance values is also very close to the one in the skin phantom tests as presented in Figure 42, at least for the G100 case. In the case for the G200 and G500, the in-vivo measurements feature much lower capacitance values across the frequency spectrum. The G500 is the least sensitive towards changes in the SC layer, although unlike on the skin phantom, here it can be

used to distinguish AD severity levels, because across 100 Hz – 1 MHz, it reveals a substantial difference of tens of picofarads. Further testing will investigate the repeatability of the sensor readings by controlling the testing conditions to determine the accuracy for longitudinal measurements.

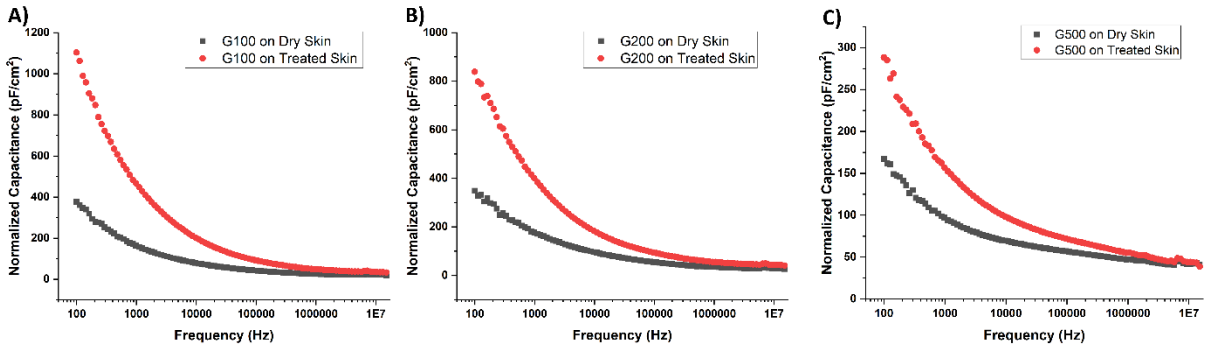

Figure 51 Normalized capacitance against frequency measurements between clinically normal (dry) skin and skin treated with humectant cream that increases SC hydration. Three IDC sizes were tested: A) G100 N32; B) G200 N16; C) G500 N10. Corneometer® readings for the dry and moisturized skin were 41 A.U. and 90 A.U, respectively.

4.4.3 Pressure Step Response Test

To determine the effect of pressure on the sensor performance, a step response test was performed, similar to the one done in section 4.3.3 using the skin phantom. Sufficient pressure is an important parameter as if too much pressure is exerted the skin layers deform, changing the dielectric properties, but with too little pressure contact is not conformal and airgaps form in the skin-sensor interface. The applied pressure was varied dynamically by increasing the tightness of the armband, following the levels outlined in Table 10. The following step procedure was performed and repeated 5 times on the volar forearm of a healthy volunteer with no treatment applied – at each step capacitance readings were recorded immediately and the procedure continued to the next step (the whole sequence took around 1 minute with 1-minute rest between cycles:

- Step 1: Tape IDC sensor onto forearm – negligible pressure exerted.
- Step 2: Position armband and increase pressure to TL 1.
- Step 3: Increase pressure to TL 2.
- Step 4: Increase pressure to TL 3.
- Step 5: Decrease pressure to TL 2.

- Step 6: Decrease pressure to TL 1.
- Step 7: Remove armband – only tape remains.
- Step 8: Peel off tape and remove IDC; wait 30 seconds; Adhere tape and IDC again and take reading.
- Step 9: Position armband and increase pressure to TL 1.
- Step 10: Increase pressure to TL 2.
- Step 11: Increase pressure to TL 3.

The removal and reapplication of the IDC in step 8 was done to test repeatability and for a dynamic reset to investigate the effect of possible hysteresis. The capacitance was recorded using an impedance analyser with the settings described in section 4.4.1. The G200 N16 IDC was used for this test, and the results are presented in Figure 52.

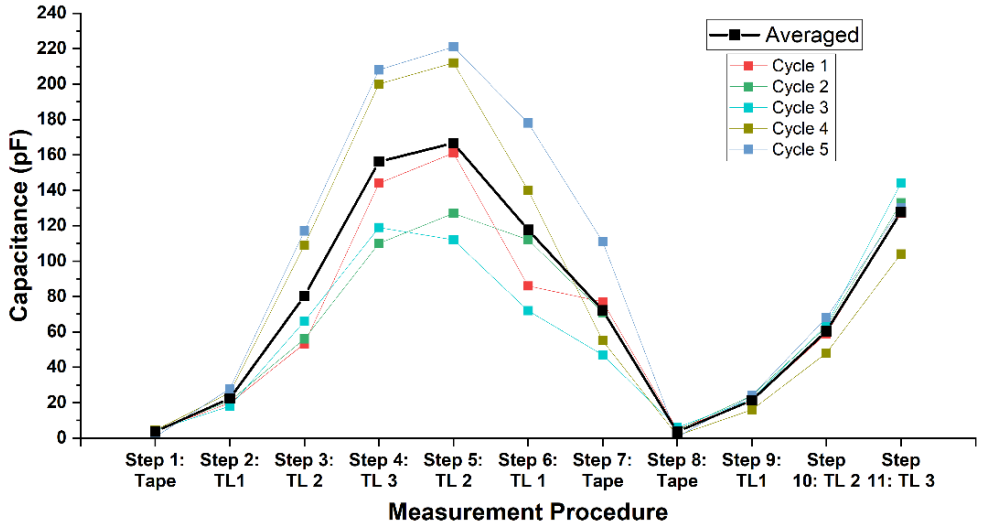

Figure 52 Dynamic variation of exerted pressure onto copper IDC in contact with skin of a healthy volunteer – step response test. Five cycles of measurement procedure were repeated, and the results were averaged. The G200 N16 copper IDC was used.

From the figure it is evident that pressure exerted by the IDC onto the skin plays a major role in the capacitance output, as values increase tenfold between TL 1 and TL 3. Moreover, the difference in capacitance values among the cycles indicate that the results are unrepeatable, even with the control of pressure through the armband. A hysteresis effect is observed at steps 5 to 7, as capacitance values continue to be elevated after pressure is released. This effect has been reported in the literature by Albulbul et.al., who noted that initial application of an applied force caused irreversible changes in the impedance [145]. The authors also used a copper electrode and noted that the changes could not be repeated or pinpointed to a single cause. Since

the sensor is occlusive (does not let water evaporate from the skin through the sensor substrate), sweat buildup over longer periods of time is a concern. The dynamic reset done with the removal and reapplication of the IDC confirms that the increase of capacitance is not caused by sweat or moisture buildup between the IDC and the skin, as the values between steps 1 and 2 and steps 8 and 9 are the same across all 5 cycles. The next study will investigate the long-term contact of IDC sensor with the skin to determine the effect and scope on the capacitance readings.

4.4.4 Longitudinal Testing and Capacitance Drift

The IDC e-textile is designed to be worn for longer periods of time, to continuously assess the condition of AD in vivo. Thus, longitudinal measurements are of utmost importance and must be performed in a repeatable and controlled manner. Previous tests hinted towards increase of capacitance values in time, even when pressure is controlled. This effect is undesirable as it diminishes the utility of the sensor as a continuous monitoring device for skin health. Thus, this section will conduct preliminary tests to determine the scope and cause of this increase in capacitance, in effort to prevent or control it.

Testing involved a healthy male volunteer with clinically normal skin (not treated with SC barrier strengthening cream). The IDC sensor was positioned on the participant's volar forearm, and the blue armband was used to secure and tighten the sensor around the forearm. TL 2 was chosen, as that was the balance between conformal fit without airgaps and comfortable for long-term wear without deforming the skin layers. The IDC sensor was kept in contact for a total of 1 hour, with a custom LabView script sampling the capacitance measurement every 10 seconds from a Wayne Kerr 6500b Impedance Analyzer. Six tests were done across 2 days, with all of the copper IDC used previously – the G100, G200 and G500. The results, presented in Figure 53, reveal the significance of the capacitance drift on the readings of the IDC and the unrepeatable nature of the measurements.

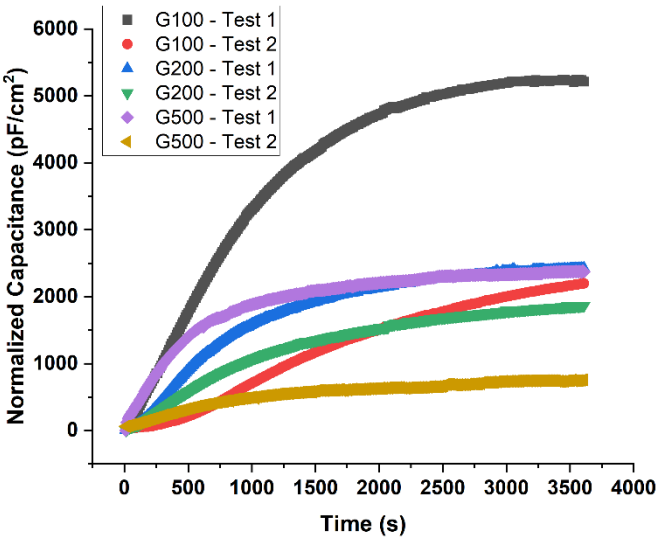

Figure 53 Longitudinal tests using various sizes of the IDC onto a healthy volunteer. Capacitance values were sampled at equal intervals of 10 seconds and were then normalized, to account for sensitivity area changes between the G100, G200 and G500 IDCs.

In all of the tests conducted a substantial and gradual increase in capacitance, labelled as capacitance drift, is observed. This drift causes readings to exceed the measurement scope of differentiating between hydration states of the SC. Therefore, in time, dehydrated skin with damaged SC barrier would produce the same capacitance measurement as clinically normal skin, which is a problem. This drift can be accounted for if it is repeatable, but initial testing suggests that it is not. The drift rate is not constant between same sensors tested on the same location across different days – for G100, the rate of change and the maximum capacitance value reached during day 1 were more than double those of day 2, whereas for G200 and G500 the opposite is observed. Also, it is not possible to draw a correlation between the size of the IDC (gap between electrodes) and the capacitance drift, as in some cases G200 and G500 produce higher capacitance output than G100, which contrasts with findings from simulation study, phantom testing, and frequency sweep tests. Because of all this, tests were halted and were not performed on skin with artificially hydrated SC layer, until this drift is resolved. One common thing across all tests is that the rate of capacitance drift decreases in time, suggesting saturation. As far as the authors are aware, this behaviour has not been reported on in the literature, thus a discussion about the possible causes is presented in Section 4.5.

4.4.5 Conclusion

Preliminary in-vivo testing performed on healthy volunteers validated the findings from the FEA simulations and characterization procedure. Smaller IDC gaps result in higher capacitance difference and greater sensitivity towards dielectric changes within the SC layer – the G100 N32

IDC serves as the best balance between sensitivity and fabrication feasibility. The frequency range of 1 kHz – 1 MHz concluded within the FEA studies remains a valid option for the excitation frequency. A standardised approach to pressure application was proposed and investigated. Results concluded issues with repeatability arising from controlled pressure application, hinting at hysteresis effects. This effect does not emerge from long-term sweat buildup, as hysteresis resets after the complete detachment of the copper IDC sensor from the skin. Long term contact of the sensor onto the skin resulted in gradual increase of measured capacitance. This phenomenon, named capacitance drift, could not be repeated, as rate of change of capacitance and maximum values achieved were all different and did not follow the findings so far. The next section discusses the results to determine the efficacy of the copper IDC sensor in the current state as a sensor for monitoring AD continuously.

4.5 Discussion and Limitations of Copper IDC Sensor

The in-vivo results confirm the trend seen in simulation and phantom testing – smaller gaps increase sensitivity to SC changes – yet they also expose fundamental limitations of the etched-copper implementation and, critically, of the skin sensor interface. In frequency sweeps before/after humectant application on the volar forearm, all three IDCs successfully separated hydration states of the SC, with the G100 N32 IDC providing the largest and most consistent capacitance contrast across 1 kHz – 1 MHz. However, when testing dynamics and longer wear, the copper devices exhibited strong pressure dependence, hysteresis, and time-dependent capacitance drift that undermine repeatability for continuous monitoring. These behaviours point to interface-dominated artefacts rather than purely dielectric changes in the SC.

The step-response experiments across different strap tightness levels showed clear pressure sensitivity with hysteresis on release and also unrepeatability during consecutive cycles. This is attributed to contact mechanics at the skin-sensor interface, indicating that there is no consistent conformity between the two surfaces. The capacitance drift observed during longer wear exceeded the measurement range for AD sensitivity and thus its origin must be understood. This behaviour has not been investigated, nor referenced in the literature, and similar work on skin capacitance sensing using electrodes omits information about this phenomenon. Several authors who use IDC sensors without electric insulation directly onto the skin do not report about impedance or capacitance drifting against time [66, 133, 134, 139].

The flattening of the drift curve indicates saturation, hence one valid reason for the appearance of the drift is sweat build-up between the IDC sensor and the skin. This is supported by Corneometer® readings taken before and after the 1 hour longitudinal test on the same spot of the skin, which featured on average a 70% increase from 31 A.U. to 53 A.U. The copper-etched

IDC is not water permeable; therefore, occlusion takes place since the skin cannot naturally evaporate sweat through the surface of the IDC. This effect is not present initially at low timescales and is therefore responsible for later stage creep of the capacitance drift, but not for the initial spike in values. Another plausible reason for the initial spike would be the IDC surface settling into the skin – since the skin is an uneven surface, during initial contact a lot of airgaps are formed which reduce capacitance. As time goes on and better contact is established, these airgaps disappear slowly.

The third reason is that the initial effect is caused because the human body acts as a battery, continuously providing ions that charge the IDC, thereby increasing its capacitance. This is the most promising reason, because when the skin is electrically insulated from the electrodes of the IDC, with a thin polymer film in between, the sensitivity decreases significantly but the capacitance drift does not appear. The dielectric in between prevents charges to traverse the skin-sensor interface and therefore affect the charge-storage capabilities and thus increase capacitance. The goal of this work is to create a sensor for measuring SC hydration accurately and repeatedly, thus investigation of this phenomenon is out of scope, but efforts will be focused to contain and control it.

Further reading into the literature highlights concerns about the usage of copper as a skin-contact electrode because it reacts chemically with the skin, forming copper oxides. This releases Cu ions which introduces half-cell potential and time-varying impedance at the interface – effectively behaving like a battery, which supports the drift theory discussed above [146]. Thus, a more stable inert conductor like noble metals (gold, silver, palladium) with an encapsulated electrode should be investigated for continuous sensing of AD biomarkers.

4.6 Conclusion

Copper IDCs validated the design principle (smaller gaps like the G100 N32 best target the SC; 1 kHz – 1 MHz is best for excitation frequency) but exposed critical limitations centred on the skin–sensor interface: strong pressure dependence, hysteresis, and non-repeatable drift over time. Consequently, the etched-copper approach is unsuitable for continuous in-vivo monitoring in its current form. Subsequent chapters build on these lessons by moving to IDCs made of noble metals, less reactive to skin contact, and printed on the textile substrate. The potential of adding electrical isolation - specifically, a thin encapsulation layer over the electrodes, was also carefully investigated, as that provides conformal contact but reduces sensitivity. The second iteration of the IDC sensor proved to be useful for repeatable, clinically meaningful tracking of AD severity.

Chapter 5 Textile-Printed Silver IDC Sensor

5.1 Introduction

The findings of the previous chapters have analytically and empirically proven the bespoke design of the IDC sensor to be most sensitive to changes in the SC's hydration, an indicator of skin barrier integrity and AD severity. The copper IDC sensor proposed so far, although accurate in its readings, proved to be limited in its utility as an in vivo sensor. Problems such as skin conformity, chemical reactivity and reading hysteresis render it unfeasible for the application of a wearable sensor for monitoring AD in patients. Thus, this chapter explores ways of improving the first iteration of the IDC sensor to suit the goal of the study. The first improvement is the change of electrode material from etched copper to printed silver. The capability of printing the silver directly on the textile makes it a better option than adhering copper-Kapton sheets onto the textile, because it allows for easier integration with a flexible garment. The second improvement is the addition of an insulation layer, that prevents direct electrical contact between the skin and the electrode but does not hinder the sensitivity. Both approaches are thoroughly investigated and incorporated into the final design of the sensing system, suitable for wider population trials.

5.2 Fabrication and Methods

5.2.1 Silver as an Electrode Material

The metal of choice for the creation of the IDC electrodes was the Smart Fabric Inks Ltd: Fabinks TC-C4001 silver conductor paste with viscosity of 4300 cP. Silver is a better alternative to copper for skin-interfacing electrodes due to its non-reactivity with oxygen, making it a more stable material [147]. Furthermore, the antimicrobial effects of silver have been well established, which is beneficial, given this sensor will come in contact with lesions and wounds of patients [148]. Two methods were investigated for the printing of silver onto textiles, based on their resolution capabilities.

5.2.2 Screen Printing

Screen printing is a technique in which a finely woven steel or polyester mesh is used as a stencil to create a thin patterned layer of given ink on a substrate. Ink paste is deposited onto the mesh (also known as a screen) and then is squeezed through the screen via a squeegee to form the corresponding pattern on the substrate. The technique, presented in Figure 54, is useful to create thin layers (less than 500 μm) of intricate patterns to build up a complex structure.

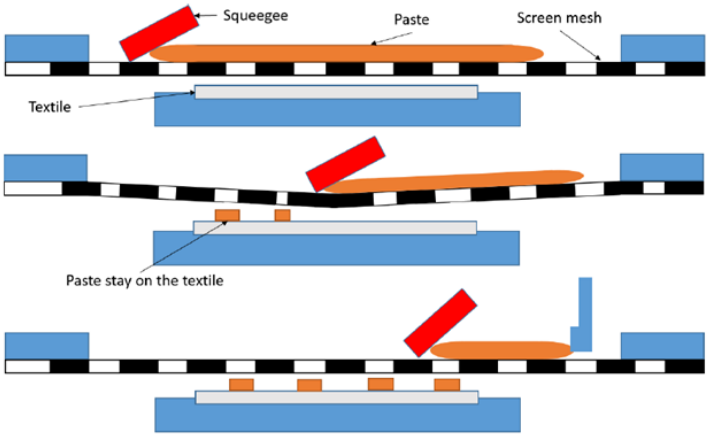

Figure 54 Illustration depicting the screen printing procedure for deposition of a single layer. Reproduced from [149].

To create the patterns of the IDC, a custom 280UTC stainless steel mesh was designed in L-Edit® software (Tanner EDA Tools) – the mesh with all of the IDC designs discussed in this thesis is presented in Appendix A. A DEK 248 Screen printer was used to deposit a single layer of silver paste using a print gap of 0.5 mm. The substrate used was an 80 µm thick thermoplastic polyurethane (TPU) film attached to removable silicon paper (Electrum Stretch HC, Policrom Screens S.p.A., Carvico, Italy). The deposited pattern is then cured in a carbolite oven at 120 ºC for 15 minutes. Once the silver has cured, the protective layer of the Electrum Stretch HC film is removed, and the substrate is ready to be laminated on any textile surface. This method is fast and allows for fabrication of IDC sensors on any textile, including curved surfaces. The G200 N16 IDC and the G400 N8 IDC were produced using this method.

The only drawback of screen printing is the limit to resolution – features below 150 µm are difficult to achieve. This limitation is due to the properties of the materials used and the resolution of the screen printing mask, as it cannot accurately control the amount of deposited ink, causing spreading and short circuits. During testing, the author managed to produce a single IDC with a feature size of 100 µm. This was only achievable with a print gap of 0.3 mm and a completely clean screen. Thus, a new method was discovered and outlined in the following section to produce the G100 N32 IDC.

5.2.3 Reverse Offset Printing

To improve the success rate of high-resolution printing an alternative method was applied. Reverse offset printing (ROP) is a method that allows for much finer paste deposition through an accurate transfer process without smudging or ink spread. The printer used for the process was developed by Dai et al. and the application of the printing process for creating fine IDC patterns for in vivo monitoring of AD severity was jointly investigated [150].

The method operates in three steps as illustrated by Figure 55 – first a moving roller, covered with PDMS, is coated uniformly with silver conductor paste using a doctor-blade coater. This ensures that only a thin layer of silver paste is used for further publication, limiting the risk of spreading [151]. The next step is the removal process where the roller comes in contact with a custom patterned cliché, made from silicon. The cliché has high surface energy, picking up unnecessary parts and leaving only the desired image on the roller. Finally, the remaining ink is deposited onto the TPU substrate (Policrom Screens S.p.A., Carvico, Italy) and then cured at 120 ºC for 15 minutes in a carbolite oven. The cliché used in this procedure featured the same pattern as the screen-printing mask, presented in Appendix A.

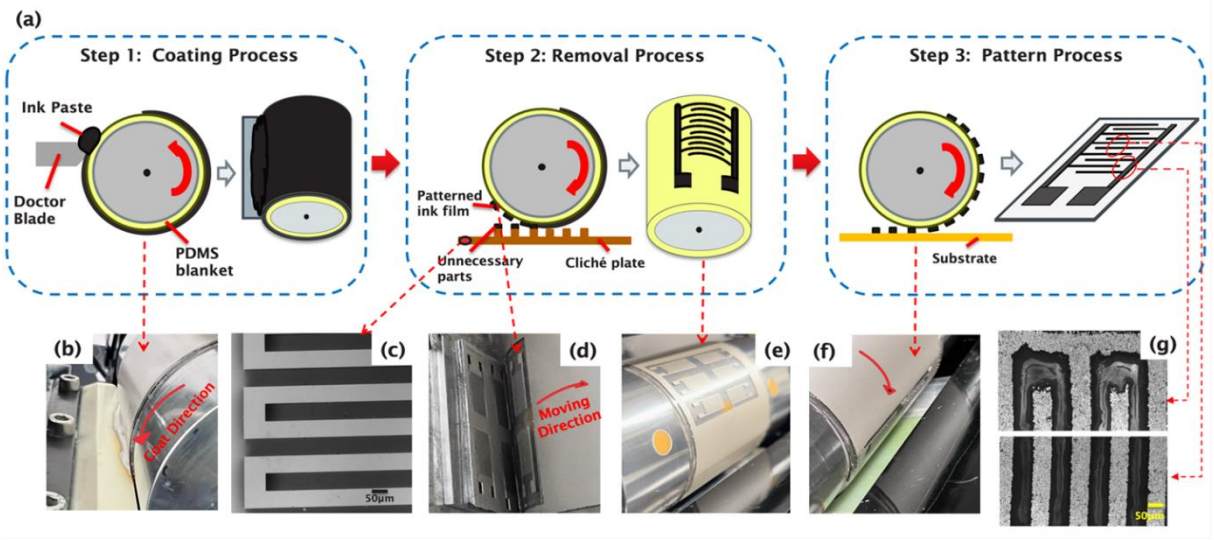

Figure 55 Reverse offset printing process during the fabrication of an IDC sensor. A) Three schematic diagrams depicting the steps of ROP. B) Roller fully coated with silver ink. C) SEM photograph of the silicon cliché. D) Roller moving across the cliché plate. E) IDC pattern on the roller. F) Transfer process of IDC pattern to TPU film. G) SEM photography of the fabricated IDC sensors. Figure is produced from [150].

The ROP method yielded fewer prints with short circuits compared to the screen-printing method. The method was applied at a later stage during the project, as its accuracy was needed to produce the silver G100 IDCs. That is why other sensors (like the G200 and the new replacement for the G500 – the G400) were produced through screen-printing and used predominantly during repeatability testing before the final IDC system was developed.

5.2.4 Lamination on Textile

The finished IDC designs had a TPU film as a substrate, allowing for lamination onto various textile carriers. It was laminated onto the skin-facing side of the elbow strap band using a hot press (Geo

Knight DK20) for 60 seconds at a temperature of 190 ºC. The cushion of the strap band achieves a better contact between the sensor and the skin, partially eliminating air gaps from forming.

5.2.5 Encapsulation of IDC Electrodes

As discussed in the conclusions of the previous chapter, encapsulation of the metal electrodes is a proposed way to eliminate the reactivity of the skin-sensor interface and control the sensor conformity. In this study, the encapsulation was undertaken after tests with the non-encapsulated silver IDC electrodes concluded and their results were assessed. To encapsulate the electrodes, a different, thinner TPU film was used – the Platilon U073 TPU film (Covestro Ltd., Cheadle Hulme, UK) with a thickness of 50 µm. It was laminated on top of the IDC using the same hot press for 60 seconds at a temperature of 160 ºC. Figure 56 shows a photograph of the e-textile G100 IDC sensor with a micrograph inset of the G100 IDC itself, where the encapsulating film is visible.

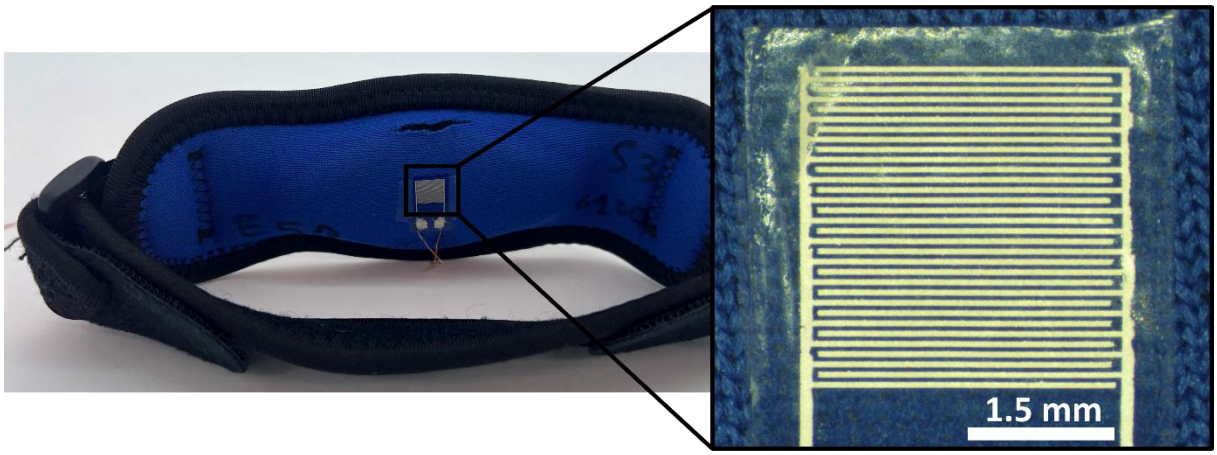

Figure 56 Photograph of the e-textile IDC sensor for monitoring AD in patients and a micrograph of just the IDC sensing element – an array of 32 interdigitated electrodes with a 100 µm width and a 100 µm separation between them.

5.2.6 Study Setup

The goal of this study is to revise the second iteration of the IDC sensor, by testing the printed silver electrodes first and then the encapsulated electrodes and comparing them to the copper IDC. Thus, a similar procedure was conducted. Capacitance readings were collected using a Wayne Kerr 6500b Impedance Analyser with an excitation signal of 1 V. Simulation and characterisation studies concluded that the high sensitivity range for the application is between 1 kHz and 1 MHz, so frequency sweeps were performed with this range. For time-based tests where frequency is fixed, previous tests used 1 kHz and 10 kHz for the excitation frequency, but 1

MHz was chosen here and for future reference, as it is also used by the Corneometer®, thus providing a better comparison between the devices.

Only the G200 N16 IDC was tested during the studies as the capacitance drift and pressure hysteresis were independent from the gap size of the IDC, and there was no need to test all of the IDCs to find a solution for these problems. Testing was conducted directly on human skin, instead of repeating the tests on phantoms that were done with the copper electrodes. Phantom testing with the silver IDC would be beneficial for comprehension, but due to timing issues with clinical trial planning meant that this step had to be skipped and is planned for a later stage in the future work. Testing involved a single healthy volunteer, and the sensor was positioned on their left volar forearm with the IDC sensor facing the skin, as per Figure 50 B). The nominal applied pressure was at TL 2, as per the classification in Table 10.

First the non-encapsulated silver IDC was tested longitudinally to determine the effect of capacitance drift and to compare to the copper counterpart. Then the IDC was encapsulated, and the time-based measurement was repeated. Following the results, a step response test was performed to cycle the applied pressure through varying TL and determine if hysteresis occurs. Finally, the stable and repeatable IDC was used to differentiate between dry and treated skin with strengthened SC barrier, to validate its utility as an AD severity monitoring sensor.

5.3 Sensor Stability and Repeatability Tests

5.3.1 Non-Encapsulated Printed Silver IDC

The printed silver IDC was tested before the introduction of the encapsulation layer. This was done to determine if the limitations with contact pressure artefacts and capacitance drift, which were present in the copper IDC, continued here. The textile strap with the G200 IDC sensor was fixated on the left volar forearm of a healthy volunteer at TL2 and capacitance was sampled continuously for 10 minutes with an excitation signal of 1 V at 1 MHz. This was sufficient time to observe the capacitance drift, so there was no need to repeat the 1-hour tests done with the copper IDC. The results are plotted in Figure 57. As evidenced by the plot, capacitance drift still occurs, as readings increase nearly tenfold between start and end values with the silver IDC sensor. The average change in capacitance across the 10-minute span is +139.853 pF with an average slope of 0.23 pF/s.

This reveals that the drift was not caused by a chemical reaction between the copper electrodes and the skin, as silver is an inert material, but more likely by the exchange of electrons that continually charge the capacitor. The difference in capacitance values and the slope of the curves

between the 3 tests indicate that unrepeatability of sensor readings is still present here, caused by contact artefacts, resulting a big spike in initial capacitance values, as referenced by Albulbul et al. [145]. So even with careful control of the applied pressure, contact artefacts at the skin-sensor interface play a major role in the total capacitance value. To solve both problems, an electrical insulating layer is introduced between the skin and the IDC sensor, as it provides a flat surface for better conformal contact (eliminating pressure artefacts) and prevents ion transportation (hindering capacitance drift). The next section will investigate the behaviour of the next iteration of the IDC sensor.

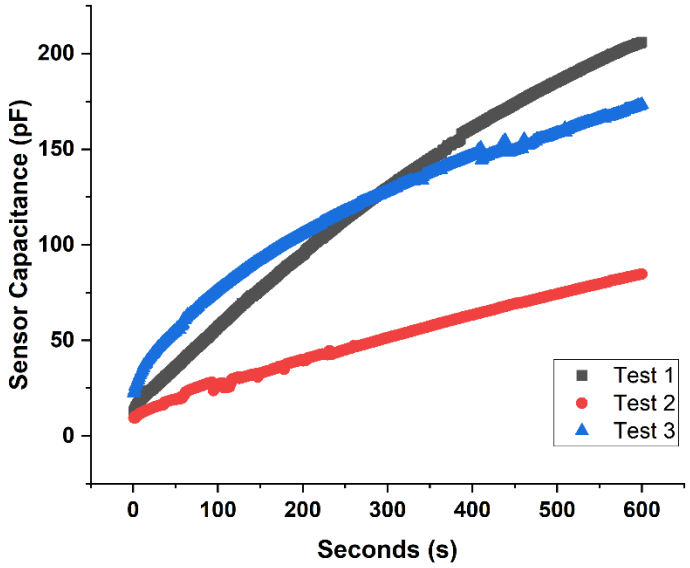

Figure 57 Longitudinal test using a G200 N16 IDC onto the left forearm of a healthy volunteer. Capacitance values were sampled at equal intervals of 10 seconds for 10 minutes. Three tests were performed with an interval of 30 minutes between them.

5.3.2 Encapsulated Printed Silver IDC

The G200 N16 IDC sensor was encapsulated following the procedure outlined in section 5.2.5. The same longitudinal test of 10-minute continuous measurement as in the previous section was performed 3 times and the results are presented in Figure 58.

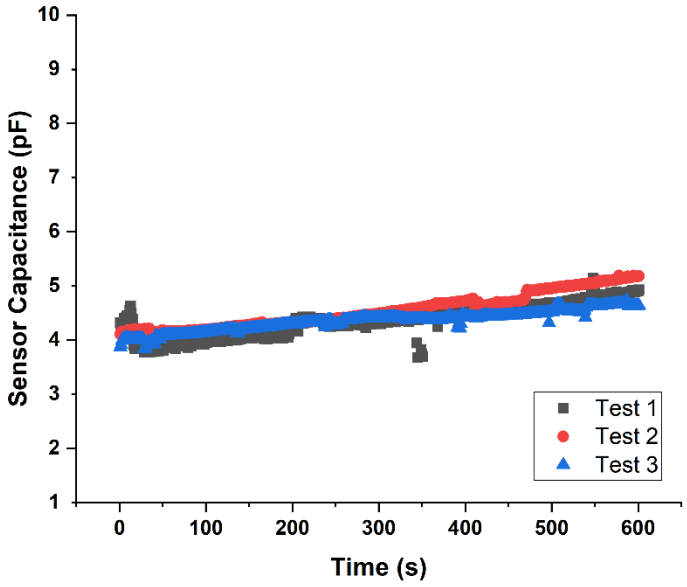

Figure 58 Longitudinal test using an encapsulated G200 N16 IDC onto the left forearm of a healthy volunteer. Capacitance values were sampled at equal intervals of 10 seconds for 10 minutes. Three tests were performed with an interval of 30 minutes between them.

Results revealed that capacitance drift does not have a fundamental effect on the readings with the encapsulated IDC compared to the non-encapsulated version. The average change between the start and end values is +0.814 pF, whereas it was +139.853 pF without the encapsulation. This is a major improvement in the stability of the sensor. The average slope of the capacitance curves is +0.00147 pF/s – again showing the diminished effect of continuous wear on the sensor readings. The positive sign of the change and slope mean that there is capacitance drift present, which is visible on the plot. This drift is the result of the occlusive properties of the IDC sensor's substrate, which prevents water molecules to permeate through it. The skin naturally loses water molecules through evaporation, thus when obstructed these molecules would condense on the skin-sensor interface. Thus, unless the substrate is completely water permeable, the effect of capacitance drift cannot be avoided entirely, but with proper measures such as an encapsulation layer it can be controlled in a repeatable manner.

The three tests proved to be repeatable, with a difference of 0.5 pF between the end readings of the 3 tests, or less than 10% of the base capacitance value of the IDC. Pressure artefacts were not observed, and to validate that the encapsulation layer assists in controlling the applied pressure, a step response cycling test was performed. The step procedure followed the sequential increase of the applied pressure from TL1 to TL3 and back, with a break between step 5 and step 6, where the IDC sensor was completely detached from the forearm of the volunteer. Capacitance was sampled using the impedance analyser with the same settings as in previous tests and the entire test was repeated 5 times with a 1-min rest between cycles. The results,

presented in Figure 59, reveal the stability and repeatability of the printed silver IDC sensor with the controllable pressure arising from the armband.

No pressure hysteresis is observed during any of the cycles. The encapsulation layer helped improve the conformity of the IDC sensor towards the skin. Furthermore, it allowed for accurate control of the applied pressure by varying the TL and achieving repeatable capacitance readings.

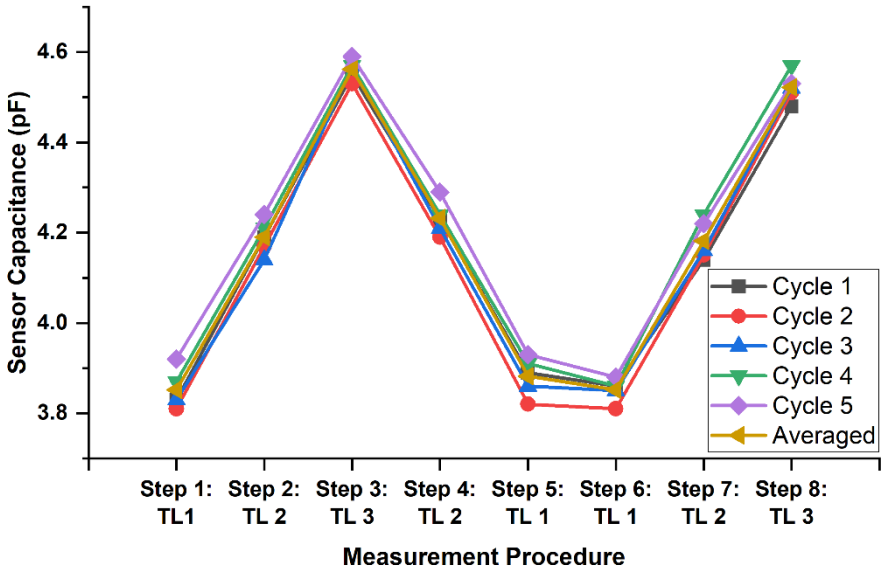

Figure 59 Dynamic variation of exerted pressure onto silver IDC in contact with skin on the left volar forearm of a healthy volunteer. Five cycles of measurement procedure were repeated, and the results were averaged. The silver G200 N16 IDC was used.

Finally, to confirm that the encapsulated printed silver IDC sensor retains the abilities of the copper IDC sensor to distinguish between varying severity states of AD, a single volunteer test was performed, in which the SC barrier of the volunteer's forearm was artificially strengthened through the addition of treatment cream and the capacitance readings were sampled before and after the application. Frequency sweep using the impedance analyser was done with a range of 1 kHz to 1 MHz. The measurements, presented in Figure 60, reveal a large difference in the capacitance between the dry and treated skin, indicating good sensitivity towards AD changes. The average delta in sensor capacitance between the two hydration states is 2.53 pF or 62% of the value of clinically normal skin. The Corneometer® was used to validate the hydration readings – 38 A.U. for the dry skin and 81 A.U. for the treated skin, in agreement with the results of the IDC sensor.

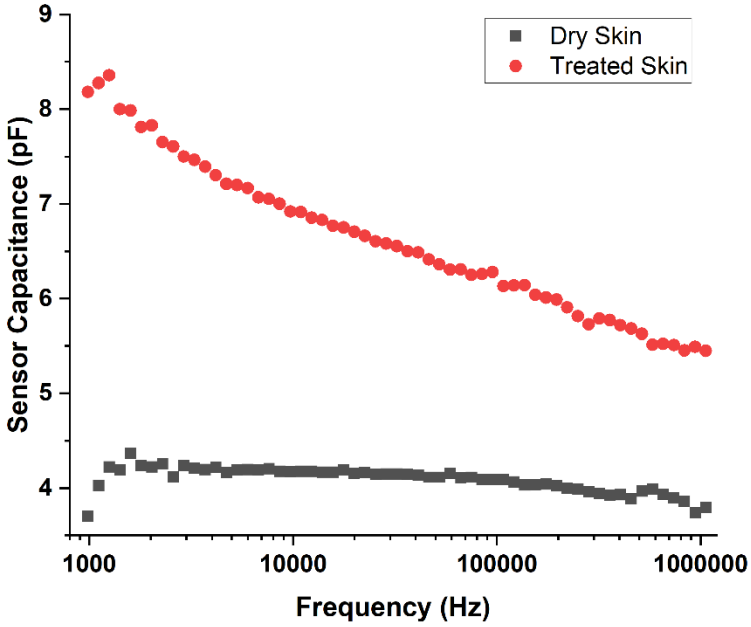

Figure 60 Capacitance against frequency measurements between clinically normal (dry) skin and skin treated with humectant cream that increases SC hydration. The G200 N16 silver IDC was used. Corneometer® readings for the dry and moisturized skin were 38 A.U. and 81 A.U, respectively.

5.4 Conclusion

This chapter has demonstrated that the second iteration of the IDC sensor, fabricated by printing silver electrodes on textile, is a viable approach for monitoring AD. The adoption of silver as electrode material enabled conformal fabrication onto curved surfaces, such as the armband, while maintaining non-reactivity with the skin. A key outcome was the confirmation that encapsulation of the sensor is essential for achieving stable and repeatable measurements. The sensitivity of the IDC sensor was decreased, compared to the non-encapsulated copper IDC sensor – difference between dry and treated skin at 1 MHz was 2 pF, rather than 19 pF with the copper one. But the encapsulation solved the capacitance drift and the pressure hysteresis problem, apart from continued drift arising from the build-up of water molecules on the skin-sensor interface because the IDC sensor is occlusive. That effect is negligible at lower timeframes, but can grow significant during very long wear, thus in the future it is worth exploring water permeable electrodes and substrates. This was not the focus of this project, hence the encapsulation layer was be used, and only short time-based tests were done, to validate the silver IDC sensor as a method of accurately distinguishing AD severity levels. The next phase of the project employed the findings of this chapter onto the G100 N32 IDC to build a device suitable for patient trials. Note that the copper IDC sensor used in the previous chapter was not encapsulated to test if capacitance drift would still occur, to accommodate more time for patient trials with the newly developed silver IDC sensor.

Chapter 6 E-Textile Sensor System for Monitoring AD

6.1 Introduction

The preceding chapters have established the design, fabrication and validation of textile-printed IDC sensors capable of stable and repeatable measurements of SC barrier function. A singular best design was chosen from simulation and empirical testing – the G100 N32 IDC with a 50 µm encapsulation layer. All previous tests approximated skin with AD and its properties, but to truly confirm the suitability of the IDC sensor, in vivo patient testing must be conducted. Building on these findings, this chapter presents the development of a complete wearable e-textile system for monitoring AD in patients. It details the design of the readout electronics and wireless communication, the implementation of a bespoke graphical user interface, and the integration of the IDC into a wearable format. The chapter further reports on system characterisation, including repeatability and environmental stability testing, and culminates in the validation of the system through patient trials.

6.2 System Design

6.2.1 System Overview

The system revolving around the IDC skin sensor has to translate the raw capacitance readings into a digital signal and then output it in a meaningful format to a general user. Thus, it requires 3 critical elements – a capacitance to digital converter, an MCU to store and transmit the digitised capacitance values, and a user interface to present the information on a host computer.

The IDC electrode was printed on a wearable textile armband, as previously done in Chapter 6. The textile armband also had a pressure sensor inside it, to continuously monitor the applied pressure – a method which will be discussed in detail in section 6.2.3. The converter circuit and the MCU transmission circuit were combined on the same PCB and connected to the IDC skin sensing textile. The collected data was then wirelessly sent to host computer for visualisation. The entire setup of the e-textile sensing system for monitoring AD is illustrated in Figure 61.

The development of each component is discussed in detail in the following subsections.

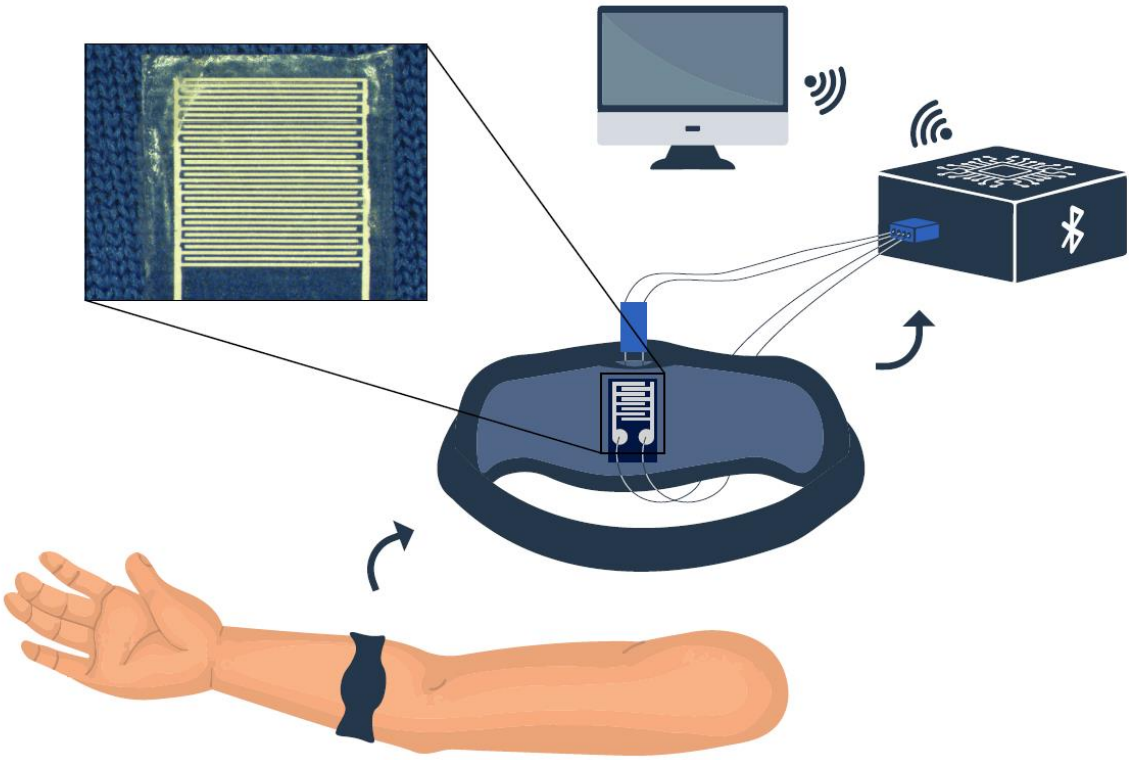

Figure 61 Graphical illustration of the e-textile IDC system for monitoring AD. The system consists of the wearable e-textile armband with the IDC printed on it (inset with photograph visible on the left); the data collection and transmission circuit; and the host computer visualising the results.

6.2.2 Capacitance to Digital Converter Circuit

From FEA simulations and tests on volunteers and skin replicas in the previous chapters, it was discovered that the measurement range of a sensor to distinguish between lesional and non-lesional skin of patients is in the tens to hundreds of picofarads. Currently, general purpose tools such as the benchtop impedance analyser were used, which had broad measurement range for various applications, but are bulky and non-portable. Thus, a measurement circuit suitable for use in this range is needed to convert the capacitance values to a digital signal locally and avoid the usage of standard benchtop multimeters and impedance analysers. The digital data can then be collected by a microcontroller unit (MCU) and transmitted wirelessly to a host computer for further processing.

The FDC2214 capacitance to digital converter (CDC) chip by Texas Instruments (Texas Instruments Ltd., Manchester, United Kingdom) was chosen as the analogue front end measuring the IDC's capacitance due to its high resolution, serial data transmission and low power consumption – around 0.3 mA per channel at 3.3 V with a 1 MHz measurement frequency [152]. The FDC2214 features 4 channels, each with 28-bit resolution, sampling the resonating

frequency of an external LC tank. Only one channel was used in this application, but the extra channels make the chip an attractive option for scaling the device to cover larger areas. The high resolution allows the CDC to detect capacitance changes in the order of femtofarads, which is more than enough for the given application. The values of the external inductor and capacitor dictate the excitation frequency of the electric field emitted onto the skin, based on Eq. 21. When an unknown capacitance is added to the circuit, the resonance frequency shifts, and the FDC2214 measures the new frequency.

$$f = \frac{1}{2\pi\sqrt{LC}} \tag{21}$$

Based on the digitised frequency value, the value of the unknown capacitance can be calculated, which in this case is the capacitance of the IDC sensor in contact with the skin, by taking the inverse of Eq. 21 and subtracting the capacitance of the LC tank – exemplified in Eq. 22:

$$C_{sensor} = \frac{1}{L(2\pi * f_{sensor})^2} - C \tag{22}$$

The LC tank values were selected to achieve an excitation frequency of 1 MHz, by using a 470 µH inductor and a 47 pF capacitor. To ensure stability of the LC circuit a high Q-factor is critical, and the selected components have Q values of 200 for the inductor and 1000 for the capacitor, resulting in a combined Q-factor of 167, well above the recommended (Q > 50) by Texas Instruments for the FDC2214 [153].The overall tolerance shift in the excitation frequency is 6%, which still fits within the high sensitivity range, discovered during previous FEA simulations, and is also the same frequency used by the Corneometer®, ensuring a comparable basis between the two devices. The LC tank is also highly temperature-stable (±30 ppm/°C), and no temperature drift was observed. Based on the LC tank and the measurement range, a drive current has to be selected, which must position the output voltage be between 1.2 V and 1.8 V, as per the FDC2214 datasheet [152].

The drive current and channel initiation of the FDC2214 IC are programmed via I2C commands. To validate the device's utility for the application the Texas Instruments EVM Development kit is used, as it comes with a MSP430 MCU and a custom graphical user interface (GUI) app built for managing the registers of the FDC2214 and for visualising the converted capacitance data [154]. The EVM board allowed for direct connection to the FDC chip via I2C and power lines to test its capabilities before building the rest of the system.

A custom circuit was designed in Kicad® 7.0, following all necessary design specifications outlined in the FDC2214 datasheet. The circuit featured all the necessary passive and active

components to power and transmit data to/from the FDC2214 IC through the I2C bus lines. The schematic and layout of the circuit are presented in Appendix B. In this layout all 4 channels are routed and made available even though only 1 will be used at this stage – this is to future proof the design for further studies on multi-channel and multi-frequency measurements. The layout was purposely made to have tracks and conductive planes on a single layer, so that it can be both fabricated on rigid PCB or etched from flexible copper-polyimide sheets, similar to the fabrication of the copper IDC sensors. The circuit will be referred to as the CDC analogue front end (AFE) or just CDC. For the course of this study, it was fabricated from a flexible copper-polyimide sheet. The inputs of the CDC's measurement channel were soldered to the ends of the IDC sensor and the I2C, power and ground lines were connected via soldered wires to the EVM board.

Measurements of capacitance were taken on healthy volunteers to test the sensitivity and determine the drive current. Tests confirmed that the most suitable value for the drive current is 3 mA, and that value was used throughout the data collection [152]. Tests were performed in a similar fashion as in Chapter 6, where the e-textile IDC sensor measured the SC barrier function of the volar forearm of a volunteer before and after the application of a SC barrier strengthening cream. Three volunteers were tested, both male and female, and the sensor sampled capacitance data continuously for 30 seconds before being removed. Then commercial cream (Eucerin®, Birmingham, UK) was applied at the location and the readings were performed again after 15 minutes. The results are presented in Figure 62.

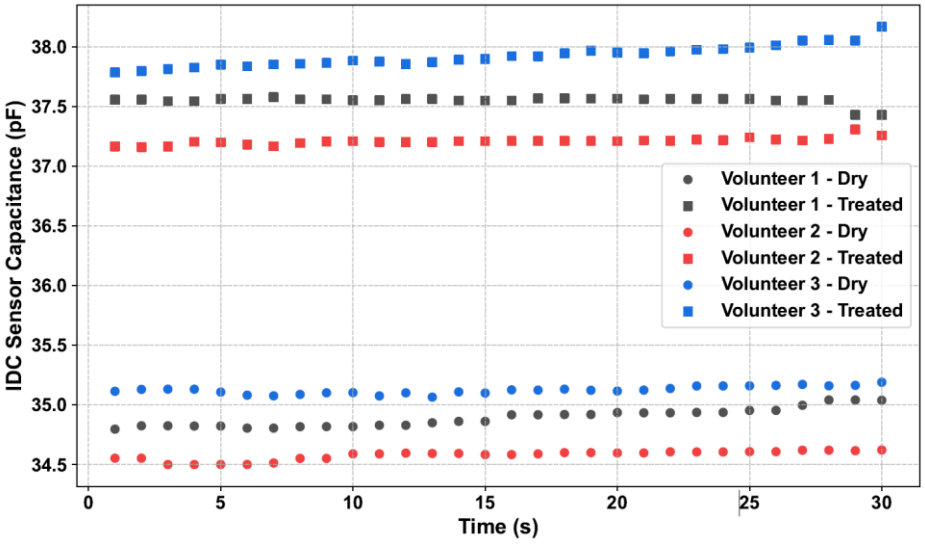

Figure 62 IDC sensor capacitance against time for varying SC barrier integrity states of 3 healthy volunteers collected via the TI EVM development kit. Volunteers are colour coded.

In all tests, the e-textile IDC sensor successfully measured the change in SC hydration arising from the improvement of the SC barrier properties, revealing an average difference in capacitance

of approximately 2.7 pF. This confirms the suitability of the FDC2214 as the main component of the CDC front end which samples the capacitance readings from the e-textile IDC sensor. The next step is to create a small and portable data transmission board, which replaces the EVM dev kit.

6.2.3 Data Collection and Transmission Circuit

To sample the frequency data from the CDC a XIAO nRF52840 module by Seeed Studio was used (Seeed Studio, Düsseldorf, Germany) [155]. This MCU board was chosen because of its miniature size, power efficiency, and BLE connectivity with built-in antenna – Figure 63 presents a photograph of the module [155]. The MCU polls the latest value from the FDC2214 every 1000 ms, resulting in a system sampling rate of 1 Hz. The module has the nRF52840 SoC by Nordic Semiconductor and it features Bluetooth low energy (BLE) connectivity with a matched on-chip antenna, I2C serial transmission at 3.3 V operation – suitable for interfacing to the FDC2214 [156]. A 3.7 V 620 mAh LiPo battery was used to power the XIAO module, which has a built-in 3.3 V voltage regulator and a power management circuit for charging the LiPo battery back through a USB port. Datasheets for the XIAO nRF52840 and FDC2214 IC indicate a current consumption of approximately 25 mA, translating to 24.8 hours of continuous usage [152, 155]. However, the device was kept fully charged in between tests, to ensure no power failure during the procedure, so this limit was never investigated.

Figure 63 Photograph of XIAO nRF52840.

The nRF52840 board was programmed via Arduino and required just 4 lines to communicate and control the CDC – the 2 I2C lines (SDA and SCL) and 2 power lines (3.3V and GND). The FDC transmits a raw 28-bit number, indicating the frequency shift (f_{sensor} in Eq. 22). It was decided that the MCU would not compute the calculation of capacitance from the frequency number, as

this required extra memory and drew more current, thereby reducing battery life. Thus, the firmware code only samples and transmits the f_{sensor} via BLE every second for further processing.

As discovered so far, pressure is an important parameter to control because if too much pressure is applied, the layers of the skin are compressed, which alters the depth of the electric field and affects the results. The TL system established in Section 4.4 was confirmed to be effective in exerting a defined amount of pressure through the controlled tightening of the e-textile strap, but it is worth to monitor the pressure to ensure it stays within range. So, to ensure consistent and repeatable pressure application between readings the FSR06 thin film pressure sensor (Ohmite, Warrenville, USA) was fit in the cushion of the strap-band, directly underneath the IDC sensor. Figure 64 shows a photograph of the pressure sensor and its position behind the IDC sensor. The pressure sensor acts as a variable resistor with one leg connected to power and the other connected to an ADC input pin of the MCU. Increasing the pressure decreases the resistance of the FSR06 and thus the ADC reading of the voltage increases. Through this technique, pressure was measured constantly, and thus, the capacitance reading from the FDC2214 chip was transmitted only when the pressure was within a certain pre-defined range. This range was empirically tested during trials to ensure proper conformal contact of the sensor on the skin without patient discomfort and set constant for the duration of the study. An updated pressure standardisation table is presented (Table 11), to link the TL of the e-textile strap with the FSR06 resistance and the approximate ADC count of the MCU for each level.

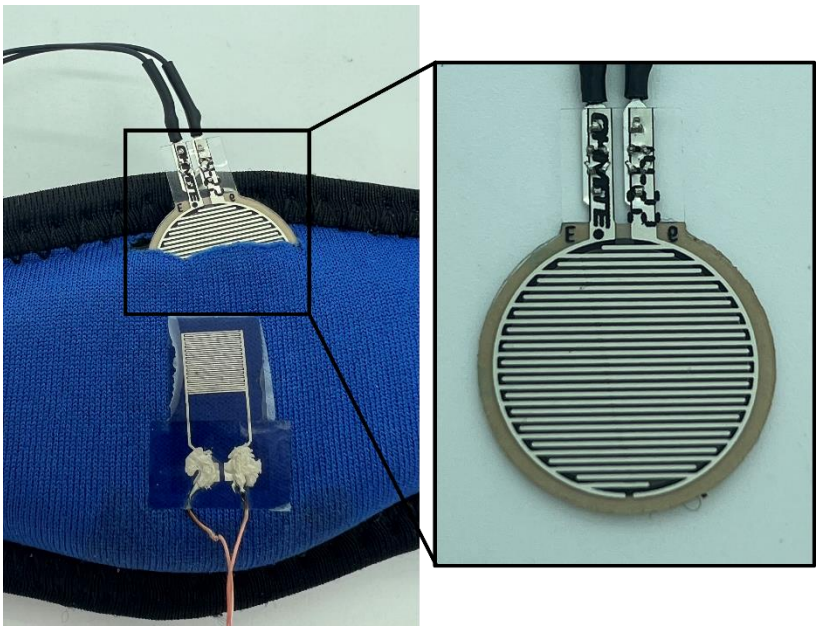

Figure 64 Photographs of the thin film pressure sensor used to control the IDC sampling, fitted in a cutout on the side of the textile armband, directly underneath the printed IDC sensor.

Table 11 Tightness/pressure standardisation levels used with the e-textile IDC sensor.

Tightness Level (TL)	FSR06 resistance (kΩ)	ADC count from MCU pin	Approx. force (N)	Approx. pressure (kPa)
1	27.5	~900	1	26.04
2	9.53	~2000	2.5	65.1
3	2.41	~3300	5	130.21

All components (CDC circuit, MCU module, battery and pressure sensor pins) were soldered together on a stripboard and a custom 3D printed box was created to house them. Pin headers were exposed to allow connection to the IDC sensor. After building the finished IDC device, the excitation frequency was verified with an oscilloscope. It was discovered that the actual frequency is around 0.95 MHz, attributed to parasitic capacitance in the PCB tracks, calculated to be 12 pF, and the capacitance of the IDC sensor itself, which is approximately 1 pF. This frequency is still within the high sensitivity range of 1 kHz – 1 MHz, so there were no alterations to the hardware. Possible mitigation options for future design would be to use shorter traces to sensor leads or an entire ground shield or ground plane directly underneath the LC circuit.

6.2.4 Graphical User Interface for Data Visualisation

To complement the bespoke IDC hardware and to extract the data wirelessly from it, a custom GUI app was developed in Python 3.12. The GUI allowed a user to connect via BLE to the IDC device, visualise the data in a table, and save the recorded data as a .csv file for further processing. The entire process of operation of the IDC system (device + app) is simplified with a flowchart in Figure 65. When the IDC device is switched on, it runs a setup sequence that starts advertising the BLE service and initiates the FDC2214 to configure the desired channel and use an external 40 MHz crystal oscillator as a clock source. Then the IDC device waits for a client to subscribe to the BLE service. On the GUI app the user can press a button to connect to the device, but no data is transmitted yet. If the connection is successful, the IDC device starts the data collection sequence. In this sequence, which repeats every second as dictated by a delay from the MCU, ADC pressure data and FDC2214 frequency readings are sampled (payload < 20 B). With default connection parameters, the end-to-end latency is sub-second and negligible relative to the 1 s sampling period, and no missing samples were observed during typical short acquisitions. If the pressure reading is within a pre-defined range, the data is written to the BLE characteristic register and advertised for a client to read. On the GUI app, the user can press the start button, which subscribes the host computer to the notifications from the BLE

advertisement, which are updated every second following the pressure-FDC reading sequence. Once a package of FDC frequency readings is read, the capacitance is calculated and printed on a table in the GUI. Afterwards, the user can choose to stop the data transmission with a stop button functionality (not shown in the flowchart), unsubscribing from the BLE service, and save the data in the GUI table as a .csv format or clear the table with a save data and clear data buttons respectively.

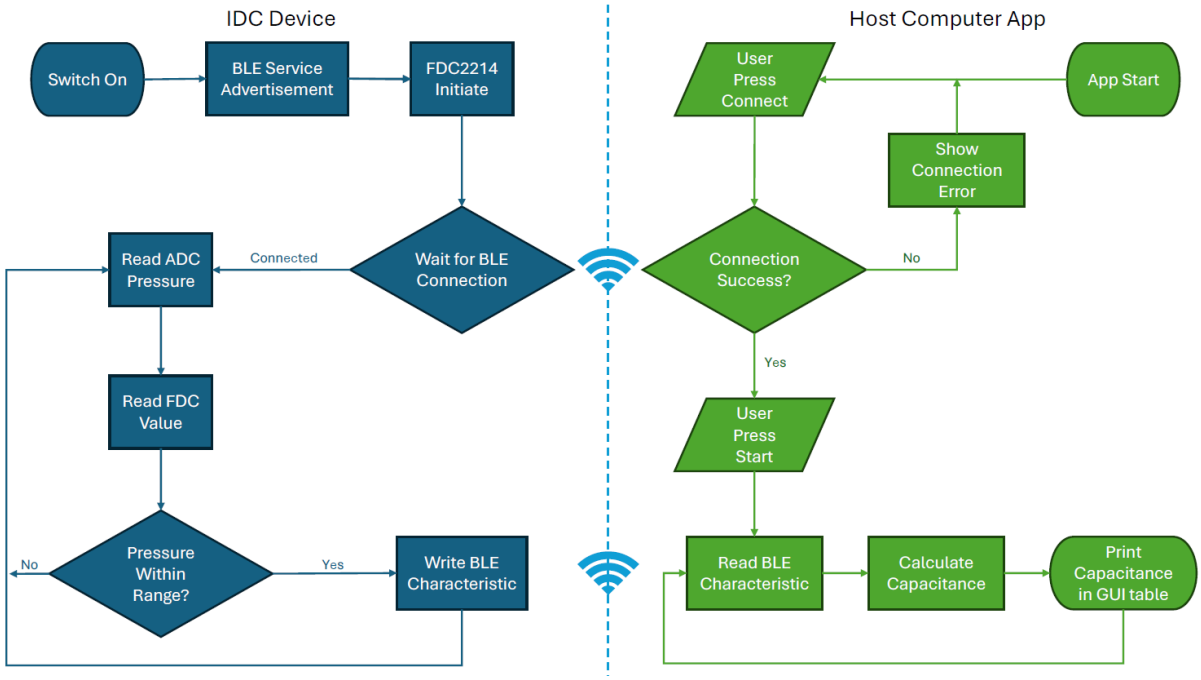

Figure 65 Flowchart describing the capacitance measurement and data transmission of the IDC wearable device. All of the processes performed by the IDC device are coloured in blue, whereas the tasks undertaken by the GUI application are coloured in green.

Tests were set up to run for 30 seconds of continuous use and collect a continuous data stream at the desired pressure range. After the 30 seconds have passed, a special notification prompts the user to remove the sensor, stop the data collection, and save the data before continuing to the next test. Further trials will explore longer wear tests. A snapshot of the GUI screen is presented in Appendix C.

6.3 Wearable IDC System Characterisation

6.3.1 Fabrication Variability Tests

Before characterising the system, the capacitance variability arising from the repeatability of the printing and assembly process was assessed. Three nominally identical IDC sensors were produced and laminated on separate textile armbands – named S1, S2 and S3. They were connected to the CDC and for each sensor capacitance was recorded for 30 seconds, 3 times in

a row. The sensors were not in contact with any medium (only air). Figure 66 presents the distribution of capacitance values obtained from the measurement protocol. The box plot shows that the median capacitance for all three sensors falls within a narrow range of 38.6 to 38.9 pF. The interquartile ranges are small, with error bars extending only slightly beyond the box boundaries. This indicates very low variability between repeated measurements of the same sensor. There is close agreement between the three independently fabricated devices, as no significant outliers or large shifts in central tendency are observed. These results confirm that the chosen fabrication process produces sensors with consistent electrical characteristics and minimal variation, demonstrating good repeatability of the manufacturing approach.

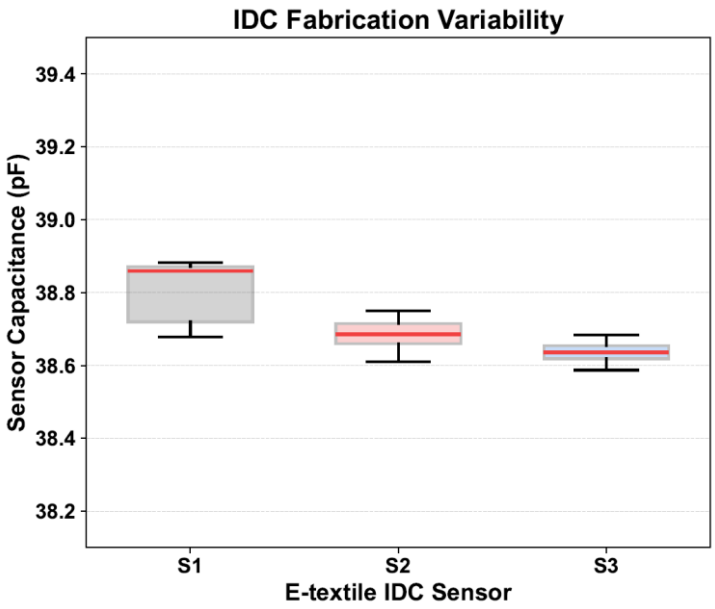

Figure 66 Box plots of the measured capacitance values from three identical e-textile IDC sensors (S1, S2 and S3). Each distribution represents the recorded samples from three repeated measurements of 30 seconds per sensor. Red line indicates the median value, box edges depict the interquartile ranges, and error bars illustrate the minimum and maximum values within 1.5 times the interquartile range.

6.3.2 Repeatability Test with a Dielectric Calibrating Weight

To validate the correct operation of the device, the stability of the readings across different days was tested before progressing with patient testing. A 3D-printed weight made of solid PLA material with a known and constant dielectric permittivity was used to test both the capacitance and the pressure sensor's outputs. In section 5.3.2, it was shown that under stable and repeatable conditions, the encapsulated silver IDC's measured capacitance does not fluctuate by more than 2 pF. The goal in this test is to confirm the result and verify that the developed system stays within that confidence interval and does not introduce too much noise into the measurement.

The calibration weight was 5 N and it was positioned on top of the skin-facing side of the strap band, in contact with the printed IDC sensor. The testing setup is presented in Figure 67. The weight was kept for 30 seconds, to replicate the setup during patient tests, and for each day the test was repeated 4 times, and the results were averaged. The relative permittivity of PLA is 3 and based on the dimensions of the IDC sensor (distance between electrodes and effective area), it is calculated that the capacitance will increase by 4 pF when the calibration weight is placed in contact with the sensor. Tests were performed under standard room temperature of 22 °C and relative humidity of 38%.

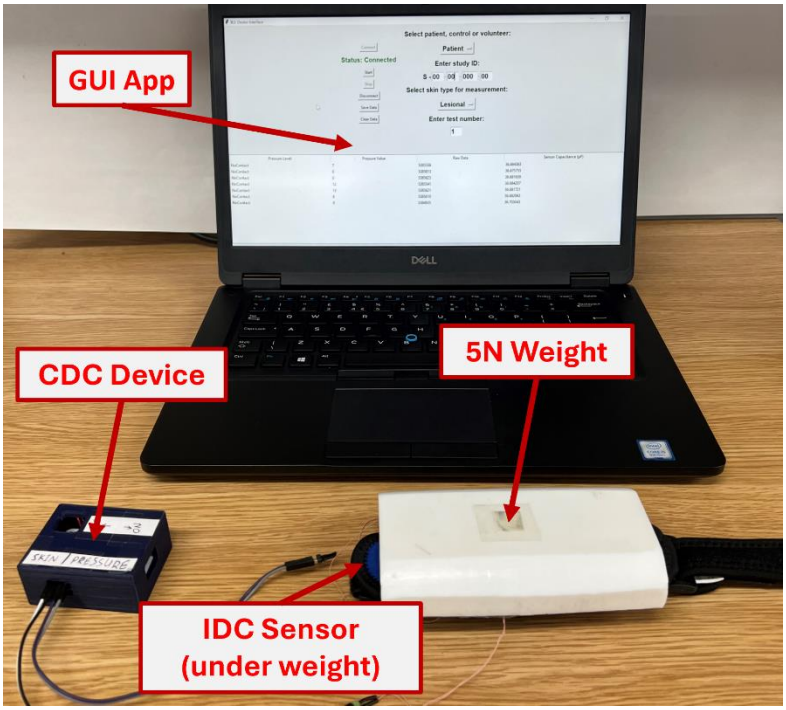

Figure 67 Photograph of the test setup used for calibration testing. The e-textile IDC sensor is positioned under the 5 N weight and is connected to the CDC device that converts the capacitance to a digital signal and transmits it to the host computer running the GUI app.

The results, presented in Figure 68, reveal the stability of the capacitance measurements, and the pressure sensors against time. It can also be observed that the readings are repeatable across different days. The capacitance of the sensor increased by about 1 pF with the addition of the calibration weight – from 38 pF when in contact with air, to 39 pF. This is less than the calculated value, but within the reasonable range. As the weight's surface is not fully flat, it is not possible to completely contact the IDC sensor, and thus the addition of air in the sensor-PLA interface reduces the measured capacitance. A slight trend of decreasing capacitance on each consecutive day is observed, but the decrease is insignificant as it is less than 0.5 pF, or less than 2 % of the total capacitance value, within the margin of error. The ADC value of the pressure reading remained around 3300 for the calibration weight across all 3 days. Without the weight,

the ADC value read was 0 for all 3 days. The calibration force of 5 N, used to achieve an ADC value of 3300, equates to approximately 130.2 kPa of pressure across the surface of the sensor.

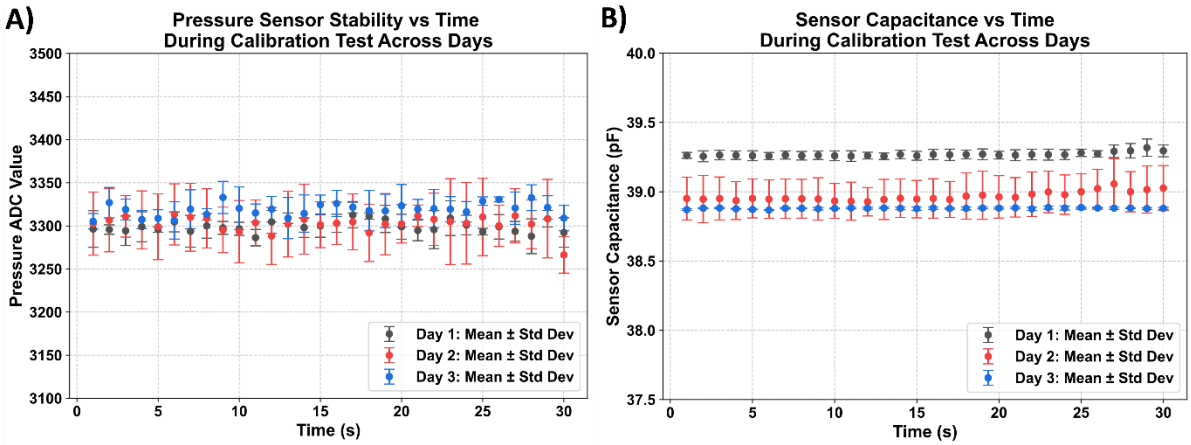

Figure 68 Results from calibration repeatability test across several days. A) Pressure sensor ADC readings against time. B) Sensor capacitance against time.

6.3.3 Relative Humidity Test

The e-textile IDC sensor was also tested against changing humidity levels in the environment, to determine the effect of relative humidity on the sensor's performance. Temperature and mechanical bending were previously found not to affect sensor performance in section 4.3.4. The IDC printed sensor was placed in a WKL100 climate chamber (Weiss Technik, Loughborough, UK), and its capacitance was measured continuously with the CDC, which was situated outside of the chamber. The following humidity profile was programmed into the chamber: 5 minutes at 40% RH; 20 minutes gradual increase to 90% RH with a step of 2.5% RH per minute; 10 minutes at 90% RH; 20 minutes decrease back to 40% RH; 5 minutes at 40% RH – for a total time of 1 hour. To measure the actual humidity, a TE-03 TH temperature and humidity data logging probe was also inserted into the climate chamber (Thermo Electric Company, West Chester, USA). The result of the test is presented in Figure 69. The capacitance of the IDC sensor changes with humidity, but for the most part the effect is minimal, less than 0.5 pF change when varying between 40% RH and 80% RH. Only when RH rises above 80%, a capacitance change of 1.5 pF is observed. The two spikes in capacitance readings at the beginning and at the end of the 90% RH programmed time can be attributed to a condensation up of water molecules on the surface of the IDC. The chamber maintains humidity by constantly switching a ventilation fan on and off, and the sudden trough after the first spike is caused by the evaporation of the water droplets due to the ventilation fan turning on. The uneven profile of the actual RH measured reveals many fluctuations in humidity, indicating frequent ventilation events. The two troughs of capacitance before and after the 90% RH range are also due to the ventilating fan, as confirmed by the behaviour of the actual RH measured in red. These troughs decrease the capacitance by about

0.4 pF, which is within the margin limit. At the end of the humidity test, the capacitance readings return to almost the same value as the start - within 0.2 pF. Overall, the IDC shows impressive stability under extreme environmental humidity conditions, as the change in capacitance is negligible compared to the change arising from a patient's skin.

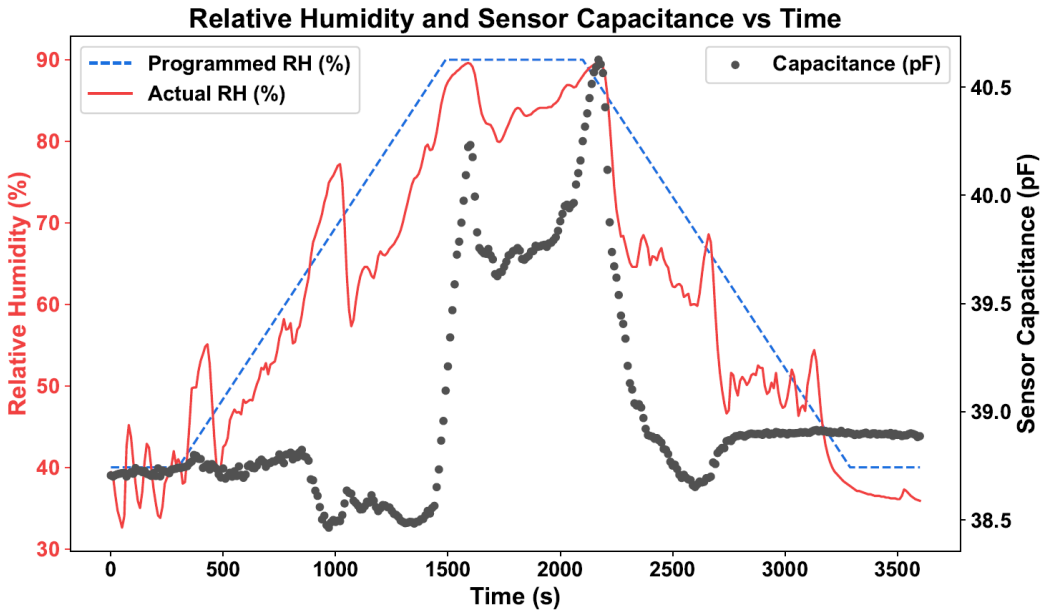

Figure 69 Change in capacitance of the IDC sensor over time for a varying change in the relative humidity of the environment.

6.4 Trials on Patients with AD in Clinic

6.4.1 Study Setup

In the patient trials, thirteen patients with AD aged 18-70, both male and female, participated in the study. The patients were recruited from the dermatological clinic, part of the University Hospital of Southampton. The study was done in conjunction with the NOMAD study, ethics approval: NRES 330915. Their skin was assessed by a dermatologist following accepted diagnostic criteria and specific areas of lesional and non-lesional skin on the arms of the patients were identified by the dermatologist. Lesional skin were areas with acute symptoms of AD, usually inflamed, red, and dry. Non-lesional skin were areas where there were no visible symptoms, and the skin appeared similar to clinically healthy skin. In some patients, almost the entire body was covered in lesions, so the least affected skin area was selected as non-lesional.

The e-textile device was located on lesional and non-lesional areas of the skin along various places of the patients' arms. The most common locations were the volar forearm and the anterior bicep. Several measurements were taken on each location to investigate sensor repeatability, with 1 minute delay between measurements. Each measurement lasted 30 seconds. The

pressure used in the characterisation tests of 3300 ADC counts (TL 3 or 130 kPa) was too high and caused discomfort in the patients; thus, it was reduced to 2100 ADC counts (TL 2 or 65 kPa). This pressure value was maintained throughout the entire patient study. The Corneometer® and the Tewameter® were used alongside the IDC device to correlate the readings to the current gold standard in skin hydration assessment. Ten readings with each of the gold standard devices were taken from the same lesional and non-lesional area on the skin, where the capacitance was sampled. Readings were taken right after the corresponding reading with the IDC device finished. The Tewameter® was used on only 7 of the 13 patients.

6.4.2 Sensitivity Test with Different E-Textile IDCs on Patients

Three of the patients were additionally tested using IDC sensors of size G200 N16 and G400 N8, printed and laminated on identical armbands – patients 3, 4, and 5. These tests were done independent from the rest of the study and a single-point reading through the e-textile CDC system was collected using the G100 N32, G200 N16 and G400 N8. G400 was used instead of the G500 because in section 4.3.3 it was discovered that overall greater area does not affect the sensitivity of the IDC sensor – only the gap between the electrodes matters. Thus, only IDCs with identical sensing area and different gap distances were used – directly comparing their sensitivity and validating the findings of the simulation, skin phantom and volunteer studies. The results were averaged and presented in Figure 70. The G100 N32 feature the highest difference in capacitance values across the inter-patient lesional and non-lesional readings of 6.9 pF, whereas the G200 N16 and G400 N8 feature lower differences of 2.8 pF and 1.5 pF respectively. Thus, the G100 N32 has the highest sensitivity towards detecting the SC barrier properties and therefore toward evaluating the severity of AD.

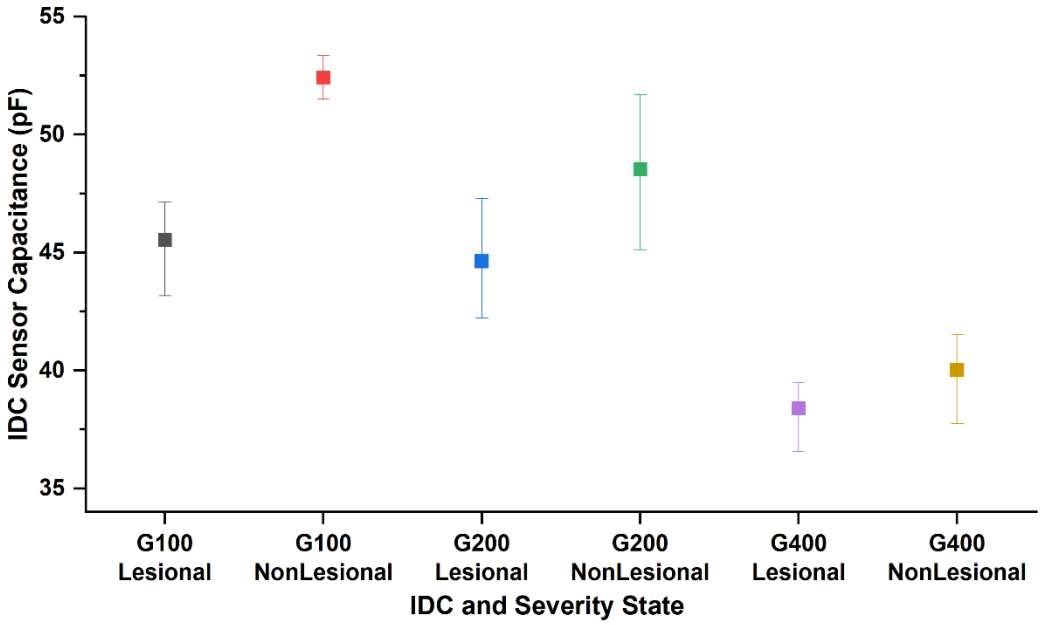

Figure 70 Averaged capacitance readings for lesional and non-lesional skin of 3 patients using 3 different IDC sizes – the G100 N32, G200 N16 and G400 N8.

6.4.3 Trial Results and Discussion

The study collected 13 datasets of longitudinal capacitance data from the lesional and non-lesional skin of the patients – numbered from 1 to 13. Figure 71 A) presents the IDC capacitance data for one of the patients (number 13), along with the averaged single-point-in-time measurements for the corneometry and TEWL. In Figure 71 B), a photograph of the skin of patient 13 is shown along with labels highlighting the lesional and non-lesional skin areas selected for this patient. The two spots selected were both on the patient's right arm. The visual difference between the two skin areas is apparent, and the capacitance readings strongly align with that. In this case, TEWL readings for the lesional skin are in the high 38 g/m^2h, hinting towards greater loss of barrier integrity and therefore higher severity of AD in skin.

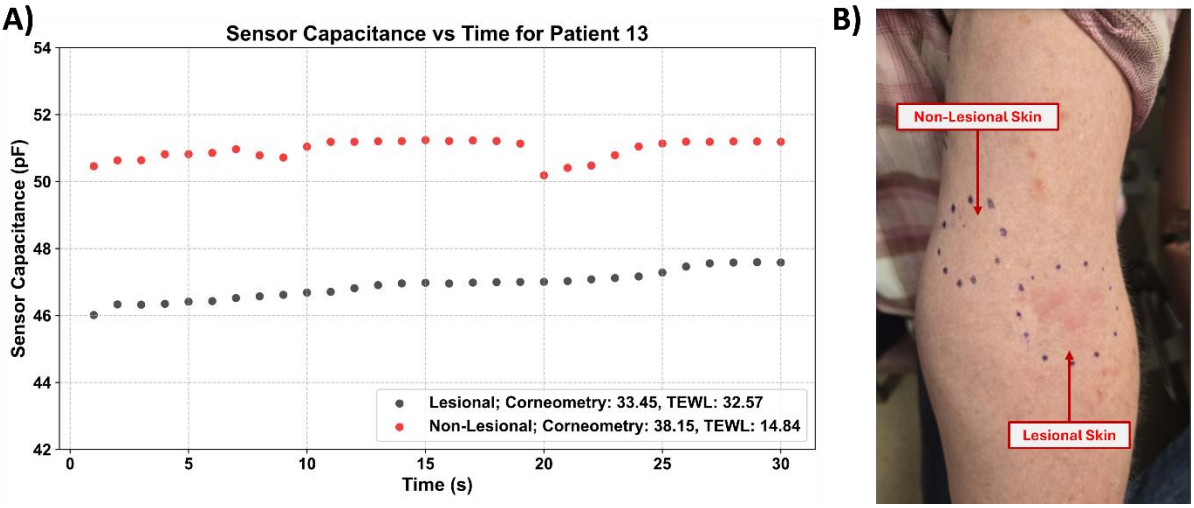

Figure 71 A) IDC sensor capacitance against time for an individual patient with AD on lesional and non-lesional areas on the skin. The legend shows the corresponding corneometry and TEWL values. B) Photograph of lesional and non-lesional areas of the skin of the right arm of patient 13.

The capacitance data for each of the patients are aggregated and presented in Figure 72, whereas the Corneometer® and Tewameter® data is presented in Figure 73 and Figure 74. The range of capacitance readings is between 40 – 55 pF across all patients, with lesional skin readings having an average of 46.71 pF and non-lesional skin readings an average of 49.25 pF. This reveals a considerable measurable difference between lesional and non-lesional skin of patients, which is also visible across all patient readings. In patients 4 and 13, this difference is the greatest, with corresponding delta values of approximately 6 pF and 4 pF. Patient 1 featured the lowest capacitance values of 40 – 42 pF, indicating that his condition was the most severe from the perspective of the IDC sensor. This is supported by the highest measured TEWL values (35 – 50 g/m^2h) and low corneometry values (16 – 26 A.U.) for patient 1. TEWL is a measure of the water loss in skin, and corneometry is a marker of skin hydration. Therefore, lesional skin with AD should exhibit high TEWL and low corneometry, which is the case here and is in line with the low IDC capacitance of patient 1. The values suggest that the condition has progressed so much in this patient, it also affects the visually non-flaky regions of the skin, thereby explaining the low capacitance and high TEWL values for non-lesional skin. The second-lowest capacitance readings are of patient 12, where there is also a small capacitance difference between the lesional and non-lesional skin, strengthening the claim that in very severe cases of AD, the barrier integrity in all areas of the skin is damaged.

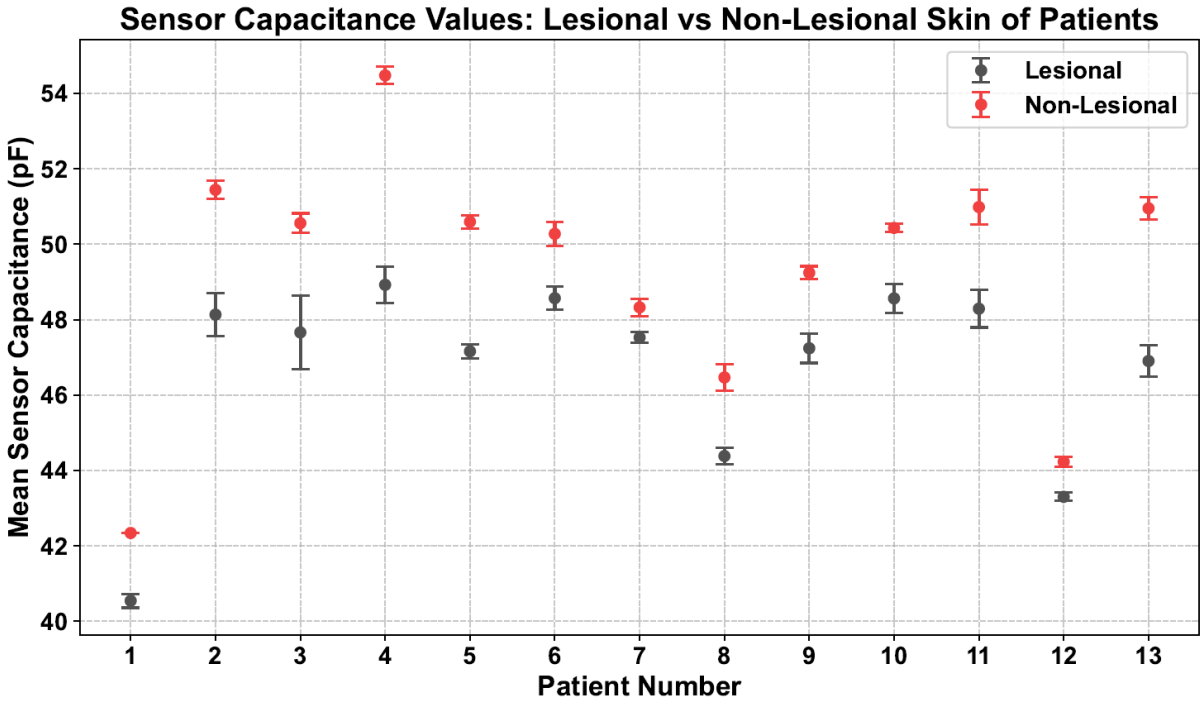

Figure 72 Mean sensor capacitance values using e-textile IDC sensor to test skin barrier integrity of lesional and non-lesional skin of 13 patients with AD. Error bars indicate standard deviation.

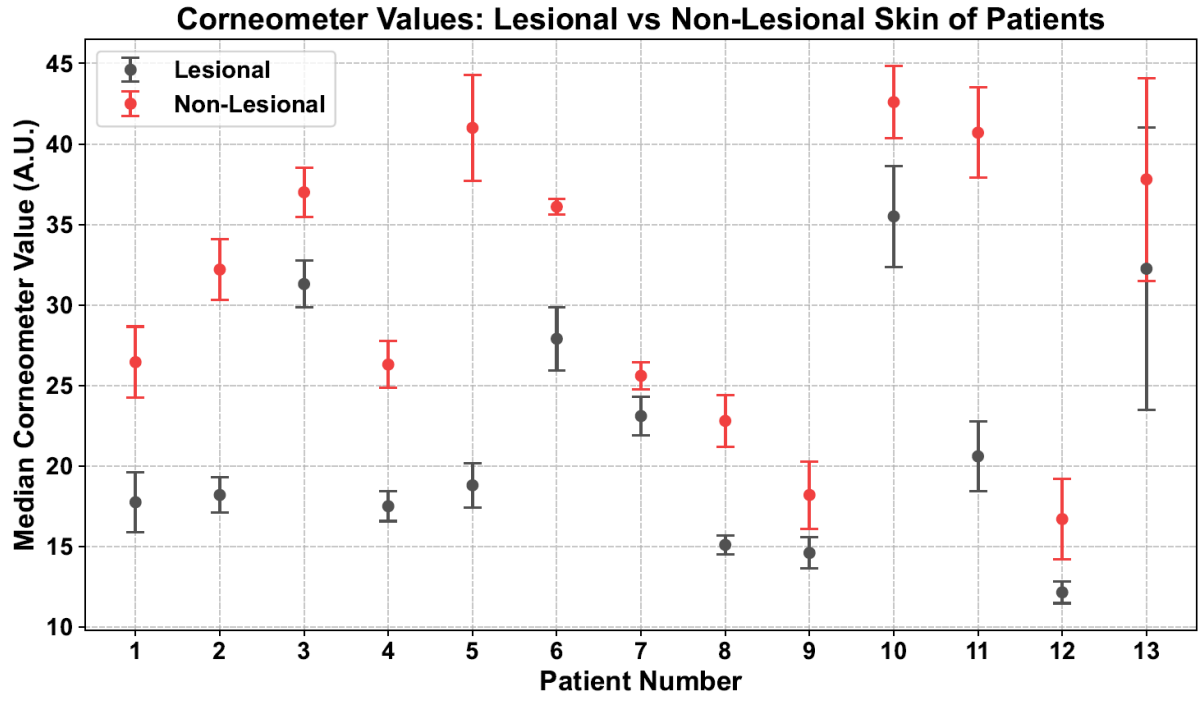

Figure 73 Median Corneometer® values to test skin barrier integrity of lesional and non-lesional skin of 13 patients with AD. Error bars indicate standard deviation.

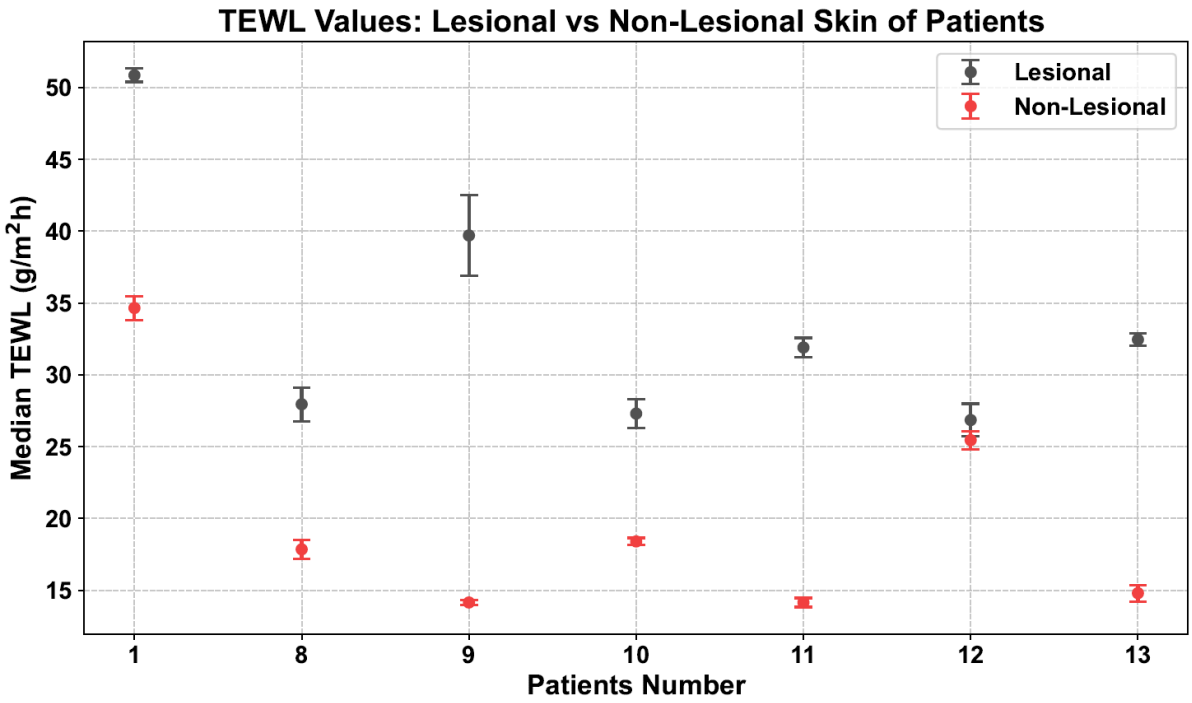

Figure 74 Median TEWL values to test skin barrier integrity of lesional and non-lesional skin of 13 patients with AD. Error bars indicate standard deviation.

For the Corneometer® and Tewameter®, the data presented is the median value of 10 iterative measurements for each patient. Median values were used instead of the arithmetic mean because it is a more accurate representation of the data extracted from the instrument, as it diminishes the effect of outliers from improper instrument application. Calculating the mean across all patients for the lesional skin gives a corneometry value of 21.9 A.U. and a TEWL of 33.86 g/m^{2}h, and for the non-lesional skin – 31 A.U. and 19.92 g/m^{2}h. Both gold standard instruments reveal a difference between the two skin types, which is the same as with the novel textile IDC sensor, thereby confirming the latter's validity as an instrument towards identifying SC barrier integrity in patients with AD. This also highlights the positive correlation between the textile IDC sensor and the Corneometer® and the inverse correlation of the former two to the Tewameter®. Pearson's correlation coefficient for the combined lesional and non-lesional data from the IDC and Corneometer® was found to be 0.595, with a p-value of 0.001, indicating a statistically significant ($p < 0.05$) strong positive correlation. Figure 75 reveals the relationship – it depicts the corresponding mean capacitance reading for each median Corneometer® reading for a patient, regardless of the severity state being lesional or non-lesional. This plotting technique allows for correlations between two measurement principles to be graphically observed and calculated. Pearson's correlation was not calculated for the TEWL readings, as there were too few to achieve statistical significance. This confirms that the novel e-textile IDC sensor's readings are accurate, as they are positively correlated with the commercial hydration measurement device. Furthermore, the readings of the IDC device feature smaller variability than the Corneometer®,

rendering it more accurate for the application. The statistical variability and its significance will be investigated in the next subsection.

Finally, to prove the repeatability of the IDC sensor readings, for one of the patients (number 8) longitudinal tests were conducted several times, with a two-minute wait between tests. The results, presented in Figure 76, reveal a maximum deviation between repeated IDC sensor readings of around 0.4 pF. This is much lower than the difference between lesional and non-lesional skin, so unlike the Corneometer®, the IDC sensor does not obscure meaningful differences due to measurement variability. In contrast, the Corneometer® showed greater inconsistency, with variations between repeated measurements sometimes exceeding the actual difference between skin types, making it less reliable for distinguishing AD severity.

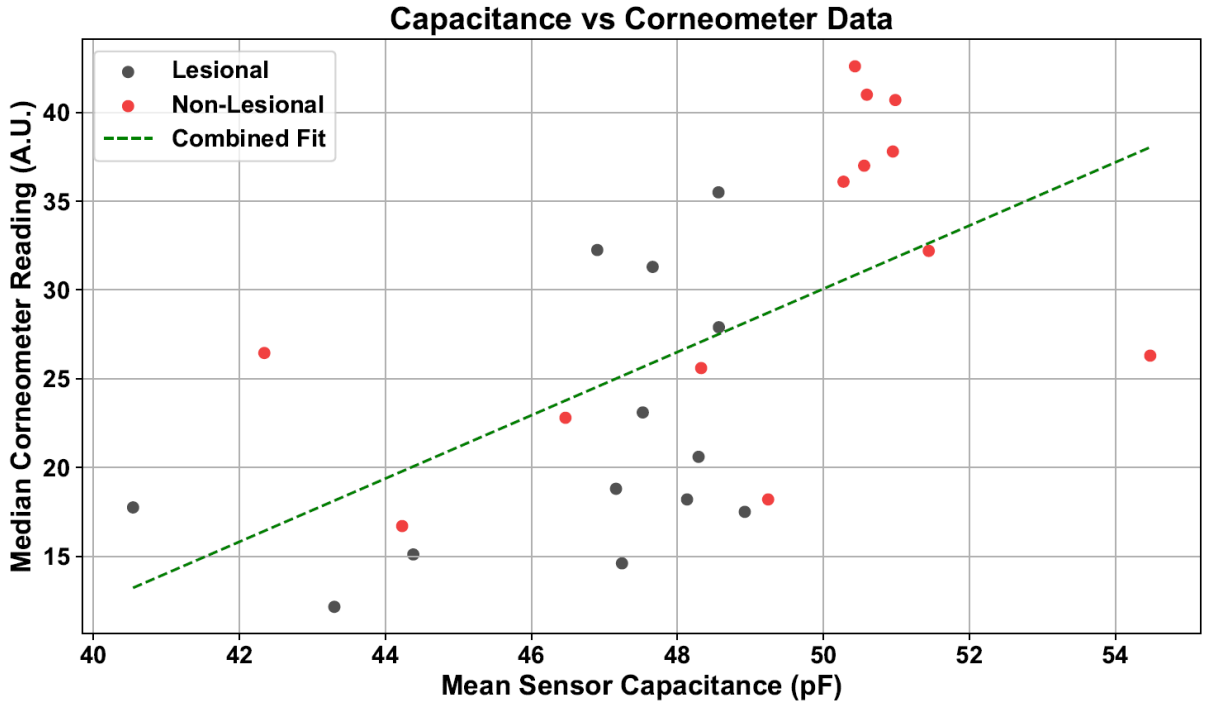

Figure 75 Correlation plot between e-textile IDC capacitance and Corneometer® data, with a combined (lesional + non-lesional) best fit line plotted in green, showing positive correlation between the two measurands.

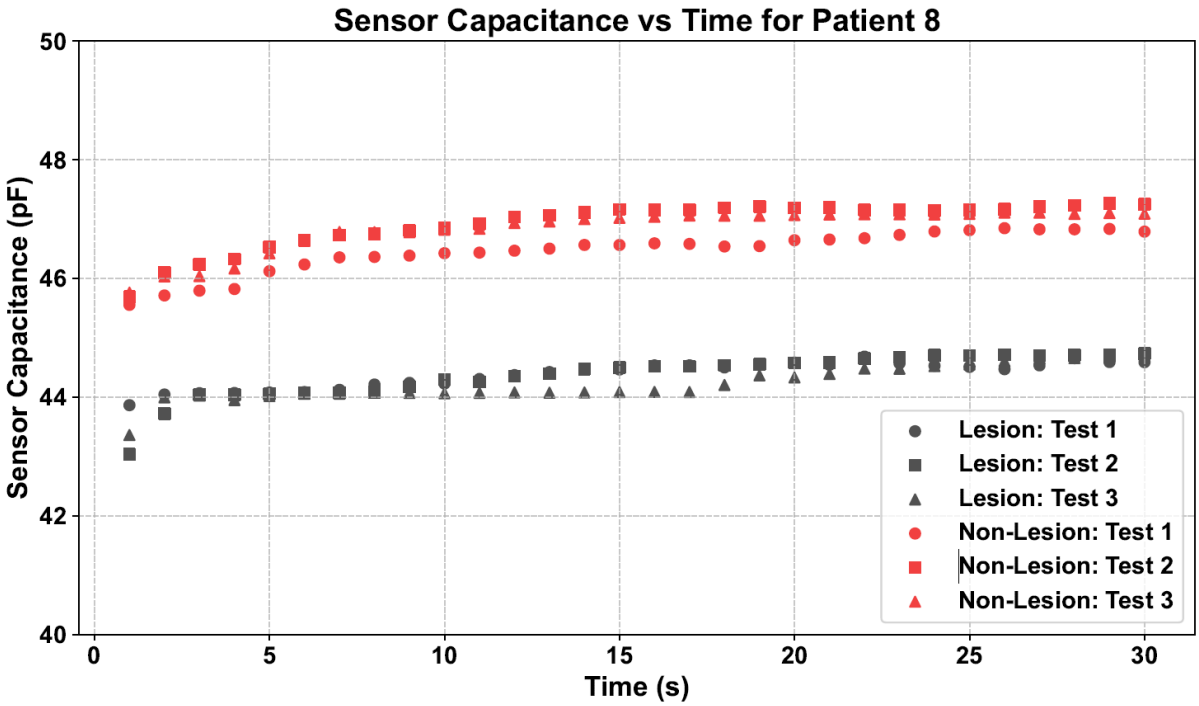

Figure 76 Repeated IDC sensor capacitance against time readings for an individual patient. Three tests were performed for each skin area – lesional and non-lesional.

6.4.4 Data Analysis and Significance

To compare the proposed e-textile sensor to commercial devices the clustering and difference of readings from lesional and non-lesional sites was examined. With each device, lesional and non-lesional skin can be clearly distinguished: lesional skin shows reduced capacitance and corneometry values, and increased TEWL, consistent with reduced stratum corneum hydration and impaired barrier function. The IDC box plot demonstrates tighter clustering of values compared to the commercial devices, indicating greater repeatability across patients. The Corneometer®, by contrast, shows broader spread, reflecting a higher susceptibility to measurement variability.

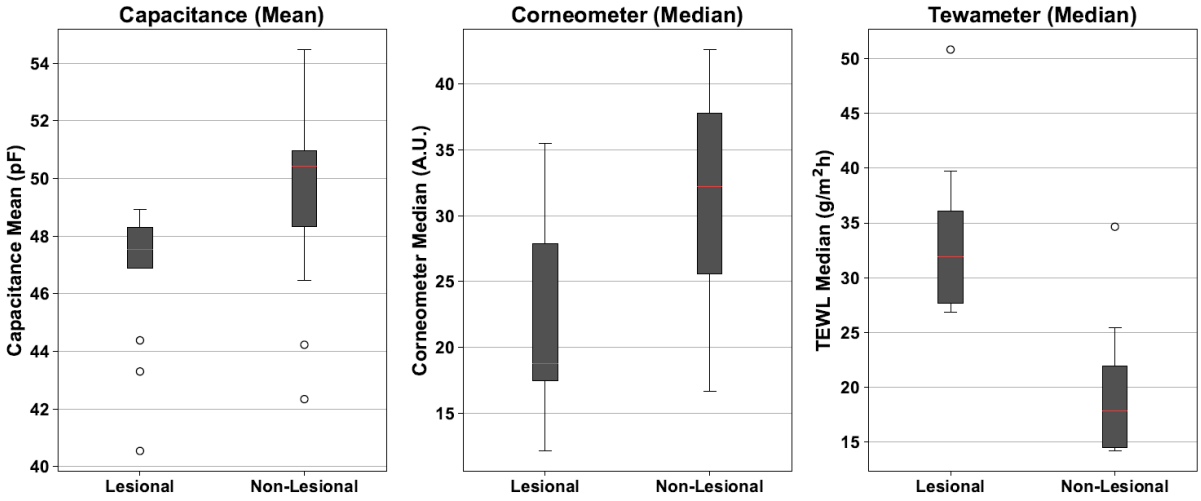

Figure 77 Box plots of capacitance (left), Corneometer® values (middle), and TEWL values (right) for lesional and non-lesional skin of atopic dermatitis patients. Each box represents the interquartile range (IQR) from the 25th to the 75th percentile, the red line indicates the median, the whiskers extend to the minimum and maximum values within 1.5×IQR, and circles mark outliers.

The variability in the Corneometer® readings is evident also in Figure 77, attributed to the wider standard deviation error bars. In the case of patient 13, the lesional and non-lesional error bars overlap, signalling issues with repeatability. This could be caused by an issue with calibrating the device. Another reason for the variability is the amount of applied pressure. The Corneometer®'s probe features a spring-loaded sensor head that depresses once in contact with the skin to ensure repeatable pressure application. Although reliable, this technique is prone to human error because even with the spring, a user can accidentally exert more pressure than needed, which alters the results. Furthermore, the rigid sensor head of the Corneometer® does not conform to the curves of the skin.

The proposed e-textile IDC sensor solves all those issues by measuring direct capacitance values, monitoring the pressure, and its flexible substrate establishes conformal contact to the skin. The e-textile IDC device surpasses the capabilities of the commercial Corneometer®, because it can provide longitudinal readings of the skin's severity, rather than just single-point measurements. The stability of the IDC sensor across time is evident with the small error bars in Figure 72. In some cases, a slight capacitance drift is noticed in the first 5-10 seconds of putting on the device, and that is attributed to the skin conforming around the sensor. Again, the limiting factor for the e-textile IDC sensor is occlusion, as the encapsulation and IDC electrodes aren't water permeable, so condensation would build up on the skin-sensor interface. For the short test of 30 seconds, this effect is negligible.

Using the per-participant mean IDC capacitances calculated for the box plot, a class separation distribution plot is built, illustrated by Figure 78. The lesional means are shifted to lower capacitance and the non-lesional means to higher capacitance, with 2 overlapping regions around 43 pF and around 47 pF, and a narrow valley of separation around 49 pF. The overlap illustrates that no single threshold can achieve perfect separation of both classes, but the valley between the two distributions could be used for an optimal decision boundary, a preliminary analysis based on this small number of participants.

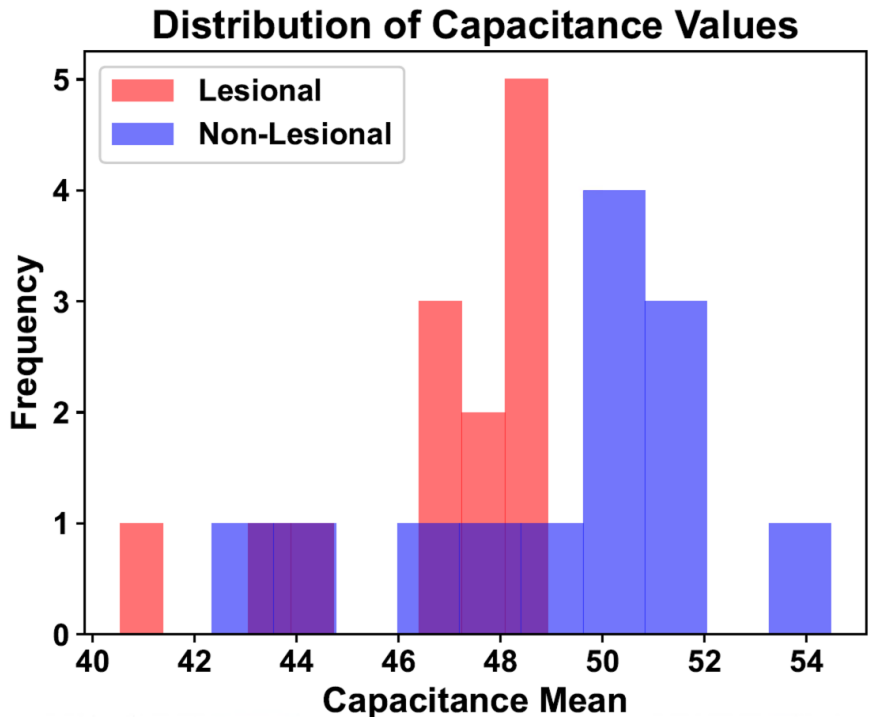

Figure 78 Distribution of IDC mean capacitance values obtained from lesional and non-lesional locations on the skin of 13 patients with AD.

Although the e-textile IDC sensor is not aimed to be used as an inter-individual diagnostic and classification tool, an attempt to investigating possible thresholds was performed. Receiver operating characteristic (ROC) analysis to the dataset of the 26 IDC mean capacitance values was applied. The ROC curve considers all possible thresholds and maps out the trade-off between sensitivity (correctly detecting lesional sites) and specificity (correctly identifying non-lesional sites). The built ROC curve is displayed in Figure 79. The overall performance of the classifier is summarised by the area under the curve (AUC), which was found to be 0.79. This value indicates good discriminative ability as it is far above random guessing (AUC = 0.5) and approaching the level of more established clinical tools. The optimum point on the curve was found to be 48.9 pF, which was the value spotted in the distribution plot. The optimum point is determined by maximising the Youden index, which is the sum of sensitivity and specificity minus 1. At this threshold the Youden index is 0.69 and it yields a sensitivity of 100%, meaning that all

lesional sites were correctly identified, while specificity reached 69%, with 9 out of 13 non-lesional sites correctly classified.

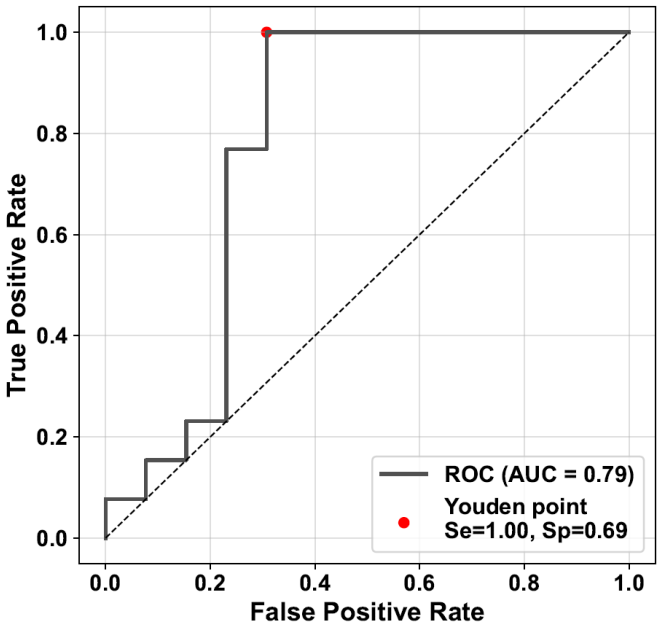

Figure 79 ROC curve generated from mean capacitance values of lesional and non-lesional skin sites of 13 patients with AD. The curve illustrates classifier performance across varying decision thresholds, with the diagonal line representing chance-level discrimination.

These findings show a consistent picture between visual inspection of the data distribution and statistical optimisation. The cut-off value of 48.9 pF corresponds closely to the region where the two distributions overlap, providing both an intuitive and a quantitative justification for its selection. At this threshold, the IDC system offers very high sensitivity. The trade-off is a moderate specificity, reflecting that some non-lesional sites still fall below the threshold.

This analysis demonstrates that a simple, single-threshold rule applied to IDC capacitance values is possible and could be used to distinguish lesional from non-lesional skin across different people. The ability to derive such a threshold directly from empirical patient data provides a practical foundation for future use of the e-textile sensor system in monitoring atopic dermatitis. These results are still preliminary, and it is not straightforward to define a threshold for lesional versus non-lesional skin at such a small population study. Still, the key benefit of the IDC sensor is the accurate assessment at an individual level and segregation of severity states of AD.

6.5 Conclusion

The results presented in this chapter demonstrate the successful development and validation of a complete e-textile IDC sensor system for monitoring AD in patients. The portable device featured a compact read-out circuit that transmits the data wirelessly via BLE over to a host computer running a custom-built app. It showed repeatability in its readings across several days during the same test conditions, and stability when subjected to extreme humidity environments. The sensor successfully managed to distinguish between lesional and non-lesional skin in all the patients with AD that participated in this study, giving 100% sensitivity and specificity for individual patients. Mean capacitance values between the two skin types were 46.7 pF and 49.3 pF, respectively. These findings correlated positively with Corneometer® readings and inversely with TEWL measurements, confirming sensitivity to impaired barrier function. Compared to commercial instruments, the IDC sensor demonstrated reduced variability and improved repeatability, enabling clearer distinction between skin states. ROC analysis further indicated that a simple capacitance threshold could classify lesional and non-lesional skin with high sensitivity and moderate specificity (AUC = 0.79). But a single population-wide threshold could not be defined as the IDC sensor is most valuable for tracking intra-individual biophysical change rather than serving as a stand-alone diagnostic tool. Collectively, the results confirm that the e-textile IDC system provides a reliable and practical platform for objective monitoring of AD severity, surpassing the repeatability of existing tools and offering strong potential for at-home and longitudinal use.

Chapter 7 Conclusion

The goal of this project to produce a device that can monitor and/or measure the severity of AD lesions in the skin, was achieved successfully. The utility of such device is to provide patients with a quantitative measurement of the severity of their condition without frequent in-person examinations from a dermatologist. Furthermore, the wearable modality can also assist in better understanding the pathogenesis of the disease, as continuous wearing could reveal physiological changes in the skin as the condition worsens or enters remission. The e-textile IDC sensor accomplished all of the above and was successfully validated not only in silica, through simulation and skin replicas, but also in vivo, through actual tests on patients with AD.

To empirically assess AD, the sensor was designed to detect one of the biomarkers of AD – change in the hydration state of the SC due to a dysfunction of the epidermal barrier. Patients' skin has a characteristic dehydration of the outermost layers of the skin, and the lack of water molecules alters the dielectric properties of said layers. The IDC sensor's capacitance output is affected by that change and thus, by focusing the electric field within the SC layer, the sensitivity towards the barrier integrity is maximized. Other measurement methods were also briefly discussed – reflectometry using RF waves and optical spectroscopy using NIR light. All three methods were compared, highlighting each one's merits and demerits and published in a review article, but the capacitance measurement through the IDC was selected as the best for the current application.

FEA simulation was performed to optimise the design of the IDC sensor. Gaps in the literature were identified – limited understanding of penetration of electric field lines into complex media and lack of comprehensive information on the dielectric properties of the different skin layers. This led to a comprehensive investigation of IDC sensor's behaviour when in contact with multi-layered tissues such as the skin. A novel skin model with layer-separated dielectric properties was proposed through analytical study and was solved both in steady-state and frequency domains to the determine the optimal IDC geometry. This resulted in 2 novel publications, laying important foundation and providing other researchers with the dataset to build accurate skin models for other applications. The FEA study concluded with several design geometries of the IDC sensor, differentiated by the gap distance (G) between neighbouring electrodes, with an overall winner being IDC sensor with a G of 100 μm and 32 electrodes (G100 N32). This design yielded the largest change in capacitance per change in dielectric properties of the SC layer. The study also discovered the target excitation frequency range for maximum sensitivity towards AD, between 1 kHz and 1 MHz.

The proposed IDC sensors were initially fabricated out of flexible copper-polyimide sheets and tested on replicas of the skin, called phantoms. A novel skin-mimicking phantom was developed

able replicate a hydration gradient of the skin on the same substrate. This phantom can mimic varying severity states of skin with AD – from severely dry to clinically normal. The characterization study showed that the G100 N32 IDC is more sensitive towards hydration changes of SC compared to the other IDC designs, with a sensitivity of 13.1 pF/cm^2 per 1 A.U. of hydration. The entire characterisation study, alongside with the novel skin phantom was published, filling the gap in the literature of empirical sensors for the application of monitoring AD.

During the testing on healthy volunteers, problems in repeatability appeared, caused by time-based drift of capacitance readings and irreversible hysteresis due to poor contact between the skin-sensor interface. Thus, the second iteration of the IDC sensor solved all of this through the addition of an encapsulation layer and accurate control of applied pressure – resulting in capacitance readings with less than 2% variability under calibration studies. The sensor's output was stable (within 5% of baseline) during relative humidity cycling of 40 – 90 RH%.

The culmination of the project was the development of a custom hardware and software system to complement the e-textile IDC sensor and pave the way for patient trials. The development system used the FDC2214 to digitise the capacitance reading and transmit it wirelessly via BLE to a host computer running a bespoke app. The system was used as part of the NOMAD study on 13 patients with the condition to distinguish through the lens of capacitance lesional and non-lesional areas of the skin. It successfully managed to achieve that, yielding 100% specificity and sensitivity in intra-patient studies, and also followed a positive correlation (0.595) with a statistical significance ($p < 0.05$) with commercial hydration measurement devices such as the Corneometer® and Tewameter®. The e-textile IDC sensor measured capacitive difference between lesional and non-lesional states of the skin of the order of 3 to 5 pF with tighter clustering of values and better repeatability and variability compared to commercial devices.

In this thesis, the complete development journey of a novel medical monitoring device for AD is uncovered. It started with a novel application and design, which were validated through analytical and simulation studies that have uncovered new insights into the well-established concept of IDC sensors. That design was fabricated into a physical sensor, validated and characterised through novel means of replicating the properties of skin with the condition. Finally, a full-scale user-friendly solution for monitoring patients is built from the ground up (software + hardware), at the centre of which is the proposed IDC sensor. The flexibility of the e-textile solution permitted two modalities – longitudinal wear or discrete singular measurements. That solution allowed for clinicians and dermatologists to empirically determine the severity of patients with the condition during patient trials, laying the foundation for wide-scale and remote assessment of AD.

Chapter 8 Future Work

This research has laid the foundation for a new generation of devices capable of providing both patients and clinicians with objective and continuous assessment of AD in vivo. It has expanded the understanding of IDC sensors and their application in medicine, by delivering a proof-of-concept prototype that surpasses current commercial devices. However, further research and development are required before this technology can be adopted into standard dermatological practice. Research will be focused to close gaps in this research, which emerged to favour conducting patient trials, such as testing the silver IDC sensors on the skin phantom and encapsulating the copper IDC sensors to determine if capacitance drift still occurs.

The first step is the continuation of the patient trials to encompass a wider pool of participants and gather more data. In order to increase the statistical significance of the results, the authors plan to test on at least 100 more patients, which is possible under the NOMAD study. With the data better analytics methods and machine learning, like the ANN models mentioned in subsection 2.2.3.5, can be employed to classify the severity and uncover new insights into better understanding the disease. An important dimension of the data-collection is to allow patients to self-record their severity readings at their own homes. Thus, multiple units of the device will be fabricated to allow regular patients and volunteers to participate in the study remotely.

The second step is to cover wide areas of the skin. The limitation of the e-textile IDC sensor as it stands is that it provides an assessment of a relatively small area. AD is a condition with lesions appearing all around the patient's body. Current diagnostic criteria, accepted in dermatology practices, evaluates the condition's severity across the entire body. It is also of clinical significance to understand what happens at the boundary of a lesion, where it borders non-lesional skin. To address this research questions, the author has already conceived a design, that was not investigated during the course of this doctoral degree. The Matrix IDC (or M-IDC) features a matrix array of individually connected IDC cells. The goal is to take precise measurements at an array of points on the skin and to produce a spatial map of hydration, much like the CMOS optical sensors. Two designs of the M-IDC are already developed and presented in Appendix D. The M-IDC will require complex read-out circuitry, but will provide beneficial data to help dermatologists distinguish between lesional and non-lesional patches better.

The third step is the overall improvement of the sensor's footprint. Miniaturising the electronics of the read-out circuit in order to fully integrate it into a wearable format is a necessary step. A textile pressure sensor to control the applied pressure will be implemented to create a seamless textile garment that can be worn by patients continuously. Patient-centric studies will be conducted to gauge the feedback from wearing the device and further improve the wearable IDC.

The goal is to produce an easy-to-use, non-invasive device, that can be integrated with patient routines at home and can provide real-time data on their condition.

Appendix A Mask for Screen Printing and ROP

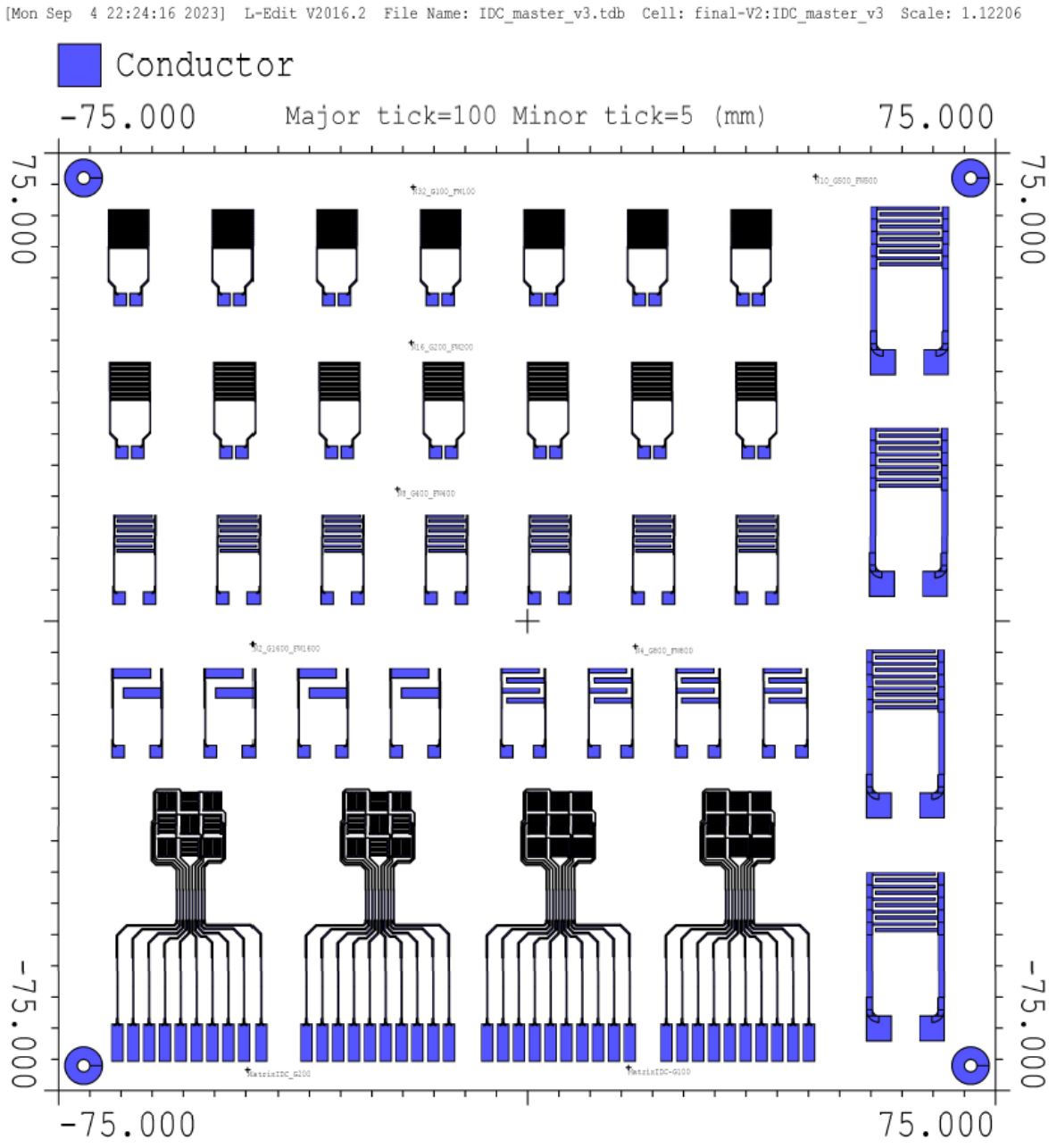

Figure 80 Rendered image of the screen-printing mask carrying all IDC designs discussed in this report. All the drawn components are part of the conductor layer, and the grid layer is just the border around the mask. Because some of the elements are considerably smaller, precise rendering was not possible, leading to distortion in the images, when embedding in text-editing software.

Appendix B CDC Circuit – Schematic

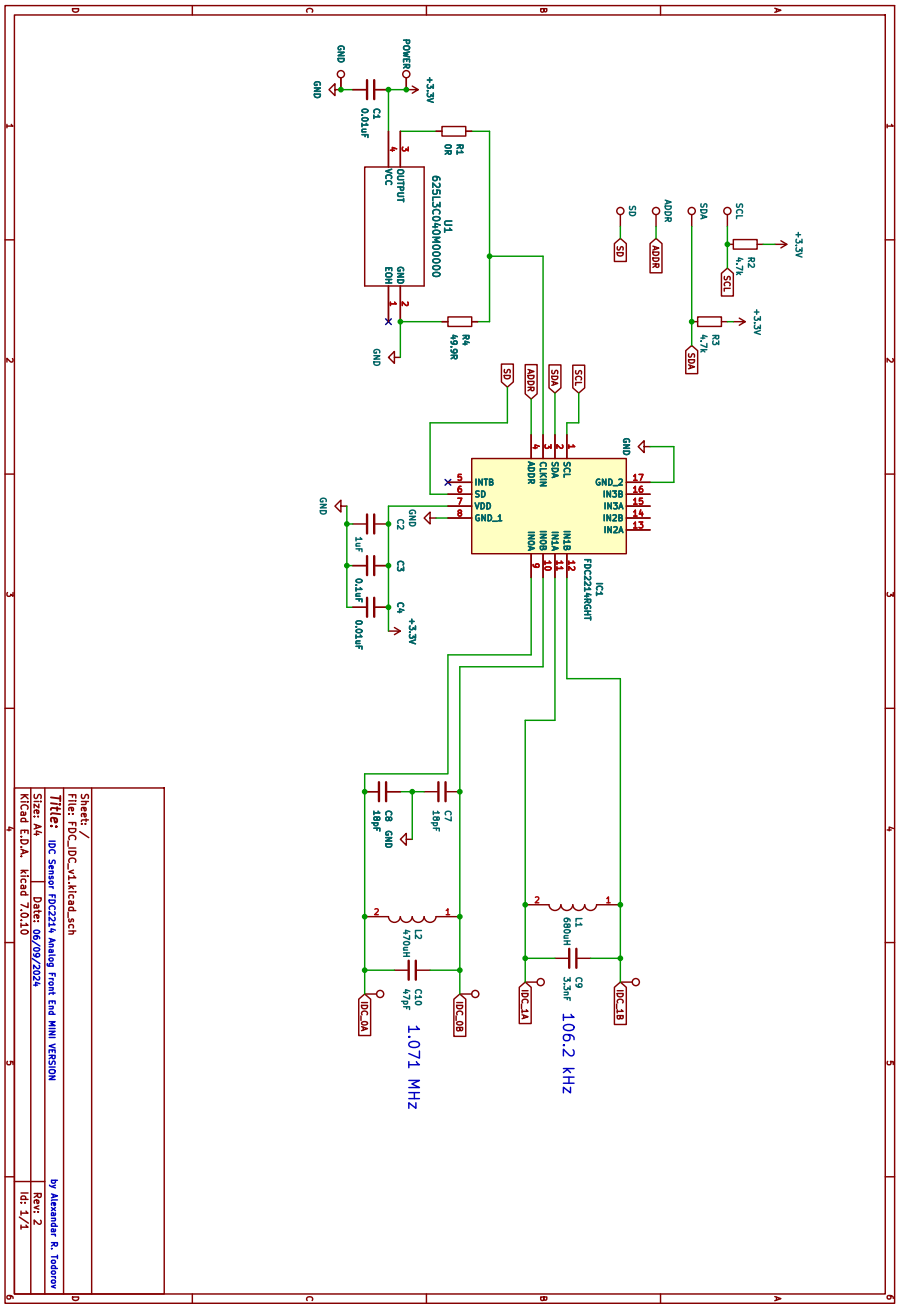

Figure 81 Schematic of the CDC circuit used to convert the raw capacitance data into digital signal. The FDC2214 is the core component of the circuit, which interfaced via soldered connectors to the XIAO nRF52840 MCU.

Appendix C Graphical User Interface

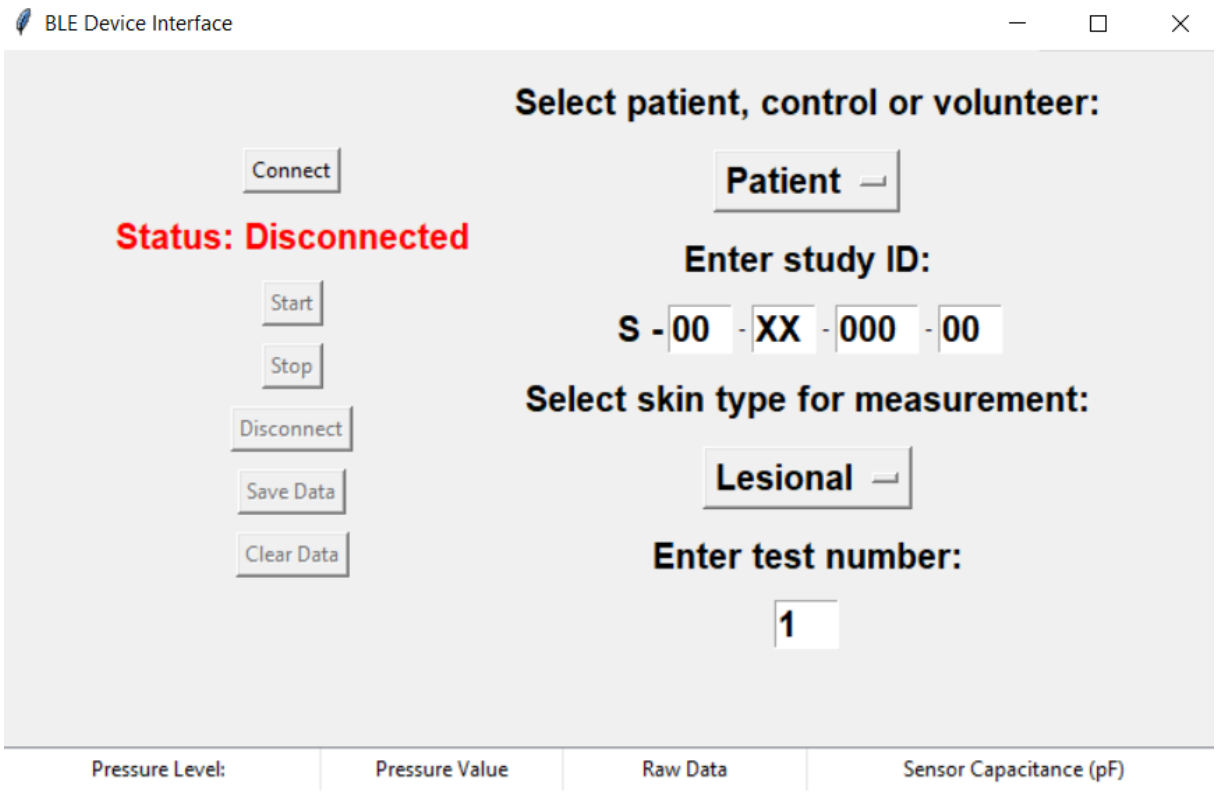

Figure 82 Snapshot of the graphical user interface developed to work alongside the e-textile IDC sensor. It was made bespoke to work with the data collection procedure of the NOMAD study.

Appendix D Matrix IDC

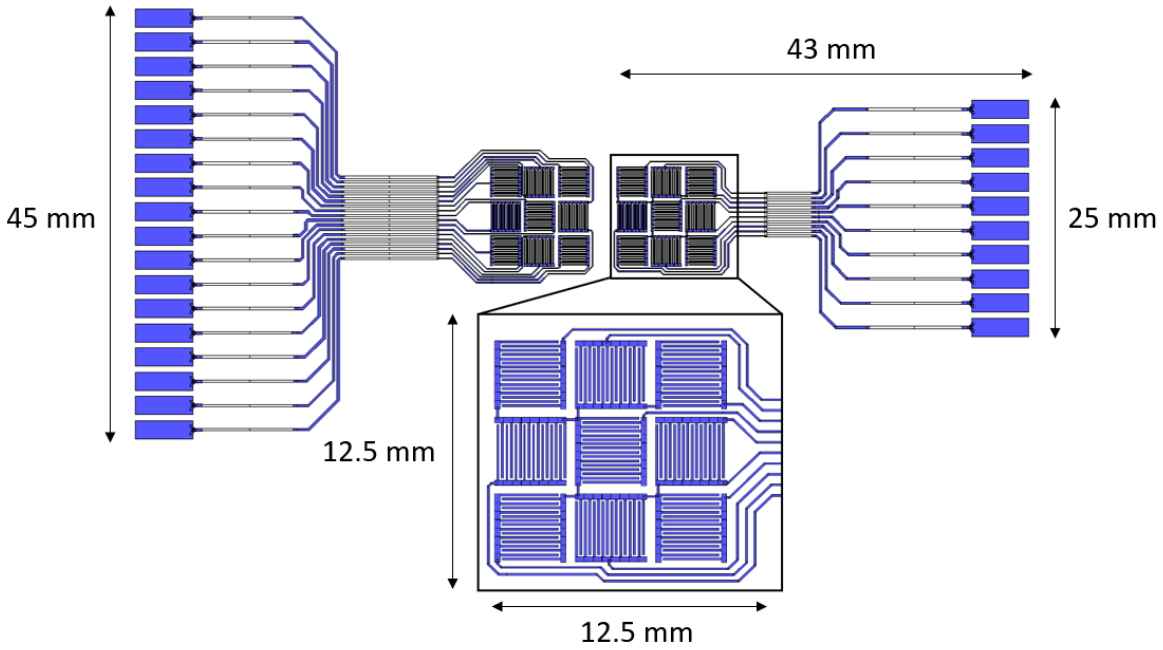

Figure 83 Schematic of the Matrix IDCs with a magnified view into the structure of the right one. The one on the left features individual connection for each cell, whereas the one on the right has a common voltage input line between cells.

The G100 N32 IDC was chosen as the base for the M-IDC sensor. The IDC cells are arranged in an alternating pattern, with neighbouring cells rotated at 90 degrees, so that there isn't any interference between them. If the cells were arranged in parallel, a signal arm on one of the IDCs will interact with a neighbouring ground arm and will introduce parasitic capacitance. Figure 83 illustrates the features of the M-IDC and shows the two approaches in wiring. The left M-IDC includes individual signal and ground connections for each of the 9 cells, resulting in 18 pins in total. In the right M-IDC, the cells share the same signal line, but each has a separate ground/return signal line. This is because the supplied voltage input in each of the cells is ultimately the same and the return output is unique and necessary to measure the capacitance of a specific cell. This reduces the footprint of the device significantly and expands the possibility of housing much more cells.

Appendix E Ethics Supplementary Materials

E.1 Consent Form

UNIVERSITY OF Southampton

CONSENT FORM

Study title: Non-invasive textile sensor for skin hydration monitoring

Researcher name: Alexandar Todorov
ERGO number: 70980
Participant Identification Number (if applicable):

Please initial the box(es) if you agree with the statement(s):

I have read and understood the information sheet (2022/06/06 v4.0) and have had the opportunity to ask questions about the study.	
I agree to take part in this research project and agree for my data to be used for the purpose of this study.	
I understand my participation is voluntary and I may withdraw (at any time) for any reason without my participation rights being affected.	

Name of participant (print name).....

Signature of participant.....

Date.....

Name of researcher (print name).....

Signature of researcher .....

Date.....

[2022/06/06] [v3.0] [ERGO 70980]

E.2 Participant Information Sheet

UNIVERSITY OF Southampton

Participant Information Sheet

Study Title: Non-invasive textile sensor for skin hydration monitoring

Researcher: Alexandar Todorov
ERGO number: 70980

You are being invited to take part in the above research study. To help you decide whether you would like to take part or not, it is important that you understand why the research is being done and what it will involve. Please read the information below carefully and ask questions if anything is not clear or you would like more information before you decide to take part in this research. You may like to discuss it with others but it is up to you to decide whether or not to take part. If you are happy to participate you will be asked to sign a consent form.

What is the research about?
This study aims to develop a wearable, e-textile device that can be used for monitoring of skin hydration. This device would allow skin hydration to be measured quantitatively and will be housed in a compact and non-invasive body that can be used for continuous measurements.

Why have I been asked to participate?
Participants that are able bodied and have no known knowledge of disabilities and are over the age of 18 are welcome to take part in this study. Participants should have no known skin disorders, history of skin irritation or sensitivity; they should have no cuts, blemishes or bruising on the skin area under test.

What will happen to me if I take part?
The study will be conducted in a single visit to a laboratory in Building 59. Participants will be asked to relax for 20-30 minutes before undertaking the study, to avoid sweat being present during the measurements. Once the study starts, an electrode patch will be adhered to the volar arm or the outside of the palm using conventional bandages. The patch will be connected to an LCR meter, which will measure the capacitance and impedance across the electrodes. The participant should not be able to feel any sensation due to the small voltage applied and the high frequency of the AC signal. Discrete measurements will be collected across a time span of 20 minutes at equal time intervals. After the first measurement procedure, the experimental conditions will be changed and moisturising cream will be introduced onto the measured area, and the test will be repeated. The entire study will last between 1-2 hours for each participant.

Are there any benefits in my taking part?
There is no direct benefit to the participant in taking part of the study. The study would yield useful results for the development of a new type of e-health devices that allow for non-invasive continuous measurements.

Are there any risks involved?
There is a very slight risk of an electric shock from the electrodes. The LCR meter (Wayne Kerr 4300) is PAT tested as of 11/2019, but its output voltage is limited to 2V (harmless). Since this is a capacitor layout, no live current will be running through the body. The frequency of operation of the machine will be in orders above 100kHz, further reducing the possibility of any sensible current to be detected.

What data will be collected?
The data collected will consist of the data readings of the LCR meter (Wayne Kerr 4300) – capacitance value and frequency range, and the age and sex of the participants. The age and sex are considered to more effectively compare the findings to other studies in the literature. Personal data will be anonymised, this study is only for testing a prototype and not for clinical trial.

Will my participation be confidential?
Your participation and the information we collect about you during the course of the research will be kept strictly confidential.

Only members of the research team and responsible members of the University of Southampton may be given access to data about you for monitoring purposes and/or to carry out an audit of the study to ensure that the research is complying with applicable regulations. Individuals from regulatory authorities (people who check that we are carrying out the study correctly) may require access to your data. All of these people have a duty to keep your information, as a research participant, strictly confidential.

Do I have to take part?
No, it is entirely up to you to decide whether or not to take part. If you decide you want to take part, you will need to sign a consent form to show you have agreed to take part.
Please contact the researcher by email (at1u18@soton.ac.uk) for more information.

What happens if I change my mind?
You have the right to change your mind and withdraw at any time without giving a reason and without your participant rights being affected.

If you wish to withdraw from the study, contact the researcher by email (at1u18@soton.ac.uk) to end your participation. Please note that once the data has been submitted for a peer-reviewed journal, it won't be possible to remove it, but this will not contain any personal information.

What will happen to the results of the research?
Your personal details will remain strictly confidential. Research findings made available in any reports or publications will not include information that can directly identify you without your specific consent.
The data obtained during this study will be used to prepare a progress report for the investigator's 9-month progression review. It would serve as evidence of the novelty of the approach taken in the context of e-textiles within e-health solutions.

The data will be stored within a repository (PURE), as per the University's policy, for 10 years. It will be actively used during the duration of the investigator's degree, because it may serve as valuable information to be published in a peer-reviewed journal.

The personal details of all participants will be kept confidential, following the University's policy.

For further questions about the results of the research contact the researcher: Alexandar Todorov (at1u18@soton.ac.uk)

Where can I get more information?
For more information contact Alexandar Todorov (at1u18@soton.ac.uk)

What happens if there is a problem?
If you have a concern about any aspect of this study, you should speak to the researchers who will do their best to answer your questions.

Investigator: Alexandar Todorov (at1u18@soton.ac.uk)
Supervisor: Russel Torah (rnt@ecs.soton.ac.uk)

If you remain unhappy or have a complaint about any aspect of this study, please contact the University of Southampton Research Integrity and Governance Manager (023 8059 5058, rgoinfo@soton.ac.uk).

Data Protection Privacy Notice

[06/06/2022] [v4.0] [ERGO 70980]

The University of Southampton conducts research to the highest standards of research integrity. As a publicly-funded organisation, the University has to ensure that it is in the public interest when we use personally-identifiable information about people who have agreed to take part in research. This means that when you agree to take part in a research study, we will use information about you in the ways needed, and for the purposes specified, to conduct and complete the research project. Under data protection law, 'Personal data' means any information that relates to and is capable of identifying a living individual. The University's data protection policy governing the use of personal data by the University can be found on its website (https://www.southampton.ac.uk/legalservices/what-we-do/data-protection-and-foi.page).

This Participant Information Sheet tells you what data will be collected for this project and whether this includes any personal data. Please ask the research team if you have any questions or are unclear what data is being collected about you.

Our privacy notice for research participants provides more information on how the University of Southampton collects and uses your personal data when you take part in one of our research projects and can be found at http://www.southampton.ac.uk/assets/sharepoint/intranet/ls/Public/Research%20and%20Integrity%20Privacy%20Notice/Privacy%20Notice%20for%20Research%20Participants.pdf

Any personal data we collect in this study will be used only for the purposes of carrying out our research and will be handled according to the University's policies in line with data protection law. If any personal data is used from which you can be identified directly, it will not be disclosed to anyone else without your consent unless the University of Southampton is required by law to disclose it.

Data protection law requires us to have a valid legal reason ('lawful basis') to process and use your Personal data. The lawful basis for processing personal information in this research study is for the performance of a task carried out in the public interest. Personal data collected for research will not be used for any other purpose.

For the purposes of data protection law, the University of Southampton is the 'Data Controller' for this study, which means that we are responsible for looking after your information and using it properly. The University of Southampton will keep identifiable information about you for 10 years after the study has finished after which time any link between you and your information will be removed.

To safeguard your rights, we will use the minimum personal data necessary to achieve our research study objectives. Your data protection rights – such as to access, change, or transfer such information - may be limited, however, in order for the research output to be reliable and accurate. The University will not do anything with your personal data that you would not reasonably expect.

If you have any questions about how your personal data is used, or wish to exercise any of your rights, please consult the University's data protection webpage (https://www.southampton.ac.uk/legalservices/what-we-do/data-protection-and-foi.page) where you can make a request using our online form. If you need further assistance, please contact the University's Data Protection Officer (data.protection@soton.ac.uk).

Thank you.

[06/06/2022] [v4.0] [ERGO 70980]

List of References

[1] H. Moghaddasi, F. Asadi, A. Hosseini, and Z. Ebnehoseini, "E-Health: A Global Approach with Extensive Semantic Variation," *Journal of Medical Systems 2011 36:5,* vol. 36, no. 5, pp. 3173-3176, 2011/11// 2011, doi: 10.1007/S10916-011-9805-Z.

[2] World Health Organization, "BUILDING FOUNDATIONS for eHEALTH," 2006. [Online]. Available: http://www.who.int/GOe.

[3] D. De, A. J. Kanwar, and S. Handa, "Comparative efficacy of Hanifin and Rajka's criteria and the UK working party's diagnostic criteria in diagnosis of atopic dermatitis in a hospital setting in North India," *Journal of the European Academy of Dermatology and Venereology,* vol. 20, no. 7, pp. 853-859, 2006/8// 2006, doi: 10.1111/J.1468-3083.2006.01664.X.

[4] E. E. A. Brenninkmeijer, M. E. Schram, M. M. G. Leeflang, J. D. Bos, and P. I. Spuls, "Diagnostic criteria for atopic dermatitis: a systematic review," *British Journal of Dermatology,* vol. 158, no. 4, pp. 754-765, 2008/4// 2008, doi: 10.1111/J.1365-2133.2007.08412.X.

[5] Z. Kirtava, T. Shulaia, N. Kiladze, N. Korsantia, T. Gogitidze, and D. Jorjoliani, "E-Health/m-Health services for dermatology outpatients screening for skin cancer and follow-up," *2016 IEEE 18th International Conference on e-Health Networking, Applications and Services, Healthcom 2016,* 2016/11// 2016, doi: 10.1109/HEALTHCOM.2016.7749427.

[6] A. Havelin and P. Hampton, "Telemedicine and e-Health in the Management of Psoriasis: Improving Patient Outcomes – A Narrative Review," *Psoriasis: Targets and Therapy,* vol. 12, pp. 15-15, 2022/3// 2022, doi: 10.2147/PTT.S323471.

[7] O. Reiter, V. Rotemberg, K. Kose, and A. C. Halpern, "Artificial Intelligence in Skin Cancer," *Current Dermatology Reports 2019 8:3,* vol. 8, no. 3, pp. 133-140, 2019/7// 2019, doi: 10.1007/S13671-019-00267-0.

[8] K. Yang, B. Isaia, L. J. E. Brown, and S. Beeby, "E-Textiles for Healthy Ageing," *Sensors 2019, Vol. 19, Page 4463,* vol. 19, no. 20, pp. 4463-4463, 2019/10// 2019, doi: 10.3390/S19204463.

[9] F. Amitrano *et al.*, "Design and Validation of an E-Textile-Based Wearable Sock for Remote Gait and Postural Assessment," *Sensors 2020, Vol. 20, Page 6691,* vol. 20, no. 22, pp. 6691-6691, 2020/11// 2020, doi: 10.3390/S20226691.

[10] A. Komolafe *et al.*, "E-Textile Technology Review-From Materials to Application," *IEEE Access,* vol. 9, pp. 97152-97179, 2021, doi: 10.1109/ACCESS.2021.3094303.

[11] M. Wagih, O. Malik, A. S. Weddell, and S. Beeby, "E-Textile Breathing Sensor Using Fully Textile Wearable Antennas," *Engineering Proceedings 2022, Vol. 15, Page 9,* vol. 15, no. 1, pp. 9-9, 2022/3// 2022, doi: 10.3390/ENGPROC2022015009.

[12] A. Boehm, X. Yu, W. Neu, S. Leonhardt, and D. Teichmann, "A Novel 12-Lead ECG T-Shirt with Active Electrodes," *Electronics 2016, Vol. 5, Page 75,* vol. 5, no. 4, pp. 75-75, 2016/11// 2016, doi: 10.3390/ELECTRONICS5040075.

[13] G. Aggarwal and Y. Wei, "Non-Invasive Fetal Electrocardiogram Monitoring Techniques: Potential and Future Research Opportunities in Smart Textiles," *Signals,* vol. 2, no. 3, pp. 392-412, 2021, doi: 10.3390/signals2030025.

[14] G. López, V. Custodio, and J. I. Moreno, "LOBIN: E-textile and wireless-sensor-network-based platform for healthcare monitoring in future hospital environments," *IEEE Transactions on Information Technology in Biomedicine,* vol. 14, no. 6, pp. 1446-1458, 2010/11// 2010, doi: 10.1109/TITB.2010.2058812.

[15] T. Hughes-Riley *et al.*, "Wearable Electronic Textiles for Healthcare, Wellbeing, and Protective Applications," 2024: ACM, pp. 1-5, doi: 10.1145/3613905.3648646. [Online]. Available: https://dx.doi.org/10.1145/3613905.3648646

[16] L. Plant, B. Noriega, A. Sonti, N. Constant, and K. Mankodiya, "Smart E-textile gloves for quantified measurements in movement disorders," *2016 IEEE MIT Undergraduate Research Technology Conference, URTC 2016,* vol. 2018-January, pp. 1-4, 2018/2// 2018, doi: 10.1109/URTC.2016.8284077.

[17] R. McLaren, F. Joseph, C. Baguley, and D. Taylor, "A review of e-textiles in neurological rehabilitation: How close are we?," *Journal of NeuroEngineering and Rehabilitation,* vol. 13, no. 1, pp. 1-13, 2016/6// 2016, doi: 10.1186/S12984-016-0167-0/TABLES/1.

[18] J. A. Bouwstra, P. L. Honeywell-Nguyen, G. S. Gooris, and M. Ponec, "Structure of the skin barrier and its modulation by vesicular formulations," *Progress in Lipid Research,* vol. 42, no. 1, pp. 1-36, 2003/1// 2003, doi: 10.1016/S0163-7827(02)00028-0.

[19] M. Mamouei, M. Qassem, M. Razban, and P. A. Kyriacou, "Measurement of dermal water content using a multi-wavelength optical sensor," in *2020 42nd Annual International Conference of the IEEE Engineering in Medicine & Biology Society (EMBC)*, 2020/7// 2020, vol. 2020-July: IEEE, pp. 4353-4356, doi: 10.1109/EMBC44109.2020.9176619. [Online]. Available: https://ieeexplore.ieee.org/document/9176619/

[20] F. Lu *et al.*, "Review of Stratum Corneum Impedance Measurement in Non-Invasive Penetration Application," *Biosensors,* vol. 8, no. 2, p. 31, 2018, doi: 10.3390/bios8020031.

[21] A. Baroni, E. Buommino, V. De Gregorio, E. Ruocco, V. Ruocco, and R. Wolf, "Structure and function of the epidermis related to barrier properties," *Clinics in Dermatology,* vol. 30, no. 3, pp. 257-262, 2012/5// 2012, doi: 10.1016/J.CLINDERMATOL.2011.08.007.

[22] Y. Abe and M. Nishizawa, "Electrical aspects of skin as a pathway to engineering skin devices," *APL Bioengineering,* vol. 5, no. 4, pp. 041509-041509, 2021/12// 2021, doi: 10.1063/5.0064529.

[23] A. O. Rinaldi *et al.*, "Electrical impedance spectroscopy for the characterization of skin barrier in atopic dermatitis," *Allergy,* vol. 76, no. 10, pp. 3066-3079, 2021, doi: 10.1111/all.14842.

[24] D. Y. M. Leung, M. Boguniewicz, M. D. Howell, I. Nomura, and Q. A. Hamid, "New insights into atopic dermatitis," *The Journal of Clinical Investigation,* vol. 113, no. 5, pp. 651-657, 2004/3// 2004, doi: 10.1172/JCI21060.

[25] J. Spergel and A. S. Paller, "Atopic dermatitis and the atopic march," *Journal of Allergy and Clinical Immunology,* vol. 112, no. 6, pp. S118-S127, 2003, doi: 10.1016/j.jaci.2003.09.033.

[26] R. M. Herd, M. J. Tidman, R. J. Prescott, and J. A. A. Hunter, "The cost of atopic eczema," *British Journal of Dermatology,* vol. 135, no. 1, pp. 20-23, 1996/7// 1996, doi: 10.1046/J.1365-2133.1996.D01-970.X.

[27] S. Reitamo, T. A. Luger, and M. Steinhoff, *Textbook of Atopic Dermatitis*. Informa Healthcare, 2008.

[28] M. Suárez-Fariñas *et al.*, "Non-lesional atopic dermatitis (AD) skin is characterized by broad terminal differentiation defects and variable immune abnormalities," *The Journal of allergy and clinical immunology,* vol. 127, no. 4, pp. 954-954, 2011, doi: 10.1016/J.JACI.2010.12.1124.

[29] C. N. A. Palmer *et al.*, "Common loss-of-function variants of the epidermal barrier protein filaggrin are a major predisposing factor for atopic dermatitis," *Nature Genetics 2006 38:4,* vol. 38, no. 4, pp. 441-446, 2006/3// 2006, doi: 10.1038/ng1767.

[30] A. De Benedetto *et al.*, "Tight junction defects in patients with atopic dermatitis," *Journal of Allergy and Clinical Immunology,* vol. 127, no. 3, pp. 773-786.e7, 2011/3// 2011, doi: 10.1016/J.JACI.2010.10.018.

[31] I. Nicander and S. Ollmar, "Clinically normal atopic skin vs. non-atopic skin as seen through electrical impedance," *Skin Research and Technology,* vol. 10, no. 3, pp. 178-183, 2004, doi: 10.1111/j.1600-0846.2004.00065.x.

[32] K. Agrawal *et al.*, "Effects of Atopic Dermatitis and Gender on Sebum Lipid Mediator and Fatty Acid Profiles," *Prostaglandins, leukotrienes, and essential fatty acids,* vol. 134, no. 530, pp. 7-7, 2018/7// 2018, doi: 10.1016/J.PLEFA.2018.05.001.

[33] Y. Kataoka, "Thymus and activation-regulated chemokine as a clinical biomarker in atopic dermatitis," *The Journal of Dermatology,* vol. 41, no. 3, pp. 221-229, 2014/3// 2014, doi: 10.1111/1346-8138.12440.

[34] K. Szegedi *et al.*, "Cytokine profiles in interstitial fluid from chronic atopic dermatitis skin," *Journal of the European Academy of Dermatology and Venereology,* vol. 29, no. 11, pp. 2136-2144, 2015/11// 2015, doi: 10.1111/JDV.13160.

[35] M. Qassem and P. Kyriacou, "Review of Modern Techniques for the Assessment of Skin Hydration," *Cosmetics,* vol. 6, no. 1, p. 19, 2019, doi: 10.3390/cosmetics6010019.

[36] K. Zafar *et al.*, "Skin Lesion Segmentation from Dermoscopic Images Using Convolutional Neural Network," *Sensors,* vol. 20, no. 6, p. 1601, 2020, doi: 10.3390/s20061601.

[37] B. Dong *et al.*, "Monitoring of atopic dermatitis using leaky coaxial cable," *Healthcare Technology Letters,* vol. 4, no. 6, pp. 244-248, 2017, doi: 10.1049/htl.2017.0021.

[38] T. Ebata, S. Iwasaki, R. Kamide, and M. Niimura, "Use of a wrist activity monitor for the measurement of nocturnal scratching in patients with atopic dermatitis," *British Journal of Dermatology,* vol. 144, no. 2, pp. 305-309, 2001, doi: 10.1046/j.1365-2133.2001.04019.x.

[39] B. G. Bender, S. B. Leung, and D. Y. M. Leung, "Actigraphy assessment of sleep disturbance in patients with atopic dermatitis: An objective life quality measure," *Journal of Allergy and Clinical Immunology,* vol. 111, no. 3, pp. 598-602, 2003/3// 2003, doi: 10.1067/MAI.2003.174.

[40] P. P. Vakharia, R. Chopra, and J. I. Silverberg, "Systematic Review of Diagnostic Criteria Used in Atopic Dermatitis Randomized Controlled Trials," *American Journal of Clinical Dermatology,* vol. 19, no. 1, pp. 15-22, 2018, doi: 10.1007/s40257-017-0299-4.

[41] D. M. Elston, E. J. Stratman, and S. J. Miller, "Skin biopsy," *Journal of the American Academy of Dermatology,* vol. 74, no. 1, pp. 1-16, 2016, doi: 10.1016/j.jaad.2015.06.033.

[42] I. Wessler *et al.*, "Increased acetylcholine levels in skin biopsies of patients with atopic dermatitis," *Life Sciences,* vol. 72, no. 18-19, pp. 2169-2172, 2003/3// 2003, doi: 10.1016/S0024-3205(03)00079-1.

[43] M. K. Kägi, B. Wüthrich, E. Montano, J. Barandun, K. Blaser, and C. Walker, "Differential Cytokine Profiles in Peripheral Blood Lymphocyte Supernatants and Skin Biopsies from Patients with Different Forms of Atopic Dermatitis, Psoriasis and Normal Individuals," *International Archives of Allergy and Immunology,* vol. 103, no. 4, pp. 332-340, 1994, doi: 10.1159/000236651.

[44] S. J. F. Salvador, "Atopic Dermatitis in Adults: A Diagnostic Challenge," *J Investig Allergol Clin Immunol,* vol. 27, no. 2, pp. 78-88, 2017, doi: 10.18176/jiaci.0138.

[45] J. Sierra, J. Marrugo-Ramírez, R. Rodriguez-Trujillo, M. Mir, and J. Samitier, "Sensor-Integrated Microfluidic Approaches for Liquid Biopsies Applications in Early Detection of Cancer," *Sensors,* vol. 20, no. 5, p. 1317, 2020, doi: 10.3390/s20051317.

[46] F.-T. Liu, H. Goodarzi, and H.-Y. Chen, "IgE, Mast Cells, and Eosinophils in Atopic Dermatitis," *Clinical Reviews in Allergy & Immunology,* vol. 41, no. 3, pp. 298-310, 2011, doi: 10.1007/s12016-011-8252-4.

[47] A. Yamamoto, S. Serizawa, M. Ito, and Y. Sato, "Stratum corneum lipid abnormalities in atopic dermatitis," *Archives of Dermatological Research 1991 283:4,* vol. 283, no. 4, pp. 219-223, 1991/4// 1991, doi: 10.1007/BF01106105.

[48] M. A. Røpke *et al.*, "Non-invasive assessment of soluble skin surface biomarkers in atopic dermatitis patients—Effect of treatment," *Skin Research and Technology,* vol. 27, no. 5, pp. 715-722, 2021, doi: 10.1111/srt.13006.

[49] S. A. Koppes, R. Brans, S. Ljubojevic Hadzavdic, M. H. W. Frings-Dresen, T. Rustemeyer, and S. Kezic, "Stratum Corneum Tape Stripping: Monitoring of Inflammatory Mediators in Atopic Dermatitis Patients Using Topical Therapy," *International Archives of Allergy and Immunology,* vol. 170, no. 3, pp. 187-193, 2016, doi: 10.1159/000448400.

[50] U. Rohrer, M. Manninger, A. Zirlik, and D. Scherr, "Multiparameter Monitoring with a Wearable Cardioverter Defibrillator," *Sensors,* vol. 22, no. 1, p. 22, 2021, doi: 10.3390/s22010022.

[51] T. Elfaramawy, C. L. Fall, S. Arab, M. Morissette, F. Lellouche, and B. Gosselin, "A Wireless Respiratory Monitoring System Using a Wearable Patch Sensor Network," *IEEE Sensors Journal,* vol. 19, no. 2, pp. 650-657, 2019, doi: 10.1109/jsen.2018.2877617.

[52] F. Antali *et al.*, "Multimodal Assessment of the Pulse Rate Variability Analysis Module of a Photoplethysmography-Based Telemedicine System," *Sensors,* vol. 21, no. 16, p. 5544, 2021, doi: 10.3390/s21165544.

[53] J. S. Talboom and M. J. Huentelman, "Big data collision: the internet of things, wearable devices and genomics in the study of neurological traits and disease," *Human Molecular Genetics,* vol. 27, no. R1, pp. R35-R39, 2018/5// 2018, doi: 10.1093/HMG/DDY092.

[54] J. Šalkevicius, R. Damaševičius, R. Maskeliunas, and I. Laukienė, "Anxiety Level Recognition for Virtual Reality Therapy System Using Physiological Signals," *Electronics,* vol. 8, no. 9, p. 1039, 2019, doi: 10.3390/electronics8091039.

[55] A. Boulemtafes and N. Badache, "Design of Wearable Health Monitoring Systems: An Overview of Techniques and Technologies," Springer International Publishing, 2016, pp. 79-94.

[56] M. Akdeniz, S. Gabriel, A. Lichterfeld-Kottner, U. Blume-Peytavi, and J. Kottner, "TEWL reference values in healthy adults," *British Journal of Dermatology,* vol. 179, no. 5, pp. e204-e204, 2018, doi: 10.1111/bjd.17215.

[57] M. Mündlein *et al.*, "Packaging of a thin-film sensor for transepidermal water loss measurements," *Proceedings of the International Spring Seminar on Electronics Technology,* vol. 2003-January, pp. 328-333, 2003, doi: 10.1109/ISSE.2003.1260544.

[58] H. Zhai and H. I. Maibach, "Skin occlusion and irritant and allergic contact dermatitis: an overview," *Contact Dermatitis,* vol. 44, no. 4, pp. 201-206, 2001, doi: 10.1034/j.1600-0536.2001.044004201.x.

[59] D.-W. Kim, J.-Y. Park, G.-Y. Na, S.-J. Lee, and W.-J. Lee, "Correlation of clinical features and skin barrier function in adolescent and adult patients with atopic dermatitis," *International Journal of Dermatology,* vol. 45, no. 6, pp. 698-701, 2006, doi: 10.1111/j.1365-4632.2005.02644.x.

[60] Y. L. V. A. Werner and M. Lindberg, "Transepidermal water loss in dry and clinically normal skin in patients with atopic dermatitis," *Acta Dermato-venereologica,* vol. 65, no. 2, pp. 102-105, 1985/1// 1985. [Online]. Available: https://europepmc.org/article/med/2408409.

[61] P. Xiao and D. Chen, "The Effect of Sun Tan Lotion on Skin by Using Skin TEWL and Skin Water Content Measurements," *Sensors,* vol. 22, no. 9, p. 3595, 2022, doi: 10.3390/s22093595.

[62] Delfin Technologies. "VapoMeter." Delfin Technologies. https://delfintech.com/products/vapometer/ (accessed.

[63] Biox Systems Ltd., "AquaFlux™ Model AF200 TEWL Measurement Device," ed, 2020.

[64] D. Sim, S. M. Kim, S. S. Kim, and I. Doh, "Portable Skin Analyzers with Simultaneous Measurements of Transepidermal Water Loss, Skin Conductance and Skin Hardness," *Sensors,* vol. 19, no. 18, p. 3857, 2019, doi: 10.3390/s19183857.

[65] K. Martin, "In vivo Measurements of Water in Skin by Near-Infrared Reflectance," vol. 52, no. 7, pp. 1001-1007, 2016/8// 2016, doi: 10.1366/0003702981944652.

[66] B. Yang and Y. Dong, "A Portable Dual-Parameter Tester for Assessing Electrical Properties of Human Skin Surface," *IEEE Sensors Journal,* vol. 16, no. 2, pp. 426-435, 2016/1// 2016, doi: 10.1109/JSEN.2015.2475747.

[67] S. Björklund *et al.*, "Skin Membrane Electrical Impedance Properties under the Influence of a Varying Water Gradient," *Biophysical Journal,* vol. 104, no. 12, pp. 2639-2650, 2013/6// 2013, doi: 10.1016/J.BPJ.2013.05.008.

[68] M. A. Yokus and M. A. Daniele, "Skin Hydration Sensor for Customizable Electronic Textiles," *MRS Advances,* vol. 1, no. 38, pp. 2671-2676, 2016, doi: 10.1557/ADV.2016.540.

[69] S. Yao *et al.*, "A Wearable Hydration Sensor with Conformal Nanowire Electrodes," *Advanced Healthcare Materials,* vol. 6, no. 6, pp. 1601159-1601159, 2017/3// 2017, doi: 10.1002/ADHM.201601159.

[70] I. M. Gidado, M. Qassem, I. F. Triantis, and P. A. Kyriacou, "Review of Advances in the Measurement of Skin Hydration Based on Sensing of Optical and Electrical Tissue Properties," *Sensors,* vol. 22, no. 19, p. 7151, 2022, doi: 10.3390/s22197151.

[71] S. Gabriel, R. W. Lau, and C. Gabriel, "The dielectric properties of biological tissues: III. Parametric models for the dielectric spectrum of tissues," *Physics in Medicine and Biology,* vol. 41, no. 11, pp. 2271-2293, 1996/11// 1996, doi: 10.1088/0031-9155/41/11/003.

[72] C. Gabriel, A. Peyman, and E. H. Grant, "Electrical conductivity of tissue at frequencies below 1 MHz," *Physics in Medicine & Biology,* vol. 54, no. 16, pp. 4863-4863, 2009/7// 2009, doi: 10.1088/0031-9155/54/16/002.

[73] A. B. SciBase, "Nevisense," ed, 2022.

[74] Courage + Khazaka electronic GmbH., "Corneometer® CM 825," ed: Courage + Khazaka electronic Gmb, H., 2022.

[75] Nova Technology Corp., "Novameter DPM 9003," ed: Nova Technology, Corp, 2013.

[76] Delfin Technologies, "MoistureMeterSC," ed: Delfin Technologies.

[77] M. Anthonissen *et al.*, "Reliability of Repeated Measurements on Post-Burn Scars with Corneometer CM 825®," *Skin Research and Technology,* vol. 21, no. 3, pp. 302-312, 2015, doi: 10.1111/srt.12193.

[78] E. E. Grinich, C. Topham, D. Haynes, J. Chung, E. Latour, and E. L. Simpson, "Validation of a novel patient-operated device for measuring skin barrier function in atopic dermatitis," *Skin Research and Technology,* vol. 27, no. 5, pp. 824-830, 2021/9// 2021, doi: 10.1111/SRT.13027.

[79] GPower Inc. "gpskin Barrier." GPower Inc. https://getgpskin.com/device (accessed.

[80] T. Matsumoto, H. Yuasa, R. Kai, H. Ueda, S. Ogura, and Y. Honda, "Skin capacitance in normal and atopic infants, and effects of moisturizers on atopic skin," *The Journal of Dermatology,* vol. 34, no. 7, pp. 447-450, 2007/7// 2007, doi: 10.1111/J.1346-8138.2007.00308.X.

[81] Scalar Corporation, "Skin Moisture Sensor MY-808S," ed: Scalar Corporation, 2009.

[82] P. G. Sator, J. B. Schmidt, and H. Hönigsmann, "Comparison of epidermal hydration and skin surface lipids in healthy individuals and in patients with atopic dermatitis," *Journal of the American Academy of Dermatology,* vol. 48, no. 3, pp. 352-358, 2003/3// 2003, doi: 10.1067/MJD.2003.105.

[83] C. Chiang and L. F. Eichenfield, "Quantitative Assessment of Combination Bathing and Moisturizing Regimens on Skin Hydration in Atopic Dermatitis," *Pediatric Dermatology,* vol. 26, no. 3, pp. 273-278, 2009/5// 2009, doi: 10.1111/J.1525-1470.2009.00911.X.

[84] Moritex, "MoistSense," ed: Moritex.

[85] Yayoi Co, "SKICON-200EX," ed: Yayoi Co.

[86] M. Jang, H.-D. Kim, H.-J. Koo, and J.-H. So, "Textile-Based Wearable Sensor for Skin Hydration Monitoring," *Sensors,* vol. 22, no. 18, p. 6985, 2022, doi: 10.3390/s22186985.

[87] H. N. Rie, J. Cho, J. Lee, S. Gandla, S. J. Kim, and J. Choi, "CMOS Skin Sensor for Mobile Skin Diagnosis Using an Electronic Cotton Pad," *IEEE Access,* vol. 8, pp. 178816-178824, 2020, doi: 10.1109/ACCESS.2020.3026382.

[88] S. Kezic, "Skin barrier in atopic dermatitis," *Frontiers in Bioscience,* vol. 19, no. 3, p. 542, 2014, doi: 10.2741/4225.

[89] Courage+Khazaka GbmH., "Cutometer® Dual MPA 580," in *Courage+Khazaka GbmH*, ed, 2022.

[90] T. Montero-Vilchez *et al.*, "Epidermal Barrier Function and Skin Homeostasis in Atopic Dermatitis: The Impact of Age," *Life,* vol. 12, no. 1, p. 132, 2022, doi: 10.3390/life12010132.

[91] T. Montero-Vilchez *et al.*, "Skin Barrier Function in Psoriasis and Atopic Dermatitis: Transepidermal Water Loss and Temperature as Useful Tools to Assess Disease Severity," *Journal of Clinical Medicine,* vol. 10, no. 2, p. 359, 2021, doi: 10.3390/jcm10020359.

[92] M.-M. Constantin, S. Bucur, E.-D. Serban, R. Olteanu, O. Bratu, and T. Constantin, "Measurement of skin viscoelasticity: A non-invasive approach in allergic contact dermatitis," *Experimental and Therapeutic Medicine,* vol. 20, no. 6, pp. 1-1, 2020, doi: 10.3892/etm.2020.9314.

[93] N. Mahadevan *et al.*, "Development of digital measures for nighttime scratch and sleep using wrist-worn wearable devices," *npj Digital Medicine,* vol. 4, no. 1, 2021, doi: 10.1038/s41746-021-00402-x.

[94] Y. Noro *et al.*, "Novel acoustic evaluation system for scratching behavior in itching dermatitis: Rapid and accurate analysis for nocturnal scratching of atopic dermatitis patients," *The Journal of Dermatology,* vol. 41, no. 3, pp. 233-238, 2014, doi: 10.1111/1346-8138.12405.

[95] J.-E. Kim, J. Lee, M. Bessho, and K. Sakamura, "Field Trial of a Wearable Itch Monitoring System for the Self-Management of Atopic Dermatitis," 2021: IEEE, doi: 10.1109/smc52423.2021.9659306. [Online]. Available: https://dx.doi.org/10.1109/SMC52423.2021.9659306

[96] J. Feuerstein, D. Austin, R. Sack, and T. L. Hayes, "Wrist actigraphy for scratch detection in the presence of confounding activities," in *2011 Annual International Conference of the IEEE Engineering in Medicine and Biology Society*, 2011 2011: IEEE, doi: 10.1109/iembs.2011.6090615. [Online]. Available: https://dx.doi.org/10.1109/IEMBS.2011.6090615

[97] Y.-P. Hsiao *et al.*, "Identification of Skin Lesions by Using Single-Step Multiframe Detector," *Journal of Clinical Medicine,* vol. 10, no. 1, p. 144, 2021, doi: 10.3390/jcm10010144.

[98] D. Padilla, A. Yumang, A. L. Diaz, and G. Inlong, "Differentiating Atopic Dermatitis and Psoriasis Chronic Plaque using Convolutional Neural Network MobileNet Architecture," in *2019 IEEE 11th International Conference on Humanoid, Nanotechnology, Information Technology, Communication and Control, Environment, and Management (HNICEM)*, Laoag, Philippines, 2019 2019: IEEE, doi: 10.1109/hnicem48295.2019.9073482. [Online]. Available: https://dx.doi.org/10.1109/HNICEM48295.2019.9073482

[99] K. Pan, G. Hurault, K. Arulkumaran, H. C. Williams, and R. J. Tanaka, "EczemaNet: Automating Detection and Severity Assessment of Atopic Dermatitis," Springer International Publishing, 2020, pp. 220-230.

[100] V. Patella *et al.*, "Atopic dermatitis severity during exposure to air pollutants and weather changes with an Artificial Neural Network (ANN) analysis," *Pediatric Allergy and Immunology,* vol. 31, no. 8, pp. 938-945, 2020, doi: 10.1111/pai.13314.

[101] A. Cataldo *et al.*, "Portable Microwave Reflectometry System for Skin Sensing," *IEEE Transactions on Instrumentation and Measurement,* vol. 71, pp. 1-8, 2022, doi: 10.1109/TIM.2022.3154804.

[102] H. Arab, L. Chioukh, M. Dashti Ardakani, S. Dufour, and S. O. Tatu, "Early-Stage Detection of Melanoma Skin Cancer Using Contactless Millimeter-Wave Sensors," *IEEE Sensors Journal,* vol. 20, no. 13, pp. 7310-7317, 2020/7// 2020, doi: 10.1109/JSEN.2020.2969414.

[103] X. Huang *et al.*, "Materials and Designs for Wireless Epidermal Sensors of Hydration and Strain," *Advanced Functional Materials,* vol. 24, no. 25, pp. 3846-3854, 2014/7// 2014, doi: 10.1002/ADFM.201303886.

[104] Y. Gao and R. Zoughi, "Millimeter Wave Reflectometry and Imaging for Noninvasive Diagnosis of Skin Burn Injuries," *IEEE Transactions on Instrumentation and Measurement,* vol. 66, no. 1, pp. 77-84, 2017/1// 2017, doi: 10.1109/TIM.2016.2620778.

[105] R. Brendtke, M. Wiehl, F. Groeber, T. Schwarz, H. Walles, and J. Hansmann, "Feasibility Study on a Microwave-Based Sensor for Measuring Hydration Level Using Human Skin Models," *PLOS ONE,* vol. 11, no. 4, pp. e0153145-e0153145, 2016/4// 2016, doi: 10.1371/JOURNAL.PONE.0153145.

[106] R. Schiavoni *et al.*, "Feasibility of a Wearable Reflectometric System for Sensing Skin Hydration," *Sensors 2020, Vol. 20, Page 2833,* vol. 20, no. 10, pp. 2833-2833, 2020/5// 2020, doi: 10.3390/S20102833.

[107] G. Monti, R. Schiavoni, E. De Benedetto, A. Cataldo, and L. Tarricone, "Low-cost System for Skin Sensing," in *2021 IEEE MTT-S International Microwave and RF Conference (IMARC)*, 2021/12// 2021: IEEE, pp. 1-3, doi: 10.1109/IMaRC49196.2021.9714692. [Online]. Available: https://ieeexplore.ieee.org/document/9714692/

[108] P. Mehta, K. Chand, D. Narayanswamy, D. G. Beetner, R. Zoughi, and W. V. Stoecker, "Microwave Reflectometry as a Novel Diagnostic Tool for Detection of Skin Cancers," *IEEE Transactions on Instrumentation and Measurement,* vol. 55, no. 4, pp. 1309-1316, 2006/8// 2006, doi: 10.1109/TIM.2006.876566.

[109] R. Schiavoni *et al.*, "Microwave Wearable System for Sensing Skin Hydration," in *2021 IEEE International Instrumentation and Measurement Technology Conference (I2MTC)*, 2021/5// 2021, vol. 2021-May: IEEE, pp. 1-6, doi: 10.1109/I2MTC50364.2021.9460018. [Online]. Available: https://ieeexplore.ieee.org/document/9460018/

[110] A. J. Moy and J. W. Tunnell, "Diffuse Reflectance Spectroscopy and Imaging," in *Imaging in Dermatology*: Elsevier, 2016, pp. 203-215.

[111] B. P. Yakimov, D. A. Davydov, V. V. Fadeev, G. S. Budylin, and E. A. Shirshin, "Comparative analysis of the methods for quantitative determination of water content in skin from diffuse reflectance spectroscopy data," *Quantum Electronics,* vol. 50, no. 1, pp. 41-46, 2020/1// 2020, doi: 10.1070/QEL17212/XML.

[112] M. Mamouei, S. Chatterjee, M. Razban, M. Qassem, and P. A. Kyriacou, "Design and Analysis of a Continuous and Non-Invasive Multi-Wavelength Optical Sensor for Measurement of Dermal Water Content," *Sensors,* vol. 21, no. 6, p. 2162, 2021, doi: 10.3390/s21062162.

[113] K. Dev *et al.*, "Machine Learning Assisted Handheld Confocal Raman Micro-Spectroscopy for Identification of Clinically Relevant Atopic Eczema Biomarkers," *Sensors,* vol. 22, no. 13, p. 4674, 2022, doi: 10.3390/s22134674.

[114] S. L. Zhang, C. L. Meyers, K. Subramanyan, and T. M. Hancewicz, "Near infrared imaging for measuring and visualizing skin hydration. A comparison with visual assessment and electrical methods," *Journal of Biomedical Optics,* vol. 10, no. 3, pp. 031107-031107, 2005/5// 2005, doi: 10.1117/1.1922347.

[115] N. Petitdidier, A. Koenig, R. Gerbelot, H. Grateau, S. Gioux, and P. Jallon, "Contact, high-resolution spatial diffuse reflectance imaging system for skin condition diagnosis," vol. 23, no. 11, pp. 115003-115003, 2018/11// 2018, doi: 10.1117/1.JBO.23.11.115003.

[116] C. J. H. Ho *et al.*, "Handheld confocal Raman spectroscopy (CRS) for objective assessment of skin barrier function and stratification of severity in atopic dermatitis (AD) patients," *Journal of Dermatological Science,* vol. 98, no. 1, pp. 20-25, 2020/4// 2020, doi: 10.1016/J.JDERMSCI.2020.02.001.

[117] F. J. González *et al.*, "Use of Raman spectroscopy for the early detection of filaggrin-related atopic dermatitis," *Skin Research and Technology,* vol. 17, no. 1, pp. 45-50, 2011, doi: 10.1111/j.1600-0846.2010.00461.x.

[118] V. Fioravanti *et al.*, "An Infrared Absorbance Sensor for the Detection of Melanoma in Skin Biopsies," *Sensors,* vol. 16, no. 10, p. 1659, 2016, doi: 10.3390/s16101659.

[119] E. S. Shin, J.-Y. Lee, S. J. Lee, and S. H. Nam, "Non-invasive method to monitor molecular changes in human stratum corneum during acute barrier disruption using reflectance NIR spectroscopy," 2018: IEEE, doi: 10.1109/embc.2018.8512567. [Online]. Available: https://dx.doi.org/10.1109/EMBC.2018.8512567

[120] P. Anker *et al.*, "Visualization of Keratin with Diffuse Reflectance and Autofluorescence Imaging and Nonlinear Optical Microscopy in a Rare Keratinopathic Ichthyosis," *Sensors,* vol. 21, no. 4, p. 1105, 2021, doi: 10.3390/s21041105.

[121] L. Yan, S. Hu, A. Alzahrani, S. Alharbi, and P. Blanos, "A Multi-Wavelength Opto-Electronic Patch Sensor to Effectively Detect Physiological Changes against Human Skin Types," *Biosensors 2017, Vol. 7, Page 22,* vol. 7, no. 2, pp. 22-22, 2017/6// 2017, doi: 10.3390/BIOS7020022.

[122] A. Todorov, R. Torah, M. R. Ardern-Jones, and S. P. Beeby, "Electromagnetic Sensing Techniques for Monitoring Atopic Dermatitis—Current Practices and Possible Advancements: A Review," *Sensors,* vol. 23, no. 8, p. 3935, 2023, doi: 10.3390/s23083935.

[123] K. Goyal, D. A. Borkholder, and S. W. Day, "A biomimetic skin phantom for characterizing wearable electrodes in the low-frequency regime," *Sensors and Actuators A: Physical,* vol. 340, pp. 113513-113513, 2022/6// 2022, doi: 10.1016/J.SNA.2022.113513.

[124] A. R. Todorov, K. Goyal, R. N. Torah, T. Greig, M. R. Ardern-Jones, and S. P. Beeby, "Skin Model for Monitoring Atopic Dermatitis Using Interdigitated Capacitive Sensor," in *46th Annual International Conference of the IEEE Engineering in Medicine and Biology Society*, Orlando, FL, 2024 2024: IEEE, pp. 1-4, doi: 10.1109/embc53108.2024.10782789. [Online]. Available: https://dx.doi.org/10.1109/EMBC53108.2024.10782789

[125] T. Greig, K. Yang, and R. Torah, "A comparative evaluation of equivalent circuit and finite element electrical skin modelling techniques," *Biomedical Physics & Engineering Express,* vol. 9, no. 6, p. 065013, 2023, doi: 10.1088/2057-1976/acfb04.

[126] A. V. Mamishev, K. Sundara-Rajan, F. Yang, Y. Du, and M. Zahn, "Interdigital sensors and transducers," *Proceedings of the IEEE,* vol. 92, no. 5, pp. 808-844, 2004, doi: 10.1109/JPROC.2004.826603.

[127] C. U. Kim *et al.*, "Numerical analysis on effective electric field penetration depth for interdigital impedance sensor," *Journal of Physics: Conference Series,* vol. 418, no. 1, pp. 012020-012020, 2013/3// 2013, doi: 10.1088/1742-6596/418/1/012020.

[128] T. H. Huang, J. C. Chou, T. P. Sun, and S. K. Hsiung, "A device for skin moisture and environment humidity detection," *Sensors and Actuators B: Chemical,* vol. 134, no. 1, pp. 206-212, 2008/8// 2008, doi: 10.1016/J.SNB.2008.04.030.

[129] K. De Guzman and A. Morrin, "Screen-printed Tattoo Sensor towards the Non-invasive Assessment of the Skin Barrier," *Electroanalysis,* vol. 29, no. 1, pp. 188-196, 2017/1// 2017, doi: 10.1002/elan.201600572.

[130] R. AlDisi, Q. Bader, and A. Bermak, "Hydration Assessment Using the Bio-Impedance Analysis Method," *Sensors (Basel, Switzerland),* vol. 22, no. 17, 2022/9// 2022, doi: 10.3390/S22176350.

[131] L. Q. Jun, G. W. bin Djaswadi, H. F. bin Hawari, and M. A. B Zakariya, "Simulation of Interdigitated Electrodes (IDEs) Geometry Using COMSOL Multiphysics," in *2018 International Conference on Intelligent and Advanced System (ICIAS)*, 2018/8// 2018: IEEE, pp. 1-6, doi: 10.1109/ICIAS.2018.8540599. [Online]. Available: https://ieeexplore.ieee.org/document/8540599/

[132] C. Xu, Y. Yang, and W. Gao, "Skin-Interfaced Sensors in Digital Medicine: from Materials to Applications," *Matter,* vol. 2, no. 6, pp. 1414-1445, 2020, doi: 10.1016/j.matt.2020.03.020.

[133] X. Huang, W. H. Yeo, Y. Liu, and J. A. Rogers, "Epidermal Differential Impedance Sensor for Conformal Skin Hydration Monitoring," *Biointerphases,* vol. 7, no. 1, pp. 52-52, 2012/8// 2012, doi: 10.1007/S13758-012-0052-8.

[134] R. Ivanic, I. Novotny, V. Rehacek, V. Tvarozek, and M. Weis, "Thin film non-symmetric microelectrode array for impedance monitoring of human skin," *Thin Solid Films,* vol. 433, no. 1-2, pp. 332-336, 2003/6// 2003, doi: 10.1016/S0040-6090(03)00389-4.

[135] X. Huang *et al.*, "Epidermal Impedance Sensing Sheets for Precision Hydration Assessment and Spatial Mapping," *IEEE Transactions on Biomedical Engineering,* vol. 60, no. 10, pp. 2848-2857, 2013/10// 2013, doi: 10.1109/TBME.2013.2264879.

[136] H. Benjamin, S. Bhansali, S. B. Hoath, W. L. Pickens, and R. Smallwood, "A planar micro-sensor for bio-impedance measurements," *Sensors and Actuators B: Chemical,* vol. 111-112, no. SUPPL., pp. 430-435, 2005/11// 2005, doi: 10.1016/j.snb.2005.03.075.

[137] R. Matsukawa, A. Miyamoto, T. Yokota, and T. Someya, "Skin Impedance Measurements with Nanomesh Electrodes for Monitoring Skin Hydration," *Advanced Healthcare Materials,* vol. 9, no. 22, pp. 2001322-2001322, 2020/11// 2020, doi: 10.1002/ADHM.202001322.

[138] S. Ramanathan *et al.*, "Elastomeric polydimethylsiloxane polymer on conductive interdigitated electrode for analyzing skin hydration dynamics," *Applied Physics A: Materials Science and Processing,* vol. 126, no. 9, pp. 1-11, 2020/9// 2020, doi: 10.1007/S00339-020-03933-4/FIGURES/8.

[139] N. Sekiguchi, T. Komeda, H. Funakubo, R. Chabicovsky, J. Nicolics, and G. Stangl, "Microsensor for the measurement of water content in the human skin," *Sensors and Actuators B: Chemical,* vol. 78, no. 1-3, pp. 326-330, 2001/8// 2001, doi: 10.1016/S0925-4005(01)00834-6.

[140] C. Malnati, D. Fehr, F. Spano, and M. Bonmarin, "Modeling Stratum Corneum Swelling for the Optimization of Electrode-Based Skin Hydration Sensors," *Sensors 2021, Vol. 21, Page 3986,* vol. 21, no. 12, pp. 3986-3986, 2021/6// 2021, doi: 10.3390/S21123986.

[141] N. Zoric, "DESIGN AND SIMULATIONS OF IDC SENSOR USING COMSOL MULTYPHYSICS AND DIELECTRIC SPECTROSCOPY OF LTCC SPECTROSCOPY OF LTCCMATERIALS," 2013. [Online]. Available: https://www.researchgate.net/publication/346442154.

[142] N. Angkawisittpan and T. Manasri, "Determination of Sugar Content in Sugar Solutions using Interdigital Capacitor Sensor," *Measurement Science Review,* vol. 12, no. 1, 2012, doi: 10.2478/v10048-012-0002-0.

[143] A. Komolafe *et al.*, "Integrating Flexible Filament Circuits for E-Textile Applications," *Advanced Materials Technologies,* vol. 4, no. 7, p. 1900176, 2019, doi: 10.1002/admt.201900176.

[144] L. Davies, P. Chappell, and T. Melvin, "Modelling the effect of hydration on skin conductivity," *Skin Research and Technology,* vol. 23, no. 3, pp. 363-368, 2017, doi: 10.1111/srt.12344.

[145] A. Albulbul and A. D. C. Chan, "Electrode-skin impedance changes due to an externally applied force," 2012: IEEE, pp. 1-4, doi: 10.1109/memea.2012.6226628. [Online]. Available: https://dx.doi.org/10.1109/MeMeA.2012.6226628

[146] H. Wu *et al.*, "Materials, Devices, and Systems of On-Skin Electrodes for Electrophysiological Monitoring and Human–Machine Interfaces," *Advanced Science,* vol. 8, no. 2, p. 2001938, 2021/01/01 2021, doi: https://doi.org/10.1002/advs.202001938.

[147] I. Hong *et al.*, "Study on the oxidation of copper nanowire network electrodes for skin mountable flexible, stretchable and wearable electronics applications," *Nanotechnology,* vol. 30, no. 7, pp. 074001-074001, 2018/12// 2018, doi: 10.1088/1361-6528/AAF35C.

[148] M. L. W. Knetsch and L. H. Koole, "New Strategies in the Development of Antimicrobial Coatings: The Example of Increasing Usage of Silver and Silver Nanoparticles," *Polymers,* vol. 3, no. 1, pp. 340-366, 2011, doi: 10.3390/polym3010340.

[149] Z. Li, "Textile Electrode Design and Simulation for Bio-signal Recording," ed, 2018.

[150] H. Dai, A. R. Todorov, S. Yong, R. Torah, M. Ardern-Jones, and S. Beeby, "High resolution reverse-offset printed wearable laminated textile capacitive sensor for continuous monitoring of atopic dermatitis," *npj Flexible Electronics,* vol. 9, no. 1, p. 78, 2025/08/02 2025, doi: 10.1038/s41528-025-00456-x.

[151] H. Dai, R. Torah, and S. Beeby, "Reverse-Offset Printing for Fabricating E-Textiles," in *5th International Conference on the Challenges, Opportunities, Innovations and Applications in Electronic Textiles*, Ghent, Belgium, 2024 2023: MDPI, doi: 10.3390/engproc2023052014. [Online]. Available: https://dx.doi.org/10.3390/engproc2023052014

[152] Texas Instruments, "FDC2214: 28-bit, 4-channel capacitance-to-digital converter datasheet," Texas Instruments, SLDS208C, 2017. [Online]. Available: https://www.ti.com/lit/ds/symlink/fdc2214.pdf

[153] KYOCERA AVX Components Corporation, "C0G (NP0) Dielectric, KGM Series MLCC Datasheet," Datasheet TDS-SMDMLCC-0036 Rev 5 [Online]. Available: https://www.mouser.co.uk/datasheet/2/40/C0GNP0_KGM-3216332.pdf

[154] T. Instruments, "FDC2114 and FDC2214 EVM User's Guide," Texas Instruments, SNOU138A, 2015. [Online]. Available: https://www.ti.com/lit/ug/snou138a/snou138a.pdf?ts=1740871626831

[155] Seeed Studio. "XIAO nRF52840 – Bluetooth 5.0 Development Board Documentation." https://wiki.seeedstudio.com/XIAO_BLE/ (accessed.

[156] Nordic Semiconductor, "nRF52840 - Multiprotocol Bluetooth 5.3 SoC Technical Documentation," Nordic Semiconductor, nRF52840, 2023. [Online]. Available: https://infocenter.nordicsemi.com/topic/ps_nrf52840/